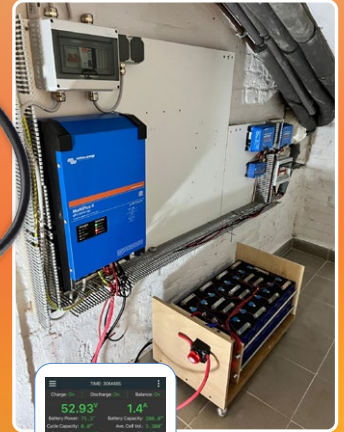


DIY Solar Energy Storage

Build Your Own Battery for a PV Solar Array

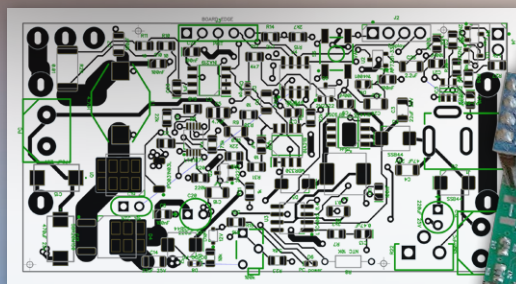
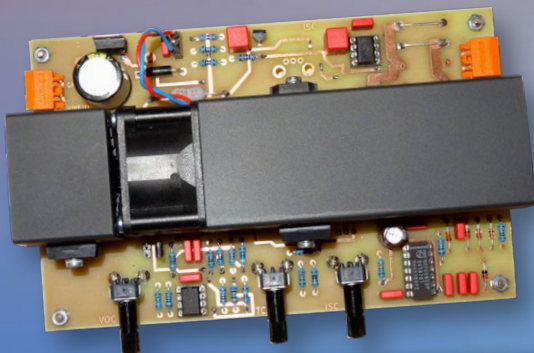


FOCUS ON

Power & Energy

Solar Panel Simulator

For Testing and Optimization of MPP Trackers and Inverters

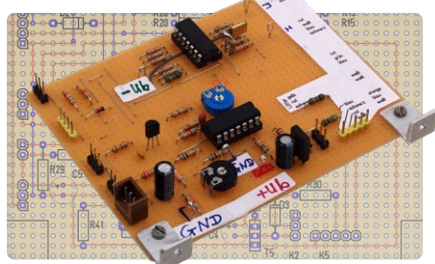


Notebook Power Bank

Extend the Life of Your Aged Laptop



STM32 Edge AI Contest €5,000 in prizes up for grabs



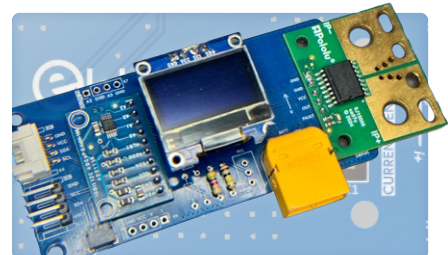
Electronic Load Resistor

Test Batteries and Solar Panels



Frost Guard for Fruit Plants

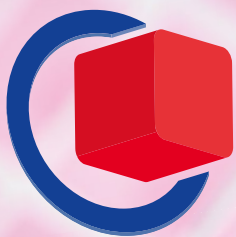
With Temperature Data Logger



AmpVolt v2.0

Measure 100 A and Beyond





embeddedworld

Exhibition & Conference

CONNECTING THE
EMBEDDED COMMUNITY

11 – 13.3.2025

NUREMBERG, GERMANY



Get your
free ticket now!

embedded-world.de/codes

Use the voucher code **ELE4ew25**

Media partners

elektroniknet.de

Markt&Technik
Die unabhängige Wochenzeitschrift für Elektronik

Elektronik

Elektronik
automotive

Elektronik
•medical

connect
professional

NÜRNBERG / MESSE

Volume 51, No. 535
January & February 2025
ISSN 1757-0875

Elektor Magazine is published 8 times a year by
Elektor International Media b.v.
PO Box 11, 6114 ZG Susteren, The Netherlands
Phone: +31 46 4389444
www.elektor.com | www.elektormagazine.com

Content Director: C. J. Abate
Editor-in-Chief: Jens Nickel

For all your questions
service@elektor.com

Become a Member
www.elektormagazine.com/membership

Advertising & Sponsoring
Büsa Kas
Tel. +49 (0)241 95509178
busra.kas@elektor.com
www.elektormagazine.com/advertising

Copyright Notice
© Elektor International Media b.v. 2025

The circuits described in this magazine are for domestic and educational use only. All drawings, photographs, printed circuit board layouts, programmed integrated circuits, digital data carriers, and article texts published in our books and magazines (other than third-party advertisements) are copyright Elektor International Media b.v. and may not be reproduced or transmitted in any form or by any means, including photocopying, scanning and recording, in whole or in part without prior written permission from the Publisher. Such written permission must also be obtained before any part of this publication is stored in a retrieval system of any nature. Patent protection may exist in respect of circuits, devices, components etc. described in this magazine. The Publisher does not accept responsibility for failing to identify such patent(s) or other protection. The Publisher disclaims any responsibility for the safe and proper function of reader-assembled projects based upon or from schematics, descriptions or information published in or in relation with Elektor magazine.

Print
Senefelder Misset, Mercuriusstraat 35,
7006 RK Doetinchem, The Netherlands

Distribution
IPS Group, Carl-Zeiss-Straße 5
53340 Meckenheim, Germany
Phone: +49 2225 88010



Jens Nickel

International Editor-in-Chief, Elektor Magazine



The Agony of Choice

Colleagues contribute to every Elektor issue, as do external experts, who provide articles on various electronics topics throughout the year. However, a good portion of each issue is filled by community authors who only occasionally send us new suggestions. When planning an issue, I look at a list of the article ideas we think are good, and the same process ensues for this issue, "Power and Energy." I was amazed at how many suitable projects were on the list! Unfortunately, space in our magazine is limited, and I was only able to include a few well-crafted suggestions, such as an electronic load (p. 94), a solar panel simulator (p. 14), and a power bank for notebooks (p. 32). This shows me how popular the power and energy topic is with electronics engineers. The solar boom and ever-cheaper Li-Ion battery technology have certainly contributed to the fact that more and more people are becoming interested in the topics of power generation/storage/conversion/measurement.

At this point — and also fittingly at the beginning of a new year — I would like to say a big thank you for the contributions from our community! My colleagues and I discuss the submissions in meetings and are always impressed by the great ideas and professional documentation! Since we have the luxury problem of receiving so many submissions, we are forced to accept only a select few of the good projects. It is not easy for us to have to reject some ingeniously designed special home automation system or professionally manufactured measuring device solely because we believe that they would only be of interest to a very small group of readers. Incidentally, our Elektor Labs project platform is particularly suitable for such somewhat exotic projects and ideas (www.elektormagazine.com/labs). I know from my own experience how much it is appreciated when one finds one, two, or three fellow innovators who are willing to give tips and advice and perhaps even collaborate on the project.

So, if you have a project in the drawer, don't hesitate to publish it on Elektor Labs. Of course, you can also send suggestions to us by e-mail at editor@elektor.com. We also welcome small circuits and background articles on all kinds of electronics topics!

Stay tuned — especially in this new year!



Submit to Elektor!

Your electronics expertise is welcome!
Want to submit an article proposal, an electronics tutorial on video, or an idea for a book? Check out Elektor's Author's Guide and Submissions page:

www.elektormagazine.com/submissions



Elektor Labs Ideas & Projects

The Elektor Labs platform is open to everyone. Post electronics ideas and projects, discuss technical challenges and collaborate with others.

www.elektormagazine.com/labs

The Team

International Editor-in-Chief: Jens Nickel | **Content Director:** C. J. Abate | **International Editorial Staff:** Asma Adhimi, Roberto Armani, Eric Bogers, Jan Buiting, Rolf Gerstendorf (RG), Ton Giesberts, Saad Imtiaz, Alina Neacsu, Dr. Thomas Scherer, Jean-Francois Simon, Clemens Valens, Brian Tristram Williams | **Regular Contributors:** David Ashton, Stuart Cording, Tam Hanna, Ilse Joostens, Prof. Dr. Martin Ossmann, Alfred Rosenkränzer | **Graphic Design & Prepress:** Harmen Heida, Sylvia Sopamena, Patrick Wielders | **Publisher:** Erik Jansen | **Technical Questions:** editor@elektor.com

DIY Solar Energy Storage

Build Your Own Energy Store for a PV Solar Array



Regulars

- 3 Colophon**
- 73 Starting Out in Electronics...**
...Filters Actively
- 100 2025: An AI Odyssey**
Some Projects to See in the New Year
- 110 Err-electronics**
Corrections, Updates, and Readers' Letters

Features

- 6 DIY Solar Energy Storage**
Build Your Own Energy Store for a PV Solar Array
- 26 Widening the Bandgap**
Why There Is So Much Interest in SiC and GaN
- 52 The Analog Thing**
The Arduino of Analog Computing?
- 76 Reducing Power Dissipation With Dropping Capacitors**
A Clever Use of Capacitive Reactance
- 80 The Affordable MCP4725 12-Bit Digital-to-Analog Converter**
An EEPROM Feature Enables Safe Switch-On Behavior
- 84 FNIRSI LCR-ST1 Smart LCR SMD Tweezers**
- 88 Elektor Books**
Raspberry Pi-Based Private Test & Measurement Lab

Projects

- 14 Solar Module Simulator**
A Solution for Testing and Optimizing MPP Trackers and Inverters
- 32 Notebook Power Bank**
Extend the Life of Your Aged Laptop
- 42 Frost Guard for Fruit Plants with Temperature Data Logger**
- 56 Energy Saving Relay Driver**
Saves 90% of Relay Drive Power
- 60 Improving the ET5410A+ DC load**
Keep Cool and Be Quiet, Please
- 94 Electronic Load Resistor**
For Up to 10 A Current
- 106 AmpVolt v2.0 Project Update**
100 Amps and Beyond!
- 116 Elektor Audio DSP FX Processor Board (2)**
Creating Applications

Widening the Bandgap
Why There Is So Much Interest in SiC and GaN



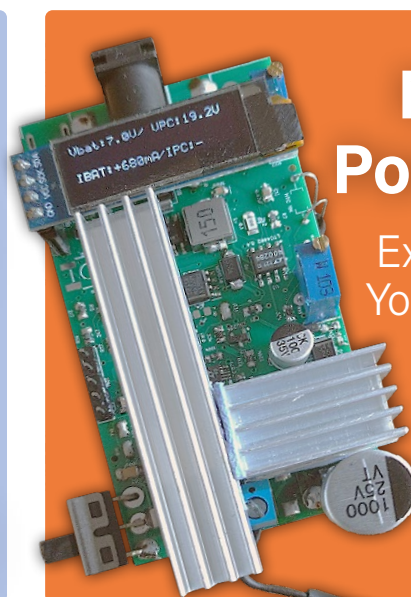
26



Electronic Load Resistor

For Up to 10 A Current

94



Notebook Power Bank

Extend the Life of Your Aged Laptop

32

Industry

22 The STM32 Edge AI Contest

Explore the New STM32N6 and Compete for a Share of €5,000 in Prizes!

39 Medical Robots

Overcoming Technical and Regulatory Hurdles

64 electronica 2024 in Review

68 Electromagnetic Compatibility

EMC in a Nutshell!

112 Unveiling Ethical Transparency

Insights from Ethics in Electronics's 2024 Survey

Elektor Magazine March & April 2025

As usual, we'll have an exciting mix of projects, circuits, fundamentals, and tips and tricks for electronics engineers and makers. Our focus will be on Embedded & AI.

- > FPGA-Based Audio Player with Equalizer
- > MCUViewer: Open-Source Multiplatform Debugging Tool
- > ESP32-S3-Based Sensor Evaluation Board
- > Wireless Mailbox Notifier
- > Maixduino AI-Powered Automatic Doorman
- > Dual-Core Programming with a Raspberry Pi Pico
- > ECG Graph Monitoring

Elektor Magazine's March & April 2025 edition will be published around **March 12, 2025**.

Arrival of printed copies for Elektor Gold members is subject to transport.

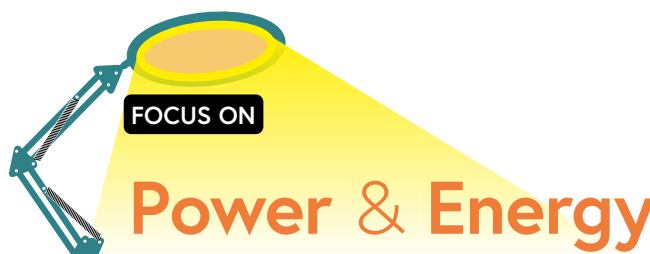
BONUS CONTENT

Check out the free Power & Energy bonus edition of Elektor Mag!

- > Speed Control of a Brushed DC Motor
- > 8-Bit Companion for the Raspberry Pi
- > Peculiar Parts: Mercury Rectifiers
- > Infographics: Power and Energy



www.elektormagazine.com/power-energy



DIY Solar Energy Storage

Build Your Own Energy Store for a PV Solar Array

By Dr. Thomas Scherer (Germany)

Over the past few years, we have witnessed a big drop in the costs of solar PV equipment. The installation of solar panels is now a no-brainer for many homeowners. The one big downside of PV arrays is the energy produced is not consistent. At night, there is no sun. During the winter months and under cloudy skies, there is a real drop in the energy produced. Adding an energy storage battery to the system can make a big difference by boosting the amount of solar energy you can actually use domestically. Here, besides general considerations, we'll take a look at the components chosen by one enthusiast to build a useful 48-V energy storage installation powered from a rooftop PV array.

Following the recent wave of "balcony power stations" (small plug-in, one-to-two panel PV systems which we've covered before [1][2]), the installation of solar storage batteries are now on the rise. It's no wonder, energy from sunlight is variable. On average, about half of each day is dark, no matter where you are in the world. There is a vanishing small level of energy that can be captured from dark current [3] or the light from the moon and stars — of course, it is not sufficient at all. And, during the day, cloud cover throttles back the maximum energy potential of your PV array. Days are shorter in winter, so there's even less solar power available right when you need it most.



Source:
OpenAI and Studio Elektor

To clarify upfront, we're not talking about batteries for small plug-in solar systems (balcony power stations). Right now, batteries for those setups aren't particularly cost-effective. This article is about somewhat larger, "normal" capacity home installations typically mounted on the roof. While you *can* build battery storage for balcony systems too, the cost savings are usually pretty minimal compared to using an off the shelf option. Storing energy from a larger solar setup is a different story.

Storing Energy

The obvious solution to the problem of fluctuating solar power output is to store any excess energy produced during the day, so it's ready for use when you need it at night or when it's cloudy. This way, you will get to use more of the energy you've generated yourself, leading to bigger savings. Of course, with higher self-consumption, you'll export less back into the grid, meaning lower feed-in payments. Even after subtracting those lost feed-in earnings from the savings on electricity you no longer need to buy, you're still left with a clear net gain.

A quick estimate shows that a solar battery can lead to significant savings. For example, if the feed-in tariff is around 10¢ per kWh and electricity from the grid costs 30¢ per kWh, you're saving about 20¢ per kWh if you can use all the energy that you generate and don't import any from the grid. The real savings potential is demonstrated in a conservative case study. Refer to the **Benefits of Using a Solar Battery in Germany** box.

On paper, the profit from a well-sized solar battery might only be around €242 per year, which isn't huge. So installing a solar battery isn't a silver bullet solution. In this study, we do not even take into account the energy lost during the charge/discharge cycles. Depending on the battery's cost, it could take a long time to pay for itself; and, in some cases, the investment may never be fully recouped. Assuming a modest interest rate of 3% would mean you'd need to make €242 annually to break even. If the battery and its installation (including the higher price of an inverter suitable for batteries) will set you back €8,000, it's unlikely to be cost-effective. In this case, you're mainly paying for the feeling of security, knowing you have better energy independence.

A solar system with a battery also comes with the bonus of backup power. Most inverters used in this sort of setup offer a mains socket outlet that, in the event of a grid outage, can be used to power essentials like a gas or oil boiler, freezer, and internet router. Having your own solar battery can add a nice level of security and comfort.

Basic Principles

A PV array with a battery added is usually configured according to the setup in **Figure 1**. An inverter with a battery connection includes a built-in charge controller, which prioritizes routing any surplus energy to charge the battery before exporting that power out to the grid. For example, if the solar system is producing 7 kW and the household is only using 1 kW, the remaining 6 kW can be diverted to charge the battery — assuming the charge controller can handle that much power and the battery has capacity to absorb it.

Battery charge level is another key factor. If the battery is already 95% full, it won't be able to absorb a charge of 6 kW, even if it's rated at 10 kWh. In this state, it would most likely charge at around 1 kWh or less. In this case, where 1 kW is being used by the household and only an additional 1 kW is being stored, the remaining 5 kW would be exported to the grid. After an hour or two, when the battery is completely full, all surplus power — in this case, 6 kW — would go to the grid. At night, when the solar panels aren't generating any power, the inverter's boost converter can draw stored energy from the battery and supply it to the household.

To make this work smoothly, sensors need to be installed in the domestic consumer unit. These sensors allow the inverter to detect how much power is being exported or imported from the grid. At night, the inverter then operates in "zero feed-in" mode, which ensures that just enough power is transferred from the battery to the home to avoid sending any power to the grid. It might be ecologically beneficial to help support the grid by sending out any privately stored energy at night, but financially it doesn't make sense. The FIT (Feed in Tariff) payments usually do not justify the higher battery wear.

With an assumed lifespan of around 8,000 cycles and a cost of €4,000 for a 10 kWh battery, each kilowatt-hour cycled through the battery ends up costing about 5¢ — and that's before installation costs are factored in. In addition, if the battery becomes discharged by early evening, it can't offset overnight usage, so electricity for night time use needs to be purchased at full rate from the utility, defeating the purpose of the storage battery.

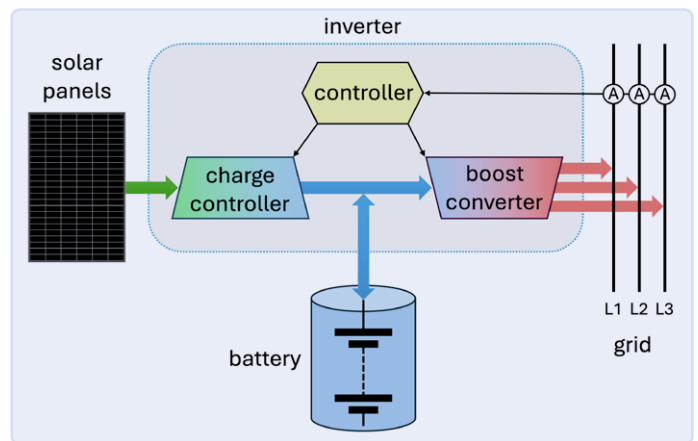


Figure 1: Block diagram showing a PV array with storage battery.

Most retrofit batteries for small plug-in "balcony" solar systems (rated at around 2 kWh) don't monitor energy usage in the consumer unit, so they can only deliver a constant power output, usually between 100 and 500 W. This doesn't adapt to the variable power needs of most households.

Battery Choice

If you want to add a battery to your home solar system, you'll need either an inverter with a connection for a battery or you'll have to retrofit or plan ahead for one. Generally, the choice is between either "high-voltage" or 48-V storage battery pack. High-voltage batteries operate at well over 48 V, usually between 150 and 400 V. Most inverter manufacturers offer compatible high-voltage batteries, usually using proprietary technology. For example, **Figure 2** shows a stackable 10 kWh model from BYD with a nominal voltage of 204 V, priced just under €1 per Wh.



Figure 2: An 11-kWh, high-voltage solar storage battery from BYD (Source: BYD [7]).

Benefits of Using a Solar Battery in Germany

Let's look at how solar battery savings work for an average three-person household in Germany, using a solar system with a 10-kW capacity and an annual electricity consumption of 3.5 MWh. Based on the published **German feed-in tariff table**, you'd get 12.73 cents per kWh if all the electricity generated was exported to the grid. Relying solely on this would mean paying far more for all the electricity you import from your energy provider, so it's not a very economical approach unless you generate significantly more power than you use. To make it worthwhile, the extra revenue from the feed-in tariff would need to outweigh the higher cost of importing all your electricity. In reality, this only works with much larger solar systems that would require significantly more roof area than most single-family homes have available.

Most households in Germany use a partial feed-in arrangement, which provides a lower rate of 8.03 cents per kWh. Meanwhile, energy providers' prices in 2024 are around 30 cents per kWh, so every self-used kWh saves you about 22 cents.

For Germany, a typical solar energy yield is around 950 kWh per year per kW of installed capacity. This means a 10 kW system should produce roughly 9,500 kWh annually. While self-consumption varies, about 20% is a fair estimate, so you'd use around 1,900 kWh domestically each year. At a cost savings of 30 cents per kWh not purchased, this equals roughly €570 saved annually. Add to that the revenue from the 80% of energy fed into the grid, or 7,600 kWh, at 8.03 cents per kWh, giving you an extra €610 per year. Altogether, a 10 kW solar system would yield about €1,180 annually.

So, how does this compare with the added benefit of a solar battery? A well-sized solar battery with effective control can theoretically more than double your self-consumption of energy generated. For a 10 kW system with an annual demand of 3,500 kWh, you'll likely only achieve an 85% self-sufficiency rate. With a battery installed, self-consumption would increase from 1,900 kWh per year to about 3,000 kWh, saving an extra 1,100 kWh per year, or about €330. On the downside, you'd now export 1,100 kWh less into the grid, lowering the feed-in revenue to about €522 annually. With a solar battery installed, the total annual savings add up to €1,422 — adding just €242 more revenue per year compared to a system without a battery.

Feed-In Tariff Table in Germany

| Installed PV Array Rating | Partial Feed in | Full Feed in |
|---------------------------|-----------------|--------------|
| ≤10 kW | 8.03 ¢/kWh | 12.73 ¢/kWh |
| ≤40 kW | 6.95 ¢/kWh | 10.68 ¢/kWh |
| ≤100 kW | 5.68 ¢/kWh | 10.68 ¢/kWh |

High-voltage batteries are typically easy to connect, but you're limited to whatever data the inverter provides about each cell's charge state. High-voltage batteries are often "cascadeable," meaning you can start with a smaller battery and then add more capacity later. The advantage is that you get a reliable, guaranteed solution without taking a deep dive into the technical details. Thanks to a major price drop over the last three years, a 10 kWh high-voltage battery now costs between €3,000 and €10,000.

Some manufacturers produce inverters for standard 48-V battery systems, which are generally cheaper due to greater market competition. The 10-kWh setup shown in **Figure 3**, for example, uses four 50-Ah batteries from Eco-Worthy and costs around €2,000. For an average three-person household, this setup would pay for itself in about eight years (10 years factoring in an interest rate of 3%). After 10 years, the battery will likely have gone through only between 500 and 1,000 cycles, so it's more likely to fail from the effects of aging rather than from overuse.

And here's the kicker: If you buy the necessary battery cells from China, add a Battery Management System (BMS), and assemble everything in an enclosure, you could build a 10-kWh, 48-V battery for just under €1,000. This DIY solution could pay for itself in about four to five years, which makes self-build an attractive option!

Now, let's talk about battery types: the best lithium-ion batteries with regard to energy density (capacity relative to size and weight) are NMC batteries (Nickel Manganese Cobalt), which are common in automotive applications. These are more expensive than LiFePo (Lithium Iron Phosphate) batteries, also known as LiFePO₄, which are better suited for static home installations, where weight and volume are not so important. LiFePo batteries will also last for up to 8,000 charge cycles, far outstripping the roughly 1,000 cycles of NMC batteries. The high-current capacity of NMC batteries is also not such an important consideration for a domestic solar battery installation.

Safety is another major advantage of LiFePo technology. LiFePo batteries are generally much safer whereas aging NMC batteries have been linked to fire risks [4]. Lithium battery fires are intense, generate toxic fumes and can't be put out with water. A large NMC



Figure 3: A stack of 48-V batteries rated at 50 Ah for wiring in parallel (Source: Eco-worthy [8]).

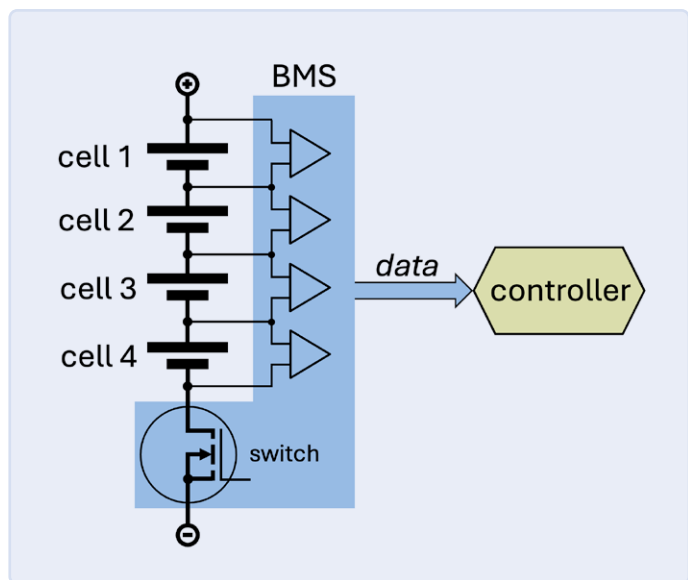


Figure 4: Basic circuit of a battery pack made from 4 LiFePo cells (12 V) with BMS.

battery in a domestic environment could pose a health and safety risk. Altogether it's best to avoid NMC batteries and go exclusively with LiFePo batteries.

Preliminary Notes

When people speak of "48 V" solar batteries, they're actually referring to a pack with a nominal voltage of 51.2 V. Why? Each LiFePo cell has a nominal voltage of 3.2 V. While theoretically 15 cells in series would make up a 48-V battery, in practice, the packs contain 16 cells in series, which brings the terminal voltage to 51.2 V. A 48-V battery can also be made by linking four 12-V LiFePo battery packs in series. These 12-V batteries are typically used as a better replacement for lead-acid batteries in marine electronics and similar applications. A nominal 12-V voltage level can hardly be produced using 3.75 cells in series. 12-V LiFePo battery packs therefore use 4 cells in series. Even the voltage of a typical lead acid starter battery for cars (which uses 6 cells) when fully charged is not 12 V, but 12.8 V. Four 12-V lead-acid batteries in series therefore also provide a nominal 51.2 V.

Unlike lead-acid cells, lithium cells aren't as simple to wire in series. Lithium cells require careful control to balance minor differences that add up in the charge level of individual cells over time. This can be managed within a BMS, which monitors each cell's charge level and uses small balancing currents to keep things even. Another approach is to use an external controller (like one built into the inverter) to monitor all cells, which at the very least can warn of major charge differences, or in some cases, employ special charging/discharging methods to correct them.

For this setup, the BMS needs a data interface compatible with the inverter's controller. A 48 V battery pack isn't always just plug-and-play; it might not work with every inverter without issues. For DIY battery setups, it's essential to pick the right BMS or opt for one that operates independently. **Figure 4** shows the basic layout of a 4-cell battery pack with a BMS. For managing these currents, N-channel MOSFETs are preferred due to better properties — they disconnect the negative side if the BMS detects overcharging or undervoltage. The data bus connection to an external controller shown on the right is optional if you're using a self-balancing BMS.

As a side note, it's not recommended to connect 48-V batteries in series unless there's electronics (like those in the inverter) ensuring that each pack maintains an even charge. Ideally, you want a BMS that monitors all cells. Even connecting batteries in parallel isn't trivial, although it's less complicated than a serial connection. If you do set up batteries in parallel, the inverter (or special monitoring electronics) should be able to connect to multiple BMS data interfaces at once. Ultimately, it's simpler and safer to plan ahead and choose a battery of the capacity you need right from the start.

The DIY Option

Building your own 48-V lithium battery pack from individual cells isn't exactly rocket science, but there are still quite a few details to keep in mind, far beyond what can be covered here. Thankfully, many others have already delved into this topic, and the online maker community is a useful resource for the exchange of knowledge. A nice report, for example, comes from Dr. Oheimb [5]. Of course, there are many more pages worth visiting.

Over three years ago, my friend Martin Jepkens (a physicist and hobby electronics enthusiast), built a hefty solar energy storage system from individual cells. The installation is still working great today. After doing a deep dive into battery science, he ordered 16 prismatic LiFePo cells from the well-known Chinese store AliExpress.

Cells

This setup is made up of 16 LiFePo₄ cells (**Figure 5**) rated at 280 Ah. Altogether, these make a 51.2-V pack with a total capacity of over 14 kWh! You can buy a similar pack today for about €1,000 to €1,500. Calling it a "pack" is a slight understatement, as the entire system weighs well



| | |
|--|-----------------------------------|
| Model: LiFePo4 3.2V 280AH | Rated Capacity: 280AH |
| Nominal Voltage: 3.2V | Max charge Voltage: 3.65V |
| AC Impedance Resistance: $\leq 0.25\text{m}\Omega$ | Maximum Discharge Current: 1C |
| Charging Temperature: 0~60°C | Discharging Temperature: -30~60°C |
| Weight: $\leq 5.6\text{Kg}$ | Dimensions(L*W*H): 173*71*204mm |

Figure 5: Technical details of the 16 280-Ah LiFePo cells (Source: Martin Jepkens).



Figure 6: The cells arrived in four cartons each containing four cells (Source: Martin Jepkens).



Figure 8: Screenshot showing the order for the BMS from Jikong (Source: Martin Jepkens).

over 100 kg with all the parts and packaging. A few weeks after placing the order, he received four boxes, each containing four well-protected cells (Figure 6).

These prismatic LiFePo cells are available in sizes ranging from less than 50 Ah to well over 400 Ah. If you want even more capacity, you can connect identical cells in parallel. If this inspires you to consider building such a setup yourself it's essential to keep product quality in mind! To avoid receiving questionable cells, only buy from sellers with good review



Figure 7: The complete solar battery system installed in the cellar (Source: Martin Jepkens).

ratings and a high volume of sales. Be sure to only connect identical cells manufactured in the same series and with the same production date, to avoid issues over time with differences in the cells' charge levels.

Of course, you don't have to go as big as Martin did — 100 Ah cells are plenty to get you started on saving money. For a typical single-family home, a solar battery with 5 kWh capacity is a good trade-off, enough to cover about 75% of your energy needs. A battery this size will store enough power to handle average night time use for about 1.5 to 2.5 days, more during the summer and sometimes not quite a full night in winter. If you are planning to store energy to cover longer outages and achieve a high level of energy independence, the rule for solar batteries is simple: bigger is better! The lifetime of larger solar batteries will also be longer since they will not be as heavily stressed.

The Inverter

When Martin designed his relatively small solar system, which uses just eight PV panels, he didn't follow the usual setup guidelines. Instead of buying a typical inverter with an additional battery connection, he put together a modular setup from components made by Victron Energy who are based in The Netherlands. They manufacture a wide range of high-quality marine tech and off-grid solutions which use open protocols.

In Figure 7, you can see the full setup in his basement, including the DIY storage battery. He's using two charge controllers (one per four solar panels) to charge the battery, and the large inverter in the foreground isn't directly connected to the solar panels. Instead, it draws power directly from the battery or indirectly through the charge controllers. In this configuration, the battery is usually fully charged by the end of

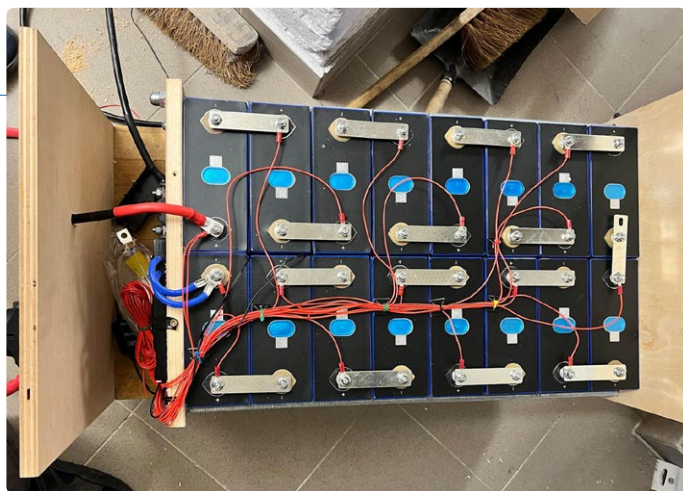


Figure 9: The solar batteries fitted into the enclosure (Source: Martin Jepkens).

a sunny day in the summer. You'll also notice a neat layout with thick cables (tens of mm² in cross-section) and a red heavy-duty isolation switch on the left side of the battery housing.

This setup is intended as a guide to the basics and an inspiration, rather than a step-by-step DIY manual with detailed instructions and a parts list. If the modular approach doesn't make sense to you, or if you're not ready to handle the calculations and component selection on your own, it might be easier to go with an off the shelf inverter, which simplifies things significantly.

The Victron modules communicate with each other over a serial bus, integrating the BMS. Victron's software supports several compatible BMS models, allowing it to read and monitor key data via its RS485 interface. A Jikong BMS controller (**Figure 8**) was ordered via AliExpress from a warehouse in Poland to avoid any customs issues. This BMS has an RS485 interface, a 300 A current rating, and support for 8 to 24 cells. Priced at less than €50 this BMS represents good value.

Battery Installation

In **Figure 9**, you can see Martin's solar battery pack close to completion. Several features stand out. First, the battery case is made of thick plywood. The BMS unit is mounted in the space on the left side, away from the battery cells, with many thinner gauge wires connecting it to each individual cell. Utmost care should be taken during wiring as any accidental short circuit with these cells could quickly draw over 1 kA. At this voltage, any short circuit could generate an arc releasing tens of kW of power as heat, light, and molten metal. The series connections between the cells are made using high-current metal straps (nickel-plated copper), shown in close-up in **Figure 10**.

One special feature isn't immediately noticeable: at the top and bottom of **Figure 9**, you'll see thick threaded rods and, at the top left, one of the four matching lock nuts. These rods are used to apply continuous pressure to the cell walls to help reduce any tendency for the cell walls to develop a bulge. This can occur during charging, discharging, or due to thermal fluctuations. Clamping should help extend the cells' lifespan. The logic behind this sounds solid, and I'd use the same approach.

It's not visible from the pictures, but a sturdy insulating plastic sheet between each cell is used as an extra precaution. With the pressure applied by the "compression housing," this is a wise move. The cells



Figure 10: Close-up showing the terminal posts (Source: Martin Jepkens).

themselves are only separated by a sort of shrink wrap, which isn't especially thick.

To ensure there were no faulty cells, the characteristics of each cell was independently tested using an adjustable load before the pack was assembled (**Figure 11**). The results showed that all the cells behaved very consistently, which remains true years later. **Figure 12** shows a screenshot of a smartphone monitoring app which lists the individual cell voltages along with some overall system parameters. Under a light load of 75 W, the lowest cell voltage is 3.307 V (shown in red, cell #8), and the highest is 3.311 V (shown in blue, cell #3) — a difference of just 4 mV!

DIY: Is it Worth the Effort?

Building your own solar storage battery pack can still be a great option. If you're not ready to dive as deep as Martin did, there are battery kits available. Unfortunately, these kits often end up costing more than a fully assembled solution. So the DIY route is the way to go. You'll learn much along the way. For anyone needing a refresher on solar module basics, please refer to another article of mine [6].

A note on battery capacity: if you combine a smaller PV array (like Martin's 3.4 kWp) with a relatively large 14.3-kWh battery, you'll get great energy independence. The degree of self-sufficiency depends not only on your battery capacity but also on your geographical location.

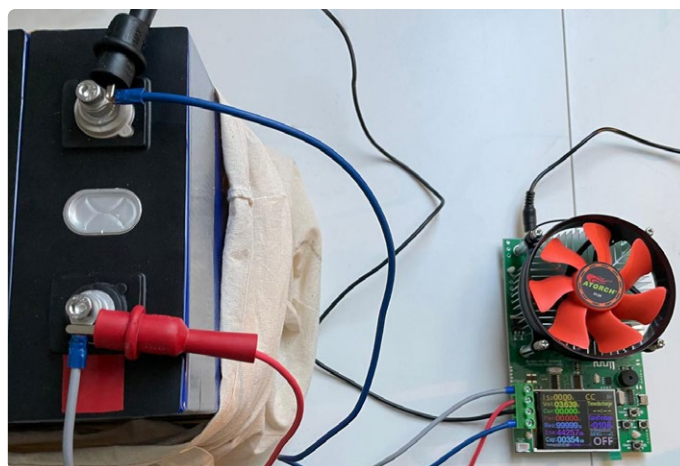


Figure 11: Testing each cell's capacity using an electronic load (Source: Martin Jepkens).

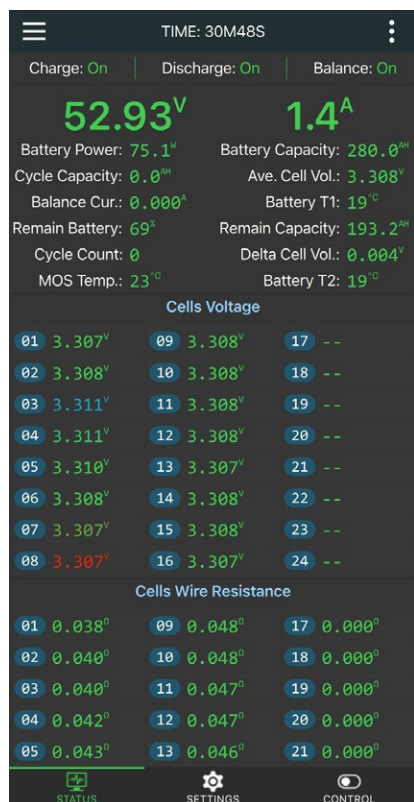


Figure 12: An app shows the terminal voltage of each cell. The reading in red shows the lowest value and blue the highest (Source: Martin Jepkens).

The relationship isn't linear; as you approach 90% self-sufficiency, the battery size required becomes less economical in most of Central Europe (or the southern half of Chile and Argentina). At that point, the storage battery may need to be as large as 50 kWh, which is not only costly but also challenging to integrate, since many standard inverters can't cope well with these high-capacity installations. Complete off-grid energy independence for a typical home using only PV charged batteries is largely a costly illusion. To get through longer periods without sunlight, you would also need some kind of backup generator. ◀

Translated by Martin Cooke — 220233-01

Questions or Comments?

If you have any comments or questions regarding this article please contact Elektor at editor@elektor.com.



About the Author

Dr. Thomas Scherer first completed an apprenticeship as a Telecommunications Electronics Technician and then worked in the Elektor editorial department from 1980. After studying psychology and several years in basic research, he now works as a freelance author and has supplied many articles for Elektor over the years. He has a large electronics laboratory and is interested in neurons as well as electrons - in other words, pretty much anything to do with electricity.



FEATURED TOPIC

Visit our **Power Electronics & Energy** page for articles, projects, news, and videos.

www.elektormagazine.com/power-energy



Related Products

- > **PCW05A True RMS Clamp Meter (600 A)**
www.elektor.com/20834
- > **Elektor-Special: Solaranlagen und Photovoltaik [German]**
www.elektor.de/20596



WEB LINKS

- [1] T. Scherer, "Balcony Power Plant," Elektor 9-10/2021: <https://www.elektormagazine.com/magazine/elektor-183/59831>
- [2] T. Scherer, "Optimizing Balcony Power Plants," Elektor 1-2/2024: <https://www.elektormagazine.com/magazine/elektor-324/62631>
- [3] Dark current: [https://en.wikipedia.org/wiki/Dark_current_\(physics\)](https://en.wikipedia.org/wiki/Dark_current_(physics))
- [4] S. Enkhardt, "Weitere Brände von Photovoltaik-Batteriespeichern," pv magazine, 2023 [German]: <https://tinyurl.com/22ztz8vb>
- [5] Report by Dr. David of Oheimb [German]: <https://ddvo.github.io/Solar/Speicher.html>
- [6] Solar panels, Elektor Special: Solaranlagen und Photovoltaik, p. 26 [German]: <https://tinyurl.com/45z2y34w>
- [7] BYD Solar batteries: <https://www.bydbatterybox.com>
- [8] Eco-worthy: <https://de.eco-worthy.com>

FREE Download Now!
Mac, Windows and Linux

Blackmagicdesign



Edit and color correct using the same software used by Hollywood, for free!

DaVinci Resolve is Hollywood's most popular software! Now it's easy to create feature film quality videos by using professional color correction, editing, audio and visual effects. Because DaVinci Resolve is free, you're not locked into a cloud license so you won't lose your work if you stop paying a monthly fee. There's no monthly fee, no embedded ads and no user tracking.

Editing, Color, Audio and Effects!

DaVinci Resolve is the world's only solution that combines editing, color correction, visual effects, motion graphics and audio post production all in one software tool! You can work faster because you don't have to learn multiple apps or switch software for different tasks. For example, just click the color page for color, or the edit page for editing! It's so incredibly fast!

Professional Editing

DaVinci Resolve is perfect for editing sales or training videos! The familiar track layout makes it easy to learn, while being powerful enough for professional editors. You also get a library full of hundreds of titles, transitions and effects that you can add and animate! Plus, DaVinci Resolve is used on high end work, so you are learning advanced skills used in TV and film.

Creative Color Correction

DaVinci Resolve's color page is Hollywood's most advanced color corrector and has been used on more feature films and television shows than any other system! It has exciting new features to make it easier to get amazing results, even while learning the more advanced color correction tools. There's PowerWindows™, qualifiers, tracking, advanced HDR grading tools and more!

Designed to Grow With You

DaVinci Resolve is designed for collaboration so as you work on larger jobs you can add users and all work on the same projects, at the same time. You can also expand DaVinci Resolve by adding a range of color control panels that let you create unique looks that are impossible with a mouse and keyboard. There's also edit keyboards and Fairlight audio consoles for sound studios!

DaVinci Resolve 19 **Free**
DaVinci Resolve Micro Color Panel **Only £405**



Learn the basics for free then get more creative control with our accessories!

Learn more at www.blackmagicdesign.com/uk
SRP is Exclusive of VAT.

Download free on the
DaVinci Resolve website



NO SUBSCRIPTIONS • NO ADS • NO USER TRACKING • NO AI TRAINING

Solar Module Simulator

A Solution for Testing and Optimizing MPP Trackers and Inverters

By Dipl.-Ing. Peter Kroll (Switzerland)

Solar installations can be seen everywhere today, and many more are planned – both large solar parks and small installations, privately on house roofs. In addition, there are even smaller applications with an output of just a few watts. Inverters or charge controllers with MPP trackers are commonly used to optimize energy yield. Optimization of a system using real light is difficult due to fluctuating conditions. This article describes a simple and inexpensive solar panel simulator that electronically mimics a 50-W solar panel.

In order for a simulator to be able to adjust parameters such as different solar radiation and other environmental influences, the short-circuit current I_{SC} , the open-circuit voltage V_{OC} , and the temperature coefficient TC are adjustable in this solar panel simulator. This means that you can also simulate other modules than the one described in the “50 W Panel from Phaesusun” text box that is simulated as an example in this article.

Simulation Circuit

Like every solar panel, the Phaesusun 50 W type has a temperature coefficient that should not be neglected. If, for example, the module temperature changes from 25°C to 60°C due to solar radiation, the open-circuit

voltage decreases from 21.6 V to 18.95 V. If the temperature drops from 25°C to -10°C in winter, the open-circuit voltage increases to 24.25 V. The temperature dependency is also reflected by the achievable power, which decreases with increasing temperature.

Figure 1 shows the internal structure of the solar panel. It consists of 36 individual cells connected in series. If you want to simulate such a panel, it makes little sense to replace it with a series circuit of 36 correspondingly powerful silicon diodes. It would be more elegant to multiply the voltage of a diode by a factor of 35, as shown in **Figure 2**, and add the result to D1. The multiplication is done by VcV — a voltage source controlled by the voltage of D1.

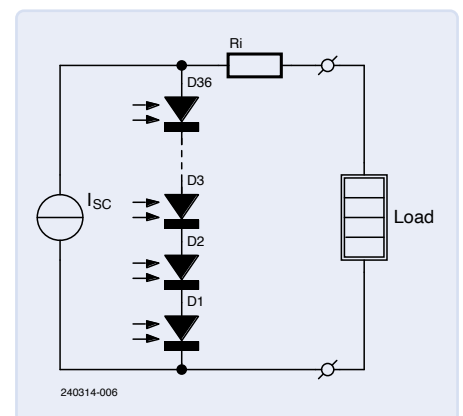


Figure 1: Equivalent circuit diagram of a 36-cell solar panel.

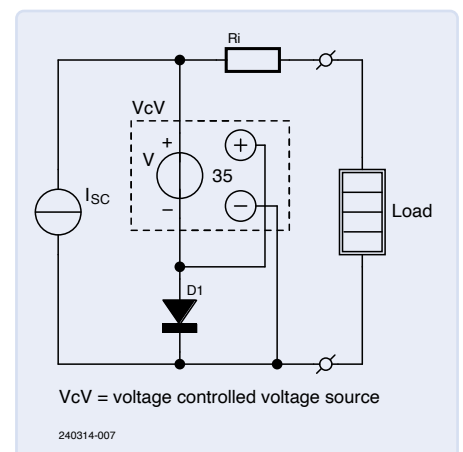


Figure 2: Equivalent circuit: multiplying the voltage across D1 by 35.

In order to implement this principle in real life, it must first be translated into a specific circuit. An initial basic circuit can be seen in **Figure 3**. The current source I_{SC} supplies a specific constant current. This current flows partly through the load resistor and partly through the (simulated) diode paths plus D1. In idle mode without load, the complete current flows through the simulated panel. In the event of a short circuit, however, all the current flows through the load with a resistance of (ideally) 0 Ω . The voltage multiplier in Figure 3 is formed by the power transistor T1, the op-amp IC1, and the voltage divider consisting of R1 and R2. The resistance of R1 is 35 times greater than that of R2. A current-limiting resistor R3 is located before the base of T1.

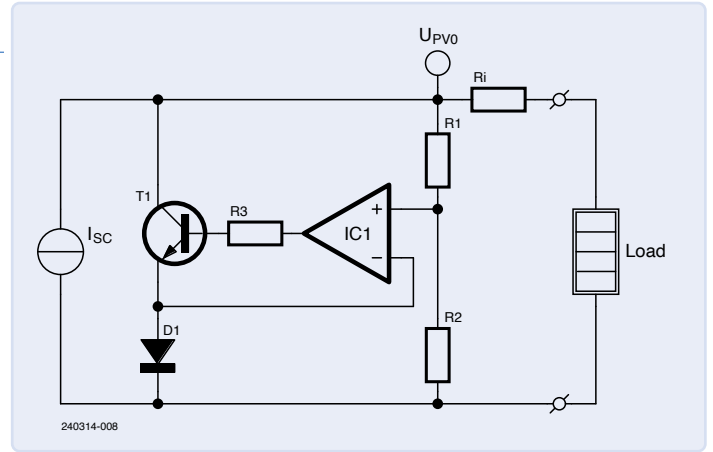
Simulation Circuit + D1

The function of the entire circuit depends largely on the properties of D1. Any deviation of its diode voltage from the behavior to be simulated is magnified by a factor of 36 by an op-amp in the circuit of Figure 3. Particularly relevant here is the temperature coefficient of the forward voltage of D1. To minimize its influence, D1 is mounted on its own heat sink which is independent of the power transistors and is cooled by air at ambient temperature. Ideally, a sufficiently resilient diode with the lowest possible thermal resistance from the junction to the housing should be selected for D1. The heat sink must be sufficiently large and have low thermal resistance. The better the cooling, the more independent the solar panel simulator is of the temperature of D1. In the specific circuit of the solar panel simulator (**Figure 4**), the body diode of an IRFP450 MOSFET is used for D1, whose gate is short-circuited to its source. This diode has a low $R_{th(j-c)}$ of just 0.66 K/W.

Please note: The circuit shown in Figure 4 is described below in the section "Initial Circuit." Even if it works, it is not yet the final solution, in which the relevant parameters can be adjusted. More on this later.

To be able to traverse almost the entire characteristic curve of the simulated solar panel, it is possible to increase R_{Load} continuously from 0 Ω to 500 Ω . R21 represents the internal resistance R_i of the solar panel. This value was determined by measurements and also depends on the diode used (the body diode of T3).

Figure 3:
Basic circuit of the
solar panel simulator.



The Maximum Power Point (MPP) shifts to smaller MPP voltages with higher internal resistance.

V2 is used in the DC simulation as a reference variable for the load resistance R8. Accordingly, V5 is used in the transient simulation as a reference variable for the load resistance: Here, an MPP tracker causes a jump in the load resistance R8 from, for example, 6 to 6.5 Ω and back to 6 Ω . To determine the optimal

operating point, an MPP tracker works with load steps. It jumps back and forth on the U/I characteristic curve, searching for the point with the highest power. Normally, the step size is small so that the MPP is hit accurately enough. V2 (DC) and V5 (transients) can be activated as an alternative if desired.

Simulation

If a DC simulation is carried out with the circuit in Figure 4 and a diode temperature

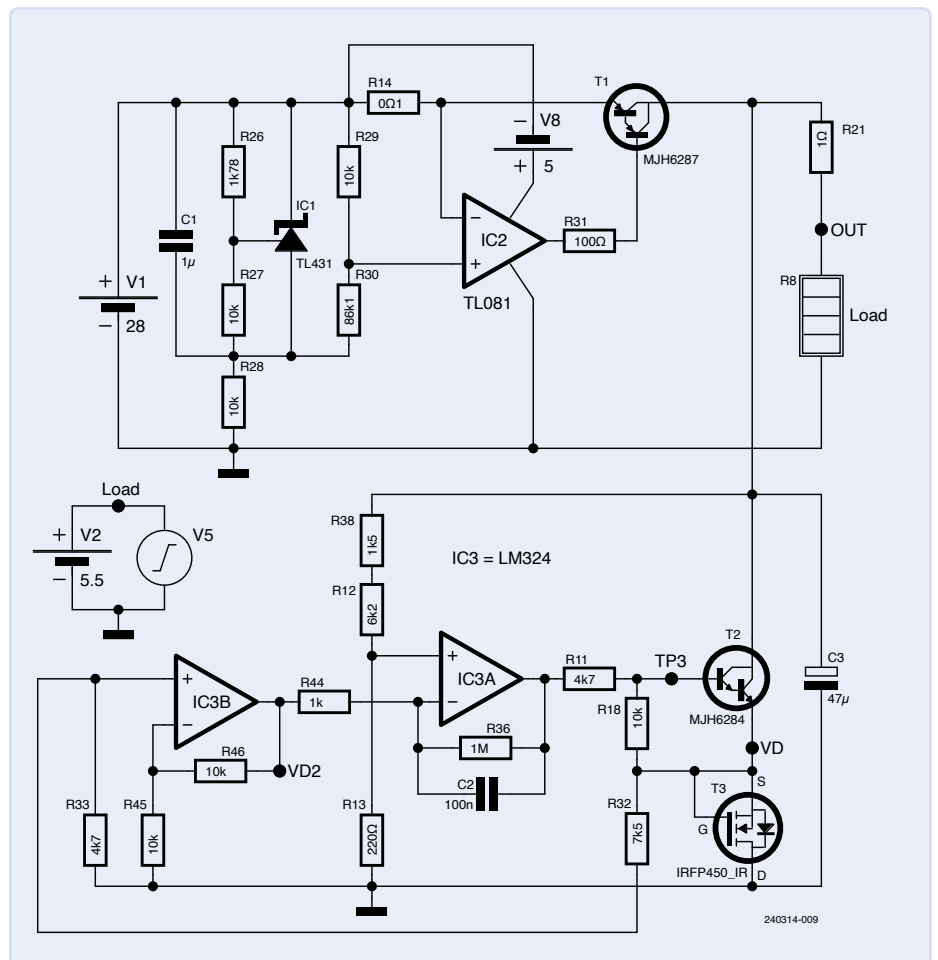


Figure 4: Simulation circuit.

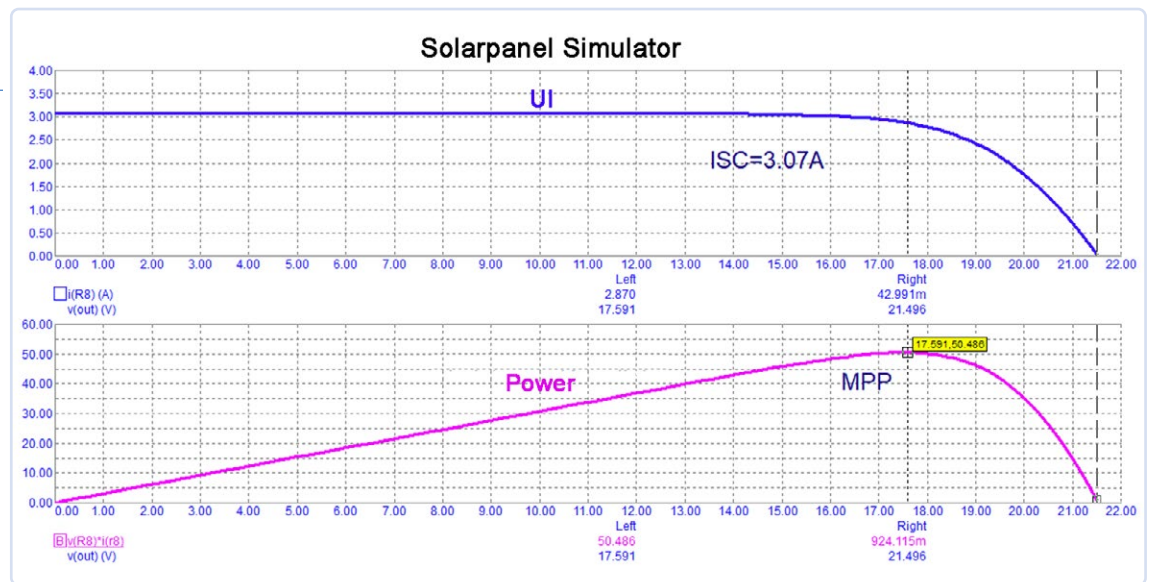


Figure 5: DC simulation at $T_{D1}(X29) = 25^{\circ}C$.

of T_3 of $25^{\circ}C$, the correct values are obtained: $I_{SC} = 3.07 A$, $V_{OC} = 21.5 V$, $V_{MPP} = 17.6 V$, and $P_{MPP} = 50.5 W$. The resulting U/I characteristic curve in **Figure 5** looks plausible and corresponds to what one would expect from a real solar panel.

The dynamic behavior of an MPP tracker in response to a step change in load is also of interest. The question is how quickly and how well the new setpoint is reached. The control behavior of the simulator and the stability of the control system are also relevant.

In the transient simulation of **Figure 6**, the already mentioned load step from 6.0Ω to 6.5Ω and back to 6.0Ω at a frequency of $50 Hz$ and $I_{SC} = 3.07 A$ is shown in the immediate vicinity of the MPP. The voltage jumps from $17.398 V$ to $18.037 V$ and back to $17.398 V$ as desired. The power jumps from $50.447 W$ to $50.052 W$ and back to $50.447 W$.

The control response time was about $3 ms$; a slight overshoot is visible in the diagram.

The control behavior is therefore fast enough, because a real MPP tracker usually works with a change rate of 1 to 10 tests per second. From the two simulations it is clear that with the given circuit dimensioning, the characteristic curve of the $50 W$ solar panel can be simulated sufficiently accurately, both statically and dynamically. For many applications, this should be sufficient.

Initial Circuit

The I_{SC} current source in Figure 3 is realized in Figure 4 by the circuit around the op-amp IC2, the Darlington PNP transistor T1, the current-sensing resistor R14, and the adjustable reference voltage source around IC1, which works with the TL431 parallel regulator. In the final circuit, which will be presented later, R29 and R30 are replaced by a poten-

tiometer, which allows the short-circuit current I_{SC} to be adjusted continuously. The voltage source V8 supplies IC2 with a slightly higher operating voltage than the $28 V$ of the operating voltage V1, so that the op-amp always works reliably, even if the reference voltage becomes small, causing the voltage at the two inputs of the op-amp to approach $28 V$. In the final circuit, this auxiliary voltage is generated by a voltage multiplier. T1 must be a Darlington type, because the base current of a conventional power transistor would be too high for the op-amp and its supply, and the collector current would deviate too much from the emitter current, which would then result in deviations via R14 and inaccurate regulation by the op-amp.

The voltage multiplier of the reference diode path of Figure 3 is realized in Figure 4 by the circuit around the op-amp IC3A, the NPN-Darlington T2, R12 + R38, R13, R18, and

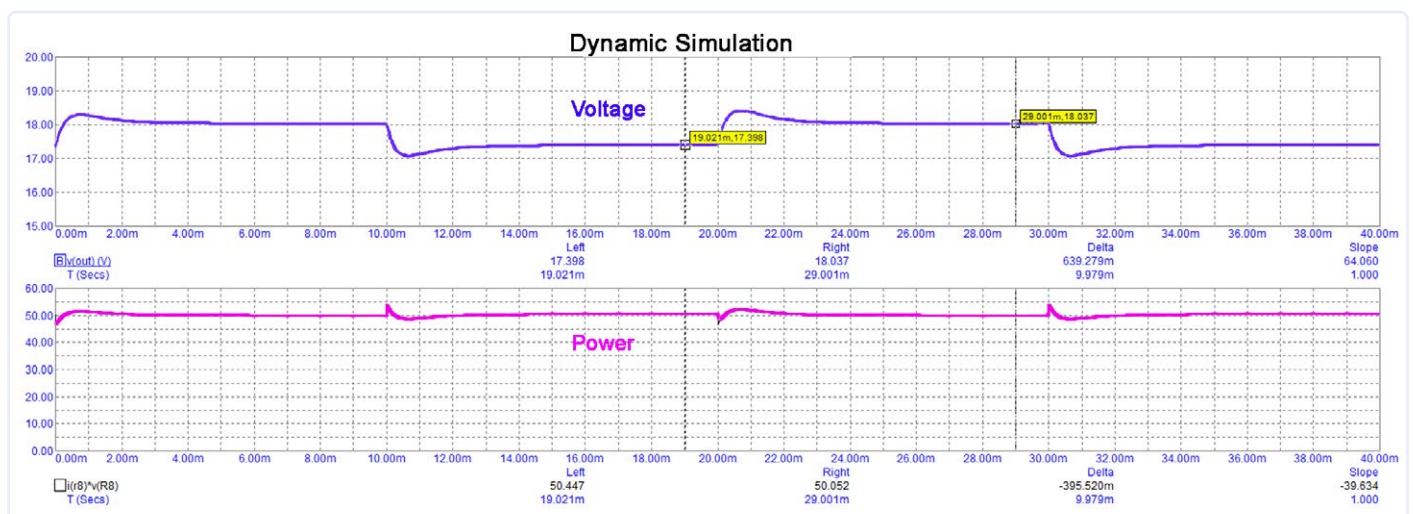


Figure 6: Dynamic simulation of a load step at $T_{D1}(X29) = 25^{\circ}C$.

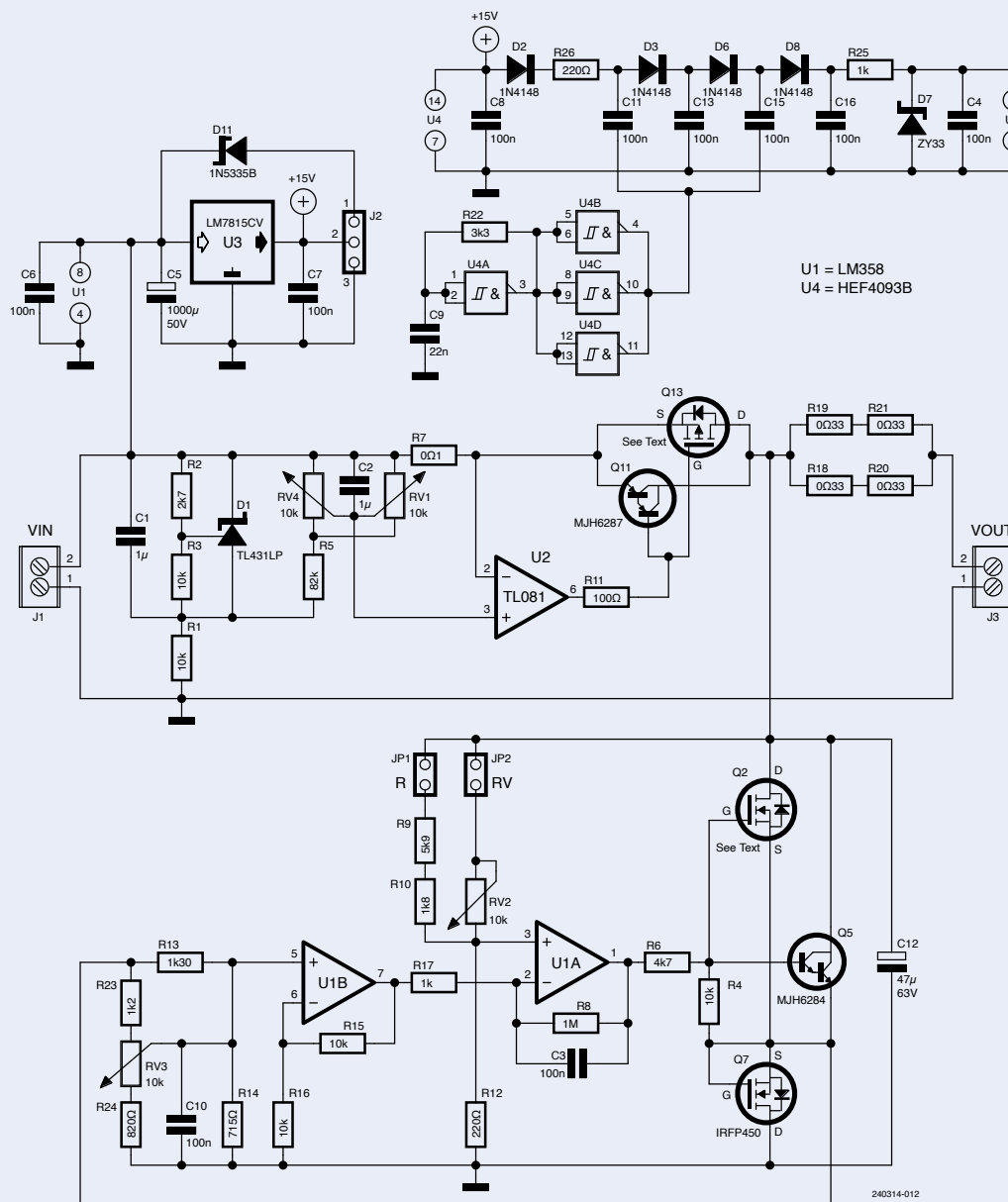


Figure 7: The final circuit of the solar panel simulator.

R11. The diode voltage V_D is tapped by the circuit around op-amp IC3B and made available as V_{D2} to the control circuit around IC3A. As already mentioned, the internal diode in T3 is the reference.

The multiplication is obtained from the ratio of $R_{12} + R_{38}$ to R_{13} and, with the given values, is exactly 35. This can also be made adjustable, either by making other resistors switchable or by adding a potentiometer.

Unfortunately, in contrast to the simulation, oscillations occurred in the real circuit. At certain operating points, the constant current source and the voltage multiplication work against each other, which led to oscillations in the 200 kHz range. The voltage amplification of IC3A is reduced by suitable dimensioning of R_{36} and R_{44} as well as C_2 . It is still large

enough for sufficient control accuracy. Oscillations and instabilities are also further eliminated by the electrolytic capacitor C_3 .

The adjustable temperature coefficient is realized with the circuit of IC3B. If the resistance ratio of R_{32} to R_{33} is made adjustable using a potentiometer, as in the final circuit, the voltage of the diode of T3 is changed (and then fed to the multiplier stage as V_{D2}). The complete circuit on the right around IC3A and IC3B acts as a kind of adjustable parallel regulator (parallel to the load R_{Load}).

Final Circuit

Compared to the initial circuit in Figure 4, the final circuit in **Figure 7** has not changed significantly. Essentially, the potentiometers have been added and the types of power semiconductors have changed. Since this

circuit was created with KiCad, the component designations have changed. As always, the KiCad files, including the PCB layout, are available for free from the Elektor website for this article [1]. The central components are, as before, the adjustable current source and the adjustable voltage multiplier.

Current Source

The reference voltage for the current source is realized by the circuit around the parallel regulator D1 and has a value of 3.17 V. A part of this voltage, adjustable via RV_1 or RV_4 , reaches the non-inverting input of U2. The nominal value of this voltage with respect to the inverting input is 0.34 V. Equilibrium is reached when the voltage drop across R_7 also amounts to 0.34 V, which it does at 3.4 A. If smaller voltages are set, the current is correspondingly lower. For lower power ratings, Q13



Component List

Resistors

Unless specified otherwise:

axial, metal film, 1%, ¼ W

R1...R4 = 10 k

R2 = 2k7

R5 = 82 k

R6 = 4k7

R7 = wirewound resistor, 0,1 Ω, 5 %, 3 W

R8 = 1 M

R9 = 5k9

R10 = 1k8

R11 = 100 Ω

R12 = 220 Ω

R17 = 1 k

R13 = 1k3

R14 = 715 Ω

R15, R16 = 10 k

R18...R21 = wirewound resistor, axial, 0.33 Ω, 5%, 3 W

R22 = 3k3

R23 = 1k2

R24 = 820 Ω

R25 = 1 k

R26 = 220 Ω

RV1...RV4 = potentiometer, 10 k, 20%, horizontal, linear

Capacitors

C1, C2 = 1 µF, 100 V, 10%, MKS2, pitch 5 mm

C3, C4, C6...C8, C10, C11, C13, C15, C16 = 100 nF, 63 V, 10%, MKS2, pitch 5 mm

C5 = 1.000 µF electrolytic, 50 V, low ESR, vertical

C9 = 22 nF, 250 V, 10 %, MKS2, pitch 5 mm

C12 = 47 µF electrolytic, 63 V, vertical

Semiconductors

D1 = TL431ACLP, TO92

D2, D3, D6, D8 = 1N4148, DO-35

D11 = Z-diode, 3.9 V / 5 W, DO201

Q2 = N-channel MOSFET as an alternative *

Q5 = MJH6284G, TO247 *

Q7 = IRFP450, TO247 *

Q11 = MJH6287G, TO247 *

Q13 = P-channel MOSFET as an alternative *

U1 = LM358, DIP8

U2 = TL081, DIP8

U3 = 7815, TO220

U4 = 4093, quad NAND Schmitt trigger

Miscellaneous

HS1 = heat sink LAM 4, shortened to 30 mm *

HS2 = heat sink LAM 4, shortened to 100 mm *

HS4 = heat sink for TO220, vertical, 18 K/W

J1, J3 = 2-pin screw terminal, pitch 2/10", angled *

J2 = 3-pin female header, pitch 1/10"

JP1, JP2 = 2-pin header, pitch RM 1/10", straight

Jumper bar, pitch 1/10", for JP1 or JP2

Circuit board 240314-01

* See text

in the smaller TO220 package can be used instead of Q11 in the TO218 package.

Only RV1 or RV4 is fitted, i.e., only one potentiometer either on the upper or lower edge of the board, as you wish. C2 blocks any interference and ensures stability.

Choosing a TL081 for U2 ensures high-impedance inputs and a low current requirement, so the supply from the voltage tripler around U4 is only slightly strained. U4A is connected as an oscillator and delivers a square wave in the two-digit kHz range. The parallel connection of the remaining three gates as a kind of output stage allows for a higher output current. The multiplier cascade itself is built with C11, C13, C15, C16, D2, D3, D6, D8, and the current limiter R26. R25 together with C4 is used for smoothing and D7 for voltage limiting. The tripler is supplied with 15 V by U3. J2 provides ground and the +15 V from U3. In addition, there is a 24 V supply for the heat sink fan, which is derived from the 28 V of VIN via D11.

Diode Voltage Multiplier

The basic principle of operation of the voltage multiplier has already been described. If JP1 (R) is in place, the circuit works with the multiplier determined by R9 + R10. If, on the other hand, JP2 (VR) is in place, the multiplication factor depends on RV2 and is thus continuously adjustable. The temperature coefficient is set using the RV3 potentiometer. A sensible adjustment range is determined by connecting R13 in parallel and R23 and R24 in series. At a temperature of 25°C, a center position of RV3 results in a voltage of 0.6 V at Q7 at the output of the op-amp U1B. If the setting range is not correct, R23 or R24 can be adjusted accordingly.

Power Resistors

When I first tried out this circuit, I had fitted the resistors R18...R21 directly on the circuit board to set an acceptable MPP voltage. At first, I used a P600G as the reference diode. The disadvantage of this choice was that this diode could not be cooled well enough, and so there was too great a thermal drift of the open-circuit voltage due to self-heating. So, I finally switched to the internal diode of the MOSFET IRFP450 (Q7) in the TO247 package and replaced the resistors R18...R21 with a wire bridge. This MOSFET has a slow internal

diode with a lower forward voltage. MOSFETs with fast diodes are not as suitable.

Settings

Short-Circuit Current I_{SC}

For this purpose, an operating voltage of 28 V with a load capacity of at least 3.5 A is applied to J1. Setting I_{SC} is relatively easy: Simply connect an ammeter in the 10 A range to the terminals of output J3. The measurement result corresponds to the short-circuit current that can be set with RV1 or RV4. I_{SC} of a real solar panel is slightly temperature dependent!

Open-Circuit Voltage V_{OC}

Here, too, the operating voltage of 28 V is first applied to the VIN input. A voltmeter in the 50-V range is now connected to the output — in the case of four-digit multimeters, this is usually the measuring range up to 199.9 V. Depending on the jumper fitted, there is a fixed V_{OC} (JP1) or it can be adjusted with RV2 (JP2).

For the correct setting, RV3 is first set to the center position. The fixed multiplication factor is calculated as $(R9 + R10)/R12$. With the given values, this results in a value of 35. Since the voltage from U1B is added to this, an output voltage of 36×0.6 V at J3 results at 0.6 V set at RV3 at pin 7 of U1B, which corresponds to V_{OC} .

Temperature Coefficient TC

Again, the operating voltage of 28 V is applied to the input. The temperature dependency of the open-circuit voltage V_{OC} is set to the desired value using RV3.

Alternative MOSFETs

Instead of the Darlingtons, the use of suitable MOSFETs offers an improvement in thermal behavior. The thermal resistance $R_{th(jc)}$ of some MOSFETs is only half as high as that of the specified Darlingtons. For Q13 instead of Q11, for example, the types IXTH80N075L2 or IXTH64N10L2 (preferably in a TO247 package) can be considered. For Q2 instead of Q5, the types IXTH26P20P (TO247) or IXTQ26P20P (TO-3P) would be suitable, for example. In these types, the silicon is thermally better coupled to the housing and thus ultimately also better coupled to the heat sink. By the way, the alternatives Q2 and Q13 are therefore drawn in the circuit diagram,

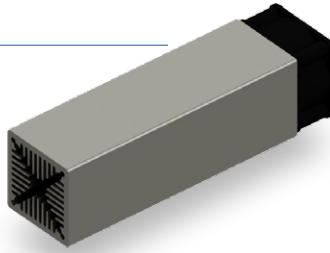


Figure 8: LAM 4 150 24 heat sink from Fischer Elektronik (Source [2]).

since their pads (due to a different pin assignment) are additionally present on the board.

With MOSFETs, the problem of derating power dissipation and the 2nd breakdown does not arise. Furthermore, the transconductance of MOSFETs is significantly lower than that of bipolar junction transistors, so oscillations do not occur as easily and it may even be possible to do without C12. This would need to be tested in practice.

Mechanical

Connectors

There are WAGO terminals on the board. When connecting and disconnecting, the forces that occur can damage the conductor tracks under certain circumstances. To avoid this, the terminals are glued to the board material so that the forces are absorbed by the material itself.

Heat Sink

A special aluminum heat sink from Fischer [2] is used to dissipate the heat. It consists of a square tube with an edge length of 4 cm and internal fins, as well as a fan with a thermal resistance of just over 0.6 K/W (see Figure 8). Two heat sinks with a length of 30 mm and 100 mm are used. The 150-mm-long original heat sink is sawn into two parts, 30 mm and 100 mm. The fan is placed between the two parts so that the intake side is on the left side of the 30 mm part. Q7 is mounted on this cold side. Q5/Q11 or alternatively Q2/Q13 are attached to the longer 100 mm tube, because a lot of waste heat has to be dissipated here. At a supply voltage of 28 V and a short-circuit current of 3.07 A, 86 W would have to be dissipated in the worst case. Fortunately, however, this rarely occurs and when it does, it is only for a short time. An MPPT charge controller connected to the simulator will only cause a fraction of this maximum power when functioning properly.

It is better to remove the fan before sawing. After sawing and tapping, any burrs must be removed with a flat key file. The heat sink then

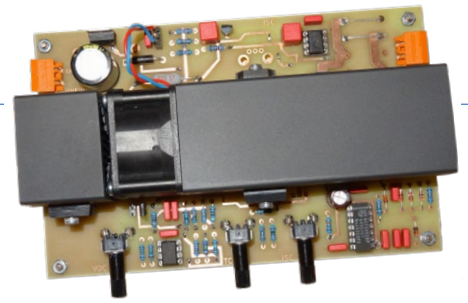


Figure 9: The fully assembled circuit board including the heat sink of the prototype.

goes, together with the fan as a package via an electrically insulating, but heat-conducting film (100 × 40 mm), on the right, warm side directly on the board. This dissipates some additional heat through the board.

The fan itself is supplied with the correct 24 V from the 28 V via the voltage reduction by D11. Due to the diameter and the relatively high speed associated with it, it is quite audible.

Assembly

The structure, including the assembled circuit board seen in Figure 9, shows what is meant. For my prototype, I blackened the aluminum heat sink so that a little more heat can be dissipated by infrared radiation. This is not really necessary for the Q7 heat sink, but since I was already at it ...

The transistors should first be mounted (isolated) on the heat sink and then soldered onto the circuit board. Small tolerances are compensated by slotted holes in the circuit board. When mounting, avoid air between the transistor housing and the heat sink. The use of commercially available thermal paste is not a bad idea.

The entire electronics, including the heat sink, fits on a two-sided Eurocard measuring 160 × 100 mm and, due to the screw connection with the heat sink, results in a fairly compact module.

Measurements

In order to assess how close the solar panel simulator comes to a real panel, I measured typical values and characteristics of the Sun Plus 50 S solar panel from Phaeson and my simulator circuitry. Due to the lack of adjustable and very expensive laboratory lighting, I took the measurements on the real solar panel outdoors. The panel was facing south, there was no wind and the sky was clear. At 1:15 p.m. — shortly after the real middle of the day during daylight saving time — the panel was aligned so that the sun's rays fell vertically on the panel.

Figure 10:
U/I characteristics of
the real solar panel (left)
and the simulator (right).
Current [A] against
Voltage [V].

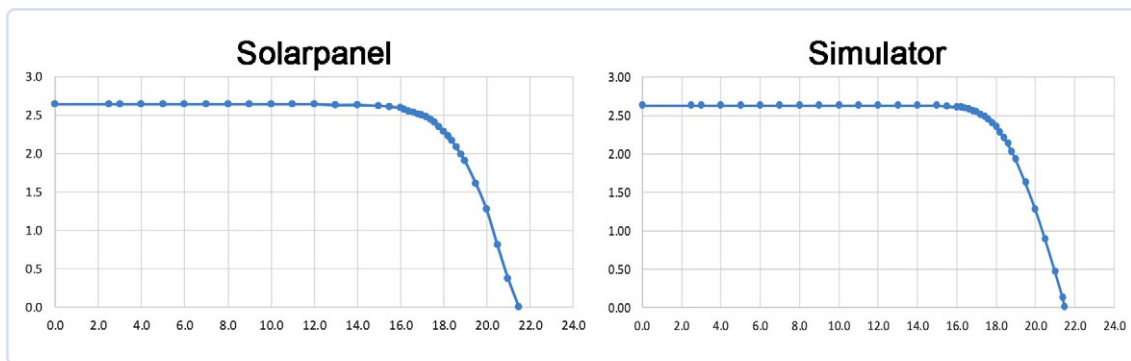


Figure 11: Power as a
function of the voltage of
the real solar panel (left)
and the simulator (right).
Power [W] against
Voltage [V].

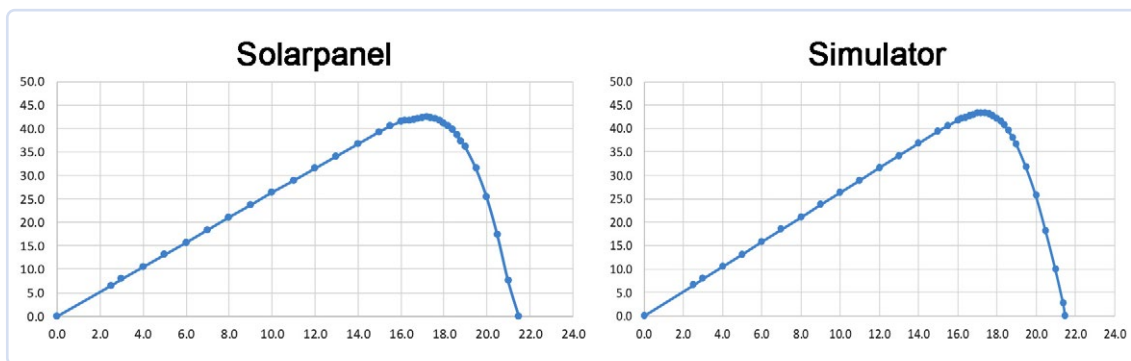


Figure 10 shows the U/I characteristics. The simulator was set to $V_{OC} = 21.5$ V and $I_{SC} = 2.64$ A. As you can see, the characteristics are almost identical. There is also virtually no difference in the power characteristics in **Figure 11**. As far as the static values are concerned, it can therefore be safely assumed that the simulator comes very close to the real panel.

To get an impression of the control behavior


of the solar panel simulator, I connected it to a programmable electronic load. In principle, this is a power Z-diode with adjustable Z voltage. Periodic jumps from 17 to 16.5 V and back with a duration of 13 ms each were set with this load. The oscillograms in **Figure 12** show the step response at the output of the simulator. On the left, the vertical resolution is 5 V/div, while on the right, a higher resolution of 200 mV/div has been set. The horizontal resolution is 5 ms/div for both oscillograms.

The step responses are certainly not ideal, but perfectly adequate for our purposes.

Power Range Up to 50 W

The solar panel simulator presented here is suitable for simulating most panels in the power range up to 50 W at a "system voltage" of 12 V, which is suitable for charging 12-V batteries, for example. The almost identical characteristics of the solar panel and the simulator indicate a good simulation result. With the help of this simulator, it is possible to check the behavior of connected charge controllers or inverters with MPP trackers in a reproducible manner, regardless of the weather.

It is not advisable to test inverters that are connected to the grid, as it is not certain that these inverters are sufficiently electrically isolated. However, even in balcony power plants, small panels with 36 cells are not used, so you are unlikely to encounter this problem.

Significantly higher MPP outputs at higher system voltages than are common in the range of ≤ 50 W should rather be realized with a different circuit technology. 

Translated by Jörg Starkmuth — 240314-01

Questions or Comments?

Do you have questions or comments about this article? Contact Elektor at editor@elektor.com.

50-W Panel from Phaesun

Typical values at a cell temperature T_j of 25°C and an irradiance of 1000 W/m².

| Manufacturer | Phaesun |
|--------------------------|--------------------------------|
| Type | Sun Plus 50 S |
| Temperature range | -40 to 85°C |
| System voltage | 12 V |
| P_{MPP} | 50 W (max. via MPPT) |
| V_{MPP} | 17.6 V (optimal MPPT voltage) |
| I_{MPP} | 2.84 A (optimal MPPT current) |
| I_{SC} | 3.07 A (short-circuit current) |
| V_{OC} | 21.6 V (open-circuit voltage) |
| Number of cells | 36 |
| Module efficiency | 15.2% |
| Temperature coefficients | |
| TC_{Power} | -0.45%/K |
| TC_{VOC} | -0.37%/K |
| TC_{ISC} | -0.081%/K |

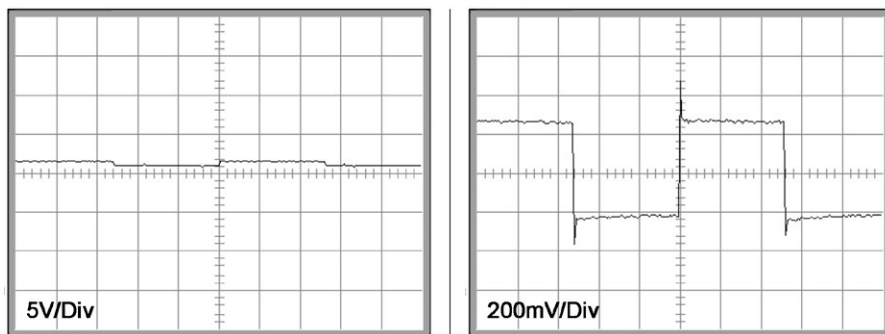


Figure 12: The step response of the simulator is not ideal, but it is sufficiently good.

About the Author

Peter Kroll has worked as a development engineer in the fields of power supplies for telecommunications applications, automation technology, medical technology, and photovoltaics. Here he has specialized in inverters for solar systems up to 15 kW, gate drivers for IGBT/ SiC- modules for railways, and energy facilities for high-power applications.



FEATURED TOPIC

Visit our **Power Electronics & Energy** page for articles, projects, news, and videos.

www.elektormagazine.com/power-energy



Related Products

- **OWON SPE6103 DC Power Supply (300 W)**
www.elektor.com/20502
- **Siglent SDL1020X-E Programmable DC Electronic Load (200 W)**
www.elektor.com/19254

WEB LINKS

- [1] Elektor web page for this article: <https://www.elektormagazine.com/240314-01>
- [2] Heat sink Fischer LAM 4 150 24: <https://tinyurl.com/Fischer-LAM>

They trust us, do you?

elektor.com

★★★★★
Great service.
Nice store, fast shipping, good packing and documentation.
Jun 27, 2024

★★★★★
Excellent product at a good price
Excellent product at a good price with fast trouble free delivery.
Date of experience: November 25, 2023

★★★★★
Easy ordering process(online)
Easy ordering process(online), good communication of delivery steps.
Overall smooth process
Date of experience: June 01, 2024

★★★★★
Great service
Great service!
Easy to purchase and delivered just in time as promised.
Date of experience: February 12, 2024



We love electronics and projects, and we do our utmost to fulfill the needs of our customers.
The Elektor Store: **'Never Expensive, Always Surprising!'**

Elektor Store

Reviews 365 • Excellent

★★★★★ 4.3

✓ VERIFIED COMPANY

Check out more reviews on our Trustpilot page: www.elektor.com/TP/en

Or make up your own mind by visiting our Elektor Store, www.elektor.com





STM32 Edge AI Contest

Explore the new STM32N6 and Compete for a Share of **€5,000** in Prizes!

By the Elektor Content Team

AI on the edge is significant for applications requiring low latency, real-time decision making, enhanced privacy, and reduced data transmission cost. With its AI accelerator and rich set of peripherals, the new STM32N657 microcontroller by STMicroelectronics is tailored for edge AI applications such as image recognition and speech processing. The STM32N6570-DK AI Development Kit, equipped with a 5" capacitive multi-touch display, microSD card slot and many other features, facilitates the development of prototypes. Creative developers have the chance to get one of these boards for free. Apply to participate in the STM32 Edge AI Contest. A share of €5,000 in prizes is up for grabs!

Artificial Intelligence (AI) is transforming our daily lives as well as industrial production, traffic, and logistics. In healthcare, AI powers wearable devices and diagnostic tools, while in industrial automation, it drives robotics and predictive maintenance, improving efficiency and reducing downtime. Smart homes benefit from AI through voice-controlled assistants and enhanced security, while autonomous robotic systems leverage AI for navigation, object manipulation, and precision tasks. Consumer electronics, such as gaming devices and cameras, use AI to deliver immersive and user-friendly experiences, making AI a cornerstone of modern innovation.

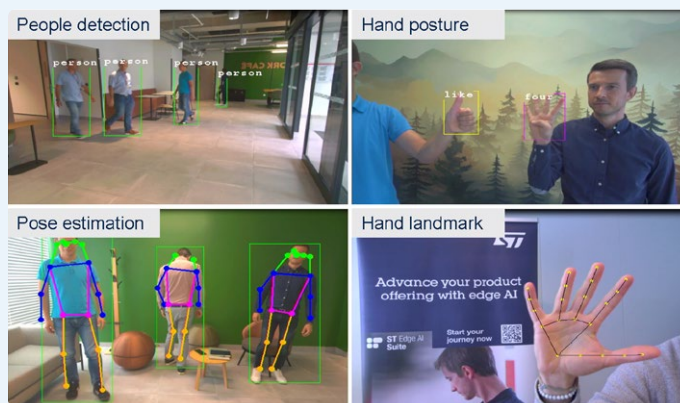


Figure 1: The Neural-ART Accelerator in action, demonstrating high-performance AI inference capabilities for edge applications.

Understanding AI on the Edge

AI on the edge involves processing data locally on embedded devices, offering low latency, enhanced privacy, and reduced reliance on cloud systems. This is particularly crucial for real-time applications such as mobile robotics or remote monitoring, where connectivity may be limited. By eliminating the need to send data to the cloud, edge AI improves response times, secures sensitive information, and lowers operational expenses. However, it requires both software and hardware optimization in order to handle computationally intensive tasks within power and resource constraints.

Enabling AI on the Edge with the STM32N657

The new STM32N6 microcontroller from STMicroelectronics is the most powerful STM32 ever, and the first one with an integrated Neural Processing Unit (NPU) — tailored to address the challenges of edge AI through efficient, real-time processing of data. The STM32N657 is one of several STM32N6 variants. Its Neural-ART Accelerator delivers 600 GOPS of AI inference ability, enabling tasks such as object- and gesture-recognition in video frames (**Figure 1**), speech processing, and anomaly detection. Powered by an Arm Cortex-M55 core operating at up to 800 MHz, the STM32N657 achieves high performance at 1,280 DMIPS and 3,360 CoreMark, making it suitable for demanding AI workloads.

From DMIPS to TOPS, the paradigm shift Opening a new range of embedded AI applications

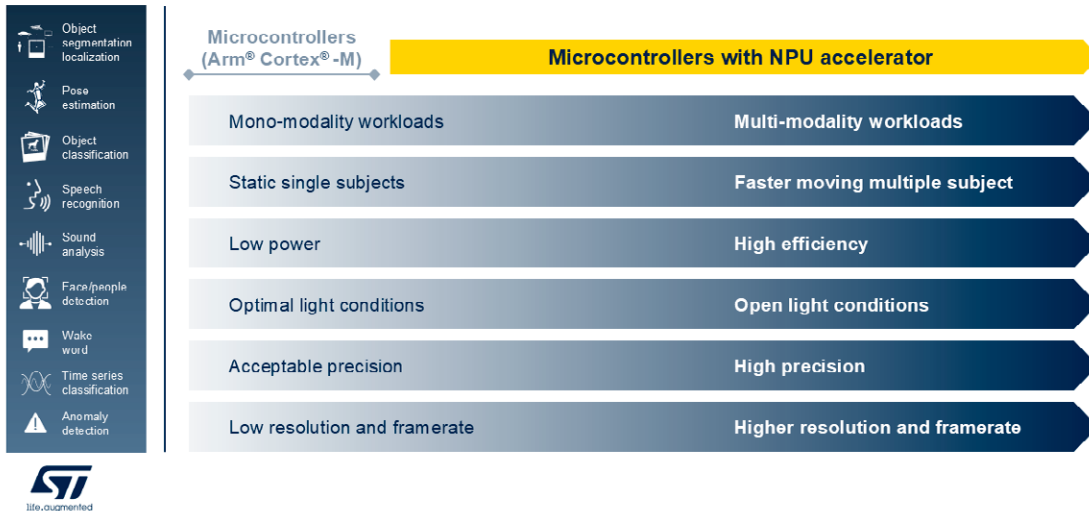


Figure 2: The Neural Processing Unit (NPU) is opening up new fields of applications.

To support the diverse needs of edge applications, the STM32N657 is equipped with a comprehensive peripheral set (**Figure 2**). Its dual-lane CSI-2 camera interfaces and integrated H.264 encoder facilitate high-resolution video input and compression, which is ideal for computer vision tasks. The device includes 4.2 MB of contiguous SRAM, enabling the execution of complex models without the need for external memory, reducing latency and energy consumption. Low-power modes, such as Sleep, Stop, and Standby, make the microcontroller well-suited for battery-operated or energy-sensitive applications.

The STM32N657 also integrates a wide range of analog and digital peripherals, including as two 12-bit ADCs with sampling rates of up to 5 MSamples/s, a temperature sensor, and extensive GPIO support for interfacing with external devices. Connectivity options include dual-USB, 1-Gbit Ethernet with TSN, I3C, and multiple UART, SPI, and I2C channels, ensuring seamless communication in embedded systems.

More on the new STM32N6 controller family and the software ecosystem behind it can be found in our AI Bonus Edition 2024, which you may download for free at [1].

The STM32N6570-DK Development Kit

To facilitate evaluation, software development and prototyping, STMicroelectronics offers a well-equipped development kit. The STM32N6570-DK is a feature-rich platform, enabling developers to build and test applications ranging from AI inference and multimedia to industrial and IoT solutions.

At the forefront, the board features a 5" capacitive multi-touch display that supports up to five touch points, providing an intuitive interface for interactive graphical applications (**Figure 3**). The display's responsiveness makes it ideal for creating user-friendly GUIs and monitoring systems. Connectivity options on the board include an RJ45 Ethernet port, supported by a Realtek controller, ensuring robust and high-speed network communication. Two USB ports — a Type-A port for external peripherals and a Type-C port for data transfer — enhance its flexibility (**Figure 4**). Additionally, programming and debugging are streamlined through a dedicated USB Type-C port equipped with ST-LINK V3, allowing efficient development workflows (**Figure 5**).

The board's expandability is one of its standout features. It adopts the Arduino UNO R3 layout, providing compatibility with a wide range of Arduino shields. For additional peripherals, it includes connectors for STMOD+, MIPI 2.0, and a ribbon cable interface for camera modules.

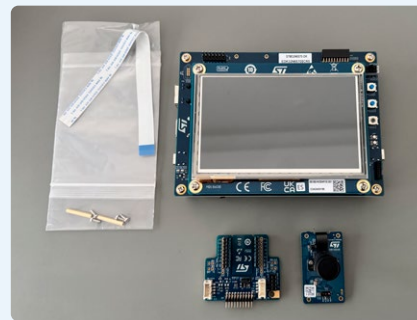


Figure 3: The STM32N6570-DK Development Kit.

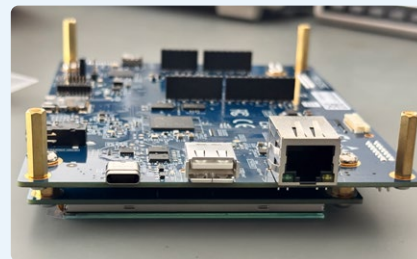


Figure 4: On-board connectivity options.

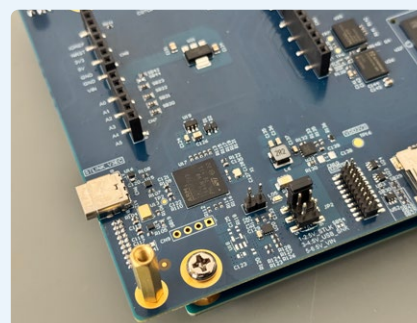


Figure 5: Dedicated USB Type-C port for programming and debugging.

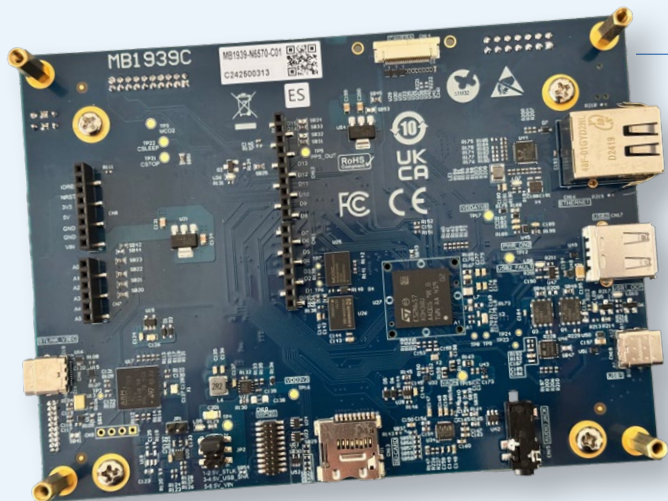


Figure 6: Rear view of the STM32N6570-DK Development Board.

These interfaces, combined with a microSD card slot and a 3.5-mm headphone jack, offer developers numerous possibilities for multimedia and storage-based projects (**Figure 6**).

User interaction and feedback are addressed with four status LEDs, including two RGB LEDs, and three buttons, one of which functions as a reset button (**Figure 7**). These features are invaluable for debugging, real-time monitoring, and custom input handling. For video and imaging projects, the ribbon cable connector supports high-resolution camera modules, leveraging the STM32N6570's built-in video processing capabilities.

Central to the board is the STM32N6570 microcontroller, designed for high-performance edge AI and multimedia applications. To ensure reliable operation even under intensive workloads, the board includes mounting points around the microcontroller, which appear to allow the attachment of a cooling solution. This thoughtful addition provides flexibility for thermal management in demanding use cases (**Figure 8**).

In addition to the main board, the kit includes the ST AI Camera Module (**Figure 9**), which enables developers to dive straight into AI-powered imaging applications such as object detection, facial recognition,

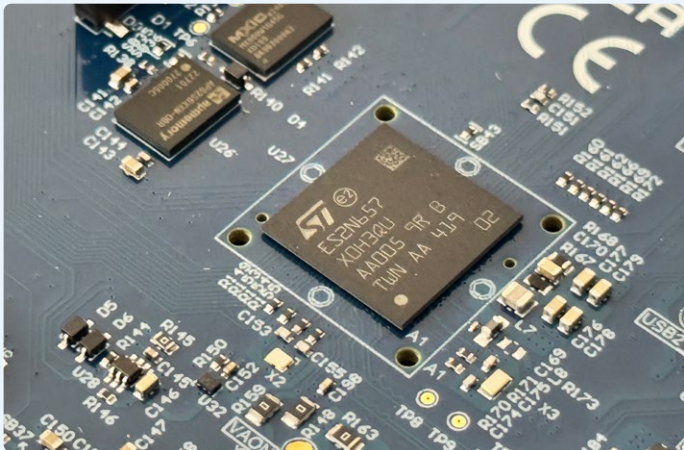


Figure 8: STM32N6570 microcontroller with cooling solution mounting points.



Figure 7: User interaction features on the STM32N6570-DK.

and more. The camera module leverages the STM32N6570's built-in video processing capabilities, making it an excellent tool for exploring computer vision at the edge.

One of the most thoughtful inclusions in the kit is the Fan-Out Board (**Figure 10**). This expansion board connects via the STMOD+ interface and provides support for the mikroBUS socket standard, a widely adopted add-on board interface designed for maximum expandability with minimal pin usage. By integrating mikroBUS, the fan-out board opens the door to thousands of Click boards from MIKROE, which offer plug-and-play solutions for sensors, actuators, displays, and communication modules. Additionally, the fan-out board includes two Grove connectors, one configured for UART and the other for I²C, enabling rapid prototyping with the vast Grove module ecosystem.

Since the STM32N6570 does not have built-in wireless capabilities, the fan-out board addresses this by providing a dedicated interface for Espressif ESP-01 Wi-Fi modules, ensuring seamless integration of wireless communication features.

As an embedded systems engineer, this fan-out board inclusion feels like a game changer. It eliminates the need for custom-designed adapter

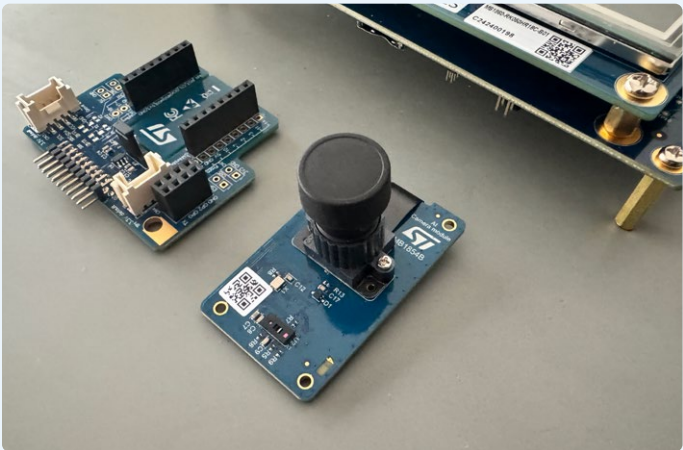


Figure 9: ST AI Camera Module.

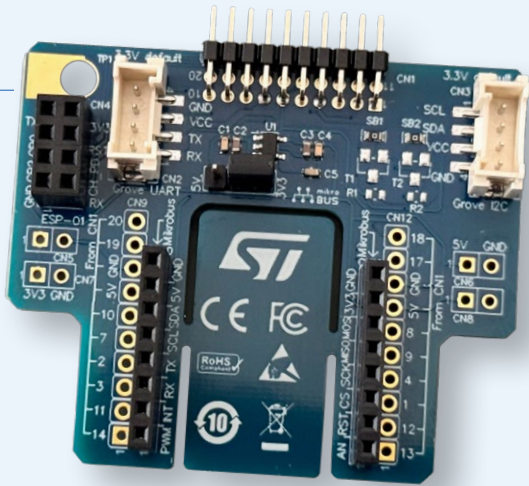


Figure 10: The Fan-Out Board and Grove connectors in the STM32N6570-DK, simplifying rapid prototyping and sensor integration.

boards — a common step many developers take when trying to interface sensors or modules with a development board. By adding this, STMicroelectronics has saved countless hours of setup time, allowing developers to focus on their actual projects instead of solving connectivity challenges.


Together, the main development board, the AI Camera Module, and the Fan-Out Board make the STM32N6570-DK an all-encompassing toolkit. With these tools at hand, developers can quickly prototype and test a wide range of applications, from AI-driven edge systems to IoT devices, multimedia interfaces, and beyond. This development kit not only offers powerful features but also emphasizes user convenience, ensuring that engineers can spend more time innovating and less time solving hardware challenges.

More on this well-equipped kit can be found at an STMicroelectronics web page [2].

The STM32 Edge AI Contest

An exciting opportunity for developers and engineers to showcase their skills: STMicroelectronics and Elektor have teamed up for the **STM32 Edge AI Contest**. Whether you're passionate about IoT, robotics, home automation, security, or anomaly detection, the possibilities are endless. The STM32N6570-DK provides all the tools you need to create cutting-edge applications, from its Neural-ART Accelerator and advanced graphics capabilities to its versatile connectivity options. The contest encourages participants to think outside the box, use the development kit creatively, and demonstrate its capabilities in real-world scenarios.

Not only is this contest a platform to innovate, but it also offers you a chance to win a share of €5,000 in prizes. It's the perfect opportunity to test your ideas, refine your development skills, and gain recognition in the embedded systems community.

Release your creativity, have fun, and bring your ideas to life with the STM32-N6 development kit. Whether it's a groundbreaking AI-powered robotics system, a smart home solution, or a novel IoT application, the contest is your stage to make a mark in the world of edge AI! 

240708-01



How to Participate in the STM32 Edge AI Contest

For developers (professionals, makers and students are welcome alike) who want to participate in this contest, STMicroelectronics is offering 100 free STM32N6570-DK development kits. To apply for a board, submit your project idea on the Elektor website:

www.elektormagazine.com/stm32ai



This phase of the contest ends 28 February 2025!

To take part in the contest and get the chance to win a prize, you have to submit documentation for your project by 30 April 2025. More details can also be found at the link above.

Prizes:

1st Prize: €2,500

2nd Prize: €1,500

3rd Prize: €1,000

Get started now and turn your innovative ideas into reality with the STM32N6!

WEB LINKS

[1] "High-Performance Edge AI: The New STM32N6," Elektor AI Digital Bonus Edition 2024: <https://elektormagazine.com/embedded-ai>

[2] Discovery kit with STM32N6570X0 MCU, STMicroelectronics: <https://st.com/en/evaluation-tools/stm32n6570-dk.html>

Widening the Bandgap

Why There Is So Much Interest in SiC and GaN

By Stuart Cording (Germany)

Silicon devices such as MOSFETs and IGBTs have been mainstays of the electronics industry since their commercialization. However, over the past decade, wide bandgap devices such as SiC and GaN have entered the scene. What are these devices, and why is the industry so excited about them?

Everyone knows the impact silicon MOSFETs have had on the electronics industry. But unless you have an avid interest in power converters, you may not be aware of the application-specific changes the semiconductor industry has made to improve them and why. Switched-mode power supplies (SMPS) have been around since the 1960s, when they were used in space applications such as the Apollo Guidance Computer [1] and early satellites. They were developed out of a need to convert between voltages more efficiently than linear regulators. Even the early BBC Micro from the 1980s quickly swapped out its linear power supply for an SMPS after its launch.

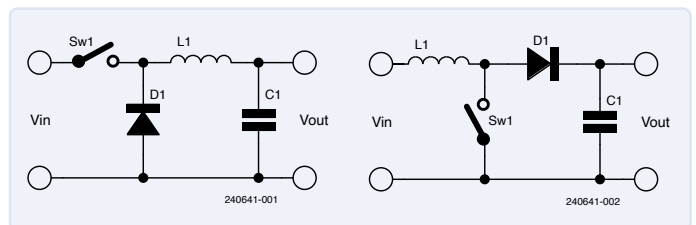


Figure 1: Circuit for a buck (left) and boost (right) converter, two of the basic switching converter architectures.

Switching converters rapidly turn their power switches on and off to convert the input voltage to the desired output voltage. Coupled with a capacitor and inductor, this chopped input is filtered to stabilize the voltage. Depending on the design, the output can be lower (buck) or higher (boost) than the input (Figure 1). A feedback loop controls the mark-space ratio, allowing the converter to respond to changes in load while minimizing variation in the desired output voltage.

Superjunction MOSFETs and IGBTs

As the rated voltage of planar MOSFETs increases, the on-resistance increases, resulting in more energy being turned into heat in the transistor. Superjunction MOSFETs were developed to overcome this limitation when used in switching converters (Figure 2).

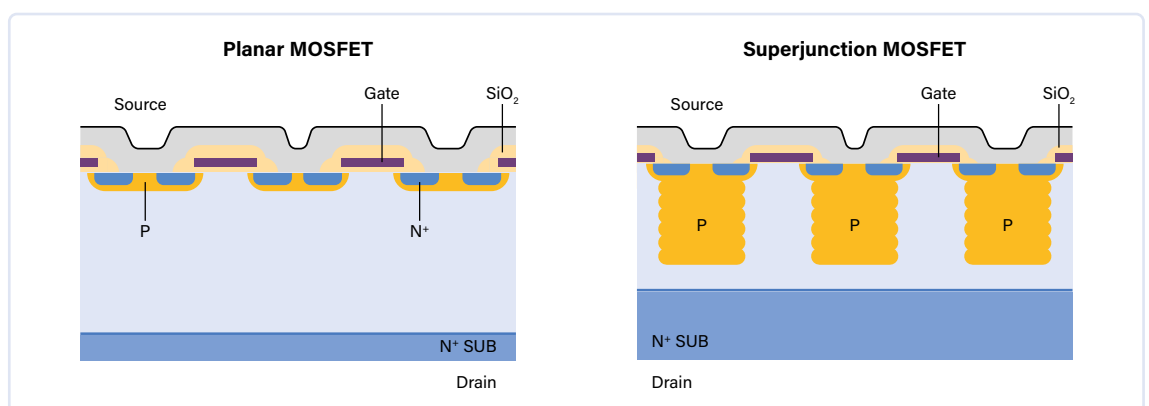


Figure 1: Circuit for a buck (left) and boost (right) converter, two of the basic switching converter architectures.

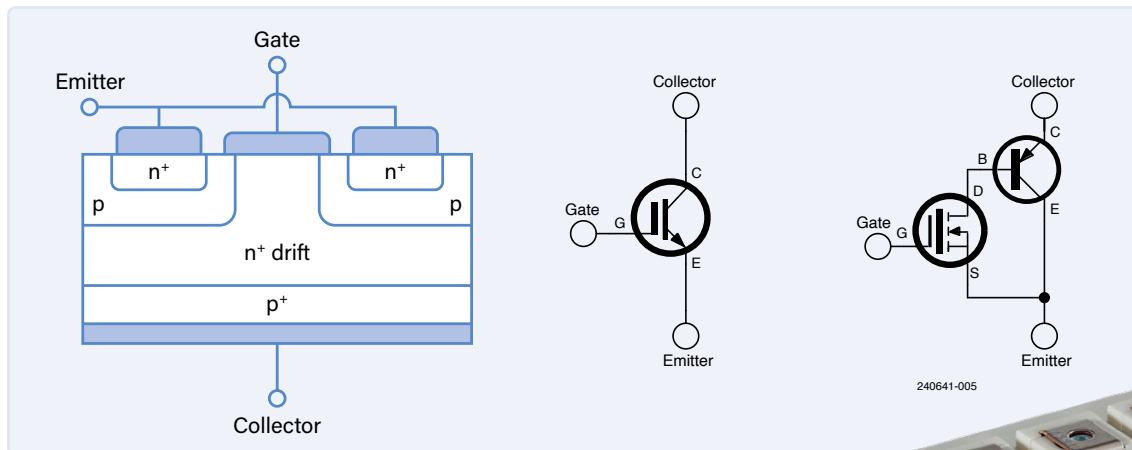


Figure 3: Cross section of an IGBT with symbol and equivalent circuit.

Superjunction devices also provide a shorter reverse recovery time [2] and lower gate and output charge. These improvements deliver further reductions in losses and contribute to reducing electromagnetic interference (EMI) challenges, which is especially important as switching frequencies increase.

MOSFETs are still limited in the upper voltage and power they can support. But massive industrial motors and wind turbines are also applications that can benefit from switched converter designs. To cover these applications, insulated gate bipolar transistors (IGBTs) were developed. With an NPNP design, they look similar to a thyristor with a metal-oxide gate (**Figure 3**).

This design allows them to have a withstand voltage rating of more than 6 kV and support switching frequencies between 2 kHz and 50 kHz. While the switching frequency range is lower than that of a MOSFET (typically up to 1 MHz), their robustness, power handling, and voltage range more than compensate. Thanks to this, they are deployed in variable frequency drives (VFDs), electric vehicle (EV) chargers, induction heating systems such as cooker hobs, and welding equipment. To get an idea of the sort of applications these devices are used in, you only need to take a look at their massive ceramic packages, complete with threaded bolt holes for the electrical connections (**Figure 4**) — a far cry from your typical TO-220 device!

Challenges in Switching Converters

Design engineers are trying to achieve an array of goals with their next switching converter design. One of these is power supply density, typically given in kW/l. Indirectly, this also indicates a lower weight since the components used are still made of the same materials. Switching frequency is a significant contributor to this figure of merit (FoM) since, as frequency increases, the size of the passives needed (capacitors and inductors) drops.

For example, in a power factor correction (PFC) stage, the DC link capacitor can consume between 20% and 50% of the available volume. Increased switching frequency can be hugely beneficial here.

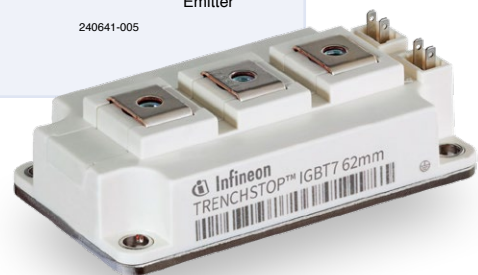


Figure 4: A 1,200 V, maximum 800 A TRENCHSTOP IGBT module from Infineon measuring 62×107×31 mm and featuring M5/M6 threaded mounts. (Source: Infineon Technologies AG)

Attempts to increase density are challenged by the risk of overheating if everything is packed closer together. This is an issue for IGBTs and MOSFETs, both of which are susceptible to thermal runaway. If the design hits a thermal boundary, forced cooling can be considered. However, this increases the cost and volume and may cause application-level issues.

Industrial applications, where many switched converters and motor inverters are used, are looking for smaller, lighter systems that can be deployed in harsh environments. Often, this implies a hermetically sealed solution, meaning forced cooling is not an option. Even wind turbine operators are keen to replace older equipment with something smaller and lighter, as this is easier to install and may generate less heat, despite plenty of space being available once the old equipment has been removed (**Figure 5**).



Figure 5: Wind turbines (left) and variable speed drives (right) are looking to benefit from innovations in power converters. (Source: Adobe Stock)

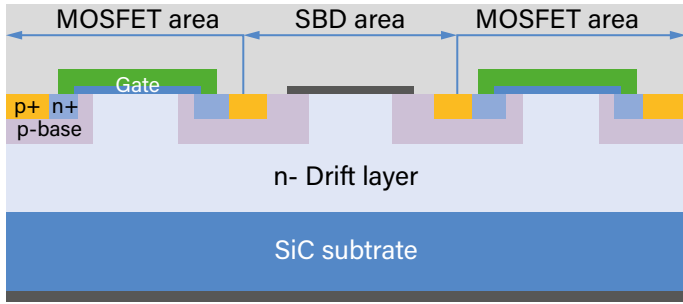


Figure 6: Cross section of a SiC MOSFET (Source: Toshiba Electronics Europe GmbH)

Silicon Carbide MOSFETs

Two key wide bandgap (WBG) semiconductor technologies are now available. The first is silicon carbide, referred to as SiC (**Figure 6**). The “wide” in WBG refers to the fact that the bandgap for these devices is wider than that for silicon. The bandgap for silicon is 1.12 eV, whereas the bandgap for SiC is around 3.26 eV, depending on the crystal lattice used [3]. This gives SiC a higher electrical breakdown field of 2.8×10^6 V/cm compared to 3.0×10^5 V/cm for silicon. SiC also offers a significantly higher thermal conductivity of 4.9 W/cmK than silicon with 1.5 W/cmK.

SiC devices are available from suppliers already known for IGBTs, like Toshiba, Infineon, STMicroelectronics, Rohm, and lesser-known players such as Wolfspeed. They typically come in voltage classes of 650 V, 1,200 V, and sometimes 1,700 V. This makes them a suitable alternative for IGBTs in this voltage range, with manufacturers promoting them for photovoltaic (PV) inverters, energy storage systems, EV charging, power supplies, and motor drives. They are also starting to be offered in lower voltage classes (400 V), making them increasingly an alternative to superjunction MOSFETs.

Because of their thermal characteristics, they are well-suited to denser designs. The on-resistance, $R_{DS(ON)}$, of silicon MOSFETs can increase by more than 1.5 times when they reach operating temperature. This results in more losses and waste heat generation. By comparison, the $R_{DS(ON)}$ of a comparable SiC MOSFET will increase by only 1.13 times. Since $R_{DS(ON)}$ is specified at 25°C, but the application will be operated at a higher temperature, a SiC MOSFET with a higher $R_{DS(ON)}$ can replace a silicon MOSFET with a lower $R_{DS(ON)}$. The thermal characteristics of SiC MOSFETs

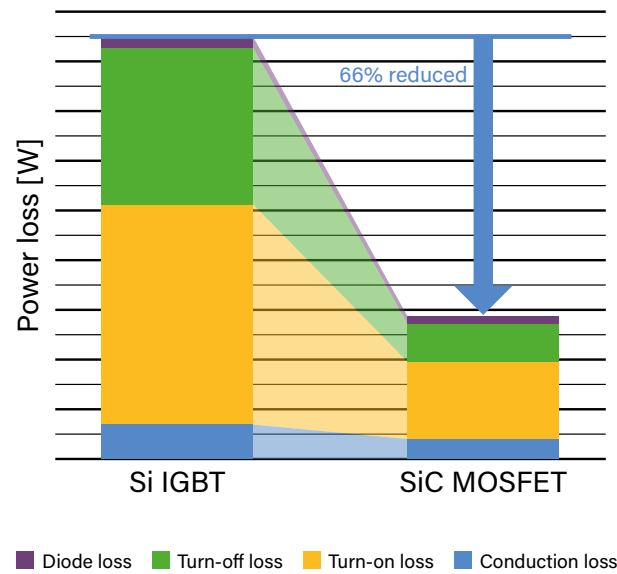


Figure 8: Using the latest generation of SiC MOSFETs can reduce power losses by 66% compared to an IGBT-based design (Source: Toshiba Electronics Europe GmbH)

also mean that they can run hotter in the application than alternative devices (junction temperatures of up to 175°C).

Losses are attributed to the device’s turn-on, turn-off, diode, and conduction characteristics. Compared to IGBTs, SiC MOSFETs exhibit significant improvements in the switching losses. For example, as an IGBT is turned on, the current rapidly flows through the device, but it takes a while (several hundred nanoseconds) for the voltage across the device to drop. During turn-off, a similar, opposite effect is seen (**Figure 7**). These “tail currents” cause power losses that reduce the power converter’s efficiency. While SiC MOSFETs don’t entirely remove the issue of tail currents, their use has been shown to reduce switching losses by more than 60% over a comparable IGBT-based design (**Figure 8**).

Driving SiC MOSFETs

$R_{DS(ON)}$ is given as a range of values in the datasheet of a SiC MOSFET for different gate voltages (V_{GS}), drain currents, and temperatures. It’s important that V_{GS} reaches the upper value given, typically 18 V;

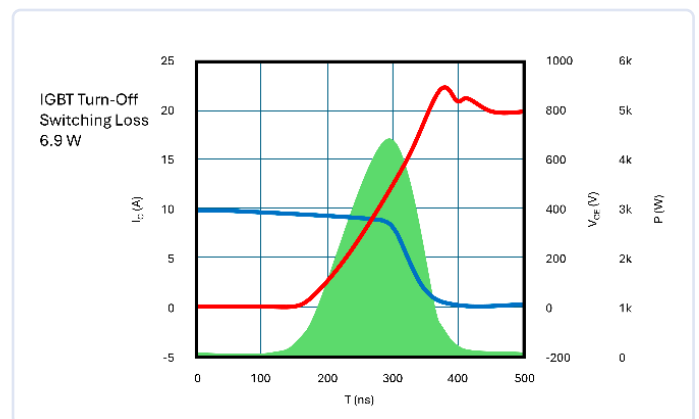
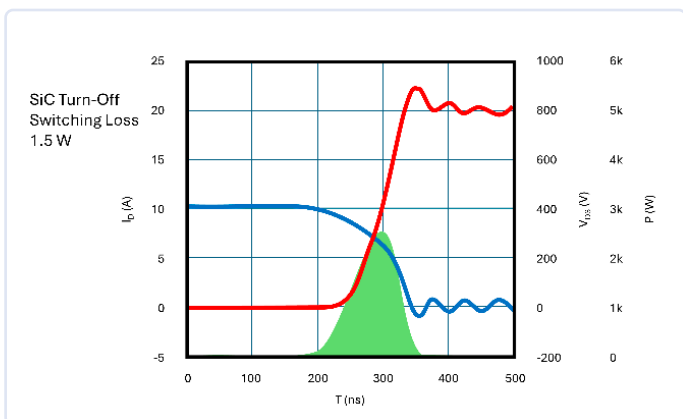


Figure 7: Turn-off power loss comparison for a SiC MOSFET (left) and IGBT (right). Voltage is in red, current is in blue, and power is in green. (Source: Toshiba Electronics Europe GmbH)

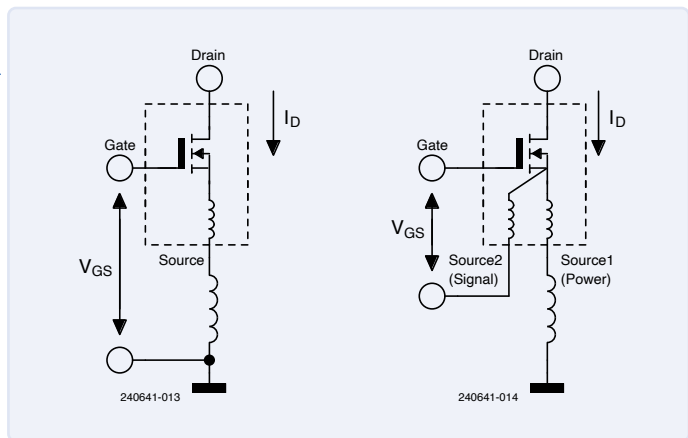


Figure 9: A Kelvin source or sense pin is often found on discrete power devices to provide a more stable gate-source or base-emitter voltage. (Source: Toshiba Electronics Europe GmbH)

otherwise, the target $R_{DS(ON)}$ won't be met, resulting in higher losses. While the task seems simple enough, controlling a several tens- or hundreds-of-kilohertz signal at the gate of a device through which tens of amps are flowing is no easy task.

Problems can be caused by the inductance of the wiring inside the MOSFET's packaging between the source on the die and the package's source pin. With high currents passing back and forth during operation, great variations in the gate-source voltage occur. To compensate, a Kelvin source pin (sometimes named Kelvin sense pin) is added and used as a source reference (Figure 9). This load-free connection between an additional package pin and the source on the die helps provide a more stable gate-source voltage. It should be noted that the Kelvin source is not unique to SiC devices, as it is a feature of many devices used in high-power applications.

Gate drivers [4] convert the controller's logic outputs (typically a microcontroller is used) to the voltage and current needed to drive the gate of the SiC MOSFET, typically peaking at several amps. Due to the high system voltages being switched, the isolated gate drivers (optoisolators) isolate the control logic from the voltage being switched. They typically use the Kelvin source pin as a ground reference.

Controlling the turn-on and turn-off speed independently is also important, leading to opposing diodes and resistors being used in the path to the gate (Figure 10). One of the diodes and resistors may be left out, depending on application needs. Some gate drivers even provide separate on and off path outputs.

SiC can also respond poorly to being subjected to negative gate voltages. Infineon recommends ensuring that the gate voltage does not drop below -2.0 V as, over time, it can cause drift in V_{GS} . This leads to an increase in $R_{DS(ON)}$ over many hours of operation. For this reason, a Zener diode may be added between the Kelvin source and gate.

GaN Transistors

The second WBG device is gallium nitride, known as GaN, a high electron mobility transistor (HEMT). It's formed from an aluminum gallium nitride (AlGaN) layer on a layer of GaN material, between which a two-dimensional electron gas (2DEG) forms (Figure 11). Their major benefit is the lack of reverse recovery charge, Q_{rr} , that is caused by the body diode in MOSFETs but isn't part of a GaN device.

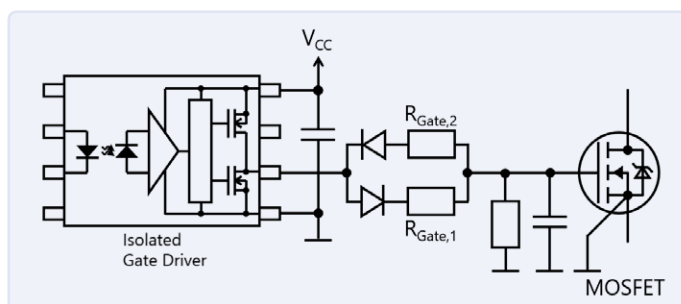


Figure 10: Opposing diodes with resistors in the gate path allow the turn-on and turn-off characteristics to be controlled independently. (Source: Toshiba Electronics Europe GmbH)

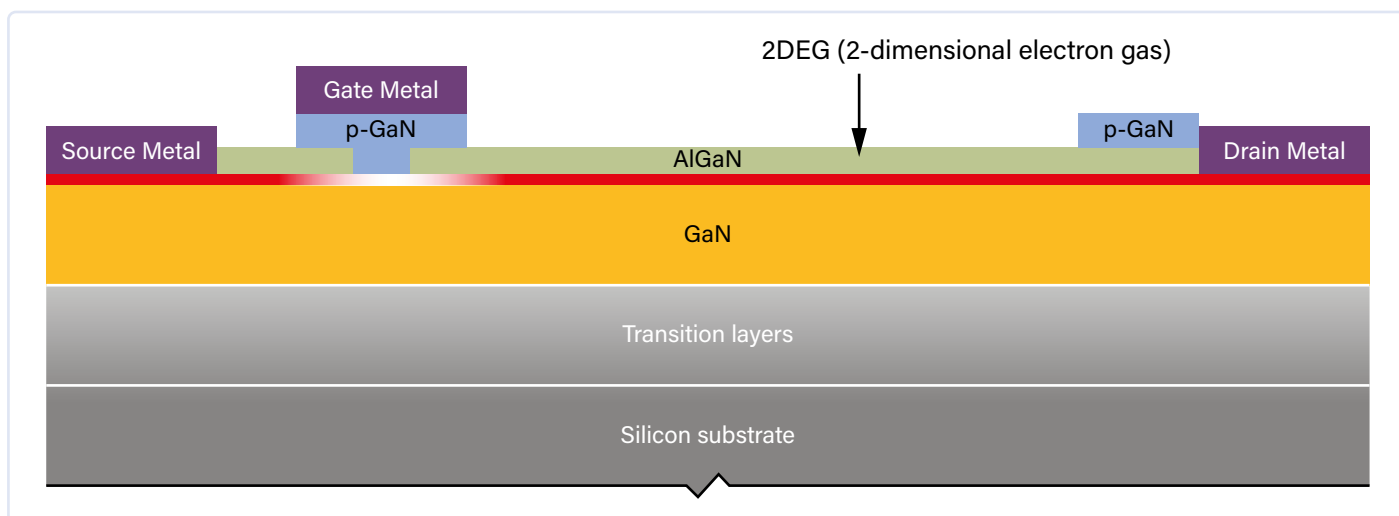


Figure 11: Cross section of a CoolGaN HEMT (Source: Infineon Technologies AG)

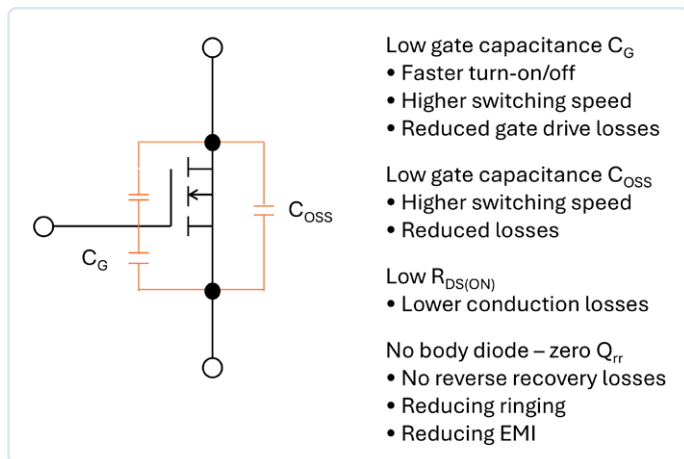


Figure 12: GaN offers reduced losses in switching applications compared to silicon, allowing for more efficient and compact power converters (Source: Texas Instruments)

This reduces losses and ringing on the switched node, improving EMI (**Figure 12**).

With a bandgap of 3.39 eV, it's similar but higher than SiC devices. They also have a similar electrical breakdown field at 3.3×10^6 V/cm. Where they sharply differ is in their thermal conductivity characteristics, which, at 2.0 W/cmK, is closer to silicon than SiC.

Infineon is also a key supplier of GaN transistors, along with Nexperia and Rohm. There are also smaller players that are leveraging the benefits it offers to innovate in the power conversion space, such as Efficient Power Conversion Corporation (EPC). However, the competition in this market is such that many smaller suppliers have already been acquired by the larger, traditional players, with Transphorm recently acquired by Renesas and GaN Systems being bought by Infineon.

The applications that make GaN so attractive are power supplies for commercial servers and consumer phone and laptop chargers. Thanks to their unique properties, GaN has rapidly made its way into these devices, giving consumers significantly smaller supplies to carry around with their computing devices. In fact, many smartphone charger manufacturers highlight that their devices use GaN, marketing its use as a benefit.

Two types are available. The depletion-mode, or d-mode, transistors are always on and require a negative voltage to turn them off. However, an always-on device in a switching power supply is challenging to use, resulting in current flowing before the control circuitry is ready to turn it off. The preferred GaN device for a power converter is the enhancement mode, or e-mode, type, that is modified to be always off.

GaN devices are available for withstand voltages up to around 800 V and junction temperatures up to 150°C. The gate-source looks like a pn-diode, and the gate threshold voltage, $V_{GS(TH)}$, required to turn

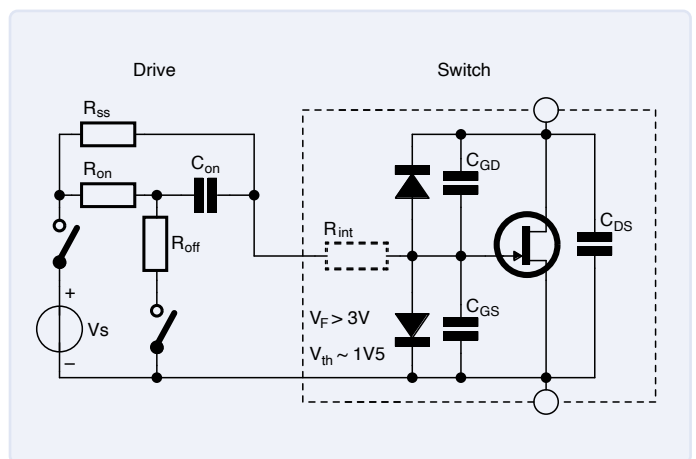


Figure 13: The drive circuitry for the gate of a GaN device is quite complicated compared to that required for other power devices (Source: Infineon Technologies AG)

on the device can be quite low at around 1.5 V with a gate resistance of a few ohms. As a result, the drive circuit can be significantly more challenging than that used in the silicon MOSFET application it typically replaces.

Adding to the challenges are the high switching frequencies of up to 10 MHz that the devices support. As already highlighted, this feature is of special interest as it allows use of smaller-volume passive components.

Driving GaN HEMT

The diode-like input at the gate makes controlling GaN devices challenging. As the control voltage is applied, it rises until it reaches the forward voltage, V_F , of this diode. After this, the device needs to be held in its on-state. Some devices will also require a negative voltage at the gate to turn it off.

Infineon proposes a simple circuit consisting of three resistors and a capacitor to control their e-mode GaN HEMTs. A driver capable of applying 8 V to 10 V is applied to the gate via a series resistor and capacitor, providing the on-transient current. In parallel, a further resistor provides the required steady on-state diode current. The turn-off process is instigated by connecting the capacitor to ground through a resistor. The voltage across this capacitor, combined with the voltage across the GaN device's internal gate-source capacitance, provides a negative gate voltage, V_G , to turn the device off again (**Figure 13**).

Like for SiC devices, specialized isolated GaN gate drivers provide separate pins for the turn-on and turn-off path. Discrete GaN device packages also provide a Kelvin source pin where appropriate.

Because of the challenges in optimally designing in GaN devices, EPC has started offering their GaN FETs with integrated drivers (**Figure 14**), offering half-bridge power stages like the EPC2152 [5]. These simplify power converter design and solve many of the

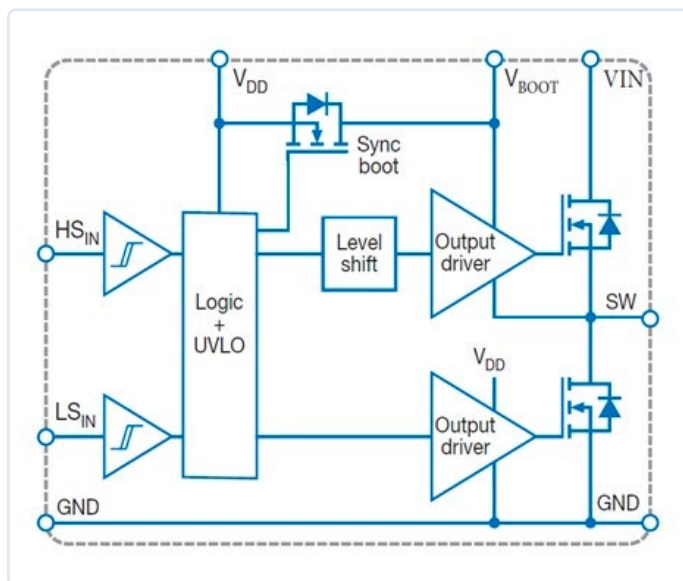


Figure 14: This half-bridge integrates GaN FETs and the necessary gate drivers in a tiny 3.9×2.6 mm package. (Source: Efficient Power Conversion Corporation)

control and EMI issues while enabling switching times of 1 to 2 ns. This move to more integrated solutions is a traditional strategy in the semiconductor industry but currently differentiates EPC from other GaN players.

Smaller, Denser, Lighter, More Efficient

Power converter designers continually look for approaches that make their products more efficient and compact. WBG devices like SiC and GaN can provide a step improvement compared to superjunction MOSFETs and IGBTs in the right applications and when using appropriate topologies.

GaN offers the highest switching frequency, meaning that those traditionally bulky inductors and capacitors can be shrunk down the most, reducing the volume, weight, and cost of materials.

They are currently seen as a replacement for superjunction MOSFETs, targeting servers and consumer power supply applications. SiC is primarily seen as an alternative to IGBTs, being deployed in industrial applications that need smaller volume, more efficient power converters and motor inverters that are robust.

What's holding adoption back is the cost of the devices compared to the alternatives. Both SiC and GaN remain more expensive than the IGBT or silicon MOSFET they replace. Suppliers often try to offer a system-level analysis of cost that factors in the lower outlay for the passives. Then, there are other benefits that customers may pay for. A more compact server power supply may enable innovation in the rest of the design, or higher efficiency may deliver energy savings that justify the higher upfront investment. The semiconductor industry is also responding by investing in their manufacturing processes to drive down the device costs for these exciting new WBG devices. One thing is for sure — WBG is here to stay and will change the power conversion industry permanently. ◀

240641-01



About the Author

Stuart Cording is an engineer and journalist with more than 25 years of experience in the electronics industry. He specializes in video content and is focused on technical deep-dives and insight. This makes him particularly interested in the technology itself, how it fits into end applications, and predictions on future advancements. You can find many of his recent Elektor articles at www.elektormagazine.com/cording.

Questions or Comments?

If you have questions about this article, feel free to email the Elektor editorial team at editor@elektor.com.

WEB LINKS

- [1] "Inside the Apollo Guidance Computer's Core Memory," Ken Shirriff's blog: <https://www.righto.com/2019/01/inside-apollo-guidance-computers-core.html>
- [2] "What Determines Reverse Recovery Time in MOSFETs," Cadence PCB Solutions: <https://resources.pcb.cadence.com/blog/what-determines-reverse-recovery-time-in-mosfets>
- [3] "What is a wide-band-gap semiconductor?," Toshiba: https://toshiba.semicon-storage.com/ap-en/semiconductor/knowledge/faq/diode_sic-sbd/sic-sbd001.html
- [4] Stuart Cording, "Why Do MOSFETs Need Drivers?," elektormagazine.com, May 2022: <https://www.elektormagazine.com/articles/why-do-mosfets-need-drivers>
- [5] EPC2152: 80 V, 15 A ePower™ Stage: <https://epc-co.com/epc/products/gan-fets-and-ics/epc2152>

Notebook Power Bank

Extend the Life of Your Aged Laptop

By Laurent Labbe (France)

If your notebook has dead batteries — perhaps no longer commercially available — or a failure on the charging circuit, this project might be for you.

It is a backup power supply system that enables you to keep the work session open on your PC for short periods, when you move it from one room to another, or keep it on standby for hours, without reconnecting it to the mains.

As it often happens, many new projects come from a special need. Since the last two years, my wife's PC has been working without the battery, and it was always powered by an external power supply.

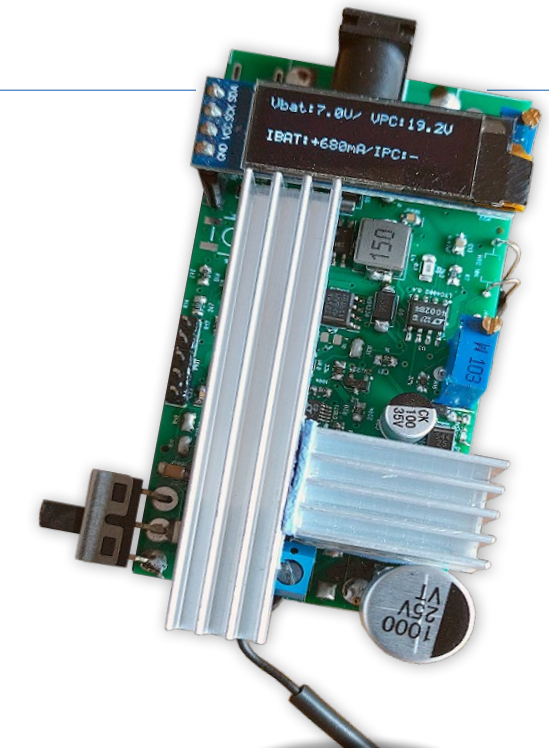
Of course, I tried to replace the battery at first, but the problem was still there. The defect was coming from the motherboard and not easy to repair. So, I proposed to her to design an external power supply, with embedded batteries, which could allow her to move with the computer without losing her working session.

The Original Design

The first design was assembled with some standard modules:

- A 3 A rated DC-DC Boost module, based on a LTC1871 by Analog Devices, stepping-up the voltage from 8.4 V (2 x 18650 cells in series) to 19 V.
- One LM317-based module for charging the batteries when the external power supply is applied.
- A DC-DC Buck from an external power source, to supply the charging module.

All in all, this was working well on her notebook, but she found it to be too bulky. Also, the boost module used was designed for 3 A output but, in real-world applications,



if the voltage difference between IN and OUT is too large (like in this case), the output current is limited to 2 A. This was still working well on her notebook but not on mine, which requests 3.2 A. The difference could be explained because my PC needs 2 A for the hardware platform itself and at least 1 A for charging the battery. On her PC, without a functional charging circuit, a current of 2 A was enough.

Furthermore, there was only a display showing IN and OUT voltages, but no information whatsoever about the current intensity.

That was the starting point of this project, that led me to redraw a power bank for PC with these further requirements:

- Usage of 2 x 18650 batteries with the highest possible capacity (LG, here).
- Capable of output up to 20 V, 3 A.
- Compact design. Should fit in a 2 x 18650 footprint.
- Display of IN (battery) and OUT (PC supply) voltage and current.

Design Choices

To achieve the latest version (schematic V2.3, illustrated in **Figure 1**), four subsequent versions were made, with four schematics and four different PCBs, whose latest release is illustrated in **Figure 2**. You can find all the details on the article published in Elektor Labs [1]. **Figure 3** shows a cluttered, earlier version of the design, which gives you an idea of the multitude of trials and variations performed before arriving at the final version.

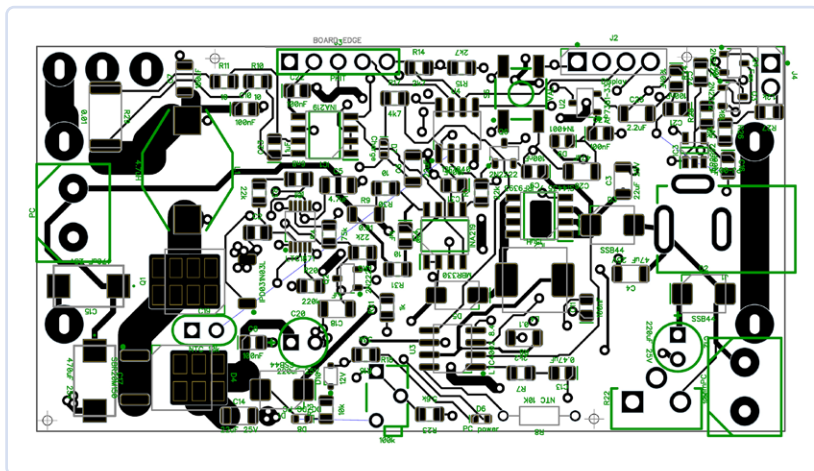
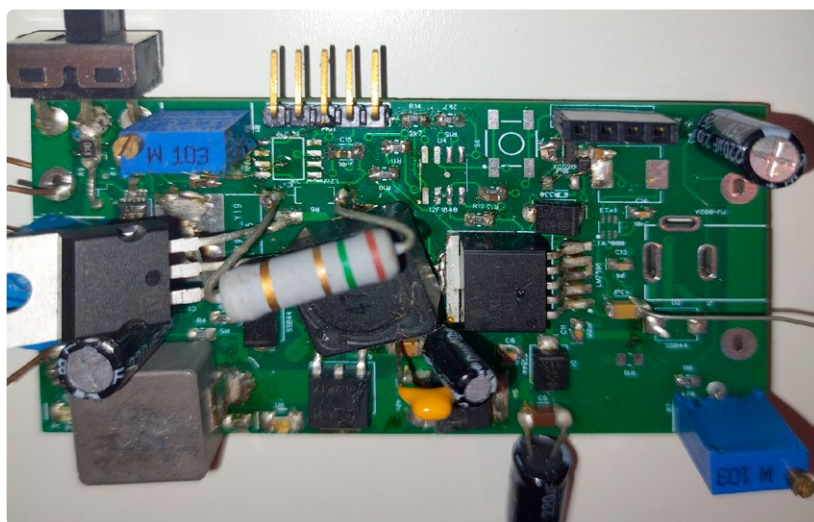


Figure 2: Layout of the latest, V2.31 version of the PCB.

The requisites for the latest version are:

- > A boost DC-DC module, still based on LTC1871.
- > A charging section, based on LTC4002-8.4 by Analog Devices, a switch-mode IC which can accept input voltages up to 22 V [2].
- > A small OLED Display, driven by a Microchip 12F1840 controller. This part just displays current and voltage values. The whole powerbank can work without this module, in case it won't be required.
- > A current monitoring section based on an INA219 sensor by Texas Instruments.
- > A high input voltage linear regulator AP7381-33 by Diodes Incorporated for the 3.3 V power supply line.
- > A 5 V fan for dissipating the heat generated by the batteries and the DC-DC converter. It's managed through a dedicated 5 V linear regulator and a special logic drive.

Figure 3: The cluttered look of a previous version of the prototype: do not try this at home!



Connections

This device needs to be connected in series between the original, external notebook's power supply and the input power plug of the same laptop. The output power to the notebook is available from the PC screw terminal block connector. The power connecting cable depends on the size and style of the PC's input power connector.

For the external power supply input, either a (standard) barrel connector, or a screw terminal block (labeled *AlimPC* on the silkscreen) can be implemented on the PCB. Again, this should match the type of plug fitted on the original laptop's external power supply.

Operating Principles

In case of no voltage is coming from the external power supply, the notebook is powered from +VBAT, by the boost DC-DC converter (U1 plus circuitry) through D1 diode, which is supplying the +VPC line. LED D8 is on.

When the PC's external power supply connected to J1 (or *AlimPC*), the notebook is powered through D2 from +VPC, and the boost DC-DC converter must be turned off, consequently. More on this below. The Zener diode D10 is used to prevent the LED D8 from staying on for a long time, due to residual charge in the capacitors, after the DC-DC converter is turned off.

The charging process starts as long as the battery temperature is not too high (monitored by R8 and R19 NTCs). D6 LED indicates that the notebook is being powered.

The final output stage to the PC has two large 470 μ F, 25 V tantalum capacitors (C15 and C17) to smoothen the ripple generated by the DC-DC booster.

Description of Each Module

DC-DC booster

This function is managed by the LTC1871. This IC is quite tricky to use and a good reading of the datasheet is needed. I've tried many configurations with different switching frequencies and inductor values.

The output voltage is fixed through FB pin and R18/R23 resistors. On the last version of the schematic, I swapped these resistors, placing R23 to the low-side (toward GND), to avoid the accidental grounding of IC's FB pin with the subsequent generation of a high voltage output. I burnt few tantalum capacitors due to that!

The frequency is set up at 100 kHz by the 220 k Ω resistor R20. INT VCC pin needs to be connected to a ceramic 4.7 μ F capacitor to stabilize the internal voltage.

This capacitor needs to be positioned as close as possible to the IC. For pin ITH, just follow the suggestions from the "Typical Application" schematic on LTC1871 datasheet [3].

The pin RUN acts like an ON/OFF function. There are 2 features here:

- The two resistors R4/R5 form a divider network, whose output to the RUN pin will stop the DC-DC conversion if the battery voltage drops below a certain value. The threshold here is 1.248 V. The values chosen here will switch off the DC-DC if the voltage of the batteries goes below 5.3 V. The voltage across R5 is filtered by a ceramic 1 μ F capacitor, to avoid that line sags might switch off the converter.
- When an external power supply is connected, its voltage is applied to R22 trimmer, acting as an adjustable voltage divider. The output from this trimmer biases the base of Q2 which, in turn, forces the RUN input of U1 to a low state, thus deactivating it. In this situation, +VPC voltage will come from D2.

To this extent, a simple adjustment is needed. Since the nominal input voltage value may differ among different PC power supplies, the turn-off threshold of U1 must be adjusted by R22. When the external power supply is connected to the device, just turn R22 until the DC-DC LED (D8) goes off.

The most difficult task in this design was finding the right MOSFET Q1 and Inductor L1. I've tried several inductors, and finally used 4.7 μ H from Coilcraft [4]. For the MOSFET, I did several tests as well. I needed to find a switch rated for at least 30 V and 30 A with the lowest possible $R_{DS(on)}$. The final choice was on a IPD031N03L by Infineon Technologies, with a $R_{DS(on)} = 2.6 \text{ m}\Omega$ (at $V_{GS} = 5 \text{ V}$) 30 V, 90 A.

The diode D4 used here is a 20 A, 150 V SBR20M150 by Diodes Incorporated. As Q1 and D4 have the same thickness, they can share the same heat sink.

After the switching diode, two ceramics capacitors (C8 and C14, 100 nF and 22 μ F, respectively) and an electrolytic one (C20, 220 μ F, 25V) stabilize and filter the output voltage.

Battery charger

The IC used in this section is an LTC4002-8.4 in SO package by Analog Devices. The LTC4002 exists in 2 versions, 4.2 V and 8.4 V. Be careful to order the 8.4 V version in this project.

The most interesting feature of this IC is the wide input voltage range, from 9 V to 22 V. As the target is to power the charging module with the standard external PC power supply, this is perfect. It is a trickle-charge switching DC-DC charging IC.

The charging module is powered by the external PC power supply and through D3, a 4 A, 40 V SMD Schottky rectifier SSB44 by Vishay.

The charging current is limited by a shunt (R6, 100 mV/ R6 [mA]). Here, the choice of using a 0.1 Ω resistor regulates the charging current around 700 mA (also depending on other parts' consumption). The choice of such a low current value for charging is not to draw too much current from the standard power supply, which will have to supply the PC as well, and could be overloaded, otherwise. It can be reduced by adjusting R6.

The inductor is 15 μ H, 1 A rated, and his choice was based on some calculations from the datasheet. For IC2 MOSFET, the maximum voltage rating needs to be considered, and must be higher than 20 V. The choice here was for a 30 V, 2 A rated Si4435 from Vishay. The IRF9393 (by Infineon) could be used as well. D5 diode is a 3 A, 30 V Schottky MBR330.

An NTC can be put on the batteries to avoid charging when their temperature too high. In this design, its use is mandatory. On the PCB, there are two possibilities for the NTC, either a SMT one (on the back side, with an adequate hole in the battery holder) or a discrete one. One LED (D7) is lit when the charging process is on.

It is interesting to note that, when the charging process is finished (low current detection), a timer will be activated and a new charge could be run (if needed) only 3 h later except, of course, when the input voltage is removed and restored subsequently.

Display section

The voltage and current display is managed by an 8-pin PIC12F1840 microcontroller by Microchip. It is powered by 3.3 V, SOT23 linear regulator AP7381-33, which has a wide input voltage spec.

The current and voltage information are using the current sensors IC INA219 from Texas Instruments. These ICs may have independent high voltage inputs (up to 30 V) on the sensor side, while their power supply can still be as low as 3.3 V. The readouts are sent to U4 microcontroller through a I²C interface.

To limit the interference of batteries voltage drop during

function, the regulator AP7381-33 is connected to VBAT through D9 diode and few capacitors. This was mandatory, as without them the 3.3 V would have never been clean enough for the INA219, and would have given erratic readings. Each of them also has a 1 μ F capacitor (C30, C23) close to their respective power supply inputs IN+ and IN-.

On the schematic diagram, the shunt resistors (R9 and R29) are connected to the INA219 through a possible filter (from datasheet proposal, see [5]). On the last PCB

I did not use it, and just replaced R30/R31/R10/R11 by soldered jumpers.

An optional push button function has been added, but it's not being used so far. Also, a link from the NTC to an analog input of the μ C is made in case of display temperature. But this function is not implemented yet in the software.

All INA219 and OLED display are managed through an I²C bus through J2 connector. This display is 128 x 32 pixels, 0.91", like this one at Smart Prototyping [6].

Program

For the software (written in MikroC and also available at the Elektor Labs page for this article [1]), I had to struggle with the limited size of the flash memory (4 kB). The I²C communication function was rewritten and optimized to reduce the memory usage. It is a simple loop to measure the PC voltage and VBAT voltage by reading VBUS and VSHUNT from both INA219. I didn't use the internal capability of the INA219 for automatic calculation of power, current and so.

The current and voltage readouts are fed to the OLED display only if their values changed from the previous loop. For the OLED display, it was needed to use a simple library, since the original OLED library couldn't fit in the 4kB size of the flash memory. The 12F1840 microcontroller is programmed through the PICkit V3 accessory and J3, where this programmer can be plugged-in directly.

An important note (since I made this mistake several times): do *not* increase the value of C25 (it has to be 2.2 μ F, or lower). With higher values, the PICkit V3 programmer does not always connect successfully to the microcontroller!

Ventilation

During all the tests with the 3 A output, which needs more than 10 A from the batteries, the heat generated by the MOSFET Q1, D4, L1 and the batteries is very high. In the case, a fan had to be provided to dissipate all the heat dissipated by all these components. The fan is a 5 V, 40 mm x 40 mm type and must be switched on under the following conditions:

- The temperature is high, i.e., more than 50°C.
- The battery voltage is higher than 5 V (2.5 V per element).

For that, a standard, 5 V SOT23 LDO was used, a LP2992 from Texas Instruments. It can source 250 mA with a low dropout and features an ON/OFF pin to control the



Component List

Resistors

R1, R3, R5 = 22 k Ω
 R2 = Not used
 R4 = 75 k Ω
 R6 = 0.1 Ω
 R7 = 2.2 k Ω
 R8, R19 = 10 k Ω NTC
 R9, R29 = 0.01 Ω
 R10, R11, R30, R31 = 10 Ω *
 R12 = Not used
 R13, R24, R25, R26 = 10 k Ω
 R14, R15 = 2.7 k Ω
 R16 = 33 k Ω
 R17 = 4.7 k Ω
 R18 = 100 k Ω Trimmer, multiturn
 R20 = 220 k Ω
 R21 = 1 k Ω
 R22 = 10 k Ω Trimmer, multiturn
 R23 = 5.6 k Ω
 R27 = 1.2 k Ω
 R28 = Not used

Capacitors

C1 = 6.8 nF
 C2 = 47 pF
 C3, C6, C14, = 22 μ F, 25 V
 C4, C26 = 47 μ F, 25 V
 C5 = 4.7 μ F, 25 V
 C7 = 100 μ F, 25 V
 C8...C11 = 100 nF
 C12, C20 = 220 μ F, 25 V, electrolytic
 C13 = 470 nF
 C15, C17 = 470 μ F, 25 V
 C18, C23, C30 = 1 μ F, 25 V
 C19 = Not used
 C25 = 2.2 μ F
 C16, C21, C22, C24, C27, C31 = 100 nF
 C28, C29 = Not used

Inductors

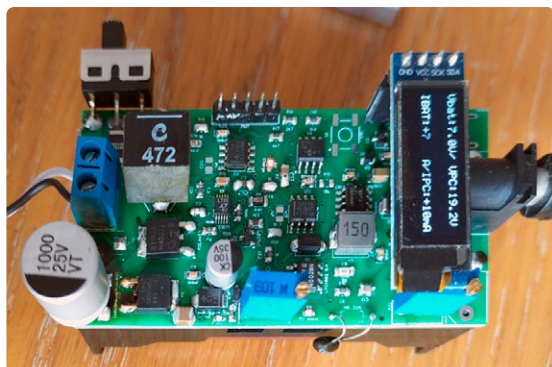
L1 = 4.7 μ H inductor, see [4]
 L2 = Not used
 L3 = Not used
 L4 = 15 μ H inductor, 1 A rated

Semiconductors

U1 = LTC1871
 U2 = AP7381-33
 U3 = LTC4002
 U4 = PIC12F1840
 IC1, IC4 = INA219
 IC2 = SI4435 or IRF9393
 IC3 = LP2992
 Q1 = IPD031N03L
 Q2...Q6 = 2N2222
 Q5 = Not used
 D1, D2, D3 = SSB44 Schottky
 D4 = SBR20M150
 D5 = MBR330 Schottky
 D6 = LED red (PC power)
 D7 = LED red (Charge)
 D8 = LED red (DC/DC Conv. on)
 D9 = 1N4001
 D10 = Zener diode, 12 V 0.5 W

Miscellaneous

2 x 18650 3.7 V cell,
 LG type LGABHG21865
 1 x 2-pole screw terminal block (PC output)
 1 x barrel-type conn., female, PCB type or
 1 x 2-pole screw-terminal block (AlimPC)
 2 x heat sink (see text)
 1 x 0.91" OLED Display, see [6]
 1 x fan, 40 x 40 mm, 5 V DC



▲ Figure 4: The populated PCB, with the display indicating the actual battery and output voltage parameters.

output (1 = ON, 0 = OFF). To achieve the two previous conditions, three 2N2222 NPN transistors are used:

- A 2N2222 (Q6) transistor with a resistor (connected to the stabilized 3.3 V line) and a 10 kΩ NTC will switch as the temperature goes high. When the temperature increases, the NTC value decreases, and at some point will turn the transistor off. By doing so, the ON/OFF pin will be enabled (high) and start supplying 5 V to the fan.
- 2 x 2N2222 transistors to monitor the VBAT (batteries voltage). If lower than 5 V, the first transistor (Q4) will be turned off, saturating the second one (Q3) and forcing the ON/OFF pin to low, thus stopping the fan.

Choice of the Battery

With the main MOSFET and inductor, the battery's choice is crucial. They must be able to deliver at least 20 A. I found some LG (LGABHG21865) which should deliver up to 30 A.

One problem here is the battery holder. The standard one will get hot quickly at currents ranging from 10 A to 20 A. Whenever possible, it should be better to solder the 18650 cells directly to the PCB.

Final Implementation

The PCB design was realized by Diptrace software and has a two-layers structure. Its design was a little bit tricky, due to the high current needed for the boost DC-DC converter. Wide tracks and large ground planes on the bottom layer have been provided for this purpose. **Figure 4** illustrates the populated board, including the OLED display reporting the actual values.

The INA219 needed to have a clean 3.3 V supply and some 100 nF decoupling capacitors close by them; therefore, the PCB routing was designed accordingly.

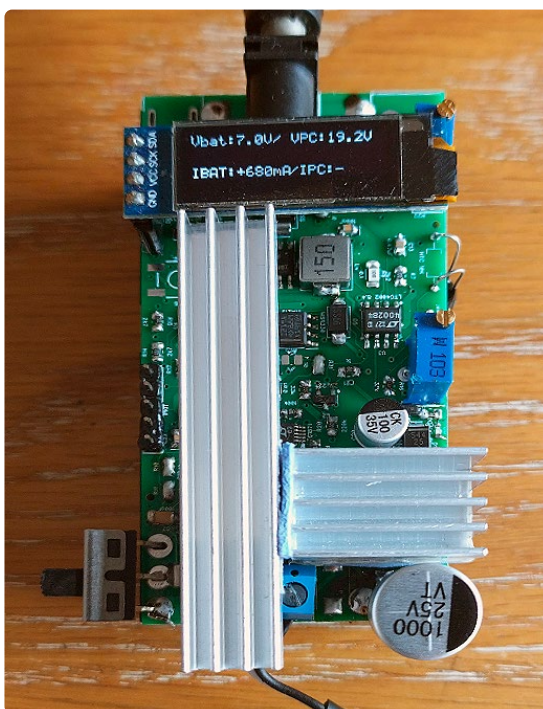


▲ Figure 5: The two 18650 Li-Po housed in the battery holder. Due to the high average current values, it's advisable to head to the PCB version of those cells (with tabs), and solder them directly to the PCB.

The dimensions of the board match the size of a 2 x 18650 battery holder, shown in **Figure 5**. However, as already mentioned, whenever possible it would be better to not use a standard spring holder, but batteries with tabs, which can be soldered directly on the PCB.

Heat dissipation

During the DC-DC boost process, a large amount of heat is generated by D4, Q1 and L1. Two heat sinks are used in this design: one for Q1 and D4, the other for L1. They are secured to the components with a double-sided heat-transferring sticking tape. **Figure 6** shows the final version of the prototype with the heat sinks already installed.



◀ Figure 6: The completed prototype board, with the heat sinks in place.



About the Author

Laurent is 60 years old, has lived in Asia for more than 20 years, and has been passionate about electronics since he was 10 years old. He's read many magazines, including Elektor since 1978. Laurent started playing with microcontrollers in the 1980s, the 8051 family and, more recently, with the PIC family and ESP32, whenever a network connection is needed. He has built many amplifiers, both solid-state (Elektor) and tube-driven (300B SE), as well as speaker systems and DACs. Laurent has been working in the mobile phone industry for more than 30 years (hardware, software, operation, quality) for a French company.

Questions or Comments?

Do you have technical questions or comments about this article? Please write to the Elektor team at editor@elektor.com.



Related Products

- > **Steffen Wolf, Ralf Regenhold,**
Abc of Power Modules (Würth, 2015, E-book)
www.elektor.com/19805
- > **AE970D Soldering Station (80 W)**
incl. extra Soldering Tip
www.elektor.com/20731

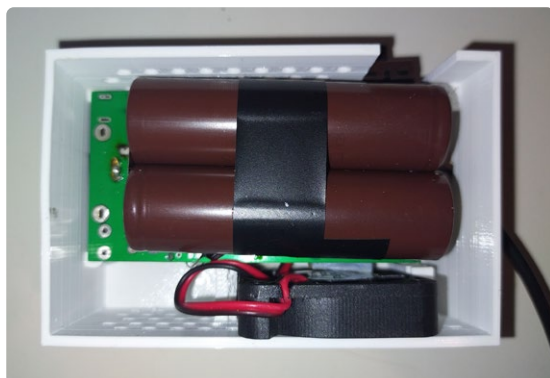


Figure 7: The small fan has enough space in the housing, tailored on purpose.

ON-OFF switch

To connect the batteries to the module, a power switch rated for more than 10 A has been used. It is not reported on the schematic but placed directly on the PCB. It must be connected between the VBATC and the "+" of the batteries.

The dedicated housing has been 3D-printed on purpose. It is slightly wider than the battery holder, due to the fan thickness, see **Figure 7**. The completed working prototype, housed in its custom-made case, is shown in **Figure 8**.

230611-01



Figure 8: The finished prototype at work, in its nicely made 3D-printed enclosure.

WEB LINKS

- [1] Elektor Labs page for this project: <https://tinyurl.com/yaxu9bk5>
- [2] Analog Devices LTC4002 web page: <https://www.analog.com/en/products/ltc4002.html>
- [3] Analog Devices LTC1871 datasheet: <https://tinyurl.com/3bzdjd9p>
- [4] Coilcraft inductor spec: <https://tinyurl.com/y7w2jkcu>
- [5] Texas Instruments INA219 datasheet: <https://www.ti.com/lit/ds/symlink/ina219.pdf>
- [6] 0.91" OLED display at Smart Prototyping: <https://tinyurl.com/ycktr2mc>

Medical Robots

Overcoming Technical and Regulatory Hurdles

By Mark Patrick (Mouser Electronics)

Designing robotics is never simple, but medical robots come with a number of unique regulatory and technical challenges that engineers must overcome.

Over the past 20 years, medical robots have evolved from being a concept in science fiction to becoming a real part of modern healthcare. Due to the arrival of sophisticated robotics in the market, numerous intricate tasks, ranging from surgeries and lab work to pharmaceutical automation and patient rehabilitation, have seen improvements.

One report by the Private Healthcare Information Network (PHIN) revealed a remarkable 524 percent surge in robot-assisted surgeries in the UK from 2016 to 2023, while in Q1 of 2024, a total of 22,700 robot-assisted procedures were carried out, illustrating the rapid expansion of robots in the healthcare sector [1].

However, despite the impressive growth, the current market is relatively immature. Continual advancements in perception, power, and control electronics, as well as artificial intelligence (AI), could drive a whole new wave of medical robot development, including advancements in surgical robots and exoskeletons.

Introducing a medical robot to market is no simple task. Any hopeful designs must provide the highest levels of precision and safety while adhering to a complex web of

technical regulations. In this article, we will explore how design engineers can navigate the unique regulatory and technical hurdles to create robots that the healthcare industry can readily adopt.

Navigating the Complex Regulatory Landscape

For engineers looking to develop medical robots for use within the European Union (EU) and the United Kingdom (UK), several key technical regulations act as a framework to ensure quality and safeguard patients from potentially harmful devices.

The EU Medical Devices Regulation (MDR) [2], which came into force on May 26, 2021, governs the manufacturing and distribution of medical devices in the European

Economic Area (EEA). It includes a certification and a risk-based system for classifying medical devices that manufacturers must comply with to legally sell their products in the EU.

MDR Article 51 categorises devices into classes I, IIa, IIb, and III based on factors like intended purpose, duration of the patient interaction, and inherent risks associated with its use [3]. Class I devices present the lowest risk and cover simple devices such as bandages, whereas class III devices represent devices with a significant impact on the human body, such as heart valves and surgical robots (**Figure 1**).

Engineering teams embarking on a medical robotics project can refer to the MDR classification guide to identify the appropriate class for their robot. This guide will establish a project framework to ensure the right level of development and clinical testing is conducted before the solution is launched.



The use and diversity of medical robots are on the rise, meaning solutions like the one pictured above could soon be a reality. (Source: phonlamaipphoto/stock.adobe.com)



Figure 1: Surgical robots are rapidly becoming a key part of modern medical institutions. (Source: MasterVideo/stock.adobe.com)

Additional Regulations and Standards

For medical robots, EU MDR — or the UK equivalent regulation (UK MDR [4]) — is just one of many regulations that must be met. Robots intended for in vitro diagnostic purposes must also conform to in vitro diagnostic regulation (IVDR), and there are numerous IEC and ISO standards that are crucial for engineers looking to develop safe medical robots, including:

- **IEC 80601-2-77:2019:** This standard sets essential safety and performance requirements for robotically assisted surgical equipment (RASE), ensuring systems are reliable and electrically safe in high-stakes surgical settings.
- **IEC 80601-2-78:2019:** For rehabilitation robots, like exoskeletons, this standard defines requirements for devices that interact directly with patients in therapeutic settings, focusing on operational safety and patient comfort.
- **IEC TR 60601-4-1:2017:** A technical guide on risk management for medical systems, this guide can assist engineers in identifying and addressing potential risks in robotic systems, aiming to enhance patient and operator safety.
- **ISO 14971:2019:** This standard provides a structured approach for managing risk in medical design, helping engineers identify and mitigate hazards early, which is critical for compliance and patient safety.
- **IEC 60601 Series:** This comprehensive series includes standards on electrical safety, electromagnetic compatibility, and performance, which are foundational for ensuring medical robots operate reliably within clinical environments.

Although robots are not explicitly mandated to adhere to IEC and ISO standards, these standards can act as essential tools for engineering teams, helping to promote best practices and guaranteeing robots' suitability for their intended use.

Strategy for Working to Standards

Navigating medical device regulations and standards is crucial for engineers developing compliant, safe, and effective medical

robots. While the exact implications of each standard and regulation vary, several working strategies can help ensure success:

- **Integrate standards early:** By incorporating applicable standards from the outset of the design process, it is possible to prevent costly redesigns and ensure that your design remains aligned with regulatory requirements.
- **Collaborate:** Collaborating with key market stakeholders — as well as regulatory and clinical experts — can make it easier to navigate the complex regulatory landscape, recognise potential compliance problems sooner, and refine approval procedures.
- **Stay up to date:** Standards and regulations evolve, often introducing new compliance requirements. Staying updated on these changes can help you anticipate adjustments in your design and keep your product development aligned with the latest requirements.
- **User-centric design:** Always keep the end user in mind, including both patients and healthcare providers. A robotic design that enhances usability, safety, and patient care will not only aid compliance but also improve the device's market adoption and practical value.
- **Documentation:** Meticulous record-keeping is essential. Document the design process, risk assessments, test results, and any modifications. Clear and comprehensive documentation demonstrates compliance and is often required for regulatory submissions.

By applying these strategies, administrators can naturally work these standards and key regulations into the development process as intended, providing engineering teams with guidance instead of creating technical hurdles.

Scaling Designs to Meet Global Demands

Creating robots for medical settings is inherently complicated. Engineers must prioritise safety while also ensuring designs can be scaled and priced to meet the budget constraints of medical institutions.

Robots have traditionally been developed and manufactured in small numbers in laboratories, often using a lot of highly skilled manual labour and bespoke hardware. However, as production ramps up to meet increasing demand, assembly speed, costs, and manufacturing consistency become critical, making the precise assembly of systems such as intricate mechanical joints with strict tolerances incredibly challenging.

For example, early robotic prototypes often use components such as high-resolution optical encoders, which, while incredibly accurate, are costly and have tight assembly tolerances. Alternatively, in many final designs, lower-resolution encoders may suffice. This means a designer could include a more cost-effective Hall effect encoder, which also has lower assembly tolerances.

For engineers designing medical robots, balancing safety, performance, and scalability is crucial if solutions are to be adopted by the market. Taking shortcuts in safety and performance can lead to catastrophic consequences, while unnecessary performance overheads can inflate costs and delay production timelines.

Selecting Components for Reliable and Accurate Operation

The complexity of interactions between medical robots and humans in tasks such as surgical procedures or assistive exoskeletons requires the highest levels of movement reliability, accuracy, and real-time responsiveness. To meet these requirements, engineers require a wide range of essential components, including sensors, motor drivers, encoders, and intelligent control systems.

Perception and Feedback

Ensuring the precise movement of medical robots in often complex environments relies on highly accurate perception technologies. Mouser Electronics [5] offers a wide range of sensor solutions that are designed to support the latest medical robotics, ranging from surgical and diagnostic systems to rehabilitation devices and patient monitoring solutions.

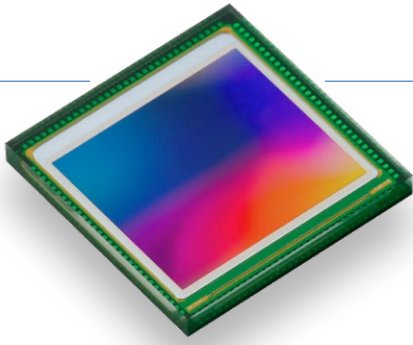


Figure 2: ams OSRAM's Mira220 provides high-performance and low-power operation. (Source: Mouser Electronics)

Sensors such as ams OSRAM's Mira220 1/2.7 2.2MP Global Shutter Image Sensors [6] (**Figure 2**) fulfil the needs of modern medical robotics by providing an ideal balance of performance and cost. In contrast to rolling shutter designs that capture images row by row, the global shutter captures the entire image at once. This enhances the precision of AI-backed machine vision operations by guaranteeing the continuous visibility of the entire current scene.

In solutions like medical service robots that must navigate hospital hallways, the Mira220 sensors' global shutter combined with the 90 fps maximum frame rate ensures control electronics can accurately perceive their surroundings.

Furthermore, the Mira220 sensors use the MIPI CSI-2[®] interface for easy interaction with microprocessor units (MPUs) and field-programmable gate arrays (FPGAs). The on-chip registers can be accessed via the standard I²C interface for easy configuration, helping to reduce integration considerations.

Motor Drivers and Control Systems

Perception is just one part of ensuring a safe and accurate medical robot. Any movement must also be smooth and controlled. This



Figure 3: The design of Broadcom's AEAT-901x-S06 reduces assembly errors and ensures accurate movement feedback. (Source: Mouser Electronics)

requires precision motor drivers and control electronics, as well as high-speed internal feedback systems.

Rotary encoders provide movement feedback in intricate robotic mechanical joints. This role has historically fallen to highly accurate optical sensors, but now more cost-effective and easier-to-assemble magnetic sensors are gaining popularity in robotics applications.

Broadcom's AEAT-901x-S06 Absolute Magnetic Kit Encoders [7] (**Figure 3**) are one such example tailored for robotic deployments. The integrated encoder housing streamlines integration and minimises assembly errors, saving time and costs.

These high-performance devices can accurately determine absolute angular position and provide resolutions of up to 18 bits, offering performance similar to optical encoders. The design's resistance to oil and dust plays a crucial role in ensuring reliability, helping to boost longevity.

Conclusion

As medical robots continue evolving, they hold the potential to transform healthcare delivery through enhanced precision and

automated solutions. However, successfully bringing a robot to market demands engineers address both regulatory challenges and high technical standards while balancing costs and scalability.

By focusing on precision, real-time feedback, and safety-compliant design, while embracing the latest advanced perception and control technologies, developers can significantly accelerate the integration of robots across medical applications. ◀

240688-01



About the Author

As Mouser Electronics' Director of Technical Content for EMEA, Mark Patrick is responsible for creating and circulating technical content within the region — content that is key to Mouser's strategy to support, inform, and inspire its engineering audience. Before leading Technical Content, Mark was part of Mouser's EMEA Supplier Marketing team and played a vital role in establishing and developing relationships with key manufacturing partners. Mark's previous experience encompasses hands-on engineering roles, technical support, semiconductor technical sales, and various marketing positions. A "hands-on" engineer at heart, Mark holds a first-class Honors Degree in Electronics Engineering from Coventry University. He is passionate about vintage synthesizers and British motorcycles, and thinks nothing of servicing or repairing either.

WEB LINKS

- [1] Phin, "New report shows record use of robot-assisted surgery technology in the NHS and private sector," Oct 2024: <https://www.phin.org.uk/news/record-use-of-robot-assisted-surgery-technology>
- [2] EU Medical Devices Regulation (MDR): <https://eumdr.com/>
- [3] Medical Device Coordination Group, "MDCG 2021-24," Oct 2021: https://health.ec.europa.eu/system/files/2021-10/mdcg_2021-24_en_0.pdf
- [4] Regulating Medical Devices in the UK: <https://www.gov.uk/guidance/regulating-medical-devices-in-the-uk>
- [5] Mouser Electronics: <https://eu.mouser.com/>
- [6] ams OSRAM Mira220 Sensors: <https://eu.mouser.com/new/ams-osram/ams-osram-mira220-sensors/>
- [7] Broadcom AEAT-901x-S06 Absolute Magnetic Kit Encoders: <https://eu.mouser.com/new/broadcom/broadcom-aeat-901x-s06-encoders/>

Frost Guard for Fruit Plants

With Temperature Data Logger



By Thomas Dausner (Germany)

With climate change, Earth's average temperature has risen, causing fruit trees and other flora to flower earlier each year. Under these conditions, overnight freezing can cause the loss of the complete harvest. The system in this project solves the problem through the so-called "crystallization heat" technique. It works!

- Irrigation magnetic valve [1] to switch irrigation on and off (top-left).
- Circular sprinkler [2] (connected to the magnetic valve output) and some meters of water hose (on top of the temperature sensor coax cable).
- USB-to-RS232 serial adapter [3] housed in shrink tubing (bottom-right).

Features

When I start a project, I usually settle on a feature proposal list:

- Temperatures for irrigation activation and deactivation must be settable.
- Date and time of irrigation must be logged.

Every spring time I admire the flowering of the fruit trees in my garden. The first to flourish is an apricot tree — so early (beginning of March) that the March and April frost in past years destroyed the entire harvest. Fruit farmers utilize the crystallization heat when water freezes below 4°C. So, I decided to irrigate my apricot tree to avoid frost damage. Commercial frost guard systems are quite expensive. Not so much the watering part, but the controller part. That's why I decided to set up my own frost guard system.

Abstract

The frost guard system (see **Figure 1**) consists of:

- Controller (bottom-center), showing a temperature of 22.0°C.
- Power supply (bottom-left).
- Temperature sensor with 15 meters of coax cable (right).



Figure 1: All the components of the frost guard system.

- Date and time must be settable.
- Logged irrigation data must be output to a serial interface.
- Irrigation must be switched on and off on demand to set up the sprinkler at my apricot tree.
- Irrigation status must be indicated by an LED.
- The hardware implementation must use standard components, mostly available in my workshop.

Use Case

Looking for a suitable temperature sensor, I decided to use a DS18S20 High-Precision 1-Wire Digital Thermometer by Analog Devices [4] instead of any analog solutions. The DS18S20 is a temperature-stabilized device offering 9-bit resolution in the range of -10°C to $+85^{\circ}\text{C}$ with $\pm 0.5^{\circ}\text{C}$ accuracy. It is easy to interface and C software is available.

My apricot tree is located about 15 m from my garden shed, so I had to configure my own temperature sensor to make use of a 15 m coaxial cable, as all available DS18S20 temperature sensors allow a maximum cable length of 10 m. 15 m Coax cables with molded BNC connectors are easily found, off the shelf. As a result, I chose a two-wire connection for the temperature sensor ("parasite power mode" requires only two pins). The sensor is epoxied into a 6 mm-diameter aluminum pipe and is thus waterproof (**Figure 2**). The temperature sensor is located at about 3 m above ground in the center of my apricot tree. After a night with morning temperatures below 3°C , it looks like crystallization heat works (see **Figure 3**)! We'll discuss the format of the log in the **Logged Data Output** section below.

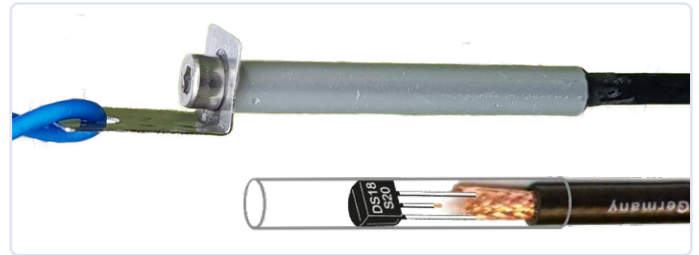


Figure 2: The sealed temperature sensor.

At the end of winter, at my latitude, temperatures don't go below a few degrees below zero for extended periods, so the water in the hose won't freeze. The controller also doesn't need military spec components, as it is sheltered in my garden shed.

Temperature Sensor

I've seen plenty of discussions on the web about possible cable lengths for DS18x20 temperature sensors. I agree, it's a matter of controller timing on one hand, and a matter of reflections in a long cable on the other. In a blog related to this specific aspect [5], the author states:

"DS18B20 works with longer cables. As it is a one-wire device, only two wires are needed. A test with 100 m of cable was unsuccessful, but at around 20 m it works well enough. Sometimes, I get a false reading of -127.0°C , but it appears that I can get this on 3 m cable as frequently as on 20 m+ cable."



Figure 3: The crystallization heat principle works!

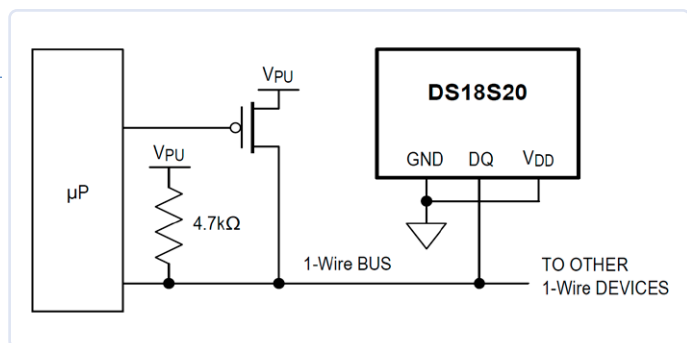


Figure 4: Supplying the parasitically-powered DS18S20 during temperature conversions. (Source: Analog Devices [4])

Parasite power mode, a method of supplying power to the IC — even during the data transmission — is explained in the “Powering The DS18S20” section of the aforementioned datasheet (see the simplified schematic in **Figure 4**):

“In parasite power mode, the 1-Wire bus and Cpp [the device’s internal capacitor, visible in Figure 5] can provide sufficient current to the DS18S20 for most operations as long as the specified timing and voltage requirements are met ... However, when the DS18S20 is performing temperature conversions or copying data from the scratchpad memory to EEPROM, the operating current can be as high as 1.5 mA. This current can cause an unacceptable voltage drop across the weak 1-Wire pullup resistor and is more current than can be supplied by CPP. To assure that the DS18S20 has sufficient supply current, it is necessary to provide a strong pullup on the 1-Wire bus whenever temperature conversions are taking place or data is being copied from the scratchpad to EEPROM. This can be accomplished by using a MOSFET to pull the bus directly to the rail, as shown in Figure 4. The 1-Wire bus must be switched to the strong pullup within 10 μs (max) after a Convert T [44h] or Copy Scratchpad [48h] command is issued, and the bus must be held high by the pullup for the duration of the conversion (tCONV) or data transfer (tWR = 0 ms).”

Thanks to this, I decided to use an engineer’s passion for trial and error and rig up a test setup on breadboard with my home-made 15 m coaxial cable. Powering the sensor up runs in parasite power mode, as you’ll (see in the schematics later on). To cut it short: Almost always, my test setup operated as expected, although in a few cases, the temperature sensor showed a nonsensical sensor value, as the

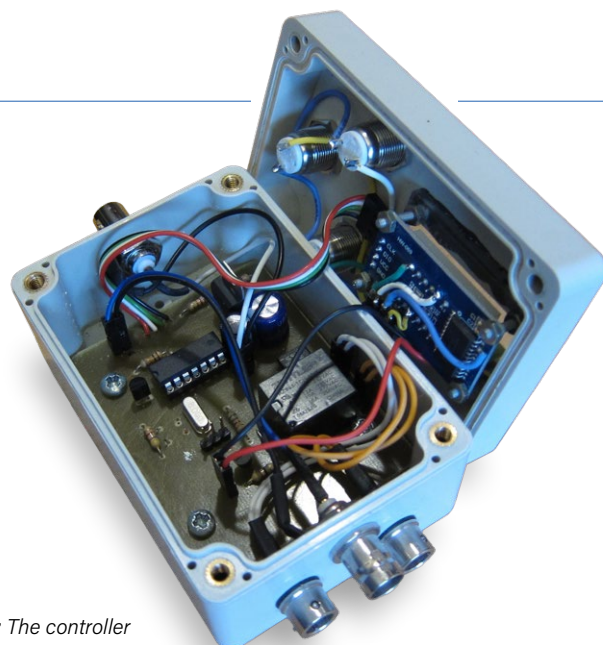


Figure 6: The controller with its connectors.

abovementioned author stated. This is reflected in the software (see the `mode_watch.c` file in the source code):

- The temperature conversion cycle starts by powering the sensor by issuing 5 V to the data line for 200 ms.
- Temperature begins.
- After a 750-millisecond delay, the sensor is read out.
- In case of an unrealistic sensor value (<-20°C or >40°C) the cycle is repeated.

Power Supply and Irrigation Solenoid

The controller has a rectifier, capacitors, and a voltage regulator on board, and draws just a few mA, mostly for the display and the irrigation solenoid. This means you can use any AC or DC power adapter, as long as the irrigation solenoid operates correctly. My power supply is an old laptop power adapter of 16 V DC/4.5 A. The irrigation solenoid is a 24 V AC type that exhibits safe switching behavior at 16 V DC.

Controller

The controller is housed in an IP65-protected 100×68×50 mm enclosure [6]. In the completed prototype illustrated in **Figure 6**, you can see the four connectors, from left to right: serial out at the back and power

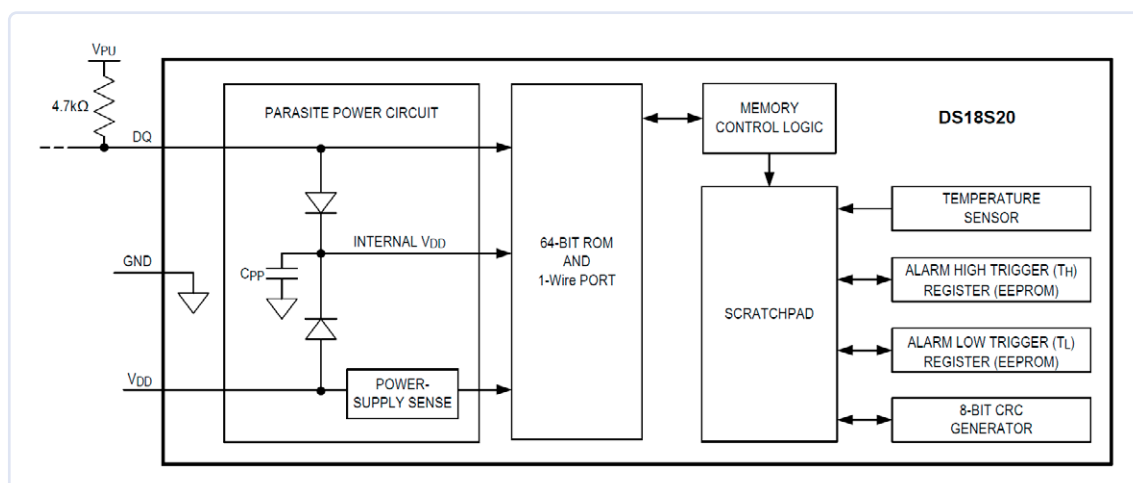


Figure 5: DS18S20 block diagram, with Cpp charged through the DQ bus line during the non-transmit time. (Source: Analog Devices [4])



Figure 7: Front view of the controller.

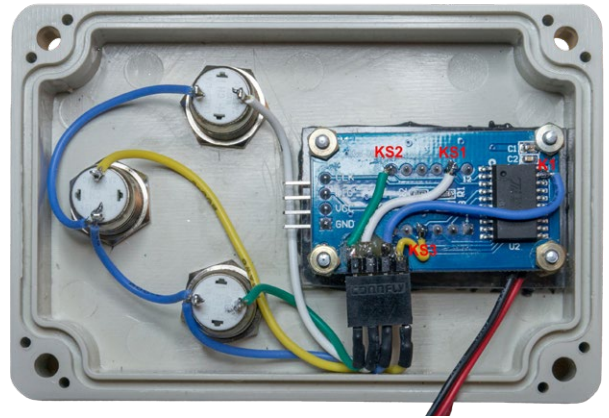


Figure 9: The modified TM1637.

supply, and temperature sensor and irrigation valve in the front. The serial output and temperature sensor connections are BNC. Spring-lock plug sets are utilized for power supply (4-pin) and solenoid (2-pin) connectors [7][8]. The display is mounted on a 5 mm-thick sheet of plexiglass, epoxy glued to the front of the enclosure. The irrigation control LED is positioned at the left of the 7-segment display. The push buttons visible in the picture were found in my collection of spare electromechanical components (**Figure 7**).

Schematics

Figure 8 shows the project's schematic. The controller hardware is simple state of the art: a Microchip ATtiny84 microcontroller [9], a Titan Micro Electronics TM1637-controlled 4-digit, 7-segment display [10], a 5 V relay, an STMicroelectronics LM317T voltage regulator, the external DS18S20 temperature sensor, and some other standard

components. The microcontroller is crystal-driven, as the controller logs all irrigation events with a time stamp. A previous version of the frost guard controller utilized the built-in clock, which proved to be too inaccurate for the purpose.

The DS18S20 temperature sensor is parasitically powered during temperature conversions by R1 and Q1, as per the recommendation in the data sheet. During conversion times, Q1 is brought to the conductive state and the DS18S20 gets charged. During communication, Q1 is blocked, and the data line is terminated by R2. Looking at the TM1637 data sheet [11], I discovered that the TM1637 controller is capable of reading up to 16 push buttons. Next, I adapted the TM1637 controller to interface the three push buttons, SW1...SW3, as shown in **Figure 9**. The push buttons are connected to the TM1637 controller's pins KS1, KS2, KS3, and K1.

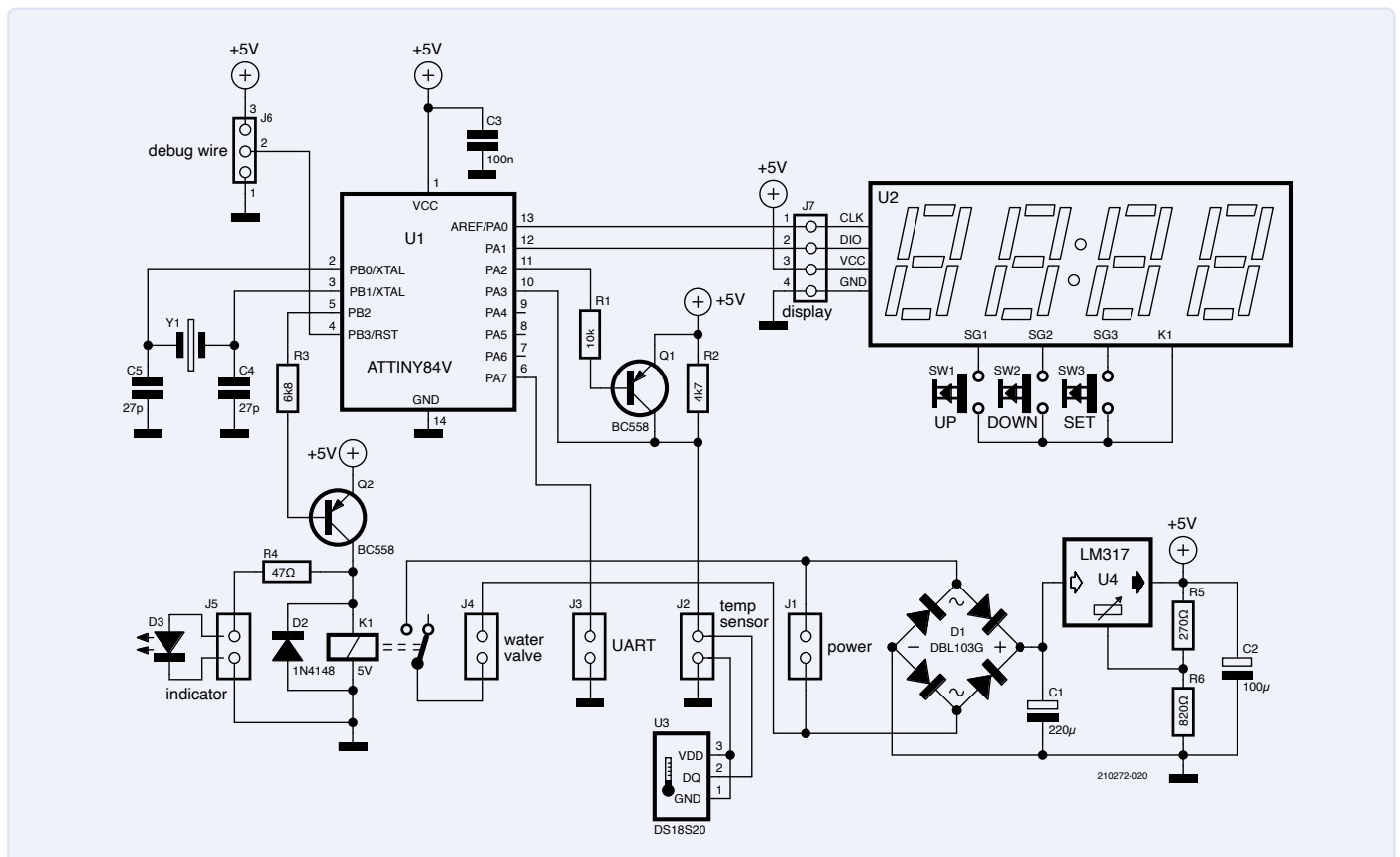


Figure 8: The project's schematic diagram.

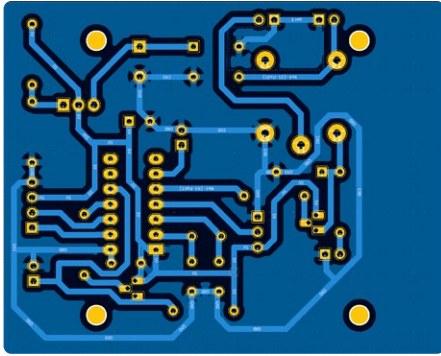


Figure 10: The PCB realized with KiCad.

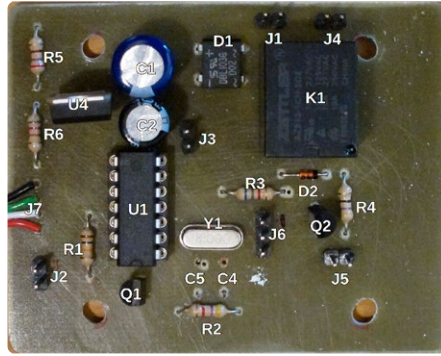


Figure 11: Top view of the populated PCB.

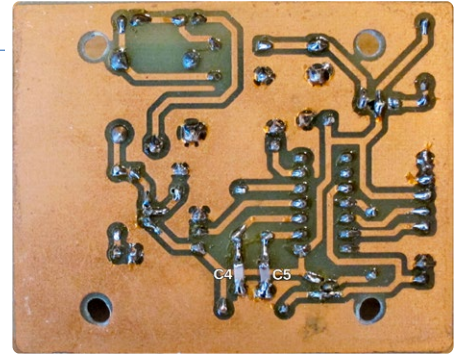


Figure 12: Bottom view of the soldered PCB, with add-on capacitors C4 and C5.

PCB

The PCB layout (Figure 10), as well as the schematics, were designed using KiCad [12]. The PCB is populated solely with through-hole components (Figure 11), and, in this prototype version of the board, some footprints were omitted: Capacitor C3 (100 nF) has been located in socket U1, while C4 and C5 (27 nF, SMD) capacitors have been soldered straight to the bottom side of the PCB, as shown in Figure 12.

Software

Features

Once again, before starting the software development, I like to put down my desired specifications:

- All user interaction must be performed using the three push buttons *UP*, *DOWN*, and *SET* on the 7-segment display.
- User dialogues for:
 - Setup of date and time — on long-pushing *UP* or *DOWN* button, the respective value must auto-increment/auto-decrement.
 - Setup of threshold temperatures for activation/deactivation of irrigation.
 - Switch irrigation on and off.
 - Send logged data.
 - Clear logged data.
 - Set display brightness.
- Communication with serial devices:
 - Temperature sensor.
 - Display (including push buttons).
 - Serial output.
- Timestamp generation.
- Log data output format must be both human- and machine-readable.
- All runtime parameters set by the user must be stored in EEPROM.
- Log data must be stored in EEPROM.

The software is set up as a state machine. The “heart” of the state machine is a timer-controlled interrupt service routine monitoring the temperature sensor and the push buttons as well as controlling the display, the serial output, and the irrigation solenoid (Figure 13).

Considering the demand for the time stamp generation on one hand and the requirement for communication with the serial devices (temperature sensor, display, and serial output) on the other, the ATtiny84 controller is configured to run at 1 MHz, which is a compromise between

power consumption and speed. This avoids problems with the available “bit-banging” serial software libraries (bit-banging is a way to use software and I/O lines to emulate serial communication, usually implemented on a specific hardware device).

As the register controlling the timer interrupt interval is 16-bit, to fulfill the feature requirement of “date and time logging” the timer interrupt interval must be an integer divisor of 1 s. So, the timer is set up to run at 20 Hz — issuing a timer interrupt every 50 ms. All operating modes (see below) are mapped to event-driven state machines [13] (no polling). Thus, all user dialogues must be designed to be non-blocking. An example of bit-banging is discussed later along with the source code for the serial output.

User Interaction

The push buttons are arranged to enable intuitive operation (see Figure 7). With a little bit of imagination, all the necessary information can be displayed on the 7-segment display (see Figure 14).

Operating Modes

One operation mode, *Watch*, is monitoring the temperature. Long-pressing the *SET* button during *Watch* mode causes a switch to *Menu* mode (the user dialog) and vice versa. In *Menu* mode (and all following user interaction modes) the irrigation solenoid is first turned off. *Menu* mode comprises a selection of sub-modes where the user can set or modify any of the controller’s runtime parameters (in order of appearance):

- Data transfer (*Data* mode).
- Irrigation on/off (*Irrigate* mode).
- Brightness setup (*Brightness* mode).
- Set up threshold temperatures (*Temperature* mode).
- Date and time setup (*Date_time* mode).

Pushing *UP* or *DOWN* repeatedly causes the menu to loop back to the other end of the menu tree (Figure 15).

On the first run after programming the ATtiny84 controller, none of the runtime parameters are configured. The controller starts in *Temperature* mode followed by *Date_time* mode to set up the initial run time parameters. In all user dialogues, long pressing the *SET* key takes the user back to *Watch* mode. The display is always switched off when leaving a user dialog.

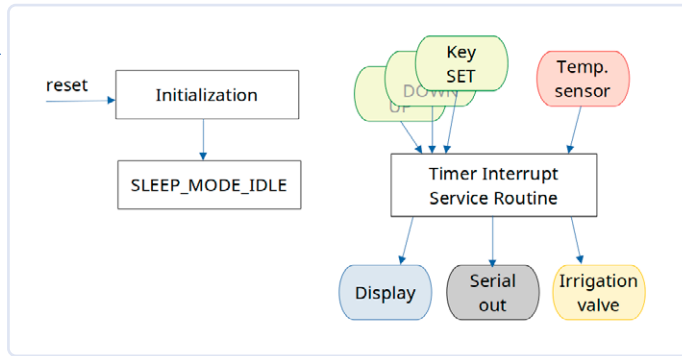


Figure 13: Software design block diagram.



Figure 14: Display messages.

User Dialogs

Each user dialog is implemented in a mode-specific module (function, subroutine).

Switching Irrigation On and Off (Irrigate mode)

As an example, let's discuss *Irrigation* mode with the aid of a flowchart (Figure 16). The event-based design demands working with internal sub modes for each module. All modules start with sub-mode 0 (for initial tasks) and perform final tasks on sub-mode *EXIT*. Sub-mode *EXIT* is set by the key monitoring part of the interrupt service routine on long-press of the *SET* button. Being quite straightforward, the irrigation module has one sub-mode (1) where the valve is toggled *on* or *off* when the user hits the *UP* or *DOWN* key. The display is set according to the solenoid status. During *on* status, the display flashes.

Setup of Date and Time (Date_time mode)

Setting the date and time requires several steps:

1. Initial Show year (display flashing).
2. UP/DOWN Increment/decrement year (display steady)
3. SET Show month (display flashing)
4. UP/DOWN Increment/decrement month (display steady).
5. SET Show day (display flashing).
6. UP/DOWN increment/decrement day (display steady).
7. SET Show hour (display and colon flashing).
8. UP/DOWN Increment/decrement hour (display steady; colon flashing).
9. SET Show minutes (display and colon flashing).
10. UP/DOWN Increment/decrement minute.
11. SET Exit. Date and stored by mode dispatcher.

On holding either the *UP* or the *DOWN* button, the respective value auto-increments/auto-decrements.

Setup of threshold temperatures (temperatures mode)

The temperature for activation of irrigation is called *low* temperature (default: 1.0°C).

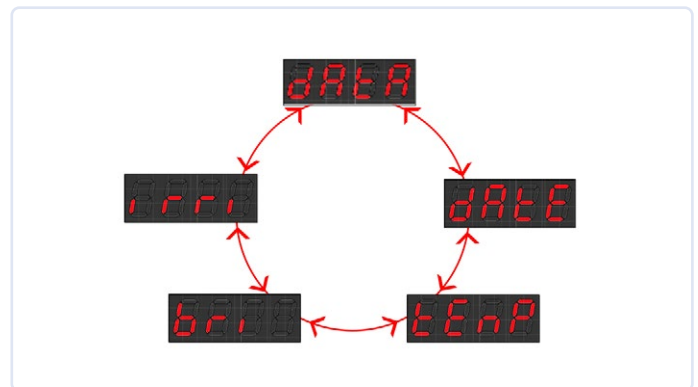


Figure 15: The round-robin menu display.

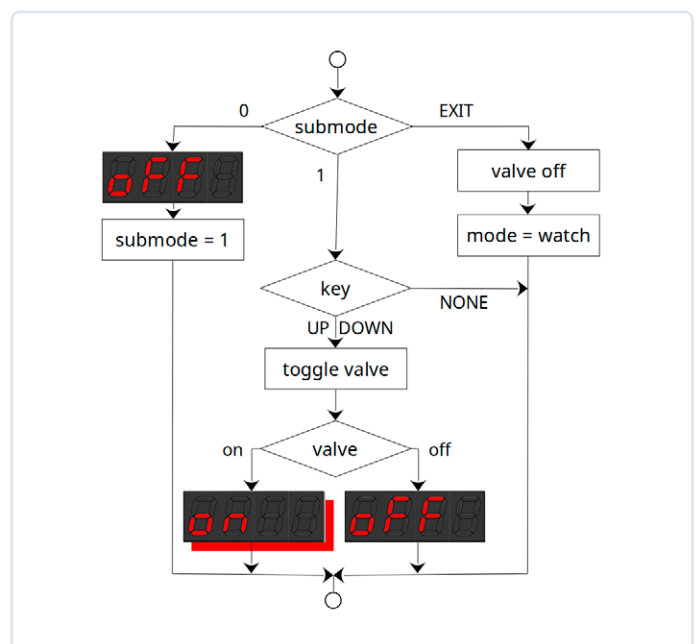


Figure 16: Flow-chart of Irrigation mode.

The temperature for deactivation of irrigation is called *high* temperature (default: 3.0°C).

Steps for *temperatures mode*:

- 1 Initial Show H in first digit, high temperature (display flashing).
- 2 UP/DOWN Increment/decrement high temperature (display steady).
- 3 SET Show L in first digit, low temperature (display flashing).
- 4 UP/DOWN Increment/decrement low temperature (display steady).
- 5 SET Exit. High/low temperatures stored by mode dispatcher.

Send/clear logged data (*data mode*)

The send/clear data dialogue depends on the state of data.

No data available:

- 1 Initial Show no d (display flashing).
- 2 SET Exit.

Data available:

- 1 Initial Show rEt (display flashing).
- 2 UP/DOWN Toggle display SEnd/rEt (display steady).
- 3 SET
- 3.1 On display rEt: exit.
- 3.2 On display SEnd:
- 3.2.1 Send data.
- 3.2.2 Display CLr (display flashing).
- 3.2.3 UP/DOWN Toggle display rEt / CLr (display stead).
- 3.2.4 On display CLr: Clear data and exit.
- 3.2.5 On display rEt: Leave.

Set display brightness (*brightness mode*)

- 1 Initial Show briX, where X in {0...7} (display flashing).
- 2 UP/DOWN Adjust brightness, show briX (display flashing).
- 3 SET Exit. Brightness stored by mode dispatcher.

Table 1. Irrigation Intervals.

| Temperature (°C) | Sensor Value | Irrigation Mode | Intervals |
|------------------|--------------|-----------------|------------------------|
| 1.0 | 2 | 1 | constantly on |
| 1.5 | 3 | 2 | 60 s on / 1 * 30 s off |
| 2.0 | 4 | 3 | 60 s on / 2 * 30 s off |
| 2.5 | 5 | 4 | 60 s on / 3 * 30 s off |
| 3.0 | 6 | 5 | 60 s on / 4 * 30 s off |

Log Data Output Format

The final feature request is fulfilled utilizing a "pretty print" JSON format.

Communication with Serial Devices

Communication is performed based on the work of Davide Gironi [14] for temperature sensor communication and Łukasz Marcin Podkalicki [15] for TM1637 display/push button controller communication. All serial communications are implemented using "bit banging" solutions.

Timestamp Generation

The timestamp is generated by counting timer events. The timer is configured in CTC mode ([8], page 74) firing an interrupt service routine every 20 ms. The timestamp is in the current epoch Unix timestamp format [16].

Watching the Temperature

The temperature is checked every 10 s. To show that the controller is operating, the display's colon is illuminated until the read out of the DS18S20 sensor is finished.

Before the start of communication with the DS18S20, it gets 200 ms power ("parasite power"). Communication begins with a device reset, performed by a 600 µs low pulse, which should be responded to with a low pulse after 100 µs. If the reset is disrupted, the display flashes and shows *no_r* for "no reset possible." Upon reset OK, temperature conversion begins. After conversion, the digital temperature data is read out from the sensor. If the sampled value exceeds 40°C or goes below -20°C, the software restarts the conversion, as the sampling result cannot initially be trusted.

Apart from *no reset possible* or a sensible converted value, the sensor might have encountered something out of the ordinary. This is displayed by flashing *no_d* for "no data."

When the *SET* button is pressed, the display shows the current sampled temperature for 10 s.

Irrigation

If the temperature reaches the low threshold (default: 1.0°C) irrigation starts. Irrigation stops if the temperature goes above the high threshold (default: 3.0°C).

| Address | Name | Value | Field | Option | Category | Setting |
|---------|----------|-------|-----------|-----------------------------------|--|--|
| 820000 | LOW | 7D | - | - | - | - |
| | | 3D | SUT_CKSEL | EXTXOSC_3MHZ_8MHZ_16KCK_14CK_65MS | Select Clock source | Ext. Crystal Osc. 3.0-8.0 MHz; Start-up time P |
| | | 1 | CKOUT | CLEAR | Clock output on PORTB2 | CLEAR |
| | | 0 | CKDIV8 | SET | Divide clock by 8 internally | SET |
| 820001 | HIGH | DF | - | - | - | - |
| | | 7 | BODLEVEL | DISABLED | Brown-out Detector trigger level | Brown-out detection disabled |
| | | 1 | EESAVE | CLEAR | Preserve EEPROM through the Chip Erase cycle | CLEAR |
| | | 1 | WDTON | CLEAR | Watch-dog Timer always on | CLEAR |
| | | 0 | SPIEN | SET | Serial program downloading (SPI) enabled | SET |
| | | 1 | DWEN | CLEAR | Debug Wire enable | CLEAR |
| | | 1 | RSTDISBL | CLEAR | Reset Disabled (Enable PB3 as i/o pin) | CLEAR |
| 820002 | EXTENDED | FF | SELFPRGEN | CLEAR | Self Programming enable | CLEAR |
| 830000 | LOCKBIT | FF | LB | NO_LOCK | Memory Lock | No memory lock features enabled |

Figure 17: Controller fuse bits.

Water crystallization is a slow process. Thinking about the nature of water running away in a liquid state and the demand to utilize the water's crystallization heat, I decided to pulse the irrigation instead of having the water flowing constantly. The temperature sensor sends the temperature as a signed 9-bit integer; the resolution is 0.5°C. The threshold temperatures are stored with the same resolution.

As shown in Table 1, irrigation is controlled by *Irrigation* mode derived from the temperature sensor value and the low threshold temperature value. The irrigation mode is registered in the data log.

Implementation

MCU Fuse Bits

The fuse bits are set to specify an external 8 MHz clock and internal divider by 8 (Figure 17).

Timer interrupt service routine

Each time the interrupt service routine is fired, it performs several tasks:

- Monitor key status
 - Status resulting is *NONE/UP/DOWN/SET/UP_LONG/DOWN_LONG/SET_LONG*
- Control of counters for display flashing period and timestamp
- Control of display/colon flashing
- Dispatch of operating mode
 - *Watch* mode
 - *Menu* mode
 - *Data* mode
 - *Irrigate* mode
 - *Brightness* mode
 - *Temperatures* mode
 - *Date_time* mode
- Update of runtime parameters to EEPROM

Globals, runtime parameters, and more

Here's the design of the runtime parameters in SRAM data memory, duplicated to EEPROM:

```
/**
 * data types
 */
typedef struct
```

```
{
    int8_t low;
    int8_t high;

} temperatures_t;

typedef struct params
// runtime parameters / copy in EEPROM
{
    temperatures_t temperatures;
    // threshold temperatures
    temperatures_t minmax;
    // min/max temperatures sampled
    uint32_t timestamp;
    // 0 is January 1st, 1970, 00:00:00
    uint8_t brightness;
    // values 0...7
    int8_t write_index;
    // event data EEPROM write index

} params_t;
```

The `params` runtime parameter structure keeps the threshold temperatures as well as the lowest and the highest temperatures registered. Structure members `timestamp` and `brightness` have already been discussed. The `write_index` member is for writing the irrigation event to EEPROM. To manage the state of the different operation modes, global structure `globals` is used:

```
/**
 * globals - see file "globals.h"
 */
typedef struct
{
    params_t params;
    // run time parameters
    uint8_t mode;
    // operation mode
    uint8_t submode;
    // sub mode
    uint8_t flash;
```

```

        // display/colon flash indicator
uint8_t    colon_status;
        // colon status off/on/flashing
uint8_t    display_status;
        // display status off/on/flashing

```

```

} globals_t;

```

Members `mode` and `submode` have been discussed in user dialog for *Switch Irrigation on and off*. Members `colon_status` and `display_status` do exactly what the comments in the listing say. Member `flash` is toggled every 400 ms between 0 and 1 and evaluated together with `colon_status` and `display_status` to perform the corresponding flashing action with the display's colon and its 4 digits. Each irrigation event is recorded with a timestamp and temperature. The recorded data is written into the controller's EEPROM memory until it's full. The ATtiny84's EEPROM has a size of 512 bytes. An event takes 6 bytes:

```

typedef struct    // irrigation event data
{
    uint32_t    timestamp;
                // time since 1970-01-01 00:00:00
    int8_t    temp;
                // binary temperature 0.5[°C] resolution
    uint8_t    irrigation_mode;
                // irrigation mode
} event_t;

```

The EEPROM also holds the runtime parameters (10 bytes — see above). Thus, the EEPROM has a maximum capacity of $(512 - 10) / 6 = 83$ events. Practice has shown that this memory size is enough for two or three nights of frost guarding.

Logged Data Output

Utilizing a mobile phone with a USB OTG adapter and an FT232RL USB-to-TTL serial adapter [17] (see **Figure 18**) and a serial terminal app, data can be dumped at 19,200 Baud in JSON pretty print format.

Here's an excerpt of logged data transfer from 2022-03-02.

Variables `tH` and `tL` represent the threshold temperature parameters. Variables `mH` and `mL` represent the maximum and minimum temperatures sampled. Irrigation event data has the variables:

```

> n    entry number
> ts   time stamp
> tm   temperature of irrigation event
> im   irrigation mode

```

```

{
  "tH": 3.0,
  "tL": 1.0,
  "mH": 12.0,
  "mL": -3.5,

```



Figure 18: The FT232RL-based USB-to-TTL serial adapter, wrapped in heat-shrink tubing to protect it from condensation.

```

"ev": [{
  "n": 0,
  "ts": "2022-03-02 20:31:14",
  "tm": 1.0,
  "im": 1
},{
  "n": 1,
  "ts": "2022-03-02 20:36:46",
  "tm": 1.5,
  "im": 2
},
...
}

```

Serial Transfer

The serial data transfer utilizes the `uart_tx()` function (from `uart.c`) performing "bit-banging" at 19,200 Baud with a bit period of 52.1 μ s.

```

void uart_tx(register char data)
{
    register uint8_t bit = _BV(0);
    register uint8_t pb;

    UART_TXDRR |= _BV(UART_TXBIT);
        // out
    UART_TXPORT &= ~_BV(UART_TXBIT);
        // start bit
    _delay_us(42);
    while (bit) {
        pb = UART_TXPORT;
        if (data & bit)
            pb |= _BV(UART_TXBIT);
        else pb &= ~_BV(UART_TXBIT);
        UART_TXPORT = pb;
        _delay_us(41);
        bit <<= 1;
    }
    _delay_us(7);
    // compensation for end of while - last bit


    UART_TXPORT |= _BV(UART_TXBIT);
        // stop bit
    _delay_us(40);
    UART_TXDRR &= ~_BV(UART_TXBIT); // in
}

```

The delay times are adjusted to the real bit time of 52 μ s, close enough to 52.1 μ s for reliable data transfer at a wide temperature range.

My first implementation was at 57,600 Baud with a 17.4 μ s bit period. This worked fine in my heated development shack, but was unreliable at low temperatures in my unheated garden shed.

Elektor Labs Webpage

The Software can be downloaded from this project's Elektor Labs page at [18]. Feel free to leave comments about the project there! 

210272-01

Questions or Comments?

Do you have technical questions or comments about this article? Email the author at thomas@dausner.de or contact the Elektor editorial team at editor@elektor.com.



About the Author

Thomas Dausner (Dipl. Ing. FH) is an electronics engineer. After he graduated in 1983, the influence of IT was becoming increasingly more important in development lab environments, and the emphasis was moving away from hardware towards software development. He was inspired to develop applications using MCUs in the 2000s by studying articles featured in Elektor. In addition to electronics and full-stack web application development, Thomas Dausner is a passionate diving instructor and underwater photographer.

List of Files in Software Download

Software can be downloaded from the project's Elektor Labs page [18].

| File Name | Purpose |
|--------------------------|--|
| <i>ds18x20.h</i> | definitions for temperature sensor |
| <i>frostguard.h</i> | project definitions |
| <i>globals.h</i> | definition of globals |
| <i>time.h</i> | definitions for CPU speed and timer control |
| <i>tm1637.h</i> | definitions for display and push buttons control |
| <i>uart.h</i> | definitions for serial TTL output control |
| <i>ds18x20.c</i> | temperature sensor control |
| <i>frostguard.c</i> | <code>main()</code> function, timer interrupt service routine with mode dispatcher |
| <i>globals.c</i> | global variables |
| <i>mode_brightness.c</i> | brightness control mode |
| <i>mode_data.c</i> | data transfer mode |
| <i>mode_datetime.c</i> | date and time setting mode |
| <i>mode_irrigate.c</i> | irrigation test mode |
| <i>mode_menu.c</i> | menu mode |



Related Product

➤ **Warwick A. Smith, *Explore ATtiny Microcontrollers using C and Assembly Language* (Elektor, 2021)**
www.elektor.com/20007

WEB LINKS

- [1] Rain Bird Magnetic Valve 100-HV: <https://mnrainman.com/100-HV>
- [2] Circular sprinkler: <https://tinyurl.com/5br2xjc6>
- [3] FT232RL USB to TTL serial adapter: <https://tinyurl.com/f6s9242w>
- [4] DS18S20 High-Precision 1-Wire Digital Thermometer data sheet : <https://tinyurl.com/4bd485aw>
- [5] Cable length for LM35 and DS18B20: <https://ogalik.ee/cable-length-for-lm35-and-ds18b20>
- [6] Module box ABS, 100x68x50 mm, IP65: <https://tinyurl.com/ypzbus49>
- [7] Plug set 8 mm 2-pin with spring lock: <https://tinyurl.com/mu263s5c>
- [8] Plug Set 12 mm 4-pin with spring lock: <https://tinyurl.com/37wvm8c3>
- [9] ATtiny24/44/84 data sheet: <https://tinyurl.com/35mf4byw>
- [10] 7 segments 4 digits display from az-delivery: <https://tinyurl.com/3s8cz7wz>
- [11] TM1637 data sheet: <https://tinyurl.com/3btawxnp>
- [12] KiCad EDA Cross Platform: <https://kicad.org>
- [13] Event-based vs polling: <https://tinyurl.com/nhdyk6t>
- [14] DS18x20 library by Davide Gironi: <https://tinyurl.com/4zk2j8ku>
- [15] TM1637 library by Łukasz Marcin Podkalicki: <https://github.com/lpodkalicki/attiny-tm1637-library>
- [16] Current Epoch Unix Timestamp: <https://unixtimestamp.com>
- [17] FT232RL USB to TTL serial adapter: <https://az-delivery.de/products/ftdi-adapter-ft232rl>
- [18] Software Download Page: <https://elektormagazine.com/210272-01>



The Analog Thing

The Arduino of Analog Computing?

By Clemens Valens (Elektor)

For most people, a computer is a digital electronic device like the laptop on which I am typing this review. There are, however, other types of computers, and one of them is the analog computer. In this review, we will examine The Analog Thing (THAT), an open-source analog computer designed by the German company Anabrid.

An Analog Computer?

Unlike a digital computer that manipulates discrete binary values, an analog computer processes data represented by continuous physical quantities, such as electrical voltages or mechanical movements. Analog computers can solve complex differential equations and simulate physical systems in real-time. They were used in early aerospace and military applications, where they helped to understand complex dynamic systems and control theory.

The complexity, limited precision and limited flexibility of analog computers make them hard to use. Therefore, they have been

superseded by digital computers in most applications. And this is where the Berlin-based company Anabrid comes in. Their (self-imposed) mission is to reintroduce the analog computer as a complement to the digital computer to help keep Moore's law alive, to save energy, and to improve security. One of their tools to achieve their mission is The Analog Thing (abbreviated to THAT).

An Intriguing User Interface (IUI)

The Analog Thing is a flat, rectangular (20 cm by 24 cm) sandwich of two white printed circuit boards (PCBs) with a height of approximately 38 mm. The lower board carries all the electronic components. The (thick) upper board provides the user interface with intriguing symbols printed in black on it. About half of its surface is reserved for a 17 × 10 patch matrix/bay/panel. Each patch hole is at the center of a graphical symbol: a circle, a diamond, or a triangle. Triangles are white, circles are white or black while diamonds come in white, black and half-white/half-black (see **Figure 1**).

The patch panel is subdivided into 17 computing elements where each element represents a mathematical function like integrator (5×), multiplier (2×), summer (4×), inverter (4×) and comparator (2×). There are also eight coefficients and four ± 1 constants.

Below the patch panel are two more rows of holes with capacitors (5×), diodes (4×), Zener diodes (2×) and four signal outputs.

The patch panel is separated from the control panel by the name of the device, printed from left to right in large characters. The control panel consists of nine potentiometers (COEFF 1 to 8 and OP-TIME) and two rotary switches (COEFFICIENT and MODE). There is also a numerical LCD panel meter, and three LEDs provide some status information.

At the top side of THAT we find all the connectors: power (USB-C, only a cable is included, not a power supply), outputs (RCA, a stereo cable is included) and extension (pin headers, one 2×5 flat cable is included).

Patch Cables

Like digital computers, THAT doesn't do anything without a program. However, loading software is not a matter of connecting a thumb drive or a microSD card. Programming is done by sticking 2-mm banana-plug patch cables into the holes of the patch panel. The Analog Thing comes with 30 patch cables in five colors.

Display Not Included

The Analog Thing produces analog signals in the shape of voltages in the range of -1 V to $+1\text{ V}$ (the precision of THAT is about 1%). A signal can be made available on four output connectors X, Y, Z and U. To visualize them, an oscilloscope or a computer with soundcard (or other analog input) is required. In many cases, you want a XY(Z) display, so the oscilloscope should have an XY(Z) mode. For optimal results, these inputs should feature DC-coupling. Therefore, a sound-card is not the best option.

THAT can output up to four signals, and so a 4-channel oscilloscope is ideal. It is therefore a bit unfortunate that the output connectors are RCA and not BNC. This was probably done to keep the costs low and make it all fit. RCA-to-BNC adapters are not included.

The panel meter is a 3.5-digit ($\pm 1,999$ count) voltmeter (**Figure 2**). However, as far as I could determine, it cannot be connected to signals produced by the unit's computing elements. Its use is to display coefficient values and show the execution speed.

Master-Minion Chaining

One last thing to mention before going into the programming of THAT is the extension option. When more computing elements are needed than are available on THAT, it is possible to connect one or more units in series. The first one will be the master, while the others are the "minions". The number of elements in a chain is said to be unlimited.

As a side note, I have come across other attempts to remove the master-slave paradigm from electronics speak, but never this one. Even though I find it quite nice, I am not sure to adopt it, as Master and Minion both start with "M". As an example, on a SPI bus, MISO (Master In Slave Out) and MOSI (Master Out Slave In) would both become MOMI. Maybe rename Master to "Gru"? Then we would get GIMO & GOMI.

What Can You Do with THAT?

Programming The Analog Thing is not done by typing strange commands into a terminal or text editor, but by plugging cables into the patch panel. It is similar to visual programming where functional blocks are connected with virtual wires.

An analog program is a mathematical expression that describes a dynamic system, i.e. a system that evolves over time according to known relationships. So, in order to make THAT do something useful, you must first come up with a suitable mathematical model. This alone makes analog computing almost inaccessible to most mortals. Believe it or not, but differential equations are just not as popular as Python or TikTok.

Example Programs

To help you get started with analog programming on THAT, its user manual features nine examples, from mathematical curiosities to real-world applications. Each example explains the model it implements, presents the mathematical equations and its corresponding signal flow diagram, the cabling diagram (the patch), and the expected output graph.

**Felonius Gru is the supervillain-turned-hero helped by an army of yellow minions made popular by the "Despicable Me" movie series.*

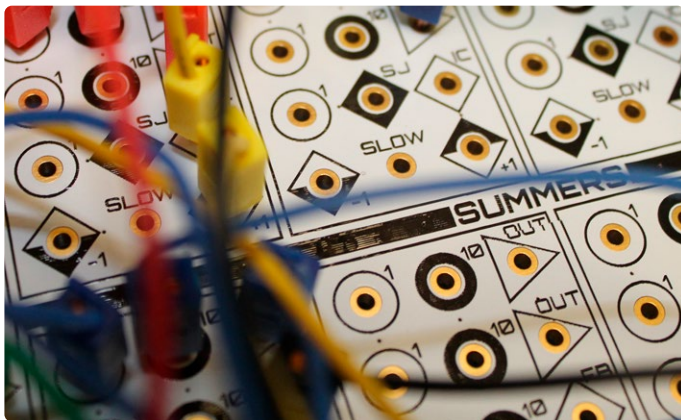


Figure 1: Strange symbols in black and white printed on the patch panel provide guidance when programming THAT.



Figure 2: The panel meter is for setting coefficient values, not for displaying signals produced by the analog program.

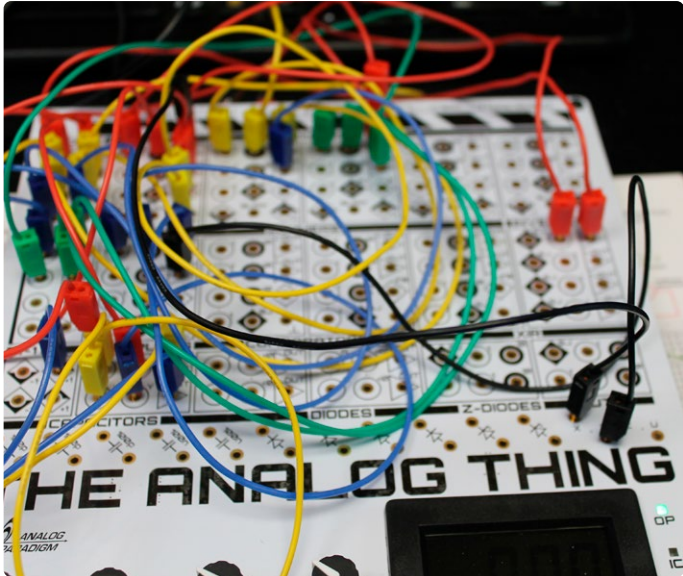


Figure 3: As the dictum says: "chaos in, chaos out." This chaotic patch-cable spaghetti implements a Lorenz attractor, the "Hello World!" of chaos theory.

To apply a patch, you plug the patch cables on THAT according to the cabling diagram. For those who are old enough to have done it, this must be done with the same care as copying a BASIC program listing from a computer magazine in the eighties. One mistake and the program won't work. The danger here is not so much plugging a cable in the wrong hole as the multicolor patch diagrams are quite clear, but to not forget a cable. Sifting through the patch cable spaghetti to figure out which wire is wrong or missing isn't easy (Figure 3).

Setting Coefficients

After patching THAT, you must set the coefficients used in the patch. A coefficient is simply a "volume" potentiometer that has its input in the COEFF section. To set the value of a coefficient, set the rotary COEFFICIENT switch to the coefficient's number (1 to 8) and set the MODE switch to COEFF. The LCD now shows the coefficient's value. You can adjust it by turning the corresponding potentiometer. Three-decimal precision is doable (with some patience). Note how in the *Lunar Landing* example two coefficients are put in series to obtain even higher precision values.

Execute an Analog Program

Now it is time to execute the patch. For this, rotate the MODE switch to the OP position. The OP LED will light up. Connect a suitable display device to the outputs of THAT. The *Lunar Landing* example has three output signals (X, Y and U) so a 3-channel display would be best.

In OP-mode, the patch is executed once. In REP-mode, the patch is executed repeatedly. REPF-mode repeats 100x faster than REP mode. Note that every repetition is preceded by a restart of the patch as the integrators must be reset to their initial condition. This makes it complicated to create a smoothly repeating patch. Those interested in using THAT in e.g., musical applications would probably be better off with continuously evolving patches than with repeating patches.

Hello, Analog World!

The first example from the user manual, *Radioactive Decay*, can probably be considered as the equivalent of the "Hello World!" example in

digital computer programming. It implements a first-order differential equation well known to electronics enthusiasts as it also applies to discharging a capacitor C through a resistor R:

$$\frac{dV}{dt} = -\frac{V(t)}{RC}$$

The example uses λ in place of $1/(RC)$ and V is called N but that doesn't change anything.

The patch requires six wires and runs in REP mode. The oscilloscope shows a nice exponential curve representing radioactive decay (or a capacitor discharging through a resistor, see Figure 4). Potentiometer 1 controls the amplitude, potentiometer 2 controls the slope.

As a second example, I tried the *Lorenz Attractor*, related to the well-known Butterfly Effect (a tiny change in an early system state can result in huge differences in later states). This complex patch consumes 22 wires (see Figure 3), and six coefficients must be carefully adjusted one by one. A 2-channel (analog) oscilloscope in XY mode gives the best results. I managed to patch the program without making mistakes and was then hypnotized by the continuously changing graph.

Mainly an Educational Tool

The quality of the Analog Thing is outstanding. It is nicely made and well thought out. Patch holes, albeit simple gold-plated holes, provide good contact, even with sometimes wiggly banana-plug patch cords. The LCD panel meter's readings are stable, and the potentiometers turn smoothly.

Electronics engineers may be attracted to THAT as they are used to circuits with integrators and other computing elements found on it. Turning a simple model into a patch diagram should be doable for certain enthusiasts but how to convert the equations of the *Euler Spiral* of example 9.5 needs a bit more explaining than provided in the "First Steps" booklet. Sticking in wires randomly will most probably result in frustratingly flat outputs clipping at the min or max value.

Maybe one day The Analog Thing will become the Arduino of analog computing, supported by thousands of community-made models and patch diagrams. The initial conditions for huge popularity have been set. Like Arduino, THAT is open source, and the design files can be found at GitHub [1]. However, until takeoff, THAT is mainly an educational tool and a curiosity for people interested in playing with mathematical models. In any case, whatever you do with it, it is a great conversation starter. ◀

240391-01

Questions or Comments?

Do you have technical questions or comments about his article? Email the author at clemens.valens@elektor.com or contact Elektor at editor@elektor.com.

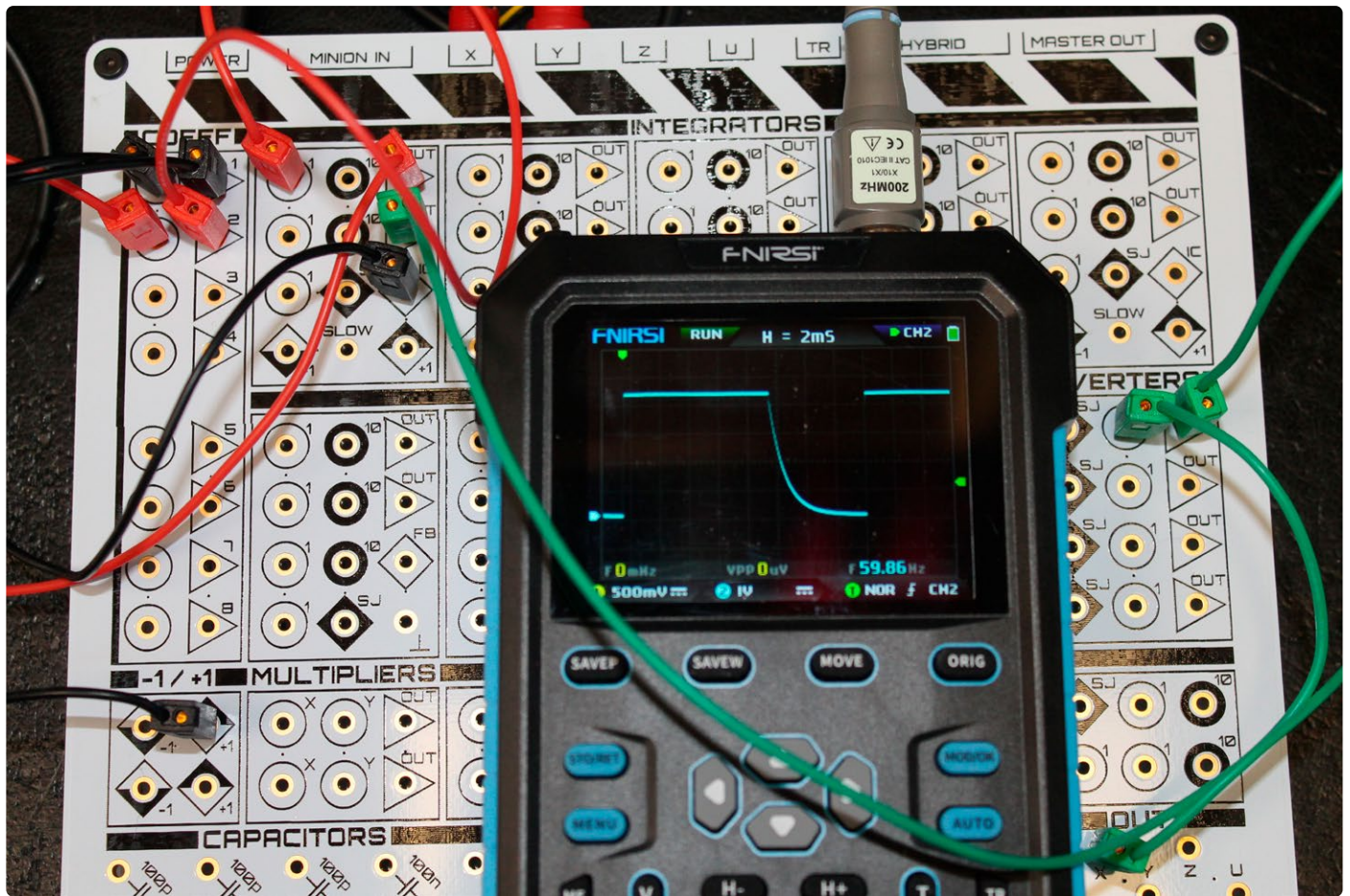


Figure 4: The "Hello World!" in analog computing is the output of a first-order differential equation. Note the horizontal part, which is due to the initialization sequence.



Related Products

- › The Analog Thing (THAT) Analog Computer
www.elektor.com/20918
- › Siglent SDS1104X-E 4-ch Oscilloscope (100 MHz)
www.elektor.com/19370

WEB LINK

[1] The Analog Thing on GitHub: <https://github.com/anabrid>



Energy Saving Relay Driver

Saves 90% of Relay Drive Power

By Frank Bachmann (Germany)

With energy costs skyrocketing, any contribution, however small, to reduce energy consumption has got to be welcome. I noticed that a relay with a coil designed for use from an AC mains supply will consume around four times more energy than an equivalent relay driven from a DC supply. By using clever coil driving, we can make even more energy savings.

The datasheet for a DC relay will typically give the rated operating voltage and holding voltage of the actuating coil. Applying the operating voltage to the coil will ensure the armature is pulled in and the relay contacts switch. Once the relay has switched it is possible to reduce the coil drive voltage to its holding level which keeps it in its switched state. Using this information we can design an efficient relay drive circuit that uses significantly less energy than the standard on/off relay control. If, for example, we halve the coil voltage, power consumption will drop to just 25%. To optimize these savings, the circuit described here reduces the hold voltage to one-third of the relay's rated voltage, which, in this case, cuts the power used by the relay coil from 400 mW down to just 45 mW!

The Circuit

The DC power supply to drive the relay is provided by a classic capacitive power supply configuration. Here the value of the coupling capacitor is calculated to ensure that the voltage applied to the relay coil is only one-third of the relay's rated operating voltage. The relay control is handled by a voltage-triggered switching stage. This ensures that the relay briefly receives the rated voltage during the switching process, to ensure fast and reliable activation. After that, the voltage drops to its holding value of 4 V for a relay rated at 12 V.

The proposed prototype circuit was first tested using MultiSim [1] (**Figure 1**), and the component values were adjusted to achieve a relay voltage of 4 V. Using this simulation it was possible to assess the energy-saving potential of the circuit. As the simulated currents and voltages showed, significant energy savings and reliable relay operation could be ensured, which allowed for the construction of a practical circuit (**Figure 2**).

A fusible resistor R1 at the mains input K1 serves both as a current-limiting resistor and fuse. Following this are capacitors C2 and C3, connected in parallel, providing a capacitive series impedance. The value of these capacitors is chosen so that about one-third of the relay's rated voltage is applied during operation. A look at the relay manufacturer's datasheet will provide information on the minimum holding voltage and the relay coil resistance. The following formula helps calculate the values for C2/C3:

$$C = \frac{I_{\text{Relay}} \times k}{2\pi \times f \times V}$$

$$= \frac{11111 \mu\text{A} \times 1.12}{2 \times 3.1416 \times 50\text{Hz} \times 230\text{V}}$$

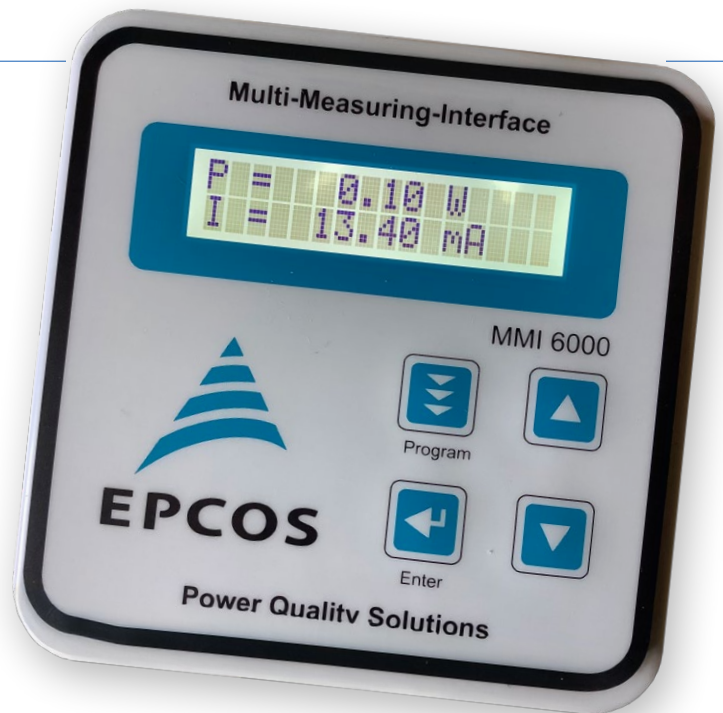
$$= 0.1722 \mu\text{F}$$

where:

- > k: Correction factor for the ratio between AC and DC current
- > I_{Relay} : Relay current at 4.0 V (360 Ω coil impedance)

The key factor in this formula is the current through the relay coil when the voltage is reduced to its holding value. The correction factor in the formula is an estimated value that takes into account the theoretical AC-to-DC voltage ratio of 1.41, the resulting current ratio, and the voltage drops across the bridge rectifier and transistors. A factor of 1.12 applies for the 12 V relay used, while for a 24-V relay, the value is increased to 1.14. These values were determined by practical testing and simulations using MultiSim. **Calculation tip:** If you scale the current in the formula in microamperes, the result will give you the capacitance in microfarads directly.

R2 and R3 are the necessary discharge resistors for the two capacitors. Two equal-value resistors are wired in series in order not to exceed the maximum allowable voltage across the wired (0207 outline) resistor. The bridge rectifier (Br1) uses capacitor C4 as a



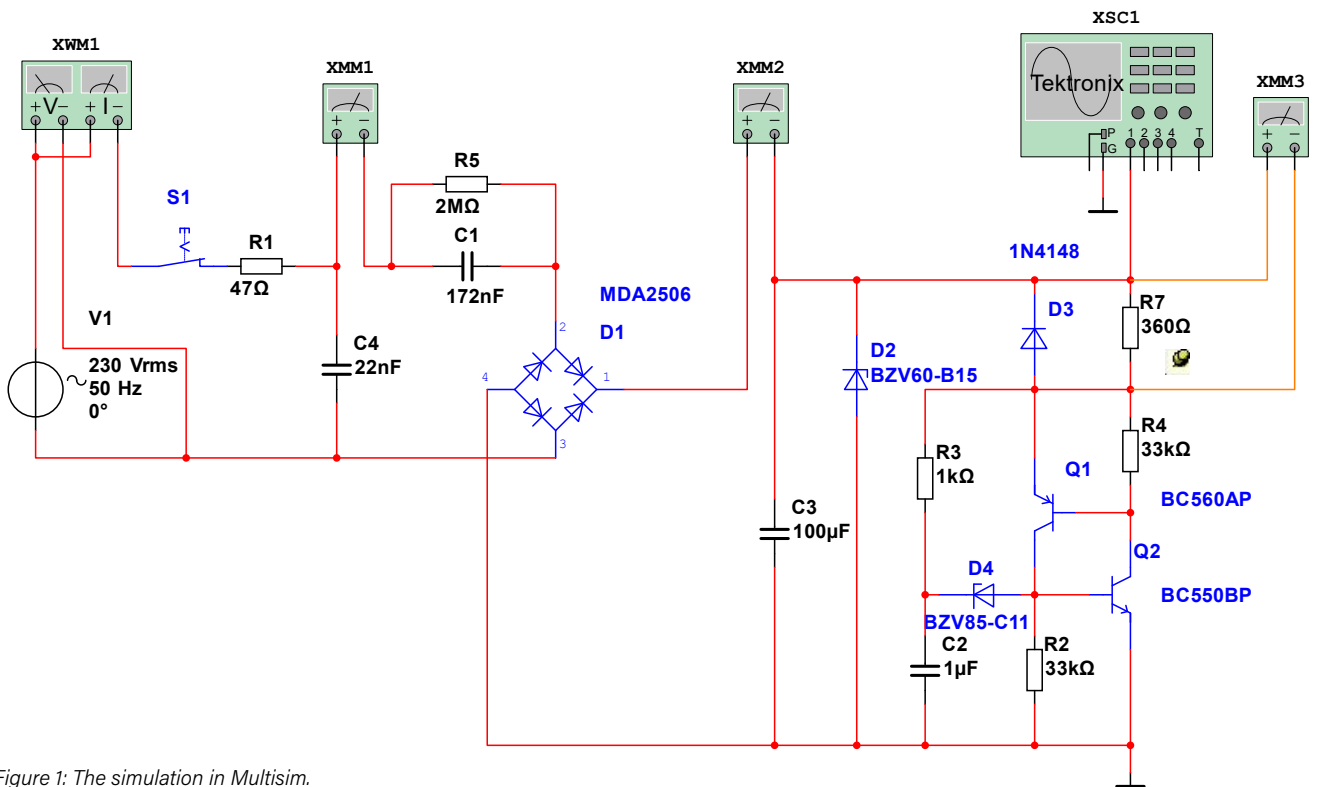


Figure 1: The simulation in Multisim.

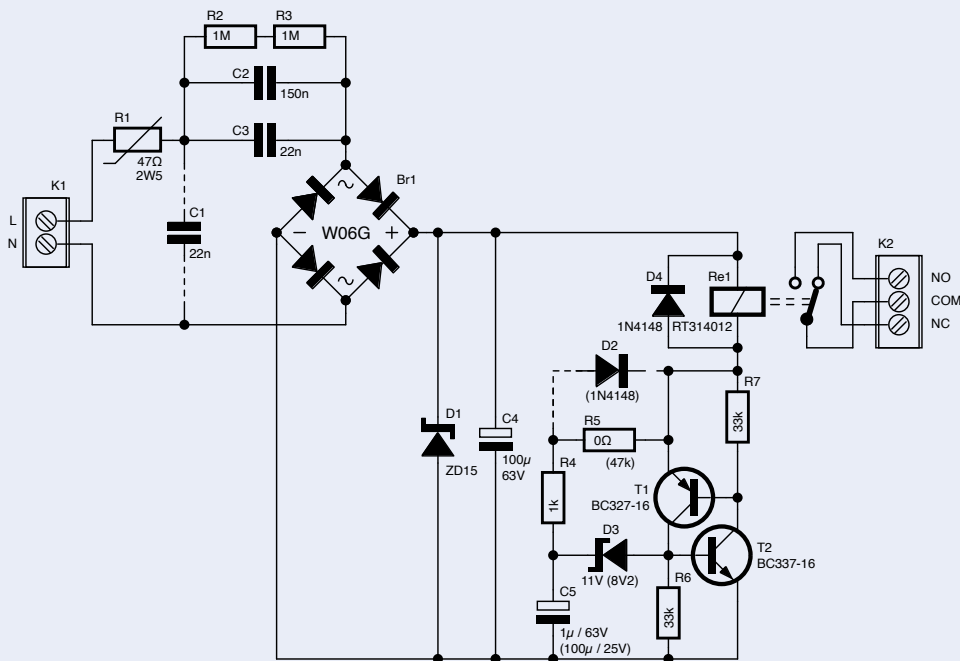


Figure 2: The final circuit of the energy-efficient mains relay. Component values for the version with a turn on delay are shown in parentheses.

reservoir and smoothing capacitor for the full wave rectified waveform. The Zener diode across C4 prevents overvoltage, which could damage capacitor C4 in the event of a relay coil failure.

Capacitor C4 begins to charge when mains voltage is applied to the circuit. This is repre-

sented by the blue trace in the oscilloscope display in **Figure 3**. C5 is charged in parallel with C4 via the relay coil and resistor R4 (green line) until the Zener voltage of D3 is exceeded. At this point, current flows into the base of T2, turning it on, which in turn causes T1 to conduct as well. This results in T2 taking over the base current for T1, and the circuit

locks in place like the action of a triggered thyristor. The relay is switched at its rated voltage (green line). The capacitive power supply can now only deliver a lower pre-defined current, and the voltage at C4 drops to its holding value. In the "trigger circuit," the current drops to zero because almost no voltage remains across the Zener diode.

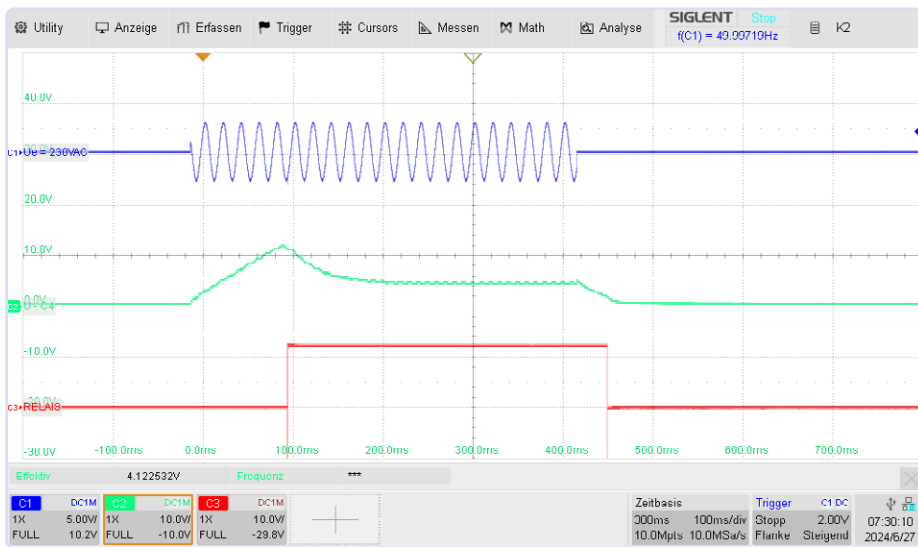


Figure 3: Oscilloscope traces showing the on/off mains voltage switching (via a divider) on channel 1 (blue), DC voltage at capacitor C4 on channel 2 (green), and DC voltage at the relay contact on channel 3 (red).

The purpose of C1 is to act as a kind of “energy sink.” In its off state, this circuit can act as a sort of “energy accumulator,” meaning that even small leakage currents or any capacitively-coupled charge can accumulate and slowly charge capacitor C4, potentially causing the relay to switch unintentionally. In this context, capacitor C1 serves as a kind of load for AC signals, though it does not increase the overall power consumption. Due to the charging curve of C4, the circuit introduces a small turn-on delay of about 100 ms.

Delayed Turn On

With a few small modifications, the same circuit on the same PCB layout can be modified to produce a longer turn-on delay. This feature can be useful as a speaker turn-on delay or for a muting function in a

power amplifier powered by a switching power supply. In such cases, fast turn-off can only be achieved by detecting the voltage on the mains side of the power supply, which can be accomplished with this simple circuit.

To create a turn-on delay with this circuit, resistor R5 is added in parallel with diode D2, the value of C5 is increased, and the Zener diode D3 is changed. The diode D2, which is reverse-biased while C5 is charging, ensures C5 will be discharged when the relay is switches on. This makes sure that the circuit will respond with the same delay time after being switched off and then back on again.

In the specified configuration, the delay time is about 4 seconds, as shown in the oscilloscope

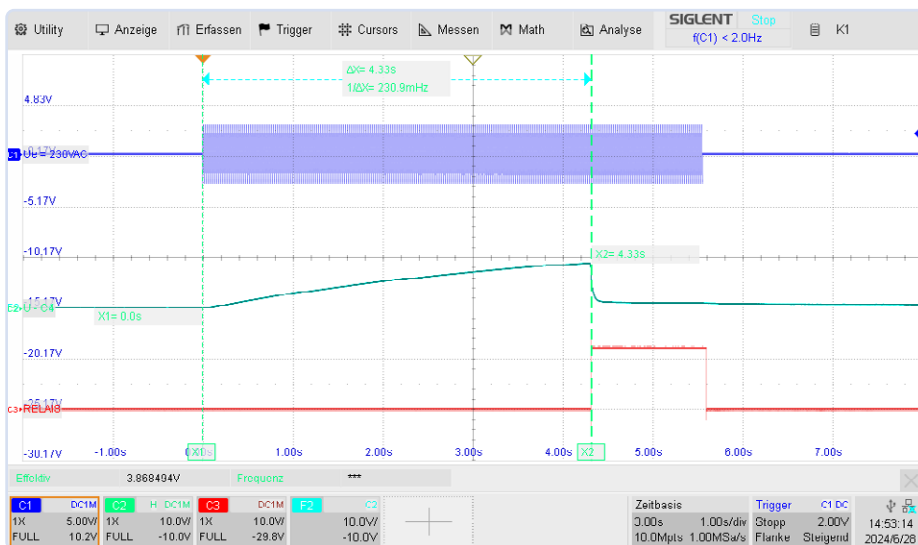


Figure 4: Mains voltage (blue), voltage on capacitor C4 (green) and relay contact voltage (red) for the version with turn on delay.

Component List

The values shown will switch the relay with a very short turn on delay (values given in brackets will produce a turn on delay of about 4 s).

Resistors:

R1 = 47 Ω , 2.5 W, Fusible resistor VSW 2.5-47
R2, R3 = 1 M Ω
R4 = 1 k Ω
R5 = 0 Ω or wire link (47 k Ω)
R6, R7 = 33 k Ω

Capacitors:

C1 = 0.022 μ F, 250 VAC, X1/X2 (optional, see text)
C2 = 0.15 μ F, 250 VAC, X1/X2, for 12 V relay with 360 Ω coil
C2 = 0.068 μ F, 250 VAC, X1/X2, for 24 V relay with 1440 Ω coil
C3 = 0.022 μ F, 250 VAC, X1/X2
C4 = 100 μ F, 25 V (12 V relay)
C4 = 100 μ F, 35 V (24 V relay)
C5 = 1 μ F, 63 V (100 μ F, 25 V for 12 V-Relay, 100 μ F, 35 V for 24 V relay)

Semiconductors:

D1 = Zener diode rated at 15 V for 12 V relay, 30 V for 24 V relay
D2 = not fitted (1N4148)
D3 = Zener diode rated at 11 V for 12 V relay, 22 V for 24 V relay
(8.2 V for 12 V relay, 16 V for 24 V relay)
D4 = 1N4148
Br1 = Bridge rectifier 1 A, >200 V, e.g. W06G
T1 = BC327
T2 = BC337

Miscellaneous:

Re1 = Relay 12 V (360 Ω coil), e.g. Schrack RT314012
Re1 = Relay 24 V (1440 Ω coil), e.g. Schrack RT314024
K1 = 2-way 7.5 mm pitch terminal block
K2 = 3-way 7.5 mm pitch terminal block

waveform in **Figure 4**. The turn-off delay — i.e., the time between cutting the mains power and the relay contact releasing — is approximately 45 ms. Reducing the value of C4 from 100 μ F to 33 μ F will reduce this time.

Power Savings

For comparison an equivalent relay with a coil rated at 230 VAC consumes around 1.6 W. The circuit presented here requires just 0.1 W! This translates to a power saving of 1.5 W, which

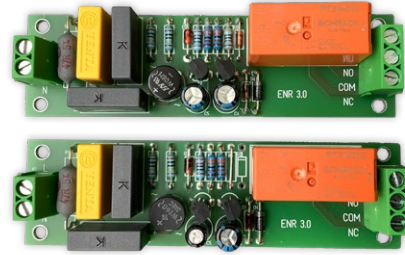
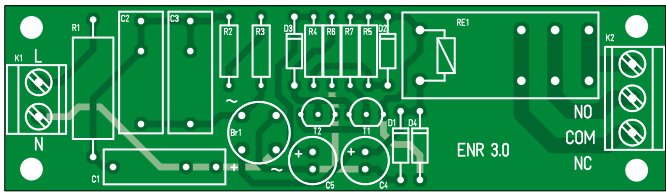



Figure 5: PCB layout with component placement and PCB image.

amounts to a saving of around 13 kWh per year in continuous operation. A DC relay also costs about half as much as an equivalent AC version.

Safety Notice: This entire circuit operates at lethal mains voltage so it is absolutely essential to install it in a housing or device to ensure that no part of the circuit can be accidentally touched or come into contact with any conductive material! When assembling the circuit, proper clearance and creepage isolation must be maintained around components and tracks carrying high voltage.

Component Selection

The efficient mains relay is built on a small PCB (**Figure 5**). You can download the layout (PDF) and a Target3001! project from the project page [2]. The fusible resistor R1 can have a value between 47 Ω and 100 Ω . Capacitors C1, C2, and C3 must be of X-certified type (X1 or X2). These capacitors can be operated directly at mains voltage.

All the remaining components are non-critical. The bridge rectifier does not necessarily need to be rated at mains voltage. You can use either a 12 V or 24 V relay, but the values of capacitors C2/C3 must be chosen to match the coil resistance. When a 24 V relay is used, the values of capacitors C2/C3 are halved, which represents another cost saving. 

Translated by Martin Cooke — 240090-01

About the Author

Frank Bachmann has been interested in electronics since childhood. After completing his apprenticeship as an electrical technician, he moved to an electronics manufacturing company and qualified as an electronics technician. From production, he moved into development, eventually taking on the role of development manager at various companies. During this time he developed hardware and software solutions for control devices to provide reactive power compensation, power meters, and switching devices for power capacitors based on thyristors. Frank Bachmann is now enjoying his retirement on the island of Rügen.

Questions or Comments?

Do you have any questions or comments regarding this article? Contact the author at wanderlumi33@yahoo.de or the Elektor team at editor@elektor.com.



Related Product

> ZOYI ZT-703S (3-in-1)
2-ch Oscilloscope (50 MHz) +
Multimeter + Signal Generator
www.elektor.com/20963



FEATURED TOPIC

Visit our **Power Electronics & Energy** page for articles, projects, news, and videos.

www.elektormagazine.com/power-energy



WEB LINKS

[1] MultiSim: <https://www.multisim.com/>

[2] Project page with PCB layout: <https://www.elektormagazine.com/240090-01>

Improving the ET5410A+ DC load

Keep Cool and Be Quiet, Please



By Jean-François Simon (Elektor)

The ET5410A+ is an affordable DC load, but its fan is very noisy. Let's modify it for both quieter operation at light loads and better performance at full throttle.



Figure 1: The ET5410A+.

When you're looking to add a DC load to your lab for testing power supplies or studying battery discharge, there are few low-cost options. I opted for the ET5410A+ (**Figure 1**), sold under the East Tester and Mustool brand names. I took advantage of a temporary offer to get it for €162. Apart from the Kunkin KP184 with identical specifications (150 V, 40 A) and a relatively similar price, the other cheaper options are almost two times more expensive, such as Korad's KEL103 which can be found for around €330. Overall, the device gets the job done, but the cooling fan is particularly noisy.

A Very Noisy Fan

At no load, or at low power dissipation, I've observed a noise level of 50 dBA, even though my lab is rather quiet (32 dBA ambient). Let's see if it's possible to reduce noise without degrading performance. Measurements have shown that the fan speed is controlled by the instrument's main microcontroller as a function of the power dissipated in the load, in three steps. The temperature sensor (RT1) attached to the heatsink is therefore only used as a safety device, and not directly for regulation. Fan speed is slowest between 0 and 125 W of dissipated power; thereafter, the fan accelerates at medium speed up to 305 W, and finally reaches maximum speed between 305 W and 400 W. Details of fan speed, fan voltage and noise level are given in **Table 1**.

It can be seen that, in addition to the relatively high speed 1, speeds 2 and 3 are very close to each other, and at speed 3, which is supposed to be maximum, the fan is not supplied with 12 V, contrary to what

might be expected. Let's see if we can both reduce the fan voltage at speed 1 and increase it at speed 3.

Table 1: Before Modifications

| Speed | Fan voltage (V) | Fan speed (RPM) | Noise (dBA) |
|------------|-----------------|-----------------|-------------|
| 1 - Slow | 5.6 | 2,660 | 50 |
| 2 - Medium | 9.6 | 3,940 | 59 |
| 3 - Fast | 9.9 | 4,040 | 59 |

The Control Circuit

The main PCB, containing three of the instrument's six IRFP250N MOSFETs, is shown in **Figure 2**. The other three are on a



Figure 2: The main PCB.

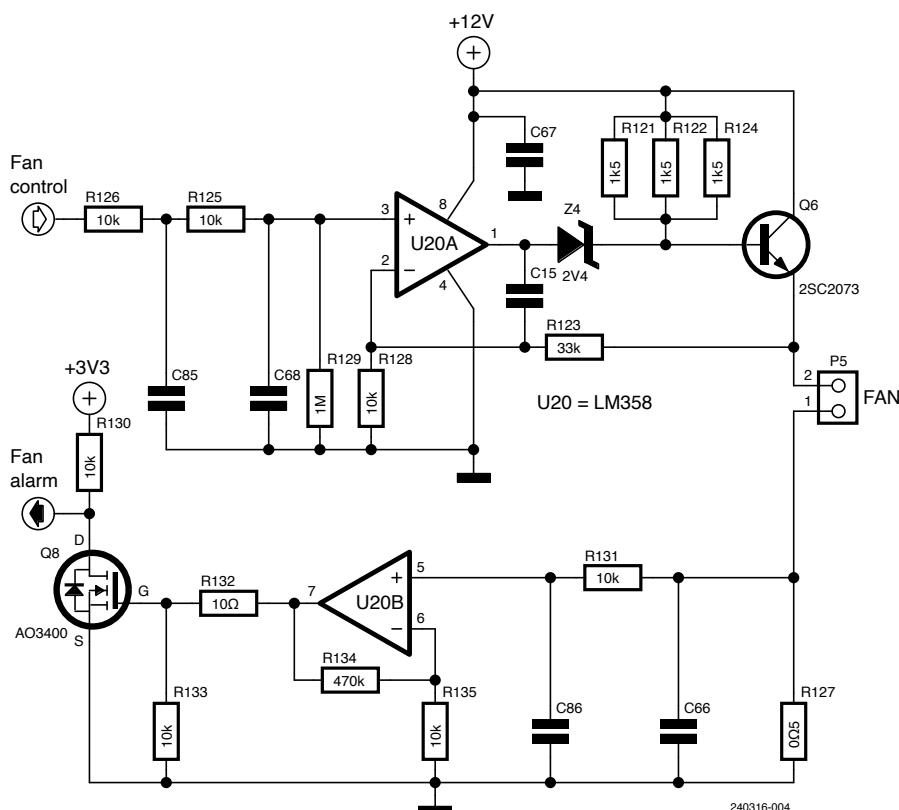


Figure 3: Schematics of the fan control circuit.

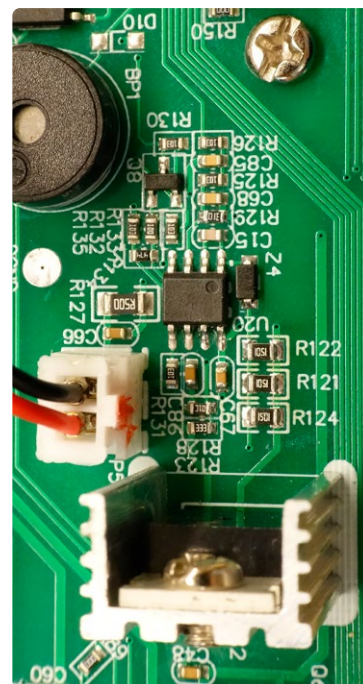


Figure 4: The original fan control circuit.

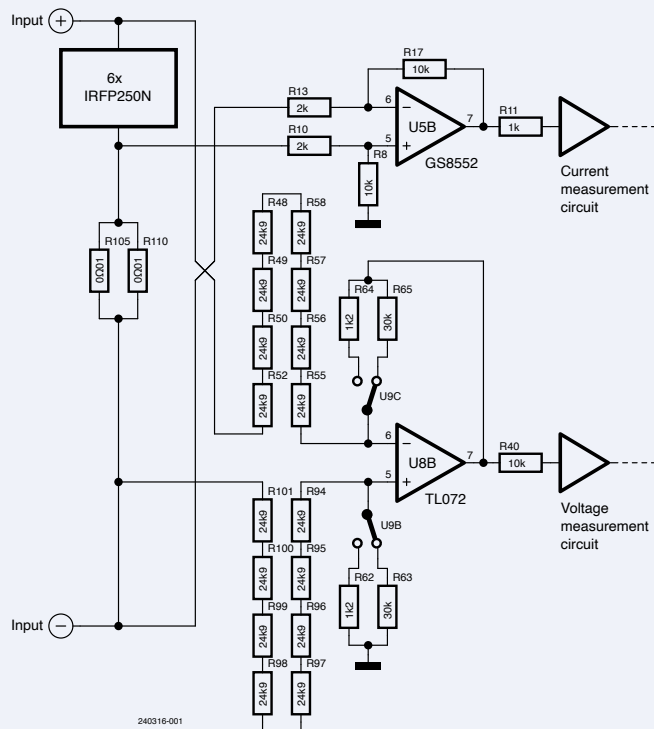
secondary PCB on the other side of the heatsink. Analysis of the fan control circuit is greatly facilitated by the remarkable work of forum user “morris6” who took the trouble to reverse-engineer the complete device schematic [1]. The partial schematic of the fan control can be seen in **Figure 3**; see the corresponding PCB section in **Figure 4**. The microcontroller transmits the speed setpoint as a PWM signal at a frequency of 5.45 kHz. The signal is transformed into a DC voltage by the dual low-pass filters R126/C85 and R125/C68 and applied to the non-inverting input of the op-amp U20A. The latter is configured as a voltage regulator, and its output controls the base of the bipolar transistor Q6, itself on the positive rail supplying the fan. The output voltage, at the emitter of Q6, is divided by the R123/R128 voltage divider to serve as negative feedback to the op-amp. Thus, each speed setpoint 1, 2, 3, corresponds to a DC voltage on pin 3 of U20 (1.27 V, 2.23 V and 3.05 V respectively) and a different output voltage supplying the fan.

Some of the design elements are surprising:

- secondary PCB on the other side of the heatsink. Analysis of the fan control circuit is greatly facilitated by the remarkable work of forum user "morris6," who took the trouble to reverse-engineer the complete device schematic [1]. The partial schematic of the fan control can be seen in **Figure 3**; see the corresponding PCB section in **Figure 4**. The microcontroller transmits the speed setpoint as a PWM signal at a frequency of 5.45 kHz. The signal is transformed into a DC voltage by the dual low-pass filters R126/C85 and R125/C68 and applied to the non-inverting input of the op-amp U20A. The latter is configured as a voltage regulator, and its output controls the base of the bipolar transistor Q6, itself on the positive rail supplying the fan. The output voltage, at the emitter of Q6, is divided by the R123/R128 voltage divider to serve as negative feedback to the op-amp. Thus, each speed setpoint 1, 2, 3, corresponds to a DC voltage on pin 3 of U20 (1.27 V, 2.23 V and 3.05 V respectively) and a different output voltage supplying the fan.
- Some of the design elements are surprising:
- ▶ The general architecture, implementing a linear regulator. With this design, the control transistor wastes some power as heat, especially at low fan speed. It would have been more efficient to connect the fan's positive terminal to +12 V, and switch its negative terminal to ground using PWM and an N-channel MOSFET. It's hard to explain this choice, except perhaps the designer's fear of potentially generating more electromagnetic noise in the latter case.
 - ▶ The use of an NPN transistor on the positive rail, controlled by an op-amp supplied with the same voltage (12 V) as the collector voltage. On the one hand, the LM358 doesn't have a rail-to-rail output, and on the other, in the absence of a higher base voltage, the transistor can never fully saturate, which explains why the fan receives, at maximum, around 9.8 V instead of the expected 11.8 V (12 V minus around 0.2 V of collector-emitter voltage when Q6 is saturated).
 - ▶ The three base pull-up resistors, in an attempt to compensate for the previous point. These provide a fairly high base current, so the op-amp only works in sink mode to regulate it. If they are removed, the voltage delivered to the fan cannot exceed 8.6 V, and speeds 2 and 3 cannot be reached.
 - ▶ The Zener diode between the op-amp's output and the base of Q6. Its only effect is to slightly increase the lowest speed, because at this speed, the op-amp is sinking its maximum amount of current (around 10 mA), to try to reduce the base current, which is driven hard by the three pull-up resistors. At this level of current sinking, the LM358 is unable to maintain a sufficiently low output voltage. Thus, the base voltage of Q6 (equal to the output voltage of the op-amp plus the Zener voltage) is too high, causing the regulator to lose regulation. The voltages on pins 2 and 3 of U20 are no longer equal, and the output voltage is higher than planned. By short-circuiting the Zener diode, regulation is restored, and the fan voltage drops to 5.4 V instead of 5.6 V.

Simulating Higher Voltages and Currents

To determine whether the fan is controlled according to actual temperature or power dissipation, it was desirable to be able to vary these two parameters independently. Here's a method for simulating high voltages and currents, without dissipating any real power (so as not to vary the temperature).



The ET5410A+ measures the current using a 5 mΩ shunt (two 10 mΩ shunts in parallel) on the negative side of its input, as can be seen on the partial schematic above. This measurement is amplified by a differential amplifier, with a gain of 5, built around one half of the op-amp U5, then the signal goes to the input of the next stage via resistor R11. By desoldering this SMD resistor and injecting a voltage there using a lab power supply and another temporary resistor, it is possible to simulate a current of 0 to 40 A by injecting a voltage of 0 to 1 V.

A similar method is used to simulate high voltages. This will allow to safely study the circuit; in any case, I don't have a 150-V DC power supply. The voltage at the input terminals is measured by the differential amplifier made with one half of the op-amp U8 and its companion resistors. This time the gain is less than 1; the circuit divides the input voltage by approximately 49.6 or 6.6 depending on the range, which is chosen by the microcontroller via relay U9. The 199.2 kΩ input resistors are made of resistor chains, each comprising eight 24.9 kΩ resistors in series. By shunting 7 of these 8 resistors with small temporary wires on each input, we can artificially multiply the gain by 8. In this way, an input voltage of 0 to 150 V can be simulated using a real voltage of 0 to 18.75 V.

The rest of the circuit is used to check that the fan is running, by measuring its current consumption through the R127 measurement shunt. The measured voltage is amplified by the other half of U20, configured as a simple non-inverting amplifier with a gain of 48. If the fan is disconnected or malfunctions, and draws a current of less than approx. 45 mA, the output voltage of U20B falls below the threshold voltage $V_{GS(th)}$ of MOSFET Q8. The MOSFET stops conducting, and the alarm output goes high.

A Few Modifications

Replacing the fan to reduce noise could be a solution, but in this particular case its disassembly isn't very easy. What's more, commercially available fans with both low noise levels and good static pressure, to overcome the heatsink's airflow restriction, are hard to find. Finally, this would not solve the issue of spacing between speeds 2 and 3.

To reduce speed 1, it may be tempting to modify the values of the R123/R128 resistor divider. The problem with this approach is that the fan voltage at speed 3 will also be reduced by the same coefficient. It is necessary to introduce a non-linearity, in order to reduce speed 1 without impacting speed 3. To this end, I propose to add a forward-biased 1N4148 diode (here in an SMD version, MMSD4148) between resistor R128 and ground, which adds an offset of about 0.5 V (i.e., the forward voltage of this diode, at a very low current) to the voltage seen by the inverting input of U20A. In practice, I installed the R128 resistor and the diode vertically, on the pads initially dedicated to R128.

In addition to this diode, in order to obtain the desired voltages and speeds, we can play with the values of R123, R128 and R129. These values have been determined by trial and error and with the help of an Excel sheet; an infinite number of combinations can work, the difficulty being to find values falling within the E12 or E24 series. The following values are suggested:

R123 = 33 kΩ (no change)
R128 = 5.1 kΩ
R129 = 47 kΩ

To increase speed 3, it is necessary to bring Q6 to saturation. To this end, U20's power supply is increased to 17 V, using a small isolated DC-DC module (Murata NME0505SC or similar), whose input is taken from the existing 5 V rail and whose output is connected in series with the existing 12 V rail. The 12 V power supply is originally brought to U20 by a very short track from a nearby via, close to pin 8; simply cut this track and solder a small wire to pin 8 to bring in the new power supply.

Having done this, pull-up resistors R121, R122, R124, and Zener diode Z4 are removed. However, a resistor is required to limit the base current of Q6 when it saturates at maximum speed. A value of 1 kΩ is suitable; it can be soldered in place of Z4. The modified circuit is shown in **Figure 5** and **Figure 6**. The voltages and speeds obtained are shown in **Table 2**. On my own ET5410A+, the 12 V supply is a little low (11.6 V), which explains the voltage observed at fan speed 3, when Q6 is fully saturated ($V_{CE(sat)}$ around 0.2 V).

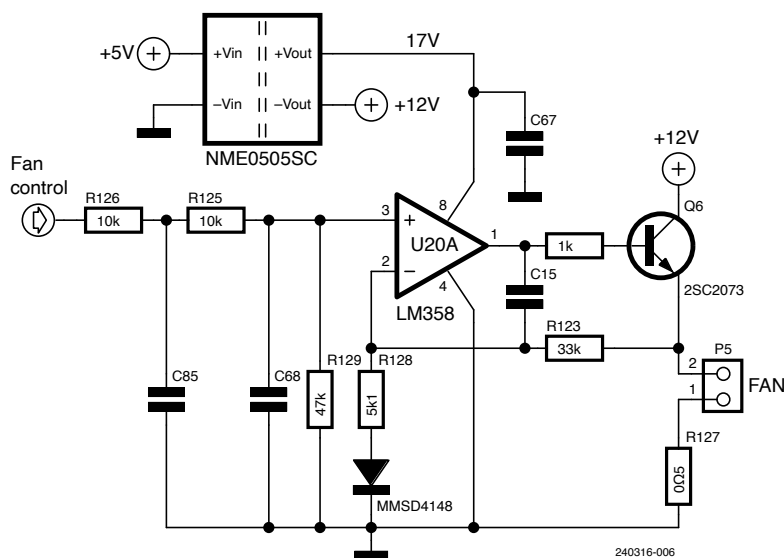


Figure 5: Modified schematic.

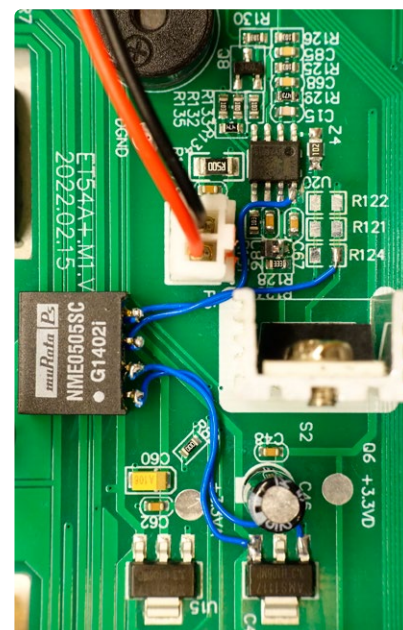


Figure 6: Modified PCB.

Table 2: After Modifications

| Speed | Fan voltage (V) | Fan speed (RPM) | Noise (dBa) |
|------------|-----------------|-----------------|-------------|
| 1 - Slow | 3.8 | 1,860 | 42 |
| 2 - Medium | 8.6 | 3,620 | 55 |
| 3 - Fast | 11.4 | 4,390 | 60 |

Testing

After these modifications, the lowest fan speed being reduced, it was necessary to check the temperature rise of the heatsink. A continuous 125 W of power was dissipated in the DC load for a prolonged period, and the temperature of the heatsink was measured with a K-type thermocouple thermometer. It reached around 45°C after about 20 minutes. The microcontroller then decided the need for further cooling, using the built-in temperature sensor. The fan was driven at full power for a few minutes, then returned to speed 1. Tests at higher power levels showed similar behavior, with no particular problems detected.

Towards Future Improvements?

The goals are thus achieved: for low-power levels, the instrument is much less noisy, and when the power dissipated or the duration of the test increases, the regulation takes over to ensure proper cooling. Operating comfort has increased significantly. Of course, this could have been tackled in many other ways: adding a microcontroller to manage speeds in a customized way via software; replacing Q6 with an N-channel FET, etc. It would also be possible to use a specific IC dedicated to fan control, such as Microchip's TC642/647/648 or EMC2301. All these solutions would have required more extensive modifications to the existing PCB, or the addition of a new PCB, which I wanted to avoid.

This DC load is obviously not perfect, but for occasional needs it does the job at an affordable price. To automate measurements and log values on PC, the manufacturer's official software leaves something to be desired, but the ET5410A+ is compatible with a very ambitious software project called Test Controller [2], which offers great scope

for experimentation. A possible next modification or improvement to the device could be, for example, to add remote sense capability, to compensate for the voltage drop that occurs in the cables when the load is used at high currents. ◀

240316-01

Questions or Comments?

Do you have questions or comments about this article? Email the author at jean-francois.simon@elektor.com or contact Elektor at editor@elektor.com.



About the Author

Jean-François Simon has a longstanding passion for electronics and enjoys topics as varied as circuit design, test and measurement, prototyping, playing with SDRs, and more. He likes to create, modify and improve his tools and other systems. He has an engineering background and also enjoys mechanics, machining, and all things technical. Jean-François joined Elektor's Lab and Content team in 2023.



Related Products

- ▶ **Siglent SDL1020X-E Programmable DC Electronic Load (200 W)**
www.elektor.com/19254
- ▶ **JOY-iT HD35 USB Load Resistor (35 W)**
www.elektor.com/19164

WEB LINKS

- [1] ET5410A+ Schematics: <https://tinyurl.com/et5411a>
- [2] Test Controller software:
<https://lygte-info.dk/project/TestControllerIntro%20UK.html>

electronica 2024 in Review

With more than 3,400 exhibitors in all 18 halls of the Munich trade fair, electronica 2024 (November 12-15, 2024) had to show more than ever in its 60-year history. Messe München and Elektor teamed up again to host the Fast-Forward Start-up Award, but that was not the only thing what was playing around the Elektor booth. Four video content creators (with over 2 million followers) presented their latest electronics projects. Elektor editors interviewed experts on stage, and talked shop about the latest developments, in our daily Lab Talk live stream. And, of course, Elektor and eeNews Europe journalists took the chance to go around and look for interesting things. Below is only a small selection of the many technologies that were presented to the more than 80,000 visitors of the event. You'll find even more on our YouTube channel, www.youtube.com/ElektorIM.



Live Streams from the Exhibition

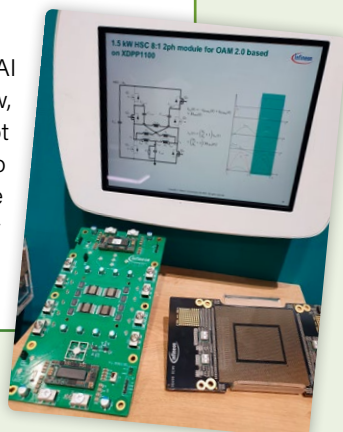
For the first time, Elektor produced daily Lab Talk livestreams from the show floor. Elektor editor Brian Tristram Williams was supported by contributions from Elektor author Stuart Cording, Jean-Pierre Joosting from eeNews Europe, and Elektor Editor-in-Chief Jens Nickel. Amongst our guests we had the influencers GreatScott!, Max Imagination, DIY Guy Chris, Edi's Techlab, Alix Paultre from ElectronicDesign, Natasha Baker from SnapMagic, and others.

But that was not all. During our "The Future Is Now" sessions, several experts took the stage stage to give live presentations. For example, well-known educator Peter Dalmaris, the author of the book *KiCad Like a Pro*, gave a live tutorial about Kicad 8.

Power, Power, and More Power

It goes without saying that we saw a lot of AI applications at the electronica. As you know, all the exciting AI applications also need a lot of power. And this power must be directed to the (gigantic) chips which do the work "in the cloud." Infineon showcased this power supply solution.

<https://tinyurl.com/infineon-we-power-ai>



Did you miss the livestreams?
You can watch the videos at
www.elektormagazine.com/electronica-2024/



electronica Fast Forward Start-Up Award

In the sixth edition of our start-up event, electronica Fast Forward 2024, which was organized by Messe München and Elektor, four startups competed for global notoriety and a share of a large marketing budget. At the world's leading electronics fair, the Elektor jury had a hard time agreeing on the winners after the short presentations candidates. The jury has evaluated the startups on criteria including their technical merit, significance for the industry, outstanding overall presentation, and potential for future development. Congrats to the winners!

1st PRIZE

(50,000 euro worth marketing package from Elektor + free booth at the next electronica 2026):

SpeedPox

2nd PRIZE

(25,000 euro worth marketing package from Elektor):

BTRY

3rd PRIZE

(10,000 euro worth marketing package from Elektor):

ICECAP

ETHICS IN ELECTRONICS AWARD

(5,000 euro worth marketing package from Elektor + Ethical Profile in "Ethics in Electronics"):

Banyan.eco

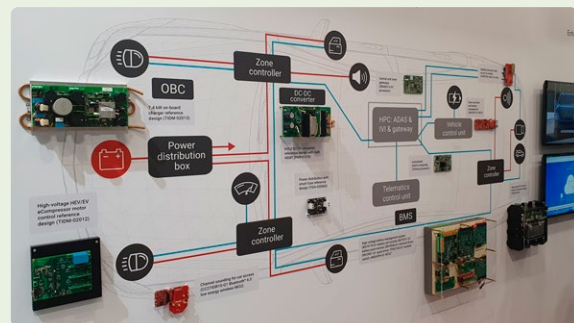
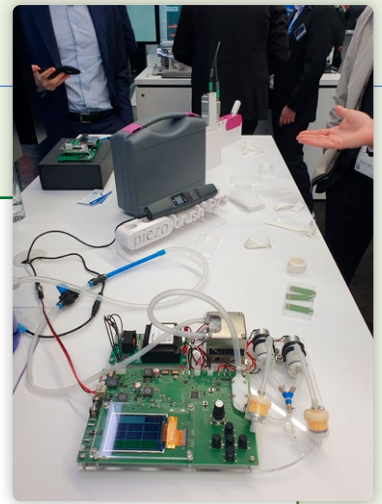
SpeedPox took first place for their fast-curing epoxy resins. BTRY and ICECAP claimed second and third prizes for their breakthroughs in ultra-fast charging batteries and portable thermo-electric cooling, respectively, while Banyan.eco received the Ethics in Electronics Award for their AI-powered carbon footprint platform. These startups highlight the event's role in driving sustainable and transformative advancements in electronics.

Find more about the start-ups:
www.elektormagazine.com/eff2024winners

Cleaning Surfaces

The PiezoBrush PZ3 from relyon/TKD is working with a plasma beam, cleaning surfaces to the max. After treating a plastic surface, an adhesive tape could be fixed that strong that there was no way to remove it without destroying it completely. An astonishing demo — we hope that it won't be used by warehouses for price tags!

www.relyon-plasma.com/piezobrush-pz3/



Automotive (Of Course!)

Enhanced by the current market upheavals (as electric drives and autonomous driving), automotive-related technologies and solutions were well represented at the booths of the semiconductor manufacturers. Here is what ST and TI had to showcase.

<https://tinyurl.com/ST-electronica-2024>

<https://tinyurl.com/hev-ev-powertrain>





Robots

One of the most attractive demos was located at the electronica Fast Forward and Elektor booth. Unitree and MyBotShop showcased not only four-legged robo-dogs, but also wheel-equipped ones and even humanoids. The humanoid guy is sold to universities and other research facilities to develop applications. Its price tag is about €85,000, but we are sure that is just the start.

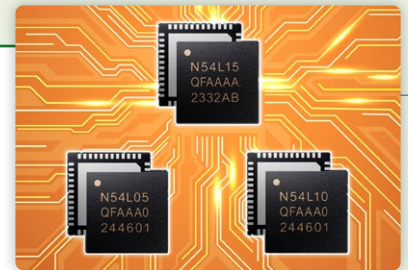
www.unitree.com

www.mybotshop.de

Wireless SoCs

Nordic Semiconductor's nRF54L series of wireless SoCs — including the nRF54L15, nRF54L10, and nRF54L05 — offers superior performance, exceptional processing power, and versatile design options for IoT applications. These devices integrate a 2.4-GHz radio module and an MCU function into a single ultra-low power chip. The nRF54L15 is intended for demanding applications, while the nRF54L10 and nRF54L05 target high-volume applications. The nRF54L series supports multiple protocols, including Bluetooth LE, Thread, and Zigbee, with extended capabilities.

<https://tinyurl.com/device-nrf54l>



Influencer Forums

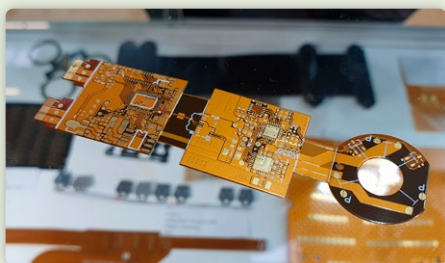
electronica 2024 was a vast exhibition featuring an extensive supporting program with practical forums, conferences, and special events. Six stages hosted discussions on various topics, including automotive, embedded systems, IIoT, power electronics, and AI-driven machine learning. One of the key venues was the Visionary Stage in Hall B4, situated near the Fast Forward area and Elektor's booth. Elektor contributed to this stage by hosting forums such as The Smart Influencer Marketing Forum and The Student & Influencer Marketing Forum. These forums at electronica 2024 offered attendees, especially students and marketing professionals, useful advice and inspiration to innovate and connect in meaningful ways.

The Smart Influencer Marketing Forum (Day 3 of electronica 2024) explored how to incorporate smart influencer marketing for your



company. Panelists included top influencers GreatScott!, Max Imagination, DIY Guy Chris, and Simon Gao (PCBWay), along with Elektor's Brian Tristram Williams. Together, they discussed strategies for their combined audience of over 2 million followers to connect with engineers, hobbyists, and makers.

The Student & Influencer Marketing Forum (Day 4 of electronica 2024) aimed to inspire students eager to enter the electronics industry. The session featured top electronics influencers and Elektor editors, sharing strategies for breaking into content creation in the industry. The event highlighted how students can combine technical expertise with creative storytelling to excel in the field.



Lightweight Solutions

These PCBs are not flexible, and because of that, adaptable to devices with space constraints. Flexible PCBs can be also made very lightweight, with weird applications like attaching to insects. PCBWay showcased this and many other (partly very colorful solutions) from their portfolio.

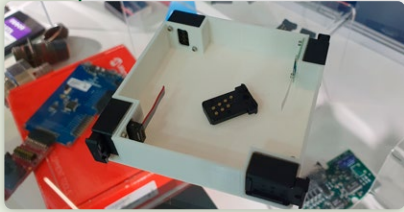
<https://tinyurl.com/PCBWay-electronica-2024>



Ruggedized Memory Stick

Up to 100,000 plug-in cycles and water-proof! For harsh environments, you need more robust solutions than fiddling with SD-cards or USB-sticks. The Datakey Minibar (with SPI or I²C interface) is mainly dedicated to host crypto keys. The receptacle can find its place (for example) at the corner of the device.

<https://tinyurl.com/datakey-minibar>

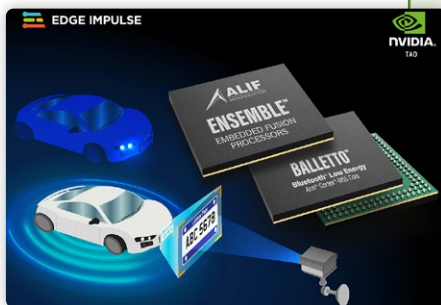


AI Vision on Edge MCUs

Alif Semiconductor and Edge Impulse have announced a significant breakthrough in implementing AI vision processing on edge microcontrollers through the introduction of full support for the Nvidia TAO model training toolkit on the Ensemble and Balletto MCU families of Alif and the Edge Impulse platform. Embedded developers seeking to implement AI vision applications — such as people counting, intruder detection, or robotics — can now utilize the TAO training toolkit and its dataset, confidently deploying either a pre-trained TAO model or a custom model developed through transfer learning via Edge Impulse on Alif Ensemble or Balletto MCUs.

www.alifsemi.com

www.edgeimpulse.com



Triple Radio Support

Ignition has announced a one-of-a-kind three-port Virtual Antenna component with simultaneous triple radio covering cellular, GNSS, and Wi-Fi/BLE. The surface-mounted passive component, called OMNIA mXTEND, turns the ground plane of a PCB into a high-efficiency radiating element that can operate between 400 MHz and 8,000 MHz, allowing device manufacturers to choose specific radio bands without requiring size modifications. Compared to three independent antennas, OMNIA mXTEND provides extra degrees of freedom, requiring a single clearance area while enabling superior long-range connectivity performance across multiple frequencies. The advanced multi-block design minimizes radio coupling, enhancing performance, reducing the matching network BoM and facilitating certifications — a crucial factor for IoT devices where every dB counts.

www.ignition.io/landing-page/discover-omnia-mxtend



GreatScott!, DIY Guy Chris and Max Imagination

Elektor has a long history of collaborating with talented influencers who have contributed articles and participated in previous events. This year, we invited some of them to participate in the electronica 2024 program, bringing their expertise and creativity to the show.

Max Imagination, the popular electronics innovator and content creator with over 145,000 YouTube subscribers, captivated the electronica 2024 audience with his live demos throughout the week. A highlight of his moment was his FPV head tracker, which he assembled live in less than an hour! While at the booth, he was working on a new robot, sparking conversations about his creative process. Watch him demo his FPV head tracker here: <https://youtu.be/Mt4MBWvempl>

GreatScott! shared his expertise with attendees about the DIY LiPo Supercharger Kit. During a livestream, he discussed his innovative projects, his journey as a content creator, and DIY electronics. And during Elektor Lab Talk #24, GreatScott! talked about new technologies and the electronica 2024 event. www.youtube.com/live/mOpgzH0GVWl

DIY Guy Chris held a live soldering competition and engaging discussions, taking questions from engineers and makers at the booth. Through his much-appreciated videos and projects, where he simplifies advanced electronics through step-by-step guides on topics like LED displays and CNC machines, Chris showcased creations like the RGB LED Cube and joined Elektor Lab Talk to offer behind-the-scenes insights into his work. www.youtube.com/live/yCYrELoGjhs

Throughout the event, Elektor's booth buzzed with activity as these influencers engaged with fans, shared knowledge, and demonstrated their projects, creating an unforgettable experience for visitors.

240678-01



Electromagnetic Compatibility

EMC in a Nutshell!

By Dr. Heinz Zenkner (Würth Elektronik eiSos)

EMC is about designing electronic products and systems in such a way that the emission of electromagnetic radiation is minimized and they are insensitive to interference from electromagnetic fields from other sources. That's what you always hear. That's what you always read. Is it really?

Yes and no, it depends on how you look at it, and it is only half the truth. Authorities mainly focus on interference emission to do justice to radio protection. Standards look at the interfaces, it is about standardized procedures with which both the interference emission and the interference immunity of the device are tested. But what does the situation look like inside the device? After all, we know from medicine

that treating symptoms is not the solution to the underlying problem.

This short article aims to show where and how the causes of "EMC problems" arise and to summarize what measures can be taken.

EMC Causes

When an electric current flows through a wire, a magnetic field is created around

the wire. This spreads out and forms a magnetic field that typically runs concentrically around the wire. The strength of the magnetic field depends on the current in the wire. If the current in the wire changes, the magnetic field around the wire also changes. This is because the movement of the charge carriers (typically electrons) in the wire changes when the current strength changes. This change in the magnetic field induces an electric field according to Maxwell's equations. The resulting electromagnetic radiation occurs when these changing electric and magnetic fields propagate through space. In a typical circuit with alternating current, the direction of the current changes periodically, which leads to a periodic change in the magnetic field and thus to a periodic generation of electromagnetic waves. These electromagnetic waves can propagate through space and influence other electrical or electronic circuits.

This mechanism, also known as electromagnetic coupling, occurs on a printed circuit board between integrated circuits (ICs) and conductor tracks due to various effects:

➤ Current flow in the conductors:

When electrical signals flow through the traces, they generate magnetic fields around the traces. This happens

when signals are transmitted between the ICs and other components of the PCB.

- **Signal changes and switching processes in the ICs:** Switching operations are constantly taking place within the integrated circuits when digital signals are processed. These switching processes generate changing electric fields within the ICs, which in turn lead to changing magnetic fields.
- **Signal reflections and impedance matching:** Signal reflections can occur when a signal crosses the boundary between different materials with different impedances. These reflections can cause signals to move back and forth along the conductive paths, which in turn can lead to increased electromagnetic radiation.
- **Capacitive and inductive coupling:** Capacitive and inductive coupling effects can occur on a PCB, where electric or magnetic fields are superimposed between the traces and the ICs. This can cause interference to propagate between the different signals.

As described above, the electromagnetic energy, i.e., the interference, “travels” from the source to the interfaces of a device and from there, via openings in housings and cable connections, into the “environment”.

On the way from the interference source, for example an Ethernet controller, to the interference sink, e.g., the Ethernet cable,

the interference signal can cause various problems:

- Coupling of the interference into neighboring circuits on the electronic module and generation of signal integrity problems and thus interference, with possible sporadic failure of functions.
- Emission of the interference as a differential mode (DM) interference signal from the interference source and decoupling as a common mode (CM) interference signal via housing openings.
- Emission of the interference signal via the Ethernet cable as an electromagnetic wave (radio interference).
- Generation of conducted interference emission on the Ethernet cable and influencing of the Ethernet signal, which can lead to a high bit error rate (BER).

In the EMC environment, the terms “spurious emission” and “immunity” are often used to describe two different aspects that are nevertheless related to electromagnetic phenomena in a similar way. Reducing the spurious emission of a device can increase its immunity to external disturbances, and improving immunity can simultaneously reduce the impact of spurious emission on other devices, because the coupling mechanisms, i.e., the coupling paths as described above, are bidirectional, i.e., they work in both directions.

There are therefore two main aspects that get to the heart of the EMC issue:

- reduction of radiation from the primary source of interference
- reduction of the potential coupling paths

These measures are not there to meet EMC standards, but to significantly increase the quality of an electronic product, a quality that the user unfortunately cannot recognize at first glance, like an apple that is rotten inside.

Uncontrolled Electromagnetic Interference

Figure 1 shows the coupling mechanism described above from interference via the electronic module to radiation via an Ethernet cable.

Starting from the current loop between IC1 and IC2, the return path via ground (GND), an electromagnetic field is emitted which:

- couples into the interface area of the module and there, also via the interface filters, into the conductors of the interface cables and leads to interference radiation via the cable. Due to the limited shielding attenuation of the cable shield, so-called common mode radiation occurs via the cable.
- couples into neighboring conductor paths and induces an interference current in them, which leads to different types of interference depending on the type of the useful signal.
- is radiated as an electromagnetic field via slots, seams, ventilation grilles, etc.

The type of electromagnetic radiation illustrated in Figure 1 is a variant of the radiation emitted by electronic circuits. Other causes are:

- Mismatch with impedance-determined lines
- Asymmetry in symmetrical signal pairs
- Poor, e.g., interrupted reference ground

A further possibility of radiation from electronic circuits, not shown here, is so-called CM radiation, which is caused

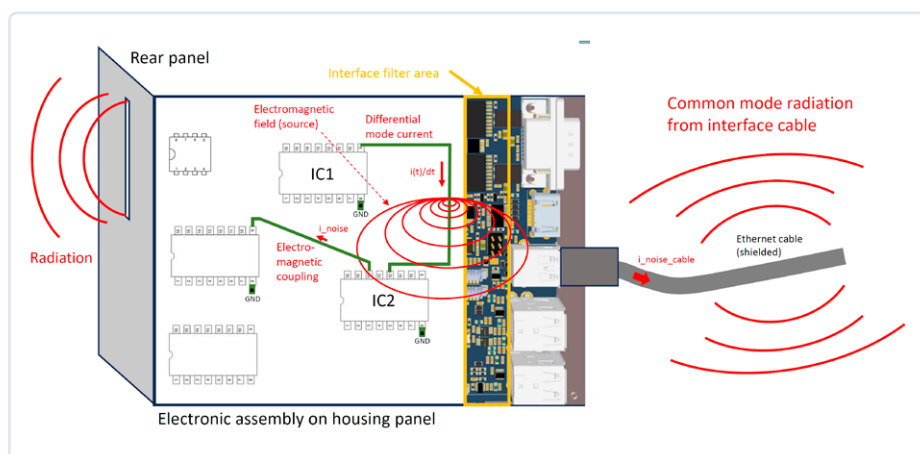


Figure 1: Uncontrolled emissions from a signal current loop on an electronic module.

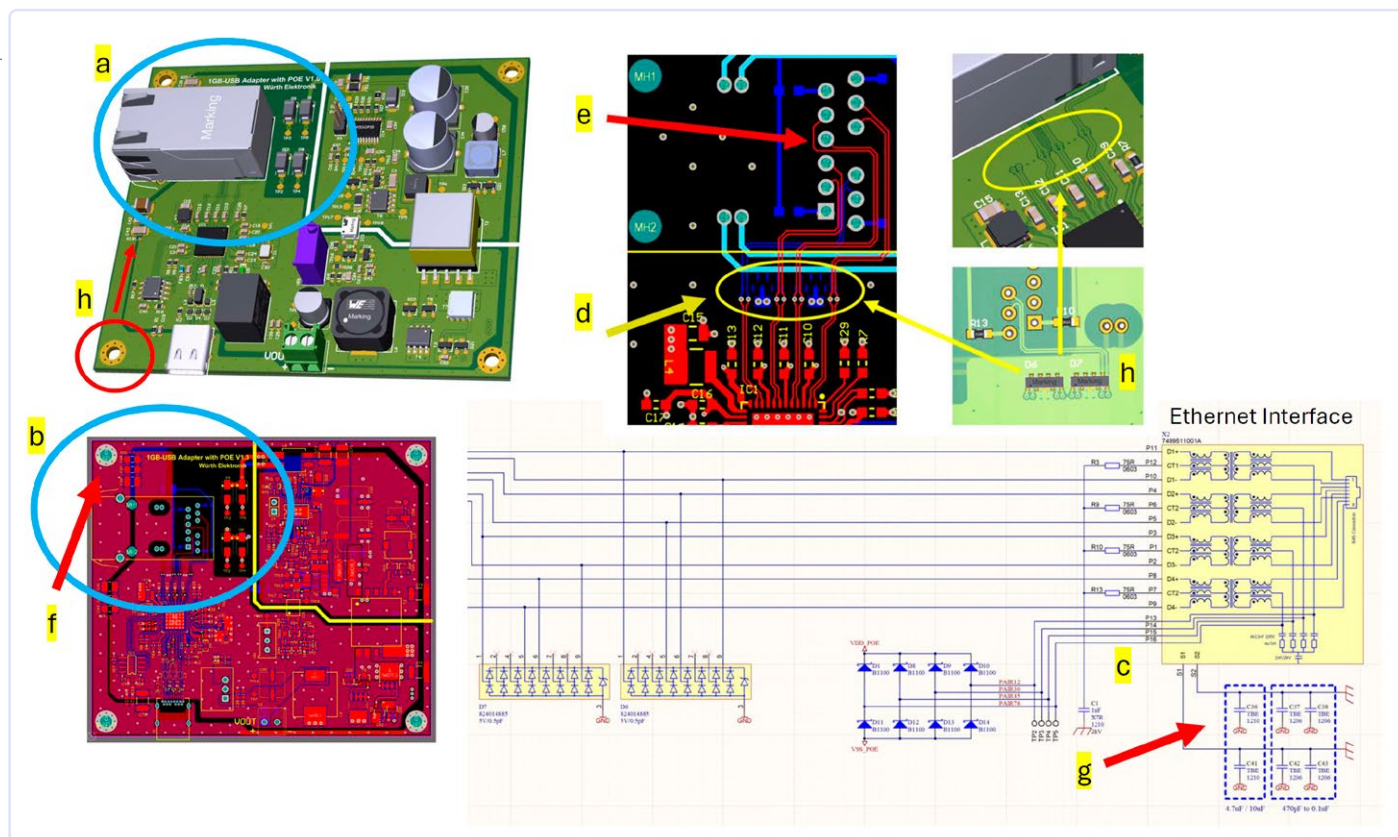


Figure 2: Important structural points of an electronic module (interface area).

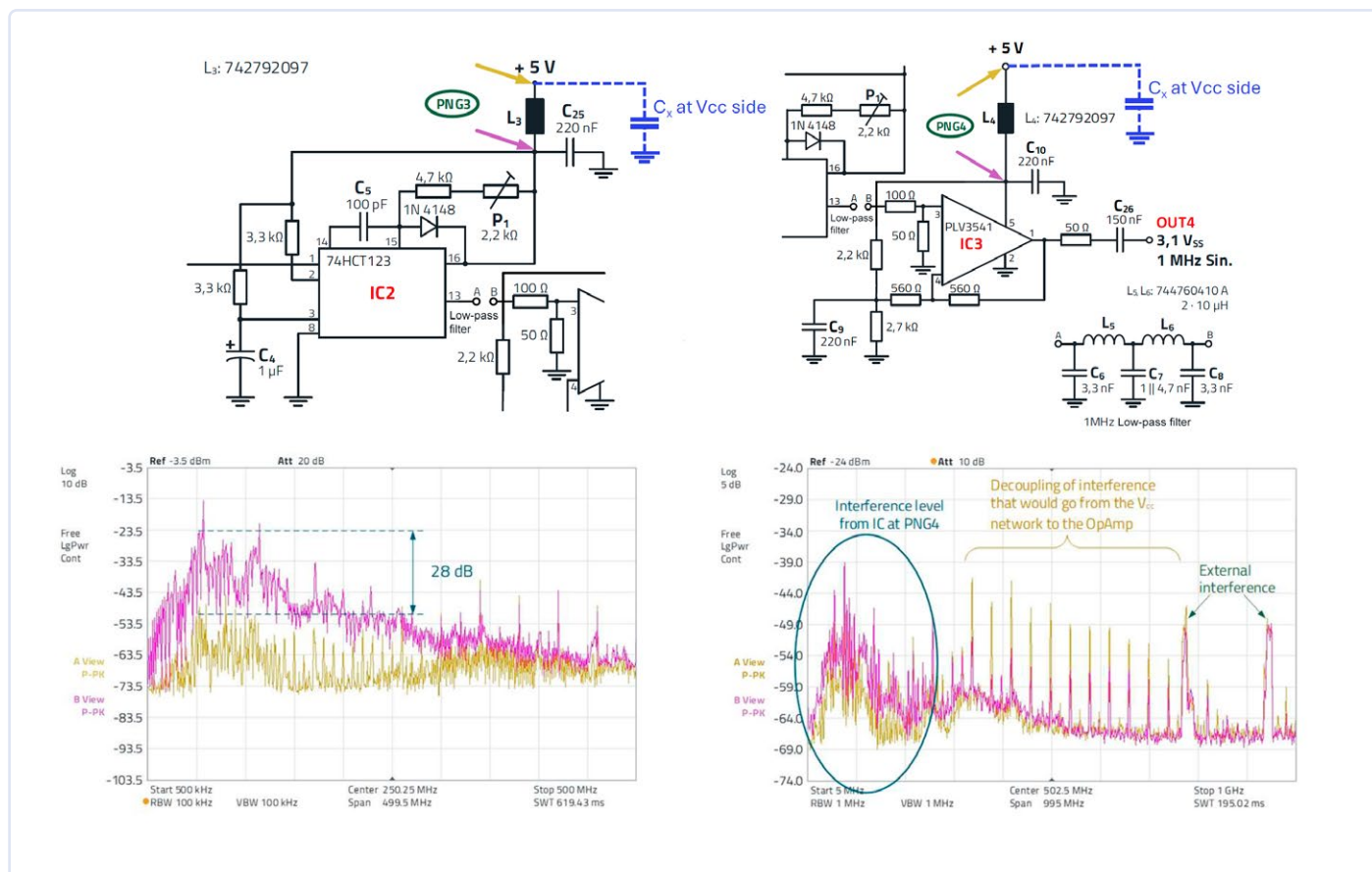


Figure 3: Illustration of the effect of Vcc decoupling filters.

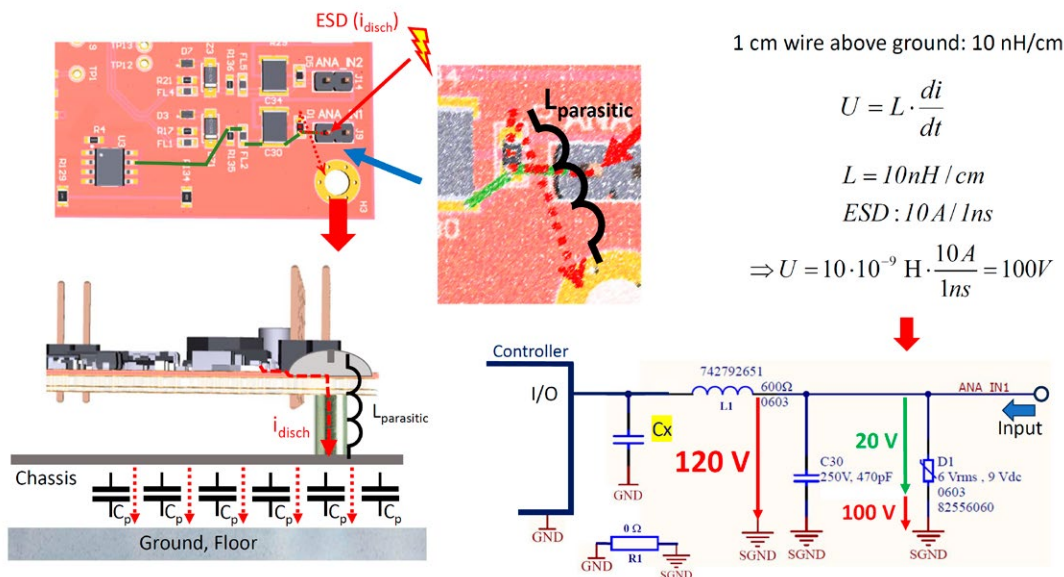


Figure 4: Filter in the interface area with associated ground concept.

by interference of the same amplitude and phase on different conductor paths (e.g., a differential USB cable pair); the reference potential of which is the ground position (GND). Ultimately, the circuit in turn forms a loop that leads to coupling mechanisms as described above.

Improving Signal Integrity and EMC

Various measures can be taken to improve signal integrity and EMC of electronic devices and thus avoid the problems described. Here are some common approaches:

1. **Layout design:** a careful layout design is crucial to ensure signal integrity and minimize electromagnetic interference. This includes minimizing signal paths, avoiding mismatches, placing components with sufficient distance to each other and using grounding and earth planes [1]. An overview is shown in **Figure 2**.

The module in Figure 2 is a GB-Ethernet front end with "Power Over Ethernet". The Ethernet connection (a) is made via a socket with an integrated interface (c), which contains transformers, matching networks and CM chokes. This shielded module, together with the board mountings (h) are the basis for a ground reference and a low impedance connection to a sheet metal housing. In addition, for installation in a plastic housing, the housing ground/PCB grounding system

can be individually designed via mounting positions (g, h). The four Ethernet channels are routed as symmetrical conductor pairs (e), into which the TVS diodes (d) are looped directly into the signal path. All balanced conductor pairs are balanced with regard to time offset (skew) in their length and system impedance (100 W balanced). Impedance-corrected shielding of the line pairs on the left and right sides with a ground plane reduces parasitic coupling (h).

2. **Decoupling capacitors and Vcc/Vdd filters:** Decoupling capacitors and filters for the IC power supply are placed directly near the power supply connections of the ICs to block high-frequency interference. They not only help to reduce voltage fluctuations and ensure a stable power supply, but also block interference from the IC. The selection of suitable filter components is essential [2]. **Figure 3** illustrates the situation.

The circuit on the left in Figure 3 shows that the π -filter, consisting of C25, the SMD ferrite L3 and the capacitors in the power supply, causes an attenuation in the system of up to 28 dB. It is important to understand that this attenuation works in both directions; this case is illustrated on the right in Figure 3. The interference potential on the power supply side in the frequency range above approx. 300 MHz is attenuated by approx. 10 to 15 dB towards the amplifier IC3, while the interference potential generated on the

amplifier side in the range up to 300 MHz is attenuated by the filter by up to 20 dB towards the power supply side.

3. **Filtering at interfaces, earthing and grounding:** The use of filters such as low-pass filters and, if necessary, band-pass filters with transient protection helps to remove or attenuate unwanted frequencies and keeps high-frequency interference and transient overvoltages away from the device's internal electronics. **Figure 4** shows an example of a filter concept at interfaces.

The π -filter has a varistor at the input to limit transient overvoltages. The reference earth for the surge arrester must be the interference potential, i.e., the housing plate and above it the capacitance to the housing base. Figure 4 shows the effect of a parasitic inductance in the supply line to the varistor. A parasitic inductance of just 10 nH increases the clamping voltage by 100 V if, for example, an ESD pulse with a current of just 10 A is used as a basis. On the controller side, filters and, if necessary, additional voltage-limiting components must be connected to the GND reference of the controller! SGND and GND are connected to each other at suitable points in the layout via zero Ω resistors, SMD ferrites or capacitors. For further explanation of the effectiveness of the ground concept, please refer to the reference design RDO16 [3].

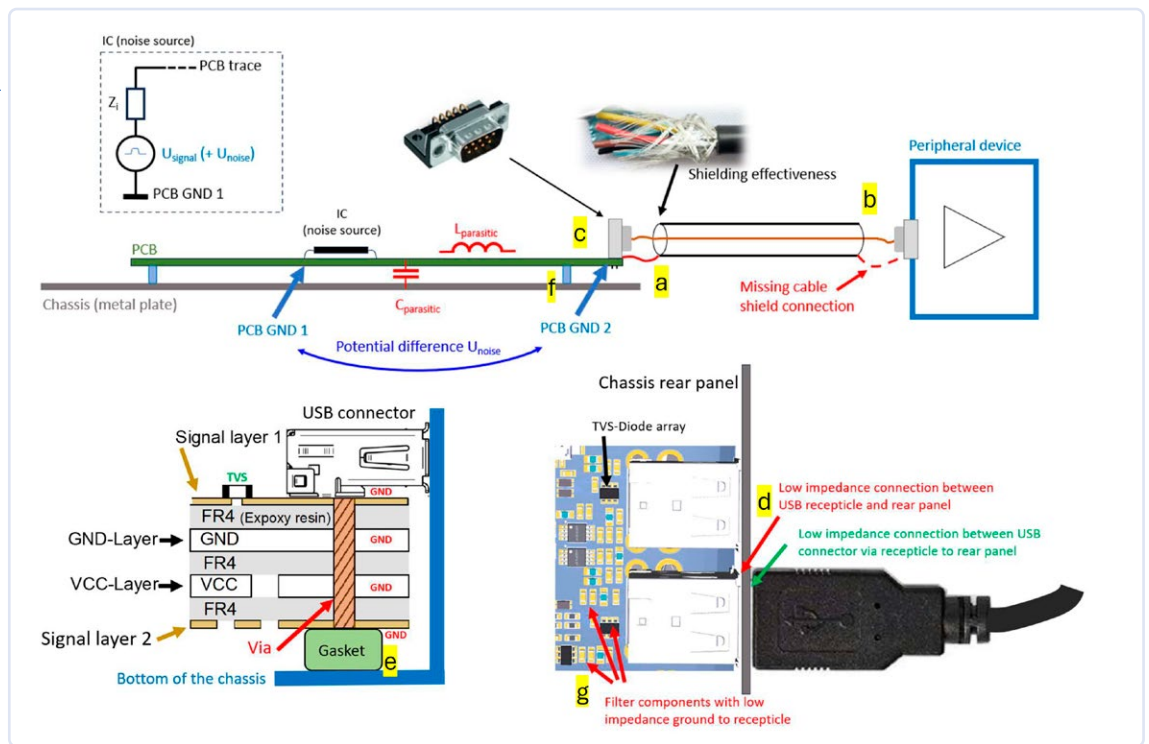


Figure 5: Illustration of the main EMC tasks of an enclosure.

4. **Shielding:** The use of shields or screens around sensitive components or conductor paths can help to contain electromagnetic radiation and reduce interference (Figure 2 h). However, the overall concept of the housing, consisting of a metal enclosure with as few gaps and openings as possible, is the decisive factor. The highest possible shielding attenuation of the housing generally also guarantees an RF-compliant ground reference for the interface filters and the connected shielded peripheral cables (**Figure 5**).

Only a cable shield connected to earth on both sides (a, b) also shields against magnetic fields. For this purpose, it is necessary that the plug connector (c) contacts the housing all around and with low impedance (d). Additional low-impedance galvanic connections can be realized by contacting the module in the filter area (e, f). This significantly improves the shielding properties of the peripheral cables and also gives TVS

diodes, SMD varistors and filter capacitors a “better” ground reference (g). A low-impedance connection of the GND reference layer (f) reduces the CM interference on the reference ground and improves the signal integrity of the entire circuit.

Holistic View of Signal Integrity and EMC

A holistic approach to the signal integrity and EMC design measures outlined above is required to ensure optimum performance and reliability of electronic assemblies. The selection of the right components, careful layout design, impedance control, proper design of signal and current loops and minimization of signal reflections are essential. A proper design of ground and earth concepts is crucial for avoiding ground loops and minimizing parasitic impedances that reduce the effectiveness of filters and cable shields. Only a combination of the above-mentioned measures can ensure a device design with both signal integrity and EMC. ◀

240683-01



About the Author

Dr.-Ing. Heinz Zenkner studied electrical engineering with a focus on telecommunication and radio frequency engineering and obtained his PhD in this field. He has been an officially appointed and sworn expert for EMC for many years. In addition to numerous scientific publications, he frequently contributes as an author in many works on EMC. Heinz has worked at various Universities, at the German Chamber of Industry and Commerce (IHK) and given numerous seminars. He has been involved with industrial electronics for years now, from initial product concept through to series production. His special interest lies in Wireless Energy Transfer, to which he has developed and patented his own theoretical and practical concepts.

WEB LINKS

- [1] Zenkner, H. “GB PoE+-Ethernet-USB adapter for industrial use with an EMC perspective,” Reference design RD022 from Würth Elektronik: <http://www.we-online.com/RD022>
- [2] Zenkner, H. “Inductive SMT Components in Comparison – the Wire Makes the Difference,” Application Note ANP129 from Würth Elektronik: <http://www.we-online.com/ANP129>
- [3] Zenkner, H. “Gigabit-Ethernet Front-End,” Reference Design RD016 from Würth Elektronik: <http://www.we-online.com/RD016>

Starting Out in Electronics...

...Filters Actively

By Eric Bogers (Elektor)

In the previous installment, we made a tentative start to discussing active filters, which offer some significant advantages over their passive counterparts, such as the ability to compensate for any losses with a little gain. In this first installment of the new year, we dive into the world of active filter circuits with fresh courage.

Low-Pass Filter with Unity Gain

Figure 1 shows a second-order low-pass filter with a gain of 1. This gain of 1 means that the signal is neither amplified nor attenuated in the pass band. Later, we will see that it can be useful to have the filter amplify a little bit.

The circuit as drawn is a so-called Sallen-Key filter — here, we are not dealing with two series-connected RC low-pass filters, but rather with a circuit with a little positive feedback by C1, which makes the filter react somewhat “sharper” at the cut-off frequency: At very high frequencies, the output of the opamp is near ground level, and capacitor C1 forms a low-pass filter together with R. At very low frequencies, the output carries the same potential as the input and C1 has no effect.

The dimensioning of the components depends on the desired filter characteristic:

- The **Linkwitz-Riley filter** is characterized by a crossover frequency at the –6 dB point. In this respect, this filter differs from other filters where the crossover frequency is defined as the frequency at which the voltage has decreased by 3 dB compared to the pass band.

When the signals from the high-pass and low-pass filters are added in other filters (assuming that the crossover frequencies

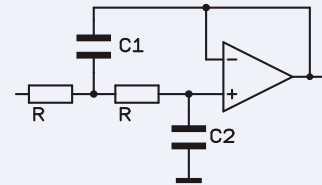


Figure 1: Second-order low-pass filter.

are the same), a peak of +3 dB is created at that frequency. This is not the case with Linkwitz-Riley filters, which is why this characteristic is often chosen for active crossover filters.

Linkwitz-Riley filters are not particularly sharp compared to other filters, but for that very reason, they do show good impulse behavior. The lack of sharpness can be compensated by using higher-order filters. The Linkwitz-Riley characteristic is therefore mostly used for fourth-order filters (with an attenuation of 24 dB/octave).

For a second-order filter, both capacitors have the same value, which is calculated as follows:

$$C_1 = C_2 = \frac{1}{2 \cdot \pi \cdot f \cdot R}$$

- The **Bessel filter** is very similar to the Linkwitz-Riley filter, but has the crossover frequency at the –3 dB point.

$$C_1 = \frac{0.9076}{2 \cdot \pi \cdot f \cdot R}$$

$$C_2 = \frac{0.6809}{2 \cdot \pi \cdot f \cdot R}$$

The two capacitors do not have the same value, and this can cause considerable problems with availability in practice. We will see later how these issues can be circumvented.

- The **Butterworth filter** is sharper, and hence has worse impulse behavior. This is a so-called critically damped filter:

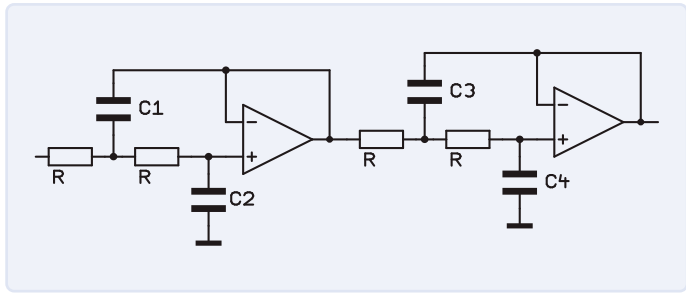


Figure 2: Fourth-order low-pass filter.

It shows the greatest possible sharpness while still having no ripple in the pass band.

$$C_1 = \frac{1.414}{2 \cdot \pi \cdot f \cdot R}$$

$$C_2 = \frac{0.7071}{2 \cdot \pi \cdot f \cdot R}$$

Sharper filters — such as the Chebyshev filter — exhibit poor impulse behavior and are therefore only used where the highest sharpness is really required.

Figure 2 shows a fourth-order filter. In principle, this involves a series connection of two second-order filters — but with adapted component values: If we were to connect two second-order filters calculated “by to the book” in series, we would get an attenuation of 6 dB or even 12 dB (Linkwitz-Riley) at the crossover frequency.

- The coefficients of the second-order Butterworth filter are used for the Linkwitz-Riley filter. As we noted earlier, the Linkwitz-Riley filter basically exhibits an attenuation of 6 dB at the crossover frequency.

$$C_1 = C_3 = \frac{1.414}{2 \cdot \pi \cdot f \cdot R}$$

$$C_2 = C_4 = \frac{0.7071}{2 \cdot \pi \cdot f \cdot R}$$

- For the Bessel filter:

$$C_1 = \frac{0.7298}{2 \cdot \pi \cdot f \cdot R} \quad C_2 = \frac{0.6699}{2 \cdot \pi \cdot f \cdot R}$$

$$C_3 = \frac{1.0046}{2 \cdot \pi \cdot f \cdot R} \quad C_4 = \frac{0.3872}{2 \cdot \pi \cdot f \cdot R}$$

- While, for the Butterworth filter, these coefficients are used:

$$C_1 = \frac{1.0824}{2 \cdot \pi \cdot f \cdot R} \quad C_2 = \frac{0.9239}{2 \cdot \pi \cdot f \cdot R}$$

$$C_3 = \frac{2.6130}{2 \cdot \pi \cdot f \cdot R} \quad C_4 = \frac{0.3872}{2 \cdot \pi \cdot f \cdot R}$$

If possible, the resistor values are chosen in the range of 2.2 kΩ to 22 kΩ. With smaller values, the operational amplifiers have to supply unnecessarily high currents and distortion is introduced with large signals; too large resistor values lead to unnecessarily bad noise behavior.

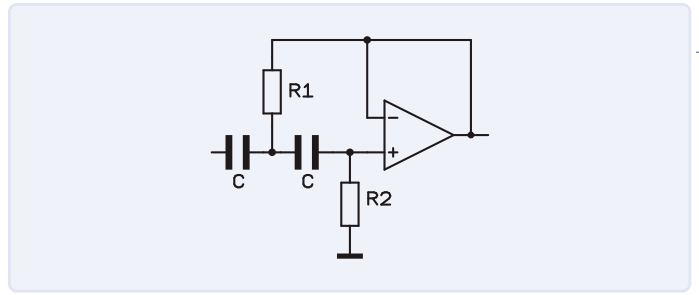


Figure 3: Second-order high-pass filter.

The coefficients do not have a convenient relationship to each other (apart from the Linkwitz-Riley filter), so the correct values have to be composed by ingenious series and parallel connection of standard values.

In the Linkwitz-Riley filter, C_1 and C_3 are exactly twice as large as C_2 and C_4 . Since the values of capacitors usually fit in the E6 or E12 series, a double value can only be obtained by parallel connection — but fortunately fairly accurately.

High-Pass Filter with Unity Gain

Compared to a low-pass filter, a high-pass filter has its resistors and capacitors reversed (**Figure 3**), while the coefficients are given their reciprocal values. Since capacitors of equal value are used, component availability is likely to be less of a problem.

- Linkwitz-Riley:

$$R_1 = R_2 = \frac{1}{2 \cdot \pi \cdot f \cdot C}$$

- Bessel:

$$R_1 = \frac{1.1017}{2 \cdot \pi \cdot f \cdot C} \quad R_2 = \frac{1.4688}{2 \cdot \pi \cdot f \cdot C}$$

- Butterworth:

$$R_1 = \frac{0.7071}{2 \cdot \pi \cdot f \cdot C} \quad R_2 = \frac{1.414}{2 \cdot \pi \cdot f \cdot C}$$

A fourth-order high-pass filter consists of a series connection of two second-order high-pass filters (**Figure 4**).

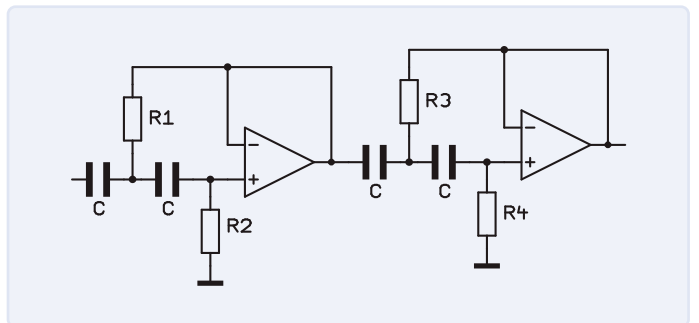


Figure 4: Fourth-order high-pass filter.

➤ Linkwitz-Riley:

$$R_1 = R_3 = \frac{0.7071}{2 \cdot \pi \cdot f \cdot C}$$

$$R_2 = R_4 = \frac{1.414}{2 \cdot \pi \cdot f \cdot C}$$

➤ Bessel:

$$R_1 = \frac{1.3701}{2 \cdot \pi \cdot f \cdot C} \quad R_2 = \frac{1.4929}{2 \cdot \pi \cdot f \cdot C}$$

$$R_3 = \frac{0.9952}{2 \cdot \pi \cdot f \cdot C} \quad R_4 = \frac{2.5830}{2 \cdot \pi \cdot f \cdot C}$$

➤ Butterworth:

$$R_1 = \frac{0.9239}{2 \cdot \pi \cdot f \cdot C} \quad R_2 = \frac{1.0824}{2 \cdot \pi \cdot f \cdot C}$$

$$R_3 = \frac{0.3827}{2 \cdot \pi \cdot f \cdot C} \quad R_4 = \frac{2.6130}{2 \cdot \pi \cdot f \cdot C}$$

That's enough formulas; we'll leave it at that for now. In any case, you can now experiment for yourself. Next time, we'll discuss filters with amplification. ◀

Translated by Hans Adams — 240637-01

Editor's note: This series of articles, "Starting Out in Electronics," is based on the book, Basiskurs Elektronik, by Michael Ebner, which was published in German and Dutch by Elektor.

Questions or Comments?

If you have any technical questions regarding this article, contact the Elektor editorial team at editor@elektor.com.



Related Products

➤ **B. Kainka, Basic Electronics for Beginners (Elektor, 2020)**

Book: www.elektor.com/19212

Ebook: www.elektor.com/19213

A green banner with a repeating pattern of electronic components like resistors, capacitors, and integrated circuits. The text "Join our Community" is prominently displayed in white and black. Below the text are four social media icons: Facebook, Instagram, Twitter, and YouTube, each with a hand-drawn, sketched style. To the right of the icons is a QR code. At the bottom left, the URL www.elektormagazine.com/community is written in white. At the bottom right is the Elektor logo, which consists of a red circle with a white 'e' inside, followed by the word "elektor" in black, and the tagline "design > share > earn" in a smaller font below it.

Reducing Power Dissipation With Dropping Capacitors

A Clever Use of Capacitive Reactance

By Christoph Biel (Switzerland)

Using dropping resistors connected in series to resistive loads often results in the dissipation of a large amount of energy. If you are working on an AC circuit, the use of dropping capacitors can reduce this to a minimum, and, for a low-power supply, they could be a valid alternative to transformers.

In electronic design, the problem of voltage drop occurs frequently. A common-sense practice is to avoid high dropout values on resistors or linear regulators, just due to the large amount of energy (and heat...) that would be dissipated — and wasted.

A First Practical Example

In AC circuits, the component most commonly employed to induce a large voltage drop is the transformer, but it is bulky, heavy and relatively expensive. To look for a possible solution, let's start from the practical example shown in **Figure 1**. It's a vacuum tube-based design, where the directly heated tube filaments are connected in series with a $22\ \Omega$ dropping resistor to 120 V AC at 50 Hz. This type of solution is cheap and easy to use in geographical areas that use 120 V.

In 230 V AC areas, if we were to apply the same principle, the power dissipated by the dropping resistor would increase from 2 W to nearly 35 W, as shown in **Figure 2** — an unacceptable waste of energy.

One possible alternative to using the dropping resistor is to exploit a feature of capacitors — the capacitive reactance. The capacitor causes phase shift ϕ between V_{out} and V_{in} . The circuit properties of **Figure 3a** (left) are calculated according to the right-angled triangles shown in **Figure 3b** (right).

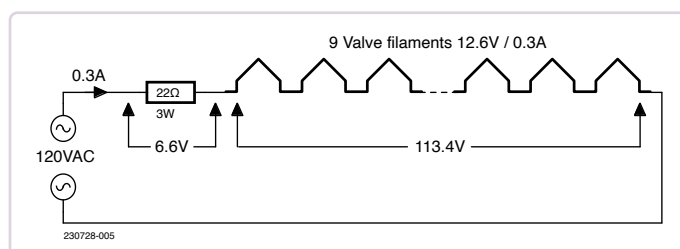


Figure 1: Starting from relatively low input voltages, in some cases the use of dropping resistors is still simple and cost-effective, even from an energy point of view.

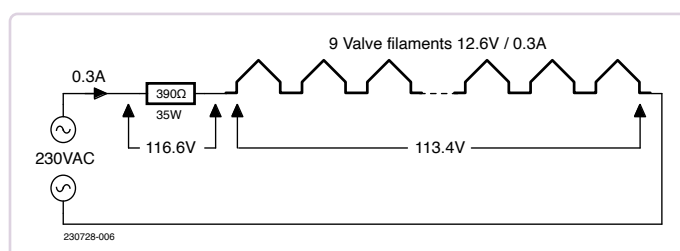


Figure 2: With higher supply voltages, as in the EU, this solution is no longer feasible, because of the high power dissipation and the large footprint that such a resistor would have as a consequence.

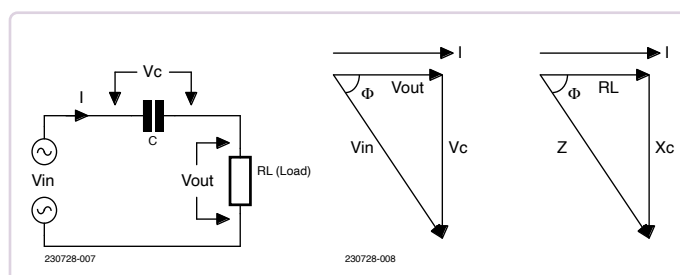


Figure 3: A capacitor used to power a resistive load by inducing a voltage drop, leveraging its typical capacitive reactance. In this design, the triangles on the right represent the relationships between V , I , C , X , and Z values.

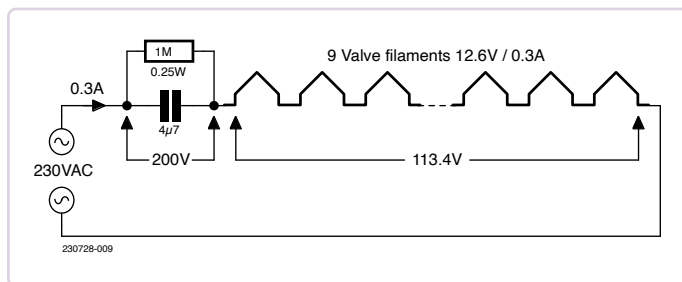


Figure 4: Using the formulas, the capacitance required to produce a V_{out} of 113.4 V was calculated from a V_{in} of 230 V AC. The 1 MΩ resistor discharges the capacitor after the circuit is turned off.

The calculations are as follows:

$$V_c = \sqrt{V_{in}^2 - V_{out}^2} \quad X_c = \frac{V_c}{I} = \frac{1}{2 \cdot \pi \cdot f \cdot C} \quad C = \frac{I}{2 \cdot \pi \cdot f \cdot V_c}$$

Where

C = capacitor, X_c = its capacitive reactance, Z = overall impedance, R_L = load

and

V_{in} = input voltage, V_{out} = output voltage, V_c = capacitor voltage, I = current.

Using a capacitor to drop the voltage in the circuit shown in Figure 2, the schematic was modified as shown in **Figure 4**.

And so, we get the formulas:

$$V_c = \sqrt{V_{in}^2 - V_{out}^2} = \sqrt{(230 \text{ V})^2 - (113.4 \text{ V})^2} = 200 \text{ V}$$

$$C = \frac{I}{2 \cdot \pi \cdot f \cdot V_c} = \frac{0.3 \text{ As}}{2 \cdot \pi \cdot 50 \cdot 200 \text{ V}} = 4.7 \text{ } \mu\text{F} \quad (3.98 \text{ } \mu\text{F in 60Hz-areas})$$

The 1 MΩ resistor has practically no influence during the operation of the circuit. Its purpose is to discharge the capacitor when the mains voltage is turned off.

Application With a Lower Voltage

In a small factory, some employees assemble PCBs and electrotechnical devices. They use Weller WTCP soldering irons (24 V/50 W), powered by a central 24 V transformer with a rated power of 600 VA.

Occasionally, PCBs containing SMD components are assembled using small soldering irons (12 V/25 W, like the Antex MLSX). For convenience, they should be supplied by the available central transformer(s) and the circuit shown in **Figure 5** could allow this, avoiding the need for a dedicated, 12 V AC transformer.

Component List

Please note: the components values of this list are only intended for the circuit and the load specifications indicated in Figure 5. For different purposes, their values will have to be re-calculated accordingly.

Capacitors

C1...C6: polymer-aluminum capacitor 220 μF (Kemet A759MY227M1JAAE045) [3]

Semiconductors

D1, D2: schottky diode SB150

Miscellaneous

X1, X2: screw terminal block, 5.08 mm pitch, 2 pole

F1: 5x20 fuse holder with fuse 2.5 A

Applying the formulas already shown, the theoretical value for the dropping capacitor should be:

$$V_c = \sqrt{V_{in}^2 - V_{out}^2} = \sqrt{(24 \text{ V})^2 - (12 \text{ V})^2} = 20.78 \text{ V}$$

$$C = \frac{I}{2 \cdot \pi \cdot f \cdot V_c} = \frac{2.083 \text{ As}}{2 \cdot \pi \cdot 50 \cdot 20.78 \text{ V}} = 319 \text{ } \mu\text{F}$$

The closest standard value available off-the-shelf is 330 μF, but film or MP capacitors of this value are not available. There are bipolar electrolytic capacitors, but they have the disadvantage of a high ESR (equivalent series resistance), which causes the warming of this component, resulting in a lifespan reduction.

The combination of two electrolytic capacitors of equal value shown in **Figure 6** behaves like a bipolar electrolytic capacitor. Note that in this application, the overall capacitance will be halved due to the series connection of two capacitors.

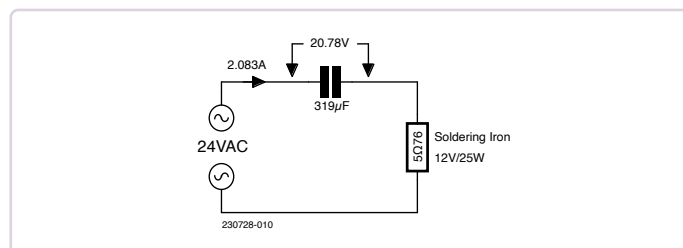


Figure 5: To power a 12 V/25 W soldering iron from a 24 V AC distribution line, this solution eliminates the need for the transformer.

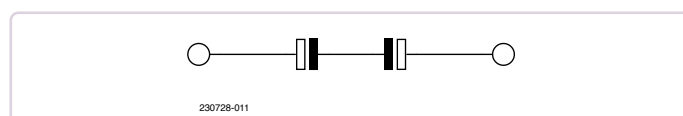


Figure 6: Since bipolar capacitors are not available, two polarized electrolytic ones can be combined. The resulting capacitance will be half of their nominal value.



Final Warning

For these designs, use only voltage-proof X2 capacitors [1] or MP capacitors for motors [2] and always insert a fuse in series with the circuit. The use of unsuitable and/or underrated capacitors in this application could cause them to be abnormally stressed, leading to possible overheating, gas discharge and housing deflation! Always observe all necessary safety precautions when working with line voltages!

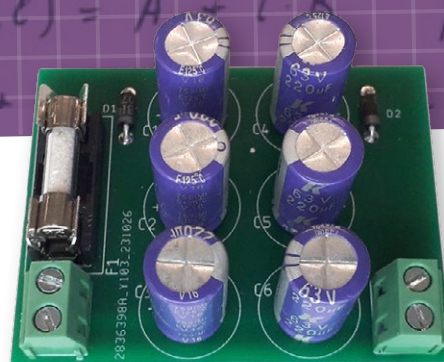


Figure 9: The finished prototype. Make sure to use capacitors of the types recommended in the article [3]. Never use ordinary, standard electrolytic capacitors in this design!

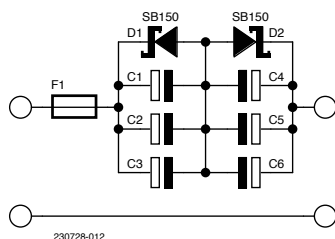


Figure 7: Design schematic for a capacitive reactance voltage dropper. Capacitance values should be calculated on a case-by-case basis, depending on the load's electrical properties.

For this reason, the circuit illustrated in **Figure 7** was developed. C1...C6 are polymer-aluminum capacitors with low ESR and high ripple current. This array works like a bipolar capacitor, but the additional schottky diodes, D1 and D2, are necessary for reverse polarity protection.

Depending on the momentary half-wave, the left side (D1 to C3) or the right side (D2 to C6) of the circuit serve as dropping capacitor. The capacitors' and diodes' voltage ratings must be higher than peak voltage V_{in} . The parallel connection of several capacitors decreases the overall ESR.

Figure 8 shows a simulation done with LTSpice. The green trace represents the peak-peak value of V_{in} (24 V_{rms} AC), the blue one the half-wave of D1, the red trace the half-wave of D2.

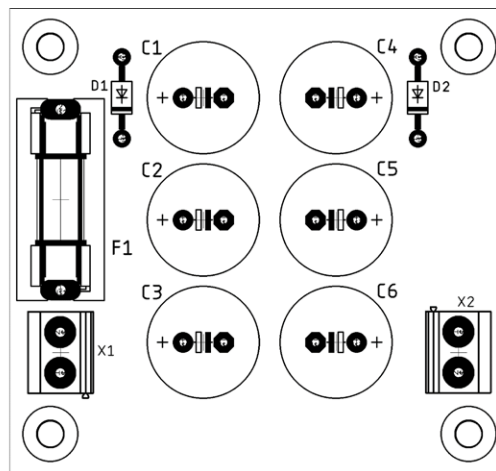



Figure 10: PCB component-side silkscreen.

The Prototype

Figure 9 shows the populated prototype PCB, **Figure 10** the component-side silkscreen.

This application can be used for our own needs by calculating the required capacitance. Determine this by combining two or more voltage-proof capacitors and appropriate schottky diodes. But please don't forget the fuse! 

230728-01

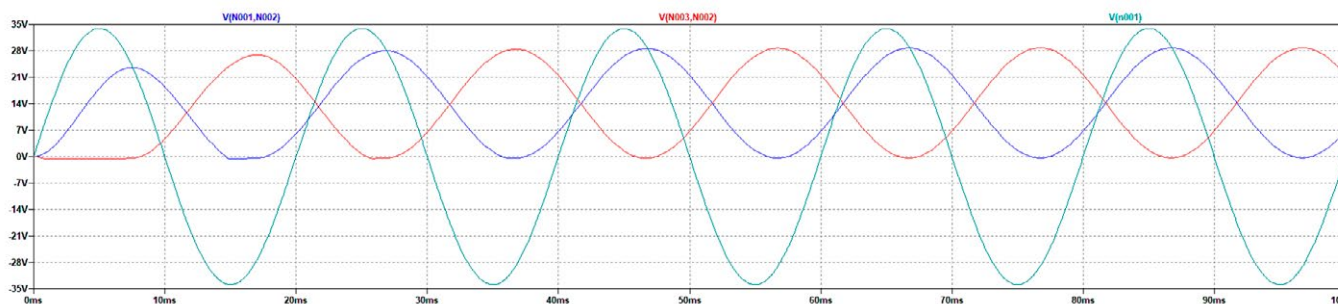


Figure 8: LTSpice simulation of this design, with an input of 24 V_{RMS} .

Questions or Comments?

Do you have technical questions or comments about this article? Please contact the author at hb9dkq@gmx.ch or the editorial team of Elektor at editor@elektor.com.




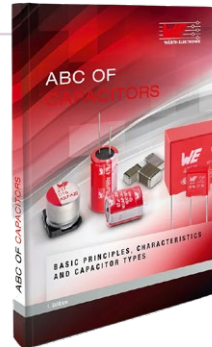
About the Author

Christoph Biel is a laboratory engineer and works in an educational institution. He trains students, apprentices, and youngsters in electronics and amateur radio technologies. He has been a radio amateur (HB9DKQ) since 1979.



Related Products

> **Stephan Menzel, ABC of Capacitors (Würth, 2021)** 
www.elektor.com/16630



WEB LINKS

- [1] Film Capacitors (Wikipedia): https://en.wikipedia.org/wiki/Film_capacitor
- [2] Motor capacitors (Wikipedia): https://en.wikipedia.org/wiki/Motor_capacitor
- [3] Datasheet — Kemet Radial Solid Polymer Aluminum Capacitors [PDF]: <https://tinyurl.com/kemetpolycaps>



Every week that you don't subscribe to Elektor's e-zine is a week with great electronics-related articles and projects that you miss!

So, why wait any longer? Subscribe today at www.elektor.com/ezine/en receive a **€5 coupon code** for the Elektor Store!



By Prof. Dr. Martin Ossmann (Germany)

A special feature of the MCP4725 from Microchip is the on-chip EEPROM. This allows the DAC to deliver a preset value immediately after it is switched on. This is of crucial importance for some applications. For example, trim potentiometers are often replaced by DACs in circuits nowadays, as this allows the parameters to be

set via software. These can be offset variables or operating point settings, for example. Normal DACs either exhibit undefined behavior immediately after being switched on or deliver a zero output value. The correct values can only be set once the CPU is ready for operation, which can take some time.



Figure 1: Connection of the MCP4725 to the Raspberry Pi Pico.

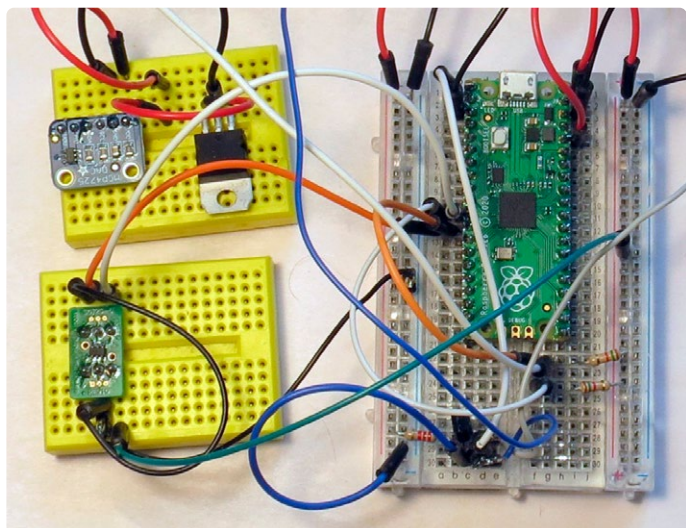


Figure 2: Setup of the test circuit on breadboards.

To illustrate this, let's take a look at **Figure 1**, which shows the MCP4725 being controlled by a Raspberry Pi Pico. Breakout boards are available for the DAC chip, for example from Adafruit, which already contain the resistors R4, R5 and R6 as well as the blocking capacitor C1. The MCP4725 normally draws the supply voltage V_{dd} via the 3V3-Out pin of the Pico.

This test circuit was set up on breadboards (**Figure 2**). The MCP4725 is connected using a simple SOT23-6 adapter (bottom left). Above this, you can also see the small adapter board from Adafruit, which is not connected in the picture.

Switch-On Behavior

Our test software toggles the DAC value back and forth between 2.5 V and 0.5 V immediately after switching on. **Listing 1** shows an excerpt of the C program, which can be downloaded from [1].

The USB power supply is switched on with a conventional mechanical switch. **Figure 3** shows the increase in the 5 V supply when switching on (cyan curve). Shortly afterward, the 3.3-V CPU supply voltage rises (purple) and is ready after approx. 1 ms. However, toggling (yellow) only starts after approximately 20 ms. This is the time the CPU needs for the boot process. This is a considerably long time, during which all sorts of things can go wrong if the DACs are not yet supplying the correct values.

This is exactly where the EEPROM feature of the MCP4725 comes in. The MCP4725 loads the DAC with the EEPROM content immediately after switching on, so that the desired values are available very quickly when switching on. This DAC can even be used with devices that do not have a microcontroller. During initial start-up, the device is connected to a controller to set the parameters, but later the EEPROM feature ensures that the correct value is available.

I²C Addresses

Internally, the MCP4725 is structured as shown in **Figure 4**. The MCP4725 has an I²C interface for communication with the CPU. In principle, eight different I²C addresses can be set, with four different addresses being preset during production (via A2 and A1). Which addresses (or address ranges) are used can be recognized by the marking of the IC according to **Table 1**. The last bit

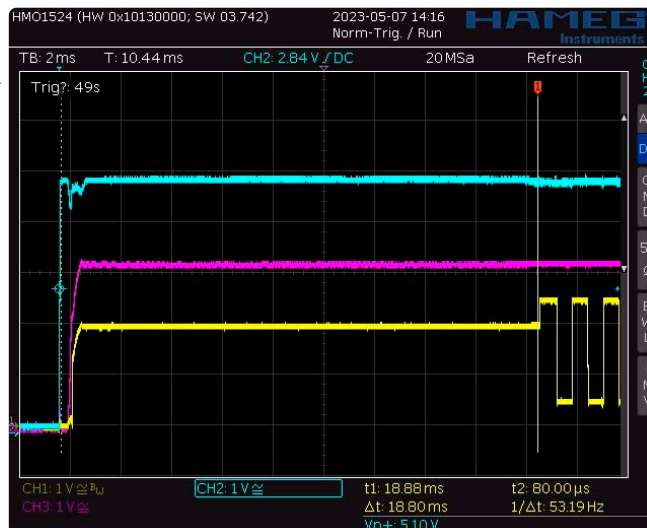


Figure 3: Switch-on process of the Raspberry Pi Pico.

of the I²C address can be set via the Ao pin (see the data sheet of the MCP4725 [2]).

The EEPROM can be accessed via the DAC; it cannot be addressed individually. The EEPROM is written to by copying twelve data bits simultaneously into the DAC register and the EEPROM using

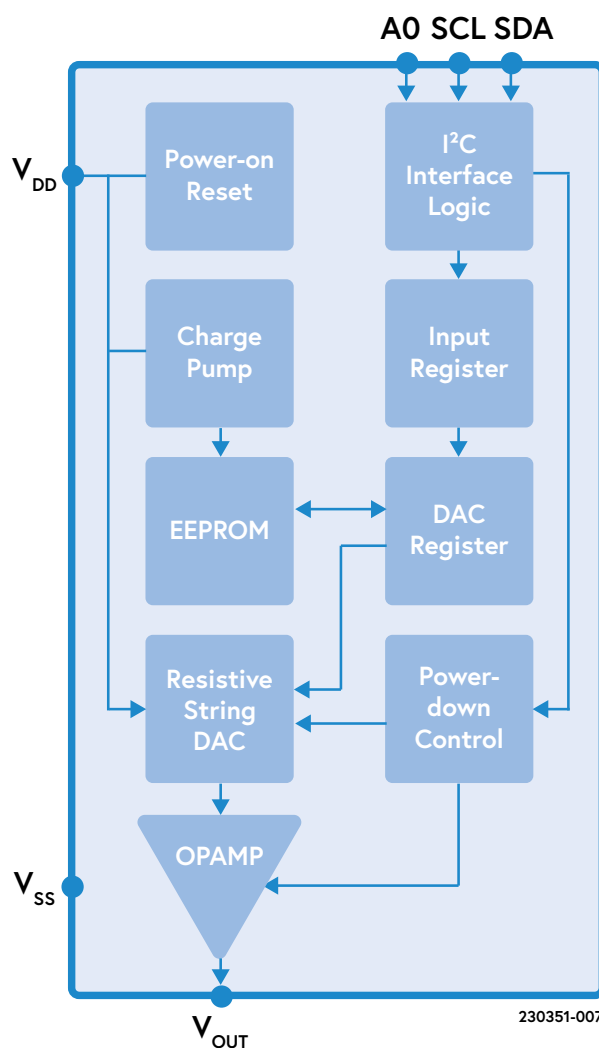


Figure 4: Schematic structure of the MCP4725 (Source: Microchip datasheet [2]).

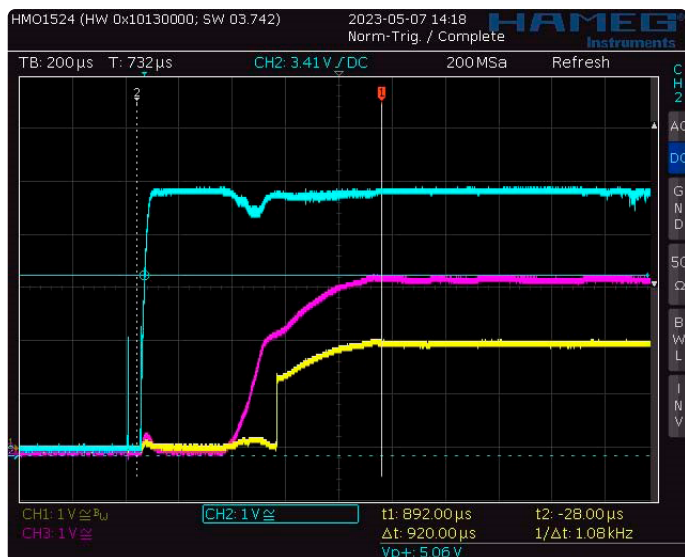


Figure 5: Switching on the Pico board with the MCP4725.

a special I²C command. A configuration bit determines whether only the DAC register or also the EEPROM is to be written. When the MCP4725 writes to the EEPROM, the RDY/BSY bit goes low and remains so until the EEPROM write process is completed. The datasheet [2] explains the write and read processes in detail in section 6.

Table 1: Marking of the SOT32 housing and corresponding I²C addresses.

| MCP4725 marking | I ² C option | I ² C address (A0=0) | Type number (MCP4725) |
|-----------------|-------------------------|---------------------------------|-----------------------|
| AJ | 00 | 060H | A0T-E/CH |
| AP | 01 | 062H | A1T-E/CH |
| AQ | 10 | 064H | A2T-E/CH |
| AR | 11 | 066H | A3T-E/CH |

Switch-On Behavior with EEPROM

The voltage curves in **Figure 5** show another switch-on process in our Pico setup, but this time using the EEPROM. The EEPROM has been programmed to supply a voltage of 2 V. This DAC voltage (yellow) is already stable approx. 1 ms after switching on the supply voltage (cyan)! And a large part of this delay is due to the fact that the CPU supply voltage of 3.3 V (purple) only starts to rise after 450 μs and then takes another 400 μs until the 3.3 V is stable. Before this is the case, the MCP4725 cannot provide a stable output voltage anyway, as the DAC uses the supply voltage as a reference. In this situation, which is already more comfortable than the original circuit, we do not even see the true speed of the MCP4725.

Fast Switch-On

To avoid this delay and get the most out of the DAC, we have equipped it with its own linear voltage regulator LF33ABV (as already shown in Figure 1). This makes the switch-on process look like **Figure 6**. Now the 3.3 V voltage (purple) is already stable about

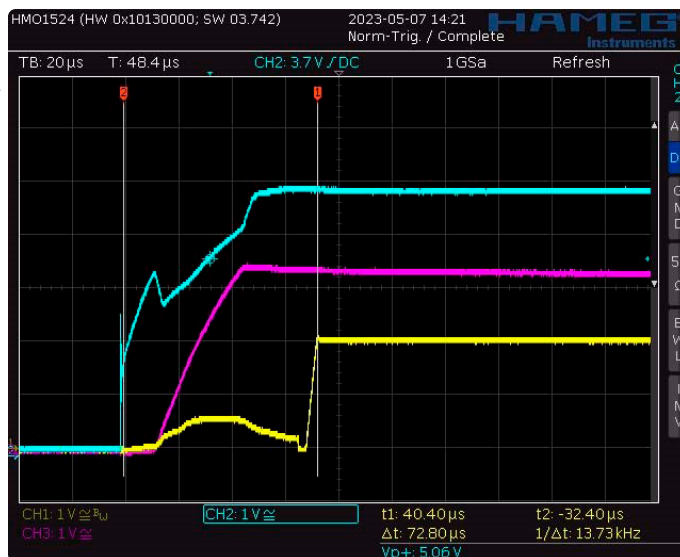


Figure 6: Switch-on process with a separate linear regulator for the DAC.

40 μs after switching on the 5 V supply (cyan). For the DAC's output voltage of 2 V (yellow), this applies after around 70 μs. That is already quite fast. Nevertheless, the "slow" increase in the supply voltage probably still accounts for around 40 μs.

To find this out, the supply voltage of the DAC was taken from a GPIO pin of the Raspberry Pi Pico. Since the DAC is a low-power IC and typically only draws 200 μA of current, a GPIO pin can easily supply this current. However, the capacitor C1 on the Adafruit MCP4725 BoB would again lead to a slow rise time here.

The MCP4725 was therefore used on a simple SOT32-6 adapter board [4] without additional circuitry (i.e., without R4...R6 and C1). Alternatively, you can obtain an MCP4725 BoB [5] and remove the blocking capacitor. A switch-on process then looks as shown in **Figure 7**. The 5 V voltage (cyan) has been stable for a long time. The firmware then sets the GPIO pin to high, whereupon the 3.3 V voltage on the MCP4725 (purple) rises very quickly and

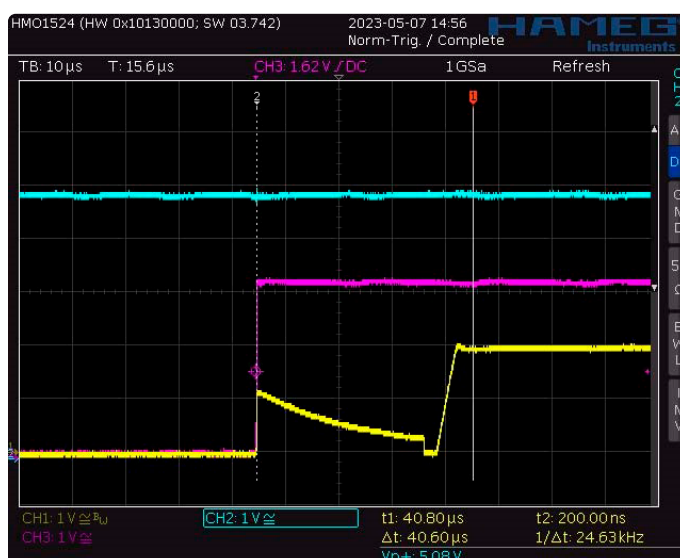



Figure 7: Switching on with GPIO pin, without C1.

is almost immediately stable. It now only takes around 40 μ s for the DAC to provide the output voltage of 2 V (yellow) in a stable manner. This is the “real” delay time of the EEPROM DAC; it can never be faster. But this delay time should be acceptable for most applications.

We operate the DAC without the normally required blocking capacitor, but this turned out to be unproblematic. You should just make sure that the supply voltage of the MCP4725 is available very quickly after switching on.

In this article, we have investigated what a power-up process of a microcontroller system with the Raspberry Pi Pico looks like and how to ensure that the digital/analog converter delivers a correct voltage value in good time. The phenomena found can typically be transferred to other systems. 

Translated by Jörg Starkmuth — 230351-01



About the Author

Martin Ossmann began reading Elektor at the age of 12 — and tinkering, of course. After studying electrical engineering and working as a development engineer for several years, he became a professor in the Department of Electrical Engineering and Information Technology at Aachen University of Applied Sciences. He is not only the author of scientific publications, but has also regularly published circuits and software projects with a great deal of technical know-how in Elektor for more than three decades.

Questions or Comments?

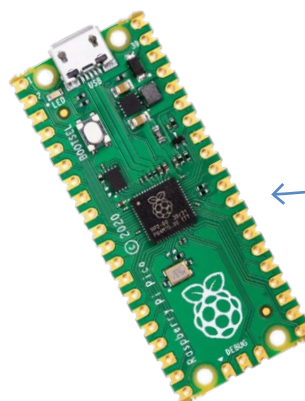
Do you have questions or comments about this article? Email the author at ossmann@fh-aachen.de, or contact Elektor at editor@elektor.com.



Listing 1: Writing the voltage values to the EEPROM (excerpt)

```
void MCP4725DACout(int DACval){
    i2cBuffer[0]=0x40 ;
    i2cBuffer[1]=DACval>>4 ;
    i2cBuffer[2]=DACval<<4 ;
    int nn=i2c_write_blocking(i2c_default,i2cAdr,
    i2cBuffer,3,false) ;
    printf("nn=%d\n",nn) ;
}

void writeEEPtest(){
    printf("writeEEPtest()...\n") ;
    float DACvalVolts=2.0 ;
    int DACvalBin=voltToBin(DACvalVolts) ;
    printf("DACvalVolts=%10.3f Volts = %04XH\n",DACvalVolts,DACvalBin) ;
    i2cBuffer[0]=0x60 ; // write DAC and EEPROM
    i2cBuffer[1]=DACvalBin>>4 ;
    i2cBuffer[2]=DACvalBin<<4 ;
    int nn=i2c_write_blocking(i2c_default,i2cAdr,
    i2cBuffer,3,false) ;
    while( getFlag()==0 ){ sleep_us(10) ; }
    printf("EEPwrite complete!\n") ;
}
```



Related Products

> **Raspberry Pi Pico**
www.elektor.com/19562

WEB LINKS

- [1] Download test program: <https://www.elektormagazine.com/230351-01>
- [2] MCP4725 data sheet (Microchip): <https://www.microchip.com/en-us/product/mcp4725>
- [3] Breakout board from Adafruit: <https://www.adafruit.com/product/935>
- [4] SOT23-6 adapter: <https://www.reichelt.de/de/en/adapter-sot23-6-1-00-mm-pitch-rm-2-54-mm-re-910-p167707.html>
- [5] Simple breakout board (with blocking capacitor!): <https://www.sparkfun.com/products/12918>

Fnirsi LCR-ST1

Smart LCR SMD Tweezers

By Harry Baggen (Netherlands)

Recently, both Zoyi and Fnirsi released affordable smart tweezers that also measure inductance, and for just a few dozen euros. In this review, I explore what the Fnirsi LCR-ST1 can do for such a low price and evaluate its practical usefulness.



Figure 1: The Fnirsi LCR-ST1 is not only useful for measuring SMDs, but also for wired components.

Identifying and measuring passive SMD components is often challenging. These parts are usually tiny, and you can't always tell by their shape whether you're looking at a resistor, capacitor, or inductor (**Figure 1**). To make measuring these SMDs easier, some manufacturers introduced "smart tweezers" years ago — a miniature [1] with tweezer-shaped probes that can clamp onto an SMD component to measure it. The original devices were (and still are) quite expensive, and soon after, affordable Chinese versions with similar designs emerged. The main drawback, however, was that these cheaper versions (with few exceptions) could only measure resistance and capacitance, not inductance.

The Fnirsi LCR-ST1: A Lot of Meter for Little Money

Opening the packaging of the Fnirsi LCR-ST1 [2], it's hard to believe what you get for under 40 euros. In a neatly lined case, you'll find the measuring tweezers themselves, two extra measuring tips with a curved front, a USB-C cable, and a magnetic plate for attaching the tweezers. There's also a small manual in Chinese and English, which, though brief, covers all the essential information you need to use the instrument (**Figure 2**).

The housing of the measuring tweezers is about 6×2.8×1.9 cm and features a 1.14-inch color display. Two measuring probes, each roughly 9 cm long, extend from the narrow end of the case.



Figure 2: You get all this for less than 40 euros.



Figure 3: The three-way switch on the side allows selecting most settings of the device.

Screws secure the metal tips at the ends, and you can tighten or loosen them without tools, making it easy to switch to the other tips that the set includes.

The controls are minimal. Next to the display, there is an on/off button and a memory button. On the side, there's a three-way toggle switch that moves left and right; you can also press down on it (**Figure 3**). I'll explain its functions in detail later. The USB-C port on the narrow side allows for charging the LCR-ST1's internal battery and connecting it to a PC.

The Possibilities of the Fnirsi LCR-ST1

When turned on, the LCR-ST1 starts in auto mode, automatically identifying whether the component under test is a resistor, capacitor, or inductor. The primary measurement (up to four digits) is visible prominently in the center, with the series resistance (R) and dissipation factor (D) below in smaller text (**Figure 4**). The

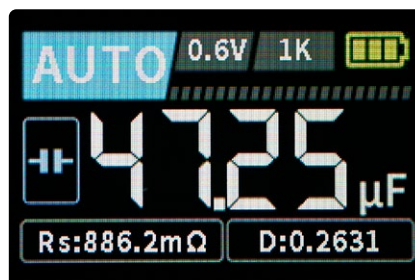


Figure 4: The bright color display shows, among other things, the measured value, the series resistance, and the dissipation factor.

measuring voltage (at the top) can be set to either 0.6 V (default) or 0.3 V by using the three-way switch. The lower voltage setting is useful for in-circuit measurements, as it avoids detecting diode transitions. The device also displays the measuring frequency. You can adjust it with the same switch to 1 kHz (default), 100 Hz, or 10 kHz. I didn't expect such versatility from such an affordable measuring probe.

Keep Track of Measurements

You can freeze measurements with the memory button. The device also stores them in its memory as a CSV file (**Figure 5**). You can access these measurements later on a PC via the USB connection. The same USB connection allows for easy firmware upgrades. Pressing and holding the memory button opens a setup menu where you can adjust settings such as display brightness, buzzer volume, and auto-off timing. The display is quite bright, so I reduced the brightness slightly for regular use.

| | A | B | C | D | E | F | G | H | I | J |
|----|-----|-------|-------------|---------------|------------------|-----------|----------|-----------|-----------|-----------|
| 1 | No. | Type | Level(Vrms) | Frequency(Hz) | Value(R nF uH V) | Rs(R) | Q | D | Z(R) | X(R) |
| 2 | 1 | C | 6 | 1000 | 10081742 | 9043 | 1745621 | 57 | 1573663 | 1578645 |
| 3 | 2 | C | 6 | 1000 | 10127062 | 9855 | 1594783 | 63 | 1566714 | 1571581 |
| 4 | 3 | C | 6 | 1000 | 10206804 | 4415 | 3531644 | 28 | 1554406 | 1559302 |
| 5 | 4 | C | 6 | 1000 | 101845 | 566898 | 2756621 | 36 | 155570918 | 156272246 |
| 6 | 5 | C | 6 | 1000 | 48851084 | 2254 | 1445650 | 69 | 325804 | 325796 |
| 7 | 6 | C | 6 | 10000 | 49499492 | 381 | 843913 | 118 | 32824 | 32153 |
| 8 | 7 | C | 6 | 100 | 49496470 | 1221 | 26334824 | 4 | 3196725 | 3215481 |
| 9 | 8 | C | 6 | 100 | 4140949687 | 1719 | 223586 | 447 | 38919 | 38434 |
| 10 | 9 | C | 6 | 1000 | 4193671562 | 730 | 51968 | 1924 | 4062 | 3795 |
| 11 | 10 | L | 6 | 1000 | 975737 | 1724 | 35552 | 2813 | 6627 | 6131 |
| 12 | 11 | L | 6 | 1000 | 48425845 | 92384 | 32935 | 3036 | 71105 | 304269 |
| 13 | 12 | L | 6 | 1000 | 101552090 | 197953 | 32234 | 3102 | 668363 | 638071 |
| 14 | 13 | C | 6 | 1000 | 41830462500 | 1051 | 3620 | 27628 | 1398 | 380 |
| 15 | 14 | C | 6 | 1000 | 48592765000 | 439 | 7464 | 13397 | 661 | 328 |
| 16 | 15 | C | 6 | 100 | 41283455000 | 706 | 54597 | 1832 | 4129 | 3855 |
| 17 | 16 | C | 6 | 1000 | 10127061 | 9573 | 1641630 | 61 | 1566727 | 1571581 |
| 18 | 17 | C | 6 | 1000 | 472154063 | 6589 | 51160 | 1955 | 34794 | 33708 |
| 19 | 18 | L | 6 | 1000 | 101610869 | 197369 | 32348 | 3091 | 668251 | 638440 |
| 20 | 19 | L | 6 | 1000 | 101573809 | 197624 | 32294 | 3097 | 668373 | 638207 |
| 21 | 20 | C | 6 | 1000 | 100283 | 51680 | 30709126 | 3 | 158705547 | 158705537 |
| 22 | 21 | DIODE | 6 | 1000 | 7116 | 139762246 | 539 | 185687 | 139441670 | 7526749 |
| 23 | 22 | R | 6 | 1000 | 101369863 | 101369863 | 0 | 417902148 | 101369863 | 2426 |

Figure 5: The measured values are stored in the internal memory and can be imported as a CSV file into Excel.

Figure 6: When measuring diodes, the polarity of the diode between the measuring pins is also shown.

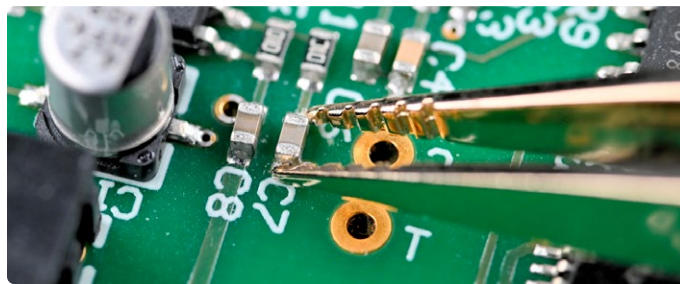
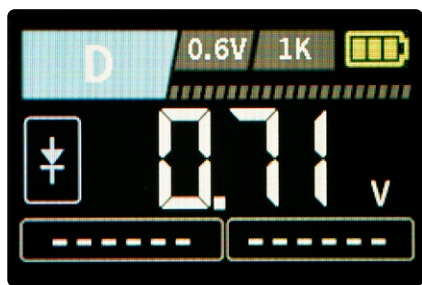


Figure 7: The measuring points are not very sharp, but they can easily be filed.

Auto and Manual Mode

Besides auto mode, you can manually select resistance, capacitance, or inductance measurement using the three-way switch. In a fourth position, the LCR-ST1 can measure diodes. Due to its low measuring voltage, it only measures standard diodes, not LEDs. A unique feature of diode measurements is that the display shows the diode's polarity, regardless of the diode's orientation, as the probe automatically detects it using alternating voltage (Figure 6).

The Fnrirsi LCR-ST1 in Practice

The LCR-ST1 is lightweight at just 40 grams and fits comfortably in hand. It powers on and is ready to use in about a second. The display is crisp, with clear, easy-to-read values from any angle. The controls are intuitive, and operation becomes straightforward after a few tries, even without the manual. The metal measuring tips are quite sharp, though some users might prefer them even sharper for measuring components soldered onto a PCB — an easy fix with a hand file (Figure 7).

In-Circuit Testing

I tested various components individually and some directly on a PCB; it was quicker and more efficient than using the SMD measuring tweezers on my larger LCR meter. When measuring components on a PCB, having the circuit diagram handy is helpful to understand which parts are connected. In auto mode, the meter reliably identified nearly everything. Wired components also measure well on this device. The grooves on the inside of the tips securely hold small component leads, like those of capacitors, for easy measurements without them slipping.

Built-In Calibration Feature

The measuring tweezers have a built-in calibration feature to compensate for the resistance between the tips. Calibration is done by pinching the tips together and briefly pressing the on/off button, though I didn't notice much effect. When the tips were closed, the meter showed a value of a few milliohms, which barely changed — a remarkably low resistance of 2 to 5 mΩ for such a basic device. There appears to be an additional calibration menu accessible by pressing the three-way switch left while turning on the device, though the exact procedure remains undocumented.

Accuracy of the Fnrirsi LCR-ST1

To test the accuracy, I measured various resistors, capacitors, and inductors, comparing results with my primary LCR meter (accurate to 0.5%). I was genuinely surprised by the results: Most measurements were within 1% of the larger meter's values. Only with larger inductors and capacitors, like a 4,700 μF electrolytic capacitor, did accuracy decrease, but stayed within Fnrirsi's specs at around 5%. The series resistance and dissipation factor also displayed impressive accuracy, though a minor drawback is the tweezers showing a dissipation (D) value for inductors rather than a quality (Q) factor — likely meant as 1/Q. This is something they could improve in future firmware, but overall, I'm very pleased with the unexpectedly high accuracy.

Final Impression

The Fnrirsi LCR-ST1 is an extremely convenient tool, essential for anyone working with SMDs. It quickly identifies components with impressive accuracy and allows for selection among three measuring frequencies and two voltages, making it suitable for in-circuit measurements as well. Wired components are also easy to measure. Although I have a "large" LCR meter, this device is far easier for quick measurements or checks — especially given its incredibly low price. It's a permanent fixture in my hobby lab! ◀

240657-01

Questions or Comments?

Do you have technical questions or comments about his article? Email Elektor at editor@elektor.com.



Related Products

- > **FNIRSI LCR-ST1 Smart SMD Tweezers (LCR/ESR Tester)**
www.elektor.com/20984
- > **UNI-T UT622E LCR Meter**
www.elektor.com/20782
- > **UNI-T UT603 LCR Meter**
www.elektor.com/20622

WEB LINKS

[1] J.-F. Simon, "LCR Meter: The UNI-T UT603 (Review)," elektormagazine.com, January 2024:
<https://elektormagazine.com/review/lcr-meter-the-uni-t-ut603-review>

[2] Fnrirsi LCR-ST1: <https://elektor.com/products/fnrirsi-lcr-st1-smart-smd-tweezers-lcr-esr-tester>

FORTEC INTEGRATED

Your project partner

- Embedded
- HMI systems
- Power supplies
- Displays and Touch

One partner,
unlimited
technology
solutions.

fortec-integrated.de
fortec-power.de



Raspberry Pi-Based Private Test & Measurement Lab

First Things First: The ADC

By Günter Spanner (Germany)

The combination of a Raspberry Pi (4 or 5) and a Raspberry Pi Pico has the potential to replace an entire “equipment park” of measuring devices like V-A-Ω meters, function generators, RF generators, oscilloscopes or transient recorders, as well as frequency counters. One must-have element in nearly all such test equipment is the analog-to-digital converter (ADC). In this article, we look at the process of implementing ADC functionality on “the Pi’s” from the Ground up (pun intended).

Editor’s Note: This article is an excerpt from the Elektor book, Raspberry Pi 4 OR 5 AND Pico. It was formatted and lightly edited to match Elektor Magazine’s conventions and page layout. The author and editor are happy to help with queries. Contact details are in the **Questions or Comments?** box.

In earlier chapters of the book, methods of displaying measurement results were covered. In the following, further possible do-it-yourself equipment will be discussed in some detail.

From Analog to Digital: Basics

The ADC in the Raspberry Pi Pico has the following performance characteristics:

- › Resolution: 12 bits
- › External inputs: 3
- › Conversion time: 2 μs, equivalent to 500 kSamples/s
- › Converter type: SAR (Successive Approximation)



The Pico actually supports five analog-to-digital converter channels internally. However, only three of them are externally available. The fourth analog channel (ADC3) can be used to monitor the input voltage V_{SY}. The fifth channel (ADC4) is connected to the internal temperature sensor. The **Table 1** shows the mapping of the ADC inputs to the pins.

Table 1: ADC inputs to I/O pins.

| ADC Channel | I/O Pin |
|-------------|---------|
| ADC0 | GP26 |
| ADC1 | GP27 |
| ADC2 | GP28 |

The ADC converters provide 12-bit values ranging from 0 to 4095 (which is $2^{12} - 1$). These values are multiplied by 16 internally by the system. Therefore, they are available as 16-bit numbers with a maximum value of 65,536. In principle, the Pico’s ADC inputs can capture voltages between 0 and 3.3 volts, which are converted into digital values by the ADC.

When reading the ADCs using MicroPython, the 12-bit data words are converted into a 2-byte value with a width of 16 bits. This corresponds to a value range of 0 to 65,535 ($2^{16} = 65,536$ discrete values).

The program `ADC_test.py` given in **Listing 1** displays the raw values of all ADC channels in the console. All programs discussed here can be downloaded free of charge from the resources page created “especially 4 U” for the book on the Elektor Store website [1].

If the inputs are left unconnected, random values will appear for channels 0, 1, and 2. The fourth



channel provides a value for VSYS, while the fifth channel provides the RP2040 internal chip temperature. However, this temperature value still needs to be converted to degrees Celsius. To obtain actual measurement values, the inputs can be connected to potentiometers as pictured in **Figure 1**. By doing so, individual voltages can be generated at each input. The output in the shell will display the results as shown in **Figure 2**. When writing the values in purely numerical form, you can also graphically represent them in the plotter:

```
...
while True:
    read0 = adc0.read_u16()
    read1 = adc1.read_u16()
    read2 = adc2.read_u16()
    read3 = adc3.read_u16()

    print(read0, read1, read2, read3)
    sleep(1)
```

Each channel will be automatically assigned its own line, see **Figure 3**.

External Power Supply by VSYS

If you want to operate the Pico as a stand-alone system without a USB connection to a PC, an external voltage can be supplied to VSYS. This voltage can be monitored using the internal ADC channel, `ADC3()`. In this case, since there is no connection to the PC, values cannot be displayed in the Thonny IDE. Therefore, you will need to rely on a directly connected display. A good choice for this is the OLED display, so all ADC values can be monitored using the program `ADC_to_OLED.py` given in **Listing 2**.

The program needs to be renamed as `main.py` so that it automatically starts after a power interruption. Then, the Pico can be powered through VSYS with an external voltage ranging from 1.8 V to 5.5 V. The following power sources are suitable for this:

- external power supply
- USB charger (5 V)
- batteries, e.g., 2× 1.5 V or 3× 1.5 V
- NiMH rechargeable batteries, e.g., 2× 1.2 V or 3× 1.2 V or 4× 1.2 V
- Li-ion batteries (3.7 V nominal)

The current input voltage is now displayed on the OLED display along with other values, allowing for monitoring. **Figure 4** shows the operation with a USB connection and two 1.2 V batteries, giving 2.4 V nominally.

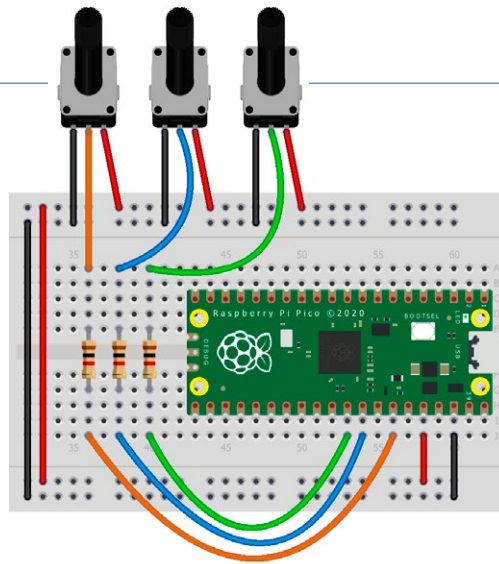


Figure 1:
A quick breadboard-build to test the ADC channels.

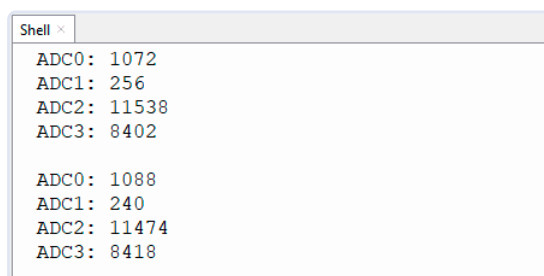


Figure 2:
Values measured from the ADC Channels.

Figure 3: Graphical output from three analog channels.

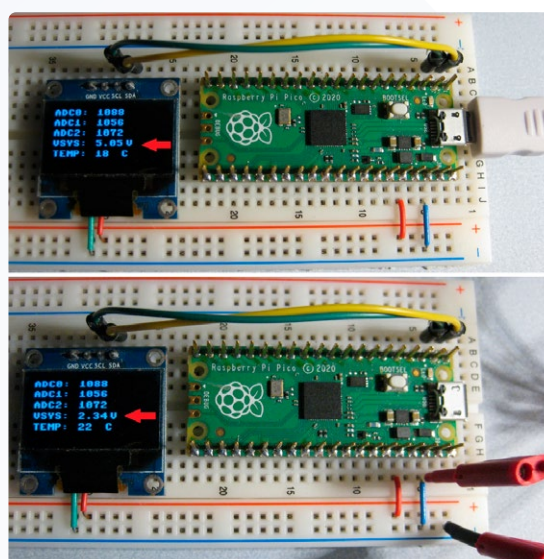
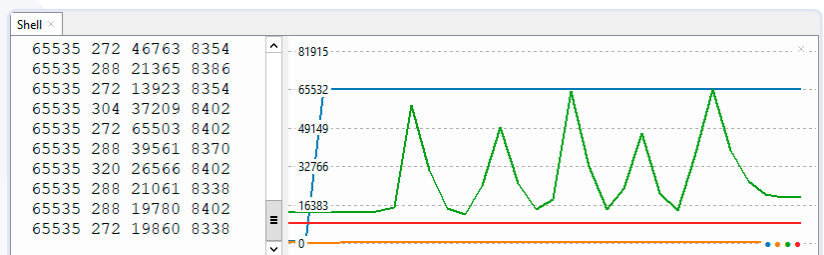


Figure 4: Operation of the Pico using external supply voltages.



Listing 1: ADC_test.py

```
adc0 = ADC(0)
adc1 = ADC(1)
adc2 = ADC(2)
adc3 = ADC(3)
adc4 = ADC(4)

while True:
    print('ADC0:', adc0.read_u16())
    print('ADC1:', adc1.read_u16())
    print('ADC2:', adc2.read_u16())
    print('ADC3 (VSYS):', adc3.read_u16())
    print('ADC4 (TEMP):', adc4.read_u16())

    print('=====')
    sleep(1)
```



Listing 2: ADC_to_OLED.py

```
from machine import ADC
from machine import Pin, I2C, ADC
from ssd1306 import SSD1306_I2C
from time import sleep

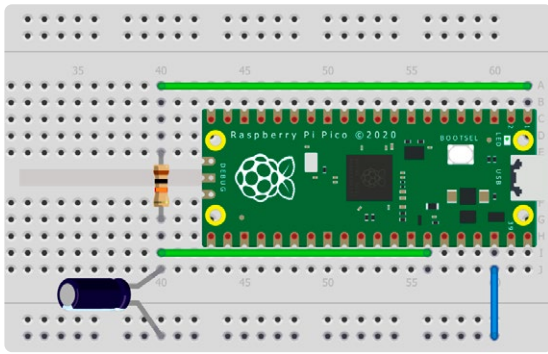
xmax=128
ymax=64
cf = 3.3 / (65535)
oled = SSD1306_I2C(xmax, ymax, I2C(0, scl=Pin(1), sda=Pin(0), freq=400_000))
adc0 = ADC(0)
adc1 = ADC(1)
adc2 = ADC(2)
adc3 = ADC(3)
adc4 = ADC(4)
while True:
    print('ADC0:', adc0.read_u16())
    print('ADC1:', adc1.read_u16())
    print('ADC2:', adc2.read_u16())
    print('ADC3 (VSYS):', round(adc3.read_u16()*cf*12,2), 'V')
    print('ADC4 (TEMP):', int(33-((adc4.read_u16()*cf)-0.706)/0.001721), '°C')

    print('=====')
    sleep(1)
    oled.fill(0)

    oled.text('ADC0:',0,0,1)
    oled.text('ADC1:',0,12,1)
    oled.text('ADC2:',0,24,1)
    oled.text('VSYS:',0,36,1)
    oled.text('TEMP:',0,48,1)

    oled.text(str(adc0.read_u16()),50,0,1)
    oled.text(str(adc1.read_u16()),50,12,1)
    oled.text(str(adc2.read_u16()),50,24,1)
    oled.text(str(round(adc3.read_u16()*cf*12,2)),50,36,1)
    oled.text('V',85,36,1)
    oled.text(str(int(33-((adc4.read_u16()*cf)-0.706)/0.001721)),50,48,1)
    oled.text('C',80,48,1)

    oled.show()
```



▲ Figure 5: ADC test circuit with low-pass filter.

```
Shell x
>>> %Run -c $EDITOR_CONTENT
Discharge...
Starting...
0 256
256 448
512 720
768 896
1024 1152
1280 1376
1536 1632
```

▲ Figure 6: Values output by the system (DAC count and ADC value).

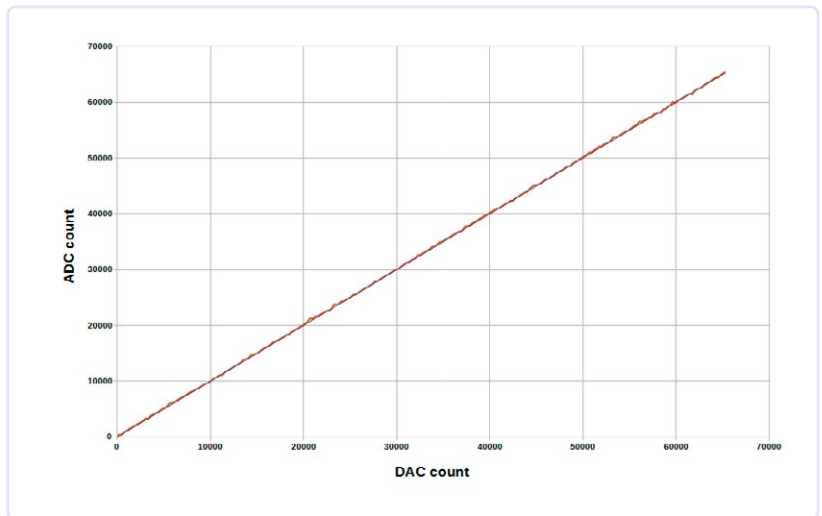
Since the Pico does not have an integrated Digital-to-Analog Converter (DAC), the ADC cannot be directly tested using a software-generated analog voltage. However, the PWM function provides a solution. By using a low-pass filter, it allows the generation of an analog voltage. A suitable low-pass filter can consist of a 10 k Ω resistor and a 100 μ F electrolytic capacitor (**Figure 5**).

The program `PWM_to_ADC.py` shown in **Listing 3** generates a slowly rising PWM voltage at Pin 0. This voltage is smoothed using the low-pass filter and measured using the ADC(2). After a 100-second discharge period due to the 100 μ F electrolytic capacitor, the measurement values are printed as a table in the Thonny shell (**Figure 6**). The data can be copied and pasted into a spreadsheet application such as LibreOffice or Excel and graphically represented as illustrated in **Figure 7**.

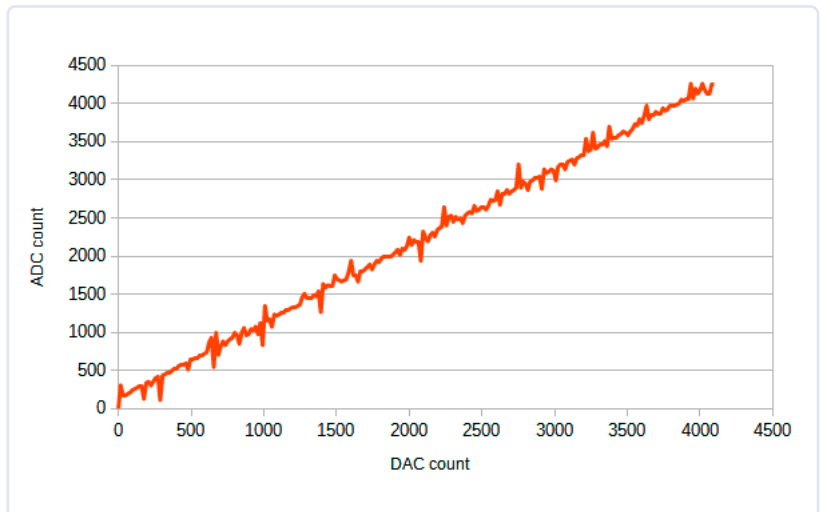
The Pico's ADC exhibits good linearity compared to other microcontrollers. However, upon closer examination of the lower ADC values (**Figure 8**), it is evident that there is a significant level of noise present. Additionally, the converter displays a certain offset. For precise results, methods such as filtering or averaging need to be applied in order to mitigate the noise. Additionally, the offset should be corrected software-wise for accurate measurements.

ADC in Practice: A Computer Voltmeter

The Pico's analog inputs are well suited for measuring voltages. Their only limitation is that they can only measure up to a maximum of 3.3 V without external circuitry. However, this is not a significant



▲ Figure 7: ADC test results.



▲ Figure 8: ADC test result for small voltages.



Listing 3: PWM_to_ADC.py

```
import time
from machine import Pin, PWM

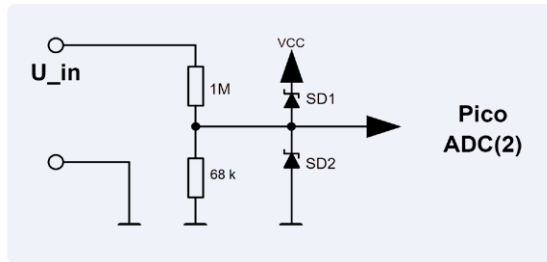
print('Discharge...')

adcPin = Pin(28, Pin.IN)
pwm0 = PWM(Pin(0))
pwm0.freq(20000)
pwm0.duty_u16(0)
time.sleep(100)

print('Starting...')

for dacVal in range(0,65540,256):
    pwm0.duty_u16(dacVal)
    time.sleep(1)
    print(dacVal, machine.ADC(2).read_u16())
```

Figure 9:
Voltage divider for
expanding the voltmeter
measurement range.



```
from machine import ADC, Pin
import time
```

```
R1 = 68
R2 = 1000
```

```
conversion_factor=3.3/(1<<16)*(R1+R2)/R1
adc=ADC(2)
```

```
while True:
    print(adc.read_u16()*conversion_factor)
    time.sleep(1)
```

As an additional protection against overload, Schottky diodes (such as the type BAT41) can be installed as shown in **Figure 9**. SD1 diverts over voltages, while SD2 protects against reverse polarity of the input voltage. By using a calibrated reference voltmeter, a high level of accuracy can be achieved. **Table 2** shows a comparison of measurement values between a calibrated bench voltmeter and the Pico voltmeter. Graphically, this can be represented as shown in **Figure 10**.

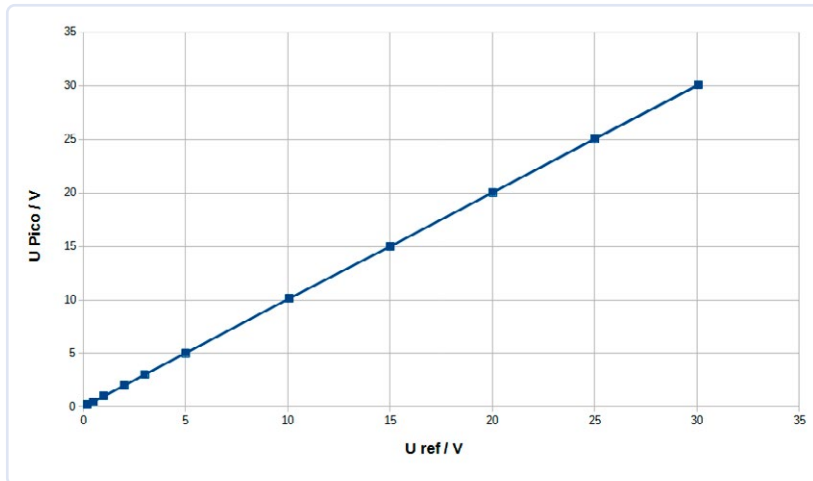


Figure 10: Calibration
graph of the Pi Voltmeter.

problem, as the measurement range can be practically extended nearly indefinitely with a simple voltage divider. **Figure 9** shows a suitable circuit. The voltage divider, consisting of a 1 MΩ and a 68 kΩ resistor, already extends the measurement range to over 50 V.

Voltages exceeding 50 V are rarely encountered in modern electronic circuits. Moreover, when dealing with such voltages, you must use safety-certified measuring devices.

Warning: Voltages greater than 50 V can be potentially life-threatening under certain circumstances.

The voltage division ratio can be calculated for the given resistors as:

$$U_o = R_1 / (R_1 + R_2) = 68 \text{ k}\Omega / 1068 \text{ k}\Omega = 0.0637$$

Thus, an input voltage of 50 V is reduced to a safe 3.18 V and can be measured using the internal reference.

The effect of the voltage divider must be considered in the software. The calibration factor “cal” is responsible for this. It incorporates both the factor from the voltage divider and an additional factor (0.94 in the example sketch below) that considers tolerance from the reference voltage source and the resistors.

Table 2: Measurements comparison: Calibrated bench voltmeter vs. Pico voltmeter.

| U_Reference [V] | U_Pico [V] |
|-----------------|------------|
| 0.202 | 0.20 |
| 0.498 | 0.48 |
| 1.002 | 1.01 |
| 2.004 | 1.99 |
| 3.006 | 3.02 |
| 5.021 | 5.03 |
| 10.082 | 10.14 |
| 15.020 | 15.01 |
| 20.018 | 20.05 |
| 25.011 | 25.06 |
| 30.082 | 30.11 |

The calibration of the voltmeter using the calibration factor is referred to as “software calibration.” Alternatively, a hardware calibration can also be performed. For this purpose, the circuit needs to be extended with a potentiometer. Spindle trimmers are highly suitable for this task. These components can be adjusted very sensitively and precisely, and they also exhibit relatively good long-term stability.



Again, a comparison is made with a calibrated reference voltmeter. However, this time, instead of adjusting a parameter in the program, the spindle trimmer is adjusted until the Pi voltmeter displays the correct value. The advantage of this method is that it avoids the need to load a new software version into the controller for recalibration. Instead, periodic calibration can be easily performed from time to time or under specific environmental conditions (e.g. very high or very low temperatures). However, the disadvantage is that an additional component is required. Furthermore, potentiometers, being electromechanical components, always introduce additional drift, meaning that environmental influences can cause changes in the electrical parameters, thereby reducing the long-term stability of the calibration.

If the selected potentiometer has a total resistance of 1 k Ω , it allows for an adjustment range of approximately 5% of the measured value. Larger potentiometer values may provide wider adjustment ranges but with lower adjustment precision. ◀

240390-01

Questions or Comments?

Do you have any questions or comments related to this article? Email the author at g.spanner@web.de or Elektor at editor@elektor.com.



Related Products

- **Günter Spanner, *Raspberry Pi 4 OR 5 AND Pico* (Elektor 2024, Book)**
www.elektor.com/20828
- **Günter Spanner, *Raspberry Pi 4 OR 5 AND Pico* (Elektor 2024, E-Book)**
www.elektor.com/20829

WEB LINK

- [1] Software Complement for: Raspberry Pi 4 OR 5 AND Pico:
<https://www.elektor.com/products/raspberry-pi-4-or-5-and-pico>

Join the Elektor Community

- ✓ The Elektor web archive from 1974!
- ✓ 8x Elektor Magazine (print)
- ✓ 8x Elektor Magazine (digital)
- ✓ 10% discount in our web shop and exclusive offers
- ✓ Access to more than 5,000 Gerber files



Take out a
membership!



www.elektormagazine.com/member



Electronic Load Resistor

An Out-of-the-Box Project

By Peter Grundmann (Germany)

If you want to test batteries or solar panels, you need a load resistor. Fixed resistors are inexpensive, but often impractical to use. With some electronics, you can not only simulate a load, but also implement useful additional functions.

As a model airplane enthusiast who only has electrically powered models, you have a lot to do with batteries that you want to test or just discharge. But also in many DIY electronics projects, such as power supplies, the question of performance often arises. Does the power source reach the targeted maximum current without a voltage drop? These and similar tasks or questions can be answered with fixed resistors, but you quickly realize that a whole lot of them are needed. Also, a reasonable structure of a load resistor is essential, especially at higher powers, to ensure safe use.

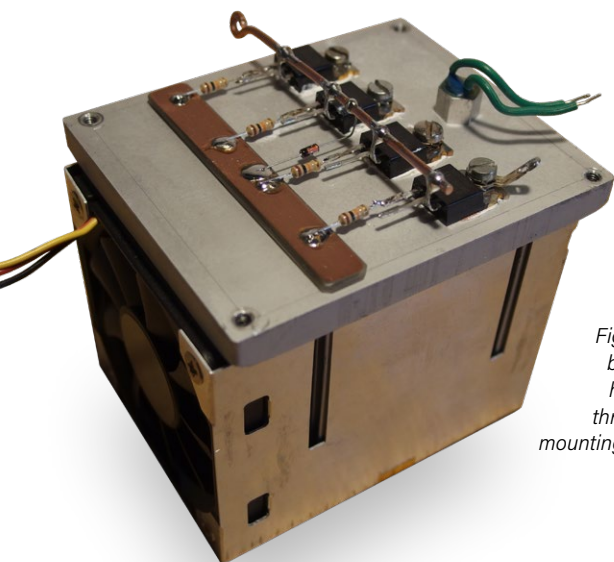


Figure 1: The solid base plate of the heatsink has M3 threaded holes for mounting the FETs, and an NTC.



While searching for an elegant solution, I came across a suggestion on the Internet that seemed to solve part of the problem [1]. However, only the heart of the circuit is documented; a power supply and even instructions for the actual implementation are missing.

However, the idea is simple and easy to explain. An operational amplifier compares a target voltage with an actual value and controls FETs that act as load resistors. The whole thing is therefore a classic control circuit. If you take the voltage across a resistor in the load circuit as a reference value, you can keep the current constant. If you switch to the voltage of the load, a constant voltage can be achieved at the connections of the current sink. The advantage of using FETs instead of bipolar transistors is that no control current flows that could complicate the measurement of the load current.

Specifications

My device should be able to handle a load current of up to 10 A at a minimum of 12 V. With a power dissipation of 120 W, the heatsink is extremely important, which would quickly become very unwieldy without a fan. In PC technology, there were and are processors that require the dissipation of considerable amounts of heat; and I still had such a cooler/fan combination from Pentium times. With a large cooling surface and a fairly quiet operation, the part recommended itself for further experiments. So, if you are thinking of building a similar device, you might want to check your "you-might-need-again" box for suitable parts, because not everything has to be bought new!

In **Figure 1**, you can see my heatsink, on which four FETs of the type IRF740, along with gate resistors, an NTC, and a protection diode have already been mounted. The semiconductors used were all still laying around in my "junk box"; many similar N-channel MOSFET types would certainly also be usable.

With the high currents involved, it is not unreasonable to think about sensibly dimensioned connections in good time. The resistors for

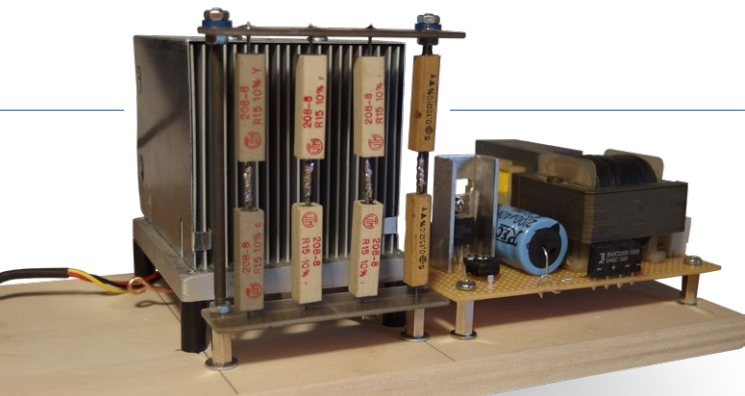
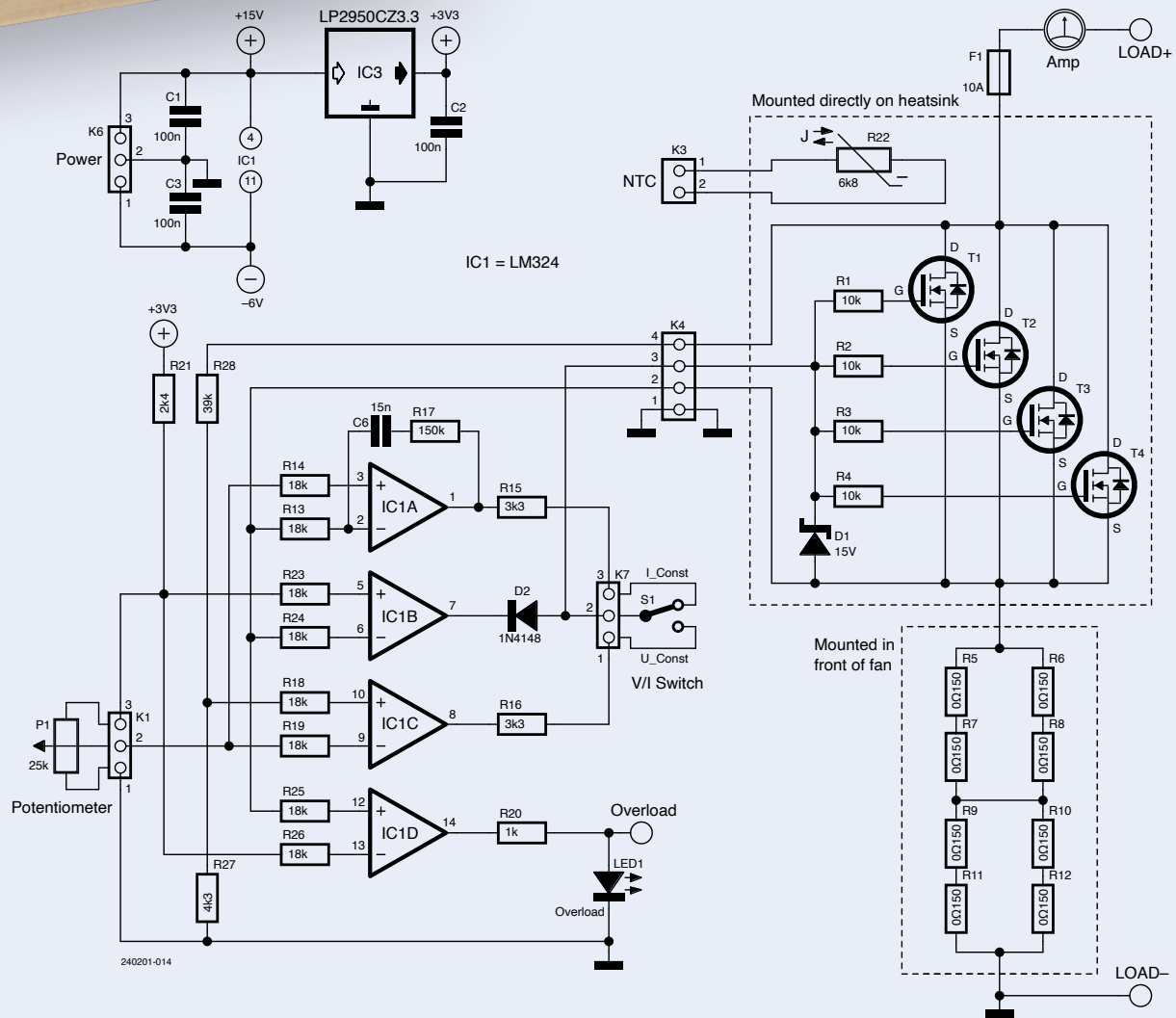


Figure 2: A total of eight resistors with a value of $0.15\ \Omega$ are connected in such a way that the total resistance is $0.3\ \Omega$. Installed in the airflow, their temperature rise remains within tolerable limits.

Figure 3: The "heart" of the electronic load resistor with the operational amplifiers, the FETs, and the power resistors.



measuring the load current also deserve attention with regard to their "heating power". In my components box, I found eight specimens of $0.15\ \Omega/5\ \text{W}$, which I connected in such a way that a total resistance of $0.3\ \Omega$ resulted (Figure 2). The resistors can dissipate up to 30 W, and placing them in the exhaust airflow of the fan prevents overheating.

Control Circuitry

The control electronics is based on a quad operational amplifier LM324 for current or voltage control, as shown in Figure 3. The positive operating voltage at K6 is first used to obtain the reference voltage with a 3.3 V fixed voltage regulator and applied to the potentiometer P1 via the resistor R21. The resistor R21, with its $2.4\ \text{k}\Omega$, is adapted to the potentiometer with $25\ \text{k}\Omega$ so that a voltage

of $0\ldots 3\ \text{V}$ can be set at the center tap of the potentiometer. Any other potentiometer between $1\ \text{k}\Omega$ and $50\ \text{k}\Omega$ should also be okay if R21 is changed accordingly. A precision shunt regulator like the TL431 with the appropriate circuitry would have been a better choice for directly generating the 3 V reference voltage, but unfortunately, it wasn't available in my box.

The wiper of potentiometer P1 is connected to the non-inverting input of IC1A, the first op-amp of the LM324. The inverting input is connected to the current sensing resistors and the output to the gates of the FETs via switch S1 in the I_{const} position. This op-amp will try to adjust the load current in such a way that the voltage drop across the measuring resistors corresponds to the voltage set with P1,

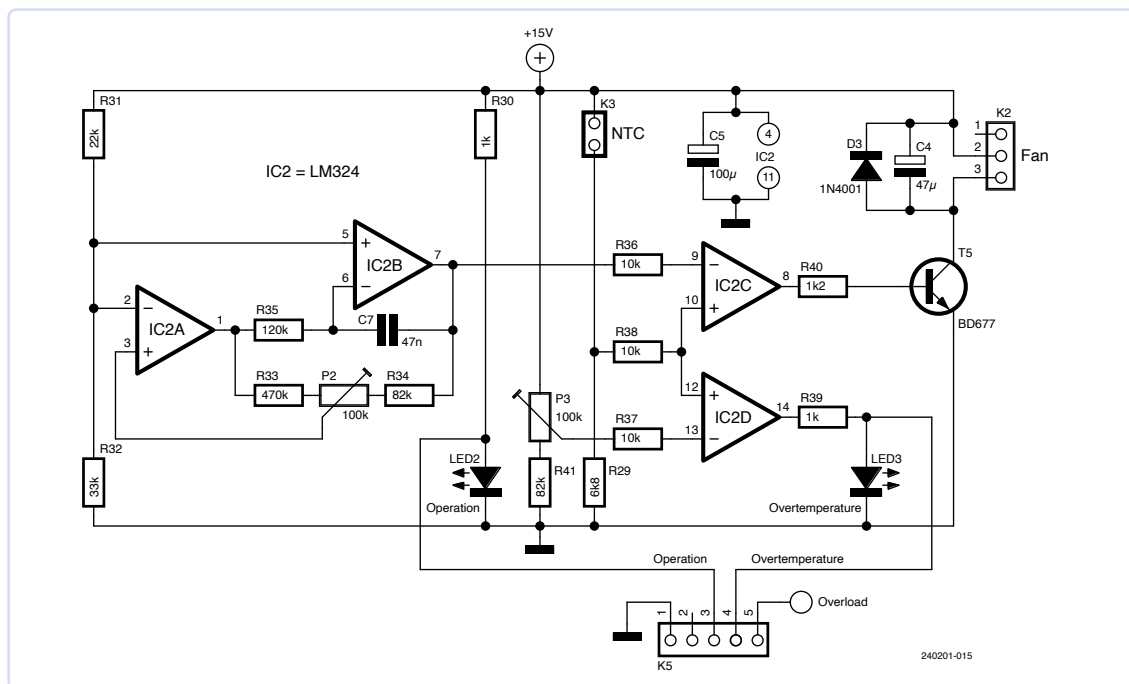


Figure 4: This circuit controls the fan speed based on the temperature.

thus ensuring a constant load current. The RC element C6/R17 was determined experimentally to prevent oscillation tendencies. This problem was only recognizable in this mode with the oscilloscope and could easily be eliminated.

The wiper voltage at the potentiometer is also fed to the inverting input of the op-amp IC1C. The non-inverting input of this op-amp is connected to the input voltage at the load (LOAD+) via the voltage divider R27/R28. If the opamp output is connected to the FETs via the switch in the *U_{const}* position (constant voltage), it will try to prevent the voltage across the electronic load from rising above the set value. The dimensioning of R27 and R28 allows a maximum voltage of about 30 V.

Since excessively high currents could occur in the *U_{const}* switch position, the opamp OP IC1B limits the maximum current. In such a

case, the diode D2 pulls the gate voltage down to ground so that the targeted maximum current of 10 A is not exceeded. To complete the quartet in the LM324, the fourth opamp IC1D controls the overload indicator LED1 in the event of an overcurrent.

To keep an eye on the load current at all times, a 10 A moving coil instrument is included in the connection to the load outside of the control loop. As you can see in the title picture, I used an ammeter with a slightly different measuring range in my device (because it was just at hand), which I adapted using a corresponding voltage divider.

Fan Control

The second circuit part around IC2 (Figure 4), which is also a quad opamp LM324, controls the fan, which should only start when necessary; thereafter, the speed should be increased with rising temperature. This helps to avoid annoying background noise as much as possible.



Component List Control Circuitry

Resistors:

(all 1/4 W, unless otherwise specified)

R1...R4, R36...R38 = 10 k

R5...R12 = 0Ω150 / 5 W

R13, R14, R18, R19, R23...R26 = 18 k

R15, R16 = 3k3

R17 = 150 k

R20, R30, R39 = 1 k

R21 = 2k4

R22 = NTC 6k8 with screw mounting

R27 = 4k3

R28 = 39 k

R29 = 6k8

R31 = 22 k

R32 = 33 k

R33 = 470 k

R34, R41 = 82 k

R35 = 120 k

R40 = 1k2

P1 = pot 25 k

P2 = trimming pot 100 k

P3 = trimming pot 100 k

Shunt resistors for ammeter, depending on type

Capacitors:

C1...C3 = 100 nF

C4 = 47 μF/25 V

C5 = 100 μF/25 V

C6 = 15 nF

C7 = 47 nF

Semiconductors:

D1 = Z-Diode 15 V

D2 = 1N4148

D3 = 1N4001

LED1 = LED 5 mm yellow

LED2 = LED 5 mm green

LED3 = LED 5 mm red

T1...T4 = IRF740

T5 = BD677

IC1, IC2 = LM324

IC3 = LP2950-CZ3,3

Miscellaneous:

S1 = toggling switch 1x

F1 = fuse 10 A with holder for front panel

K1, K2, K6, K7 = 1x3-pin header with plug

K3 = 1x2-pin header with plug

K4 = 1x4-pin header with plug

K5 = 1x5-pin header with plug

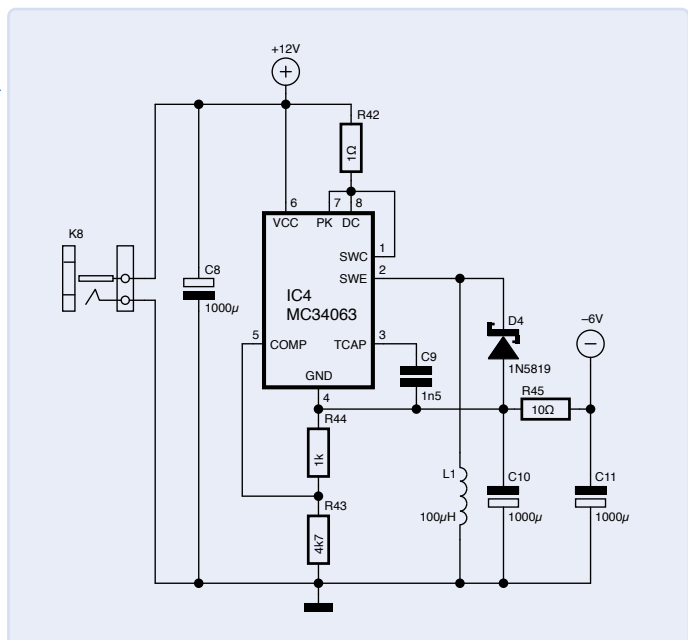


Figure 5: From the simple positive output voltage of a plug-in power supply, the inverter generates a negative operating voltage according to the manufacturer's application.

The opamps IC2A and IC2B are used to construct a triangle generator that oscillates around the voltage set with R31 and R32. This voltage is chosen so that at room temperature the negative peaks of the signal are above the value at the voltage divider NTC and R29. IC2C compares the voltage at the NTC with the triangular signal and switches T5 on when the temperature rises (i.e., when the voltage at the NTC/R29 node increases). This results in a pulse/pause ratio (duty cycle) of 0...100%. The amplitude of the signal can be influenced using the trimming potentiometer P2. This changes the two temperature values that define the PWM end points. Since the usual fans do not start at very low duty cycles, the electrolytic capacitor C4 extends such short pulses.

The warning function for excessive temperature is realized with trim potentiometer P3 and IC2D. You can adjust within wide limits at which temperature LED3 starts to light up. This should only be the case when even the fully rotating fan is unable to dissipate the waste heat (i.e., the temperature of the heat sink continues to rise). The three signals for overload, overheating, and fan operation (plus ground) are available at connector K5 for connecting corresponding LEDs on the front panel.

Negative Voltage

I had a spare power supply lying around that could be used to supply the control electronics and the fan control. It provided 12...15 V in the positive branch and -6 V in the negative branch, which was a good match. If it hadn't been available, I could have used one of the numerous plug-in power adapters that were available. A unit from an old router with a +12 V output voltage, supplemented by a small switching regulator to generate the negative voltage, might even have been the better choice, because an external power adapter is an advantage in terms of safety, as it keeps the mains voltage away from the device.

The data sheet circuit [2] in **Figure 5** shows the few components around the MC34063 switching regulator from Texas Instruments that can generate such a negative voltage of -6 V. Whether the RC filter R45/C11 is actually necessary was not investigated in detail. It may be possible to do without it if the output ripple is not a problem, or

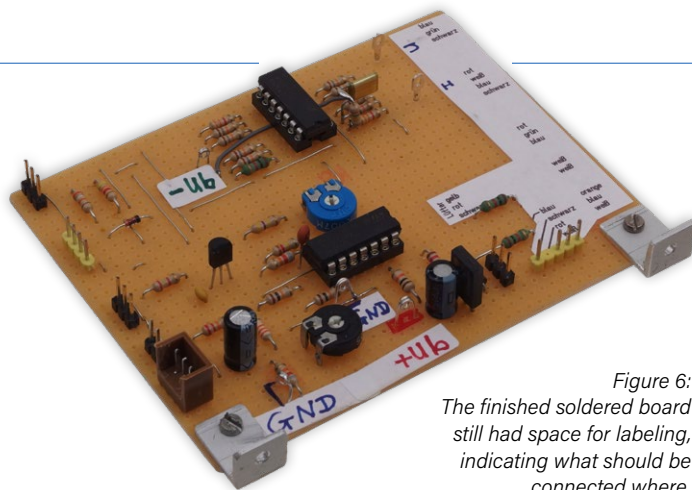


Figure 6: The finished soldered board still had space for labeling, indicating what should be connected where.

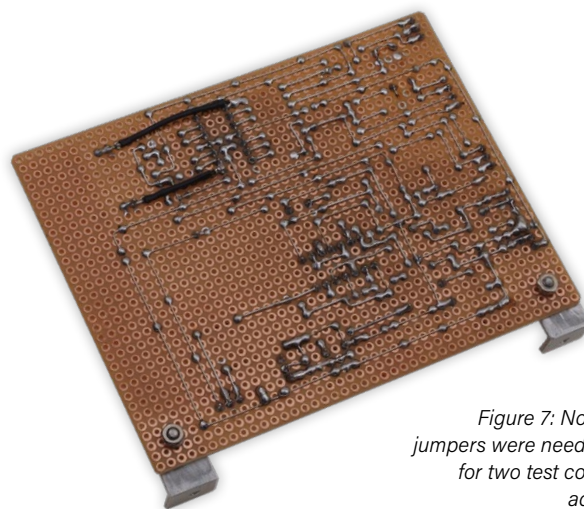


Figure 7: No insulated jumpers were needed except for two test connections added later.

to replace R45 with an inductance of 1.0 µH, so that the ripple of the output voltage is significantly reduced.

Routing on Perfboard

Despite the rather extensive circuitry, I was keen to build and wire the electronics on a perfboard. However, my first attempt was ultimately unworkable, with a total of 19 soldered connections leading from the board to externally mounted components — a nasty tangle of wires!

Finally, I configured my PCB software TARGET 3001! so that I could easily and reliably simulate the routing on a perfboard. The displayed grid is set to 2.54 mm, but components can also be placed outside the grid, since their reference point, the cross handle, is not always on a solder point. In this case, the software does not directly support the process; you have to make sure that the solder pads are placed only on the grid points. So if you place the components correctly and lay "conductor tracks", i.e. wires on top or bottom, only vertically or horizontally, the result is a flawless suggestion. The board routed in this way makes it much easier to achieve a correct and space-saving layout on a perfboard. Almost all of the plug-in connectors were even located on the sides of the board, making them easily accessible.

Figure 6 shows the component side, **Figure 7** the bottom side and **Figure 8** the TARGET component placement plan (with a highlighted hole pattern graphic), with the blue connections on the top and the red connections on the bottom of the board.

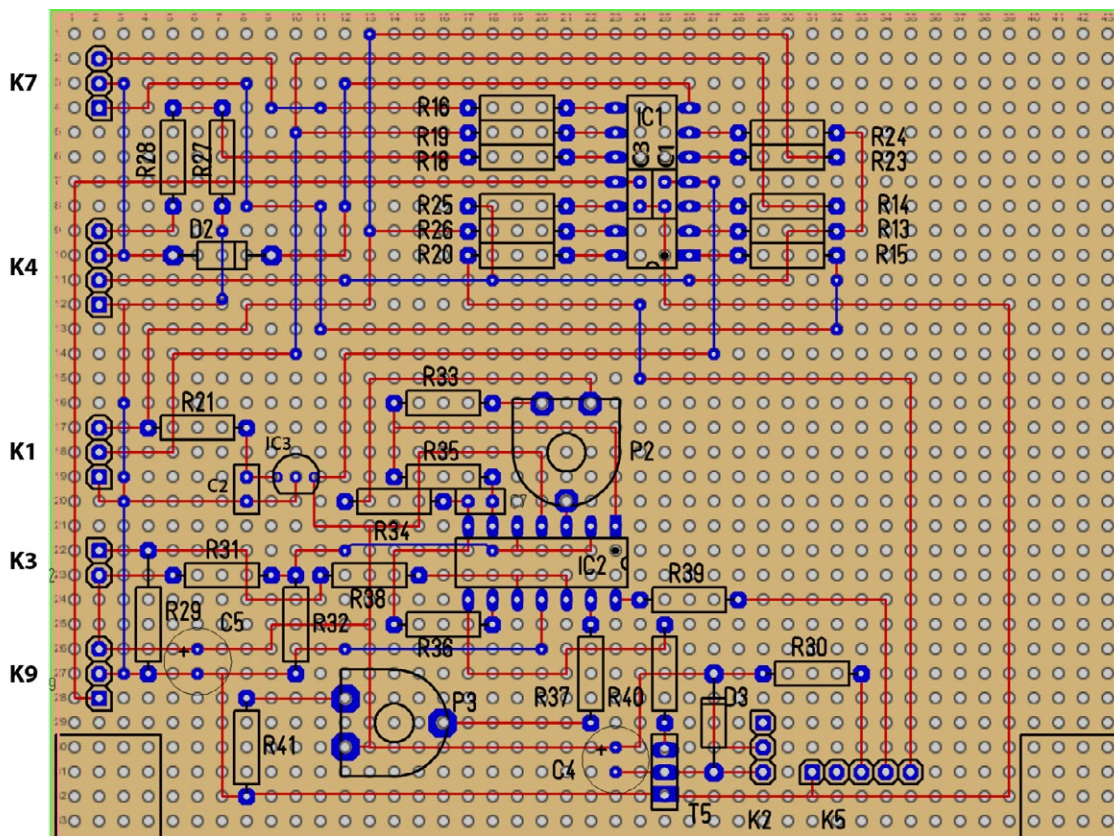


Figure 8: The result of the routing process. Connectors from old PC cases with their colorful cables can be plugged onto the single-row pin headers. The black squares at the bottom indicate areas that must be kept free for mounting brackets. The small capacitors C1 and C3 are mounted inside the socket of IC1.

In and On the Casing

You have probably noticed that I try to recycle used components from my box of left-over parts wherever possible. The display instrument that can be seen in the title photo was originally designed for 100 μ A. However, it was adapted to the current sensor resistor combination of 0.3 Ω with resistors in such a way that full deflection is reached at 10 A. A switch next to the instrument also allows a finer display range up to 1 A. If this display had not already been present, I would have used a suitable 10 A moving coil instrument, of course.

When mounting the device in its case, you should make sure that the fan can only draw in air from the outside and that the exhaust air actually leaves the case. Otherwise, at least part of the airflow would just circulate in the case, impairing cooling. Since heated air expands, the outlet should be larger than the intake vent.

Figure 9 shows something amazing: My case is made of 4-mm-thick plywood. The width of 13 cm and the height of 11.5 cm resulted from the dimensions of the heat sink and the resistors mounted in front of it. The power supply board mounted horizontally in the rear part of the case resulted in a depth of 26 cm. Since a decent surface treatment can take a lot of time, I (as I have done before [3]) applied a transparent foil to the visible parts of the case, as used in model aircraft construction to cover the wings. This foil is coated with a hot-melt adhesive and tightens when heated. It is ironed onto the finely sanded but otherwise untreated wood, thus creating an appealing surface.



Figure 9: The round opening corresponds to the diameter of the intake side of the fan. The bars ensure that almost all the air drawn in is from outside.



Component List Voltage Inverter

Resistors:

R42 = 1 Ω
R43 = 4k7
R44 = 1 k Ω
R45 = 10 Ω

Capacitors:

C8 = 1000 μ F/25 V
C9 = 1n5
C10, C11 = 1000 μ F/16 V

Inductance:

L1 = 100 μ H

Semiconductors:

D4 = 1N5819
IC4 = MC34063

Miscellaneous:

K8 = socket for coaxial power connector
Plug-in power supply 12 V with a minimum of 0.5 A load capacity

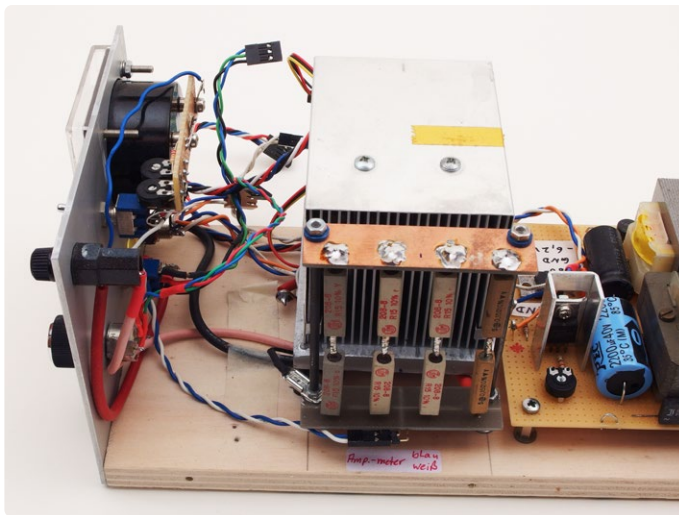


Figure 10: The base plate is 12-mm plywood, which also allows screws in the end faces. The series resistors and trimmers of the ammeter are attached directly to the instrument to simplify wiring. Epoxy base material, M3 threaded rods, and insulating bushings were used to mount the high-power resistors.

No Criticism!

To forestall any critical comments: I never intended my electronic load to compete with professional measuring equipment manufacturers. I never gave any thought to accuracy, temperature response, and so on. My display instrument with its range switching is calibrated as accurately as possible with a multimeter. However, if, for example, the values of the high-power resistors or the reference voltage have a significant temperature response, this is not compensated for and leads to errors. I can live with that!

This device is orders of magnitude better than anything I had previously used for such purposes. What's more, I enjoyed building it and came up with a device that is very well suited to my needs at a relatively low cost. In terms of its ecological footprint, my creation is also impressive: A great many parts have been given a second life here. All in all, this circuitry suggestion may at least serve as a suggestion for you, although it may be unsuitable as an addition to a professional laboratory. ◀

Translated by Jörg Starkmuth — 240201-01



About the Author

Peter Grundmann (born in 1956) was interested in electrical engineering from an early age. He later completed a commercial apprenticeship, but for the last 25 years before his retirement, he worked in software development. He always remained loyal to his hobby of electronics – this includes analog and digital circuits as well as microcontroller projects. He now has a wealth of experience in areas such as creating lighting effects and using servos in model railways. You can contact him by email at peter@groupiemebtron.de.

Questions or Comments?

Do you have questions or comments about this article? Email the author at peter@groupiemebtron.de or contact Elektor at editor@elektor.com.



Related Product

► Joy-IT HD35 USB Load Resistor (35 W)
www.elektor.com/19164

WEB LINKS

- [1] "Power MOSFET is core of regulated-dc electronic load," EDN.com, March 2005: <https://t1p.de/pt534>
- [2] MC34063A data sheet (Texas Instruments): <https://t1p.de/votu9>
- [3] Peter Grundmann, "Milliohm-Meter," elektor-labs.com: <https://www.elektormagazine.com/labs/milliohm-meter>

STILL 24 REASONS TO CONNECT WITH US

USB TYPE-C™

GND TX1+ TX1- +V CC1 D+ S-BU1 +V RX2- RX2+ GND



GND RX1+ RX1- +V SBU2 D- D+ CC2 +V TX2- TX2+ GND

© eiCan/eiS05



**WURTH
ELEKTRONIK**
MORE THAN
YOU EXPECT



Learn more about
the new Power Only
Connector!

USB-C Becomes Mandatory Charging Standard in the EU

Starting December 28, 2024, all mobile phones, tablets, and cameras sold in the EU must have a USB-C charging port. We offer a complete range of products for EMC interference, ESD protection, and power supply.

Ready for Design-In? Our technical sales team is here to support you. Samples are available for free. www.we-online.com/still24

Highlights

- USB-licensed Type-CTM connector WR-COM
- 60 W and 100 W Vbus filter
- Compact power inductors WE-MAPI & WE-MXGI
- Low parasitic ESD protection with WE-TVS



#USBTYPEC

2025

An AI Odyssey

Some Projects to See in the New Year

By Brian Tristram Williams (Elektor)

It's January 2025 and I'm looking forward to keeping up with a new year of developments in the insanely — and rather suddenly — fast-paced world of artificial intelligence. Over December, I took some time trying to get creative, and using AI to help me with some fun projects. Will they turn out to be useful? Maybe, maybe not — but the point, at the end of the year, was to have fun.

At the time of writing, I'm actually looking forward to December 2024 and thinking about what I'll be spending some of my December "fun time" on, so I would love your suggestions and ideas for a follow-up. You can find my contact details in the **About the Author** text box at the end of this article!

There are at least four things I'm whimsically looking to achieve, in part for fun, in part for practical real-world usage, and maybe a couple will turn out to be both.

Video Archive Metadata

I have been banging this drum for a couple of decades now, as is evidenced even by mentions in previous installations of this column. But, each time I revisit the subject, it becomes far more feasible to extract useful information from low-resolution archival video (read: PAL or NTSC standard-definition video, typically off videotape).

A quick summary of the "why:" I have over a thousand hours of video, primarily recorded from television in the late '80s and in the '90s, and much of the content is not available anywhere online. A lot is news coverage, but even TV ads of the time are valuable historical relics, especially for those who happened to be involved in any of it.

For example, your child was 8 and was in a TV ad for Tamagotchi, and, perhaps you never had a copy, or maybe time and moving house a few times have taken their toll, and it's lost to history. Or, your grandmother was interviewed for a news story on her winning "Gardens of the Year" in 1997, and now it's 28 years later and all you have left is her name and the contest's name?

For those two examples, perhaps, somewhere, in someone's closet gathering dust, there lies a tape with that ad or that news story, and it will

never see the light of day. No one has the time to sit through every home-recorded videotape they come across and annotate it manually. My goal for the last couple of decades is to get computers to help me do the heavy lifting, and my most recent chat with GPT-4o has really been encouraging.

In the 2000s, OCR (optical character recognition) had existed for a good few years already. It worked pretty well on high-resolution scanned documents, but I tried it with frame grabs from video, and it was pretty useless, even on text so large that it filled perhaps one-eighth of the screen height. I tried again relatively recently, and it was still disappointing.

Voice recognition has also come a long way, from Milton Bradley offering the MBX Expansion system [1] for the Texas Instruments TI-99/4A computer, complete with a headset — just so it could detect you saying one of two words, "yes" or "no," — to *Dragon Dictate* in the '90s, which was expensive, but passable if you were a CEO and didn't know how to type, to today's automatic caption generators that do an OK job but don't take any context



Source: Adobe Stock

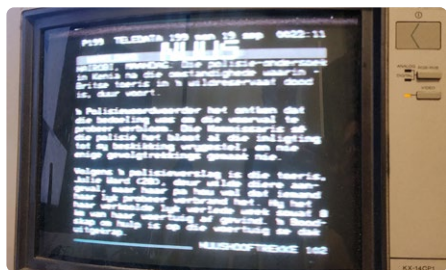


Figure 1: South African Teletext Nuus in the 1980s.

into consideration, resulting in an annoying disconnect between what's been said and what Computer-Brain heard.

Object detection came around more recently, having been feasible for security surveillance cameras in single-board computers even six years ago. With today's AI accelerators for Raspberry Pi and the like, it's possible to do 30-frame-per-second detection from pre-trained models for objects such as "dog" and "human," which suffices for security, but is nowhere near adequate for the infinite variety of things you'll see going on in any given frame of video.

Enter ChatGPT (Again)

Each new version of the generative AI behemoth seems to deliver new surprises. Never mind trying to OCR only the very largest

text in a TV news report or having object metadata that consists of only very generic real-world physical objects; I uploaded some images of varying quality, at one point even taking bad photos of the CRT video monitor and sending them directly via my phone, and I was astonished at how good ChatGPT was at telling me exactly what was going on in the image. One of the images was blurry (because the video jitters about so much while the phone takes a low-frame-rate photo), and from a bad Betamax tape of a Teletext broadcast (Figure 1), and the bot did a better job of making out most of that text than I did (Figure 2). (It made this strange guess: The dusty old KX-14CP1 monitor is made by Sony, and the AI guessed it was a Panasonic despite Panasonic never having made such a model.)

Then I tried a sample from a tape recorded in roughly 1993 from a weak TV station with an inadequate antenna. If you take a look at Figure 3, you may be hard-pressed to tell who that is. ChatGPT was equally hard-pressed, until I insisted with a "take a guess," to which it responded:

"If I had to guess based on the limited and heavily distorted visual, it looks like it could be a figure from a mid-20th-century TV broadcast. The suit and posture are reminiscent of someone like Carl Sagan (from Cosmos) or a similar educator/scientist who often appeared on TV giving lectures or presentations."

Yes, it was Carl Sagan in *Cosmos*.

Could you imagine having a thorough description (or best guess) of every frame of every video in some sort of SQL-type database, ready for a search, at your fingertips? I can.

But, the problem is far from solved for me. Firstly, this was obviously a manual process, grabbing a frame and sending it to ChatGPT, but that's not a huge obstacle — it's easy enough to access an API from OpenAI to carry out any task you can do manually. However, there are two immediate problems that come to mind.

The first problem is processing speed. At 25 frames per second in PAL video (50 different images a second if you don't deinterlace), we're talking having to analyze 270,000 frames from a three-hour tape, or 90 million frames in a 1,000-hour archive. ChatGPT works as fast as it works, and there's only so much tweaking you can do to speed it up. Perhaps generative AI running locally could tackle it (if I can find one that does as good a job), but you'll probably need deep pockets to get useful performance at that scale. So, the speed thus also becomes a cost problem.



Figure 3: Somehow it managed to identify Carl Sagan from this photo of a screen of a capture of a bad recording.

This is another teletext page, labeled **P199** on **TELEDATA**, likely from the late 1980s or early 1990s, based on the style and context. The title is **"NUUS"** (Afrikaans for "News"), and the content describes an incident involving the police.

Key observations:

- The text mentions a **police investigation** into a case involving the death of a British tourist in a neighborhood. The word **"polisie-ondersoek"** (police investigation) and related terms suggest a criminal or suspicious incident.
- Details involve actions taken by a **police spokesperson**, referencing a 20-year-old female named **Julie Hart** and possibly a suspect or related individual. There is mention of a **father** and what appears to be a **rescue or intervention attempt**.
- This text is written in Afrikaans, common in South Africa's teletext services, particularly during the SABC's broadcast dominance.

The teletext is being displayed on a **Panasonic KX-14CP1** monitor, a 14-inch CRT often used for professional purposes like video editing or teletext systems in that era.

Would you like me to fully translate and analyze the news text for more insight?

Figure 2: ChatGPT's analysis of the barely-legible Teletext.

```

Coming up on Larry King Live, America's sweetheart,
Mary Tyler Moore, dressed as Larry King,
talking about the ups and downs of her career and her life,
plus Dolly Parton, a sassy new video,
a super new album.
It's all next.
Don't go away.
For more than 120 million viewers
in over 200 nations and territories,
no one covers the world like CNN International.
Hi, everyone.
Here's a look at world weather.
Notice the bright white clouds
that are found in northern Argentina.
And here's a look at what's going on in South Africa.
And here's a look at what's going on in South Africa.
And here's a look at what's going on in South Africa.
And here's a look at what's going on in South Africa.
And here's a look at what's going on in South Africa.
And here's a look at what's going on in South Africa.
And here's a look at what's going on in South Africa.
And here's a look at what's going on in South Africa.
And here's a look at what's going on in South Africa.
And here's a look at what's going on in South Africa.

```

Figure 4: *Whisper AI* having a meltdown because it heard some music somewhere.

The second problem is also cost: If you're using the OpenAI API, every call comes at a cost. If you want to analyze 90 million frames, it's going to bankrupt a small nation.

Moving on to audio, I also tried *Whisper* [2] for voice transcription, and it worked pretty well when the audio was speech-only and relatively clear. But, as soon as music started, it got totally confused and went haywire with the transcription (**Figure 4**). A little music in a promo caused the AI to allow the weatherman four good sentences, after which, well, you can guess he never said exactly that.

So, my December “fun” challenge here is to generate useful metadata using methods that are as efficient and cost-effective as current technology will allow, whether it be online or on the edge (that is, run on local hardware). Of course, any tips from out there would be great. Reach out to me at the contact details at the end of this article.

Text Adventures in 2025?

“Back in the ‘80s,” to overuse a phrase, text adventures felt like early AI: You spoke to the computer game in English, it responded in English. This next idea, I think, has the potential to become an Elektor undertaking ... but before I get to that, let's start at the beginning for those of you too young to know what a text adventure is.

Before computers became accessible to many households, there were already experiments in creating interactive adventure games. The idea was for the player to direct their own story, by telling the game's main character what to do next, and the outcome would play out accordingly. Did you pull a book out from that bookshelf? Ah, a secret passage

opened beyond. Did you smash that glass without wearing your safety sneakers? Sorry, you bled to death.

The challenge was that in the '70s and early '80s, computers were lacking in processing and graphical ability, not to mention the storage required to save the kind of graphics you'd need to carry a story's worth of graphics. So, instead of interactive movies, we got interactive books, that is, text-only. Did the lack of pictures ever stop me from enjoying a good book? Well, yes, when I was a boy, I preferred comics, but let's put that aside.

Even without graphics, the systems of yore were limited in how much text it was feasible for them to process, so they did their best to simulate a kind of “AI” while understanding a very limited vocabulary — around 120 words in the case of the Scott Adams *Pirate Adventure* game [3]. So, in the Scott Adams *Adventure* series of games, your instructions to the computer would be at most two words, such as **TAKE BOOK** (**Figure 5**). Even with such limitations, you could have hours of fun with these, or even days or weeks (it was possible to save your game status to a cassette tape or floppy diskette).

So, aside from these being early demonstrations of pretend-AI based on a glorified haystack of IF-THEN-ELSE logic, why am I thinking about this into 2025? It's something that's been in the back of my head since I got SMS on my phone back in 1998; a text-only interface limited to 160 characters per message (it's in the name: Short Message Service). Later, Twitter was invented, and it had its 140-character post limit informed by SMS. Yes, there was a time in 2008 when I sent and received tweets using SMS!

```

I'm in a alcove. Visible items are:
Open window, Bookcase with secret
passage beyond
Obvious exit: DOWN
I'm carrying: Large blood soaked book
<----->

WHAT SHALL I DO?
WHAT SHALL I DO? TAKE BOOK
There's a strange sound.

WHAT SHALL I DO? GO STAIRS
* Welcome to Adventure number 2!
* 'Pirate Adventure' by Alexis & Scott
Adams, dedicated to Ted Heeren & Paul
Sharland. Remember, you can always ask
for 'HELP'.

```

Figure 5: Screenshot of *Pirate Adventure* on the Texas Instruments TI-99/4A shows what happens when you **TAKE BOOK**.

Now, in 2025, of course X (formerly Twitter) can do live video, images, voice notes, and the like, and it also has primary competitors in the form of Threads, BlueSky, and so on, but the fact that their all of their DNA comes from a text-first, threaded reply-based origin makes them well-suited to text-based interactions.

We've seen those tree-based customer “help” systems on WhatsApp, USSD, and SMS, where you reply in simple commands or just select a number from the menu. But how about, instead of being tortured, having some fun with it in the form of an interactive text adventure. The adventure could be themed according to any topic we want, so it could even work for us at Elektor. For example, we could host a game online where followers like you could compete to solve an electronics-related adventure to win the “Engineer Extraordinaire” prize for solving it first!

I imagine the game would start by a follower visiting our profile page and posting to us:

START GAME

and that data would go into the social media platform, be picked up on the back end by our own code running on a server somewhere else and interacting via API. It would then process the response logic and update the game session status, and then respond to the user accordingly, for example:

You are standing in the lobby at Elektor. At the end of the hallway is a door. The sign on it says “LAB.” It is slightly ajar and the lights inside are flickering. Obvious exits are EAST, WEST.

Then the player responds, and back and forth until the player is defeated or the game is won.

Because default posts and responses on these platforms are public, you are not limited to one person sitting alone at home playing a

game that no one else will see, but now one host account can be running simultaneous games with many players, each of whom can be looking over others' "shoulders" to glean tips and strategy, until eventually the final challenge falls and we have a winner.

With ideas like this, I'm glad one of the platforms is called BlueSky.

I'm enthused about this one, and I'd like to dig deeper into the server-side logic of how these games are interpreted. ChatGPT has given me some good ideas on that end, and also ideas on themes and gameplay. I won't go into too much detail here, but suffice it to say that resistor colors are always welcome in a puzzle for an electronics engineer. We'll see how much I can crack this idea open in the next month.

MIDI Audio Synthesis

This one is only tangentially AI-related, but we'll touch on that later.

In 1994, I bought a Roland JV-30 keyboard [4] with built-in music synthesizer. Not only could it play any music you banged away at on its keyboard, but it would also send out every key press via its 5-pin DIN MIDI (Musical Instrument Digital Interface) OUT connector, so it could control other synthesizers if you weren't in favor of the native sound. Likewise, it could also be given playback instructions via its MIDI IN connector, which I used to use back in the day to have the *DOOM* game music play via the synth, rather than the PC's sound card, for higher quality. Later, I got it to play music from an Arduino UNO connected to MIDI IN (see my video at [5]).

Then, a few years ago, disaster. I tried to dry my child's school jersey by draping it over the keyboard and using a hairdryer. When I removed the jersey, the keyboard smiled at me as if it were making a case for better national dental care — half of the keys were warped, and replacement keys, collectively, cost much more than the keyboard was worth. (Its synthesizer still works, so I haven't thrown it out.)

This tragedy provided the opportunity to replace it and upgrade from its limiting 61 keys. So, I got an M-Audio Keystation 88 [6], which has the full 88-key piano range.



Figure 6: Minecraft helps children thing logically and systematically, when it's needed.
(Source: Adobe Stock /@Wirestock)

However, the Keystation lacks a synthesizer, meaning it is only a keyboard, and you need to have some other device, such as a PC or cellphone, to create the audio. I knew this, but I didn't realize how much of a hassle that would be. I just want to switch on and play, and not have to find an external device that isn't dedicated to the task.

First I thought of upgrading directly from the Keystation to another keyboard / electric piano capable of making sounds, but after talking to ChatGPT for a bit, I ended up buying a standalone synthesizer, the Roland D-110 [7], which was released in 1988. Yes, the '80s in a box, as someone coined it — hear how it sounds at [8]! I got it for a bargain, but right after I had paid online for it, ChatGPT came up with a better idea (thanks?).

Its idea wasn't even that original. It was one of those "why didn't I think of it!?" moments, accompanied by a head slap: Use a Raspberry Pi!

The initial idea didn't seem *that* attractive — I was thinking of a GUI, having to boot up, open some specific application, having to have a monitor, keyboard, and mouse, and so on. That's not any better than using a PC, except that the Raspberry Pi is affordable enough and small enough to dedicate to the task.

However, the bot suggested a headless installation, which is my preferred means of using any Raspberry Pi. "Headless" means you don't need a big "head," in the form of monitor, keyboard, and mouse, on your server or embedded board. All necessary configuration interactions with the board take place via a terminal window on another computer, but, for daily use, you could have something as simple as a Raspberry Pi double-sided-taped to the back of your keyboard, et voilà, your keyboard-only musical instrument now makes sounds.

Now for the tangential AI reference. There's been widespread interest in AI accelerators for single-board computers, whether external, such as with the Raspberry Pi AI Accelerator, or on-board, such as in the case of the BeagleY-AI [9] from BeagleBoard. With this power now available on the edge, it's not far-fetched to imagine having AI "listen" to what you're playing (via MIDI data), and not only synthesize your notes, but also accompany you — your own free backup keyboard player, anyone?

I happen to have a BeagleY-AI, so that will be my platform of choice for this December experiment.

Minecraft Automation

You may have seen your kids playing *Minecraft* for hours on end (**Figure 6**), but what not everyone realizes is that it's more than just a game — it's a powerful platform for creativity, problem-solving, and even engineering. Whether automating massive builds or simulating real-world logic with its "Redstone" circuits, Minecraft offers a sandbox where coding, electronics, and design come to life in ways that resonate with professionals and hobbyists alike.

Now, I'm a little late to the party, since Minecraft has been available in one form or another since 2009 — before my daughter was born in 2010. I was averse to putting a lot of time into "playing a game," but now that she's old enough to get it (and teach me a few tricks), I've been looking into the engineering education aspect of it (and manually making "art" that could also be automated — see **Figure 7**).

I know that people have been building computers within Minecraft worlds for years, starting with first principles: logic gates. You can see a great intro video at [10], but you can go down quite the rabbit hole on this topic.

Figure 7: But that doesn't mean you can't be creative — this manual Texas Instruments logo artwork could have been a script that converts GIFs to automated Minecraft builds.



In real life, when you program FPGAs (field-programmable gate arrays), you also begin with first principles, and can replicate almost any digital logic circuit. I have no experience in the field, but my engineer colleagues have given it a go, including Jean-François Simon in his “A VHDL Clock Made with ChatGPT” article [11].

Being a retro computing fan, I'm keen to see what I can replicate in Minecraft, from simple 74x-series digital logic up to more ambitious computing projects. Yes, the “physical” circuits you build in Minecraft are massive and unwieldy and run extremely slowly, but being able to emulate an 80s microcontroller or (gasp) microcomputer down to the gate level is extremely cool — look how *SethBling* did it for the Atari 2600 [12].

The problem is the complexity. It would take me too many hours to place thousands of components manually. It seems there are ways to drag and drop copies of large structures that you'd need to replicate, for example RAM, but ultimately, I want to be able to script and automate this stuff, just as I did when I created Conway's Game of Life in Roblox [13], using the Lua programming language. Who knows,

I might dabble in FPGA programming at the same time, turning to trusty Elektor engineers.

Outcomes: Too Ambitious or Overly Optimistic?

We shall see, but I'm looking forward to these experiments, and I will let you know some of my learnings. Again, if you have any ideas, questions, suggestions, comments, or just want to wax lyrical about that favorite thing you did once back in the '80s, you can reach me via the email in the **Questions or Comments?** text box. ◀

230181-K-01

About the Author

Brian Tristram Williams has been fascinated with computers and electronics since he got his first “microcomputer” at age 10. His journey with Elektor Magazine began when he bought his first issue at 16, and since then, he's been following the world of electronics and computers, constantly exploring and learning. He started working at Elektor in 2010, and nowadays, he's keen on keeping up with the newest trends in tech, particularly focusing on AI and single-board computers such as Raspberry Pi.

Questions or Comments?

We'd love to hear about how you are using AI and how it has affected you over the past two years. If you have questions or comments, email me at brian.williams@elektor.com. You can also catch me on Elektor Engineering Insights each month on YouTube, and you can find me @briantw on X.



FEATURED TOPIC

Visit our **Embedded & AI** page for articles, projects, news, and videos.

www.elektormagazine.com/embedded-ai



Related Products

- > **Angelo La Spina, Analogue Video (E-Book)**
www.elektor.com/16889
- > **Pimoroni Piano HAT for Raspberry Pi**
www.elektor.com/20552
- > **Raspberry Pi AI HAT+ (26 TOPS)**
www.elektor.com/21038
- > **BeagleY-AI SBC with GPU, DSP and AI Accelerators**
www.elektor.com/20991

WEB LINKS

- [1] MBX Expansion System for the Texas Instruments Home Computer: <https://videogamehouse.net/mbx.html>
- [2] Introducing Whisper: <https://openai.com/index/whisper/>
- [3] Pirate Adventure: https://en.wikipedia.org/wiki/Pirate_Adventure
- [4] Vintage Synth Explorer: The Roland JV-30: <https://vintagesynth.com/roland/jv-30>
- [5] Arduino Playing a Roland JV-30 MIDI Keyboard/Synthesizer: <https://youtu.be/1M0ADumGuHw>
- [6] M-Audio Keystation 88 II: <https://m-audio.com/legacy/keystation-88.html>
- [7] Music Magazine — The Roland D-110: <https://muzines.co.uk/articles/roland-d110/2282>
- [8] Roland D-110 Synthesizer Module Patches and Tunes: <https://youtu.be/u3oQoMtZeTl>
- [9] BeagleY-AI: <https://beagleboard.org/boards/beagle-y-ai>
- [10] Computer Architecture Explained with Minecraft: https://youtu.be/dV_lf1kyV9M
- [11] J.-F. Simon, “A VHDL Clock Made with ChatGPT,” Elektor AI Edition 2024: <https://elektormagazine.com/240602-01>
- [12] 1 FPS Atari 2600 Emulator in Vanilla Minecraft 1.13: https://youtu.be/mq7T5_xH24M
- [13] Conway's Game of Life in Roblox: https://youtu.be/2q_v1aw4-kQ

Douk Audio P6 mini Tube Preamplifier

Elevate your audio experience with the Douk Audio P6 mini Tube Preamplifier, a perfect blend of modern connectivity, HiFi sound quality, and vintage charm. Whether you're an audiophile or just starting your journey into high-quality audio, this compact yet powerful preamp offers everything you need.



Price: ~~€74.95~~

Special Price: €59.95

www.elektor.com/21014

Raspberry Pi 500 (US)

The Raspberry Pi 500 (based on the Raspberry Pi 5) features a quad-core 64-bit Arm processor, RPi I/O controller, 8 GB RAM, wireless networking, dual-display output, 4K video playback, and a 40-pin GPIO header. It's a powerful, compact all-in-one computer built into a portable keyboard.



Price: €104.95

www.elektor.com/21074

FNIRSI GC-02 Nuclear Radiation Detector (Geiger Counter)



Price: €49.95

Member Price: €44.96

www.elektor.com/21046

M5Stamp Fly Quadcopter (with M5StampS3)



Price: €79.95

Member Price: €71.96

www.elektor.com/21008



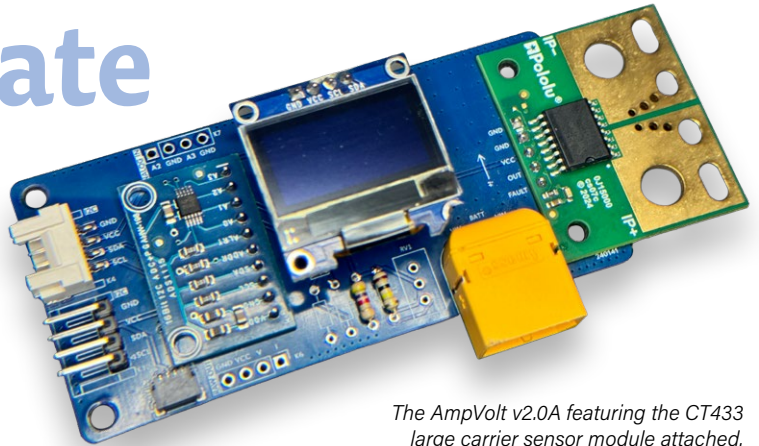
AmpVolt v2.0

Project Update

100 Amps and Beyond!

By Saad Imtiaz (Elektor)

In the previous article in the AmpVolt series, a modular PCB was presented that could measure DC power and energy consumption up to 50 V and 5 A. In this article, an updated version of the project is shared that can measure up to 60 V and 100 A (and beyond).



The AmpVolt v2.0A featuring the CT433 large carrier sensor module attached.

Before diving into the latest update, let's revisit the concept and the motivation behind its development. While USB-based power and energy measurement modules are abundant, solutions for measuring higher DC voltages beyond 12 V, and especially beyond 24 V, remain limited. This voltage range is becoming increasingly relevant with the growing adoption of battery-powered solar systems, electric bicycles, electric vehicle chargers, power tools, garden equipment and more. Recognizing this gap, the AmpVolt project was conceived to provide an efficient, reliable, and flexible solution for high-voltage and current measurements, particularly in such modern applications.

In its initial iteration, simplicity and practicality were prioritized. The design focused on integrating off-the-shelf modules into a single PCB that could handle precise current and voltage sampling while maintaining accuracy through a high-precision analog-to-digital converter (ADC). This approach allowed the AmpVolt to remain versatile yet efficient.

For the first version [1], the project set its measurement capabilities at up to 50 V and 5 A, leveraging the INA169 current sensor paired with a voltage divider circuit and a 12-bit ADS1015 ADC module. Together, these components ensured reliable and accurate current and voltage readings across a broad range of applications. To maximize compatibility, the module was designed to interface with 3.3-V or 5-V microcontrollers using a standard I²C interface.

To enhance usability and adaptability, the PCB included an OLED display, also controlled via the I²C bus, to provide real-time readings

directly on the device. Multiple I²C connectivity options were incorporated, such as Grove and Qwiic connectors, and a JST XH connector with a 2.54-mm pitch, allowing seamless integration into various systems. Furthermore, XT60PW connectors were chosen for connecting to the load and power source, ensuring compatibility with commonly used battery systems. This modular design allows you to build your own version with readily available components. The first iteration laid a solid foundation, and now we move forward to the latest updates that improve on this design.

In this article, our main objective remains consistent with the original idea: providing a simple and reliable way to measure higher currents and voltages. As you've likely noticed from the subheading, the significant update in this version is the ability to measure up to 200 A and 60 V. This improvement was made possible by transitioning to a Hall-effect current sensing method instead of the shunt resistor approach.

Technical Features

- › Voltage Range: Up to 60 V
- › Current Range: Up to 200 A (variant-dependent)
- › Current Sensing Technology: Hall-effect-based and TMR-based sensors (Allegro Microsystems)
- › Sensor Compatibility: Pololu compact and large carrier modules (e.g., CT433, CT432, ACS72981 and more)
- › Connectivity Options: XT60 connectors for easy integration
- › Data Communication: I²C interface compatible with 3.3 V and 5 V microcontrollers
- › Direct soldering pads for compact sensor modules (variants B and C)

Comparison of Pololu Current Sensor Modules

Source: [2]

| Sensor Type | Sensor Technology | Current Range | Sensitivity (mV/A) | Max Bandwidth | IC Path Resistance | Size | Over Current Fault Output | Common Mode Field Rejection | Non Ratiometric Output |
|------------------|---|---|-------------------------|---------------|--------------------|-------------|---------------------------|-----------------------------|------------------------|
| CT432/CT433 | XtremeSense TMR (tunneling magnetoresistance) | ±20 A / ±30 A / ±50 A / ±100 A / ±200 A | 20 / 10 / 5 | 1 MHz | 1 mΩ | 1.4" × 1.2" | x | x | x |
| CT432/CT433 | XtremeSense TMR (tunneling magnetoresistance) | ±20 A / ±30 A / ±50 A / ±100 A / ±200 A | 20 / 10 / 5 | 1 MHz | 1 mΩ | 0.8" × 1.1" | x | x | x |
| ACS71240 | Hall effect | ±10 A / ±30 A / ±50 A | 132 / 44 / 26.4 | 120 kHz | 0.6 mΩ | 0.7" × 0.8" | x | x | x |
| ACS72981 Compact | Hall effect | ±50 A / ±100 A / ±150 A / ±200 A | 26.4 / 13.2 / 8.8 / 6.6 | 250 kHz | 0.2 mΩ | 0.7" × 0.8" | | x | |
| ACS72981 Large | Hall effect | ±50 A / ±100 A / ±150 A / ±200 A | 26.4 / 13.2 / 8.8 / 6.6 | 250 kHz | 0.2 mΩ | 1.4" × 1.2" | | x | |
| ACS37220 Compact | Hall effect | ±100 A / ±150 A | 13.2 / 8.8 | 150 kHz | 0.1 mΩ | 0.7" × 0.8" | x | x | x |
| ACS37220 Large | Hall effect | ±100 A / ±150 A | 13.2 / 8.9 | 151 kHz | 0.1 mΩ | 1.4" × 1.2" | x | x | x |

Hall-Effect vs. Shunt Resistor

At first impression, you might question whether this change sacrifices accuracy, but modern Hall-effect current sensors have advanced significantly. They now offer impressive precision, smaller footprints, higher efficiency, and simplified integration, making them an excellent choice for high-current applications.

If we were to achieve 200 A measurements with a shunt resistor, the design would face several challenges. High-current shunts require careful consideration of power dissipation, as they can generate significant heat at such currents. Additionally, designing an accurate measurement circuit with low noise would demand careful PCB layout and thermal management. Shunt-based systems also often require amplifiers to handle the small voltage drop generated, adding complexity to the circuit.

By contrast, Hall-effect sensors inherently isolate the measurement circuitry from the current path, eliminating most of the heat and safety concerns while maintaining accuracy and reducing overall system complexity. These advantages make them an ideal solution for this upgraded version of the AmpVolt Project.

The Path to AmpVolt v2.0

I received several emails from readers suggesting that the project should support current exceeding 20 A. This feedback motivated me to develop a second version of the project. After researching various current sensor modules online, I discovered the Pololu sensors [3]. Their design, quality, and specifications immediately stood out, prompting me to order them for testing. Upon arrival, the sensors exceeded expectations, both in build quality and performance, aligning closely with their listed specifications. (Disclaimer: While I haven't tested them beyond 30 A, I trust their documented capabilities.)

The Pololu current sensor modules, built around Allegro Microsystems chips [4], are industrial-grade sensors, and they are well known for offering high accuracy, reliability, and safety. A key factor in choosing



Component List

Resistors

- R1 = 170 kΩ
- R2 = 10 kΩ
- R3, R4 = 22 kΩ
- RV1 = 170 kΩ (multi-turn trimmer or as required)

Modules and Connectors

- K1 = Pololu Current Sensor
- K2 = ADS1015
- K8, K9 = I2C OLED Screen
- K3 = Qwiic Connector
- K4 = Grove Connector
- K5, K11 = AMASS XT60PW-M
- K7, K10= Pin Header 1x4, 2.54 mm Vertical

these sensor modules was their compact and consistent form factor. The larger modules measure 35.56 × 30.48 mm [5], while the compact variants are 17.78 × 20.32 mm [6], except for the CT432/433-based compact modules, which are slightly larger at 20.32 × 27.94 mm [7].

The CT432/CT433 and ACS series sensors by Allegro cater to different needs, each offering distinct advantages for diverse applications. The CT432/CT433 modules, built on TMR (Tunnel Magnetoresistance) technology [8], provide ultra-low resistance (0.2 mΩ) and high bandwidth up to 1 MHz, making them ideal for high-speed, high-current applications like motor control, welding equipment, or dynamic power monitoring. Their superior sensitivity, reduced noise, and energy efficiency also make them suitable for precision and low-power designs. In contrast, the ACS series, based on Hall-effect sensing, strikes a balance between affordability, noise rejection, and integration flexibility. Compact variants are perfect for space-constrained IoT and embedded systems, while large carriers excel in high-current applications such as EV charging and battery management.

To accommodate this wide array of sensor capabilities, the AmpVolt v2.0 was designed in three variants (A, B, and C), supporting both compact and large modules. This modular approach ensures compatibility across

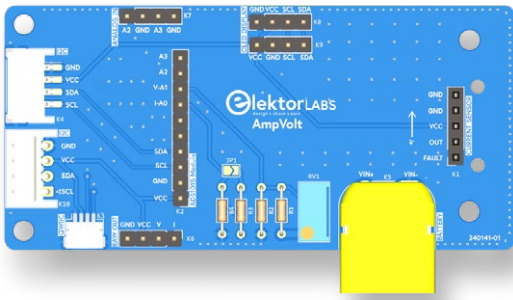


Figure 1: The AmpVolt v2.0A Variant was designed for both large and compact carrier sensor modules.

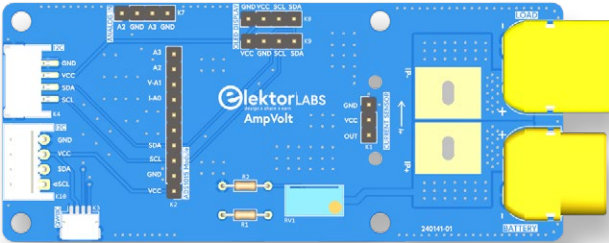


Figure 2: The AmpVolt v2.0B Variant was optimized for compact sensor modules with support for XT60 connectors.

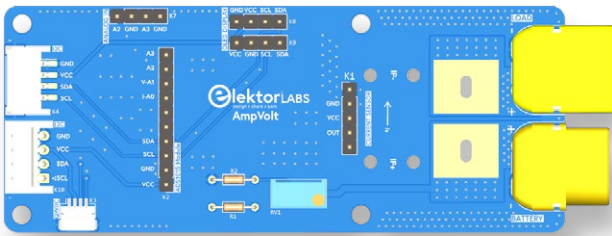


Figure 3: The AmpVolt v2.0C Variant was configured for compact sensor modules based on the CT432/433.

different use cases, allowing users to tailor the solution to their specific requirements.

- AmpVolt v2.0A: This variant supports both large and compact carrier modules, making it suitable for high-current applications by directly utilizing the pads on the sensor modules. However, it does have a limitation due to its size. It cannot accommodate XT60 connectors like the previous version. To handle high-current loads, increasing the PCB from 2 to 6 layers is necessary (**Figure 1**).
- AmpVolt v2.0B: This variant retains the compact design of AmpVolt v1.0 while allowing direct soldering of the ACS-based compact current modules. It also supports XT60 connectors on the PCB for easy integration. However, for safety, I recommend limiting the current load to 20 A for short durations to avoid overheating and eventually magic smoke (**Figure 2**).
- AmpVolt v2.0C: Similar to v2.0B, this version is specifically designed for compact modules based on the CT432/433 current sensors (**Figure 3**). As with v2.0B, the same current load recommendations apply to ensure reliable operation and prevent damage.

These three variants provide flexibility, catering to different requirements and applications.

Design Considerations and Challenges

Integrating the new current sensor modules into the design was relatively straightforward, thanks to the detailed dimensions provided in the

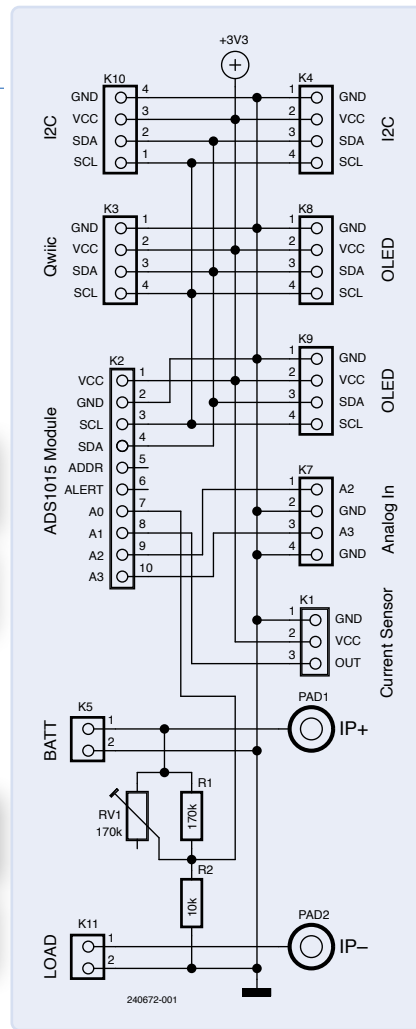


Figure 4: Schematic diagram for the AmpVolt v2.0B variant.

design files. However, achieving a robust and optimized PCB layout required careful attention to several parameters.

In the schematic (**Figure 4**), you'll notice it retains much of the core structure from the previous version, with some small updates. Specifically, this schematic corresponds to the B variant, featuring additional pads that allow the sensor module to be directly soldered onto the PCB for easier integration (**Figure 5**). For those interested in exploring or building upon this project, all design files, including the schematic, PCB layout, and firmware, are available in the project's GitHub repository [7].

One key improvement from the previous design was reducing the I²C track width to 0.20 mm. This adjustment minimizes unwanted capacitance, which

can otherwise lead to signal degradation and communication errors. In variants B and C, mounting pads were added to accommodate compact series sensors directly on the PCB. This allows for the integration of XT60 connectors, providing convenience for high-current connections. However, designing a 2-layer PCB with Outer Copper Weight of 1 oz capable of handling up to 20 A without overheating or posing safety hazards presented significant challenges.

To address this, both PCB layers were used to evenly distribute the current and manage heat effectively. Thermal vias were added between the layers to improve heat dissipation and handle the current load reliably. For a 20 A load, calculations suggest that around 10 vias with a hole diameter of 0.4 mm and an external diameter of 0.8 mm would suffice, maintaining a current density of around 2 A per via. However, to stay on the safe side and account for any unexpected conditions, 37 vias were placed. This ensures better current handling and reduces the risk of overheating during operation.

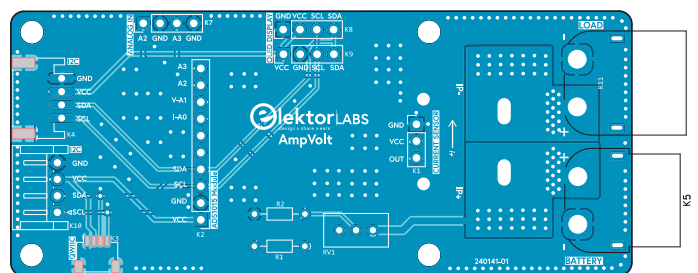


Figure 5: PCB layout of the AmpVolt v2.0B variant.



Figure 6: The AmpVolt v2.0A in action demonstrating current measurement during testing.

However, this current limit can further be pushed by increasing the copper thickness to 2 oz/ft², which can significantly enhance the current-carrying capacity of the traces. For current paths, copper zones were used, designed to handle current densities below 35°C rise per IPC-2221 standards, ensuring the PCB remains within safe operating temperatures.

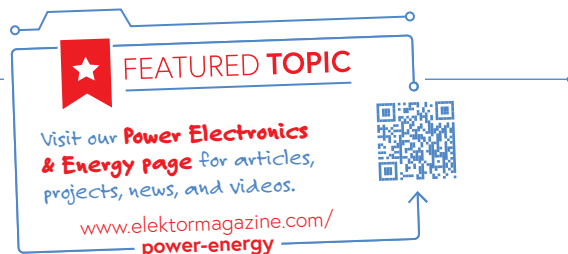
Testing the AmpVolt v2.0

For testing, I was able to measure currents up to 30 A using a friend's DC arc welder. However, in my lab, my power supply couldn't push beyond 6 A. In the **Figure 6**, you can see the OLED displaying a current draw of 6 A. The voltage and power readings are shown as 0, since I didn't connect the XT60 connector for voltage sampling during this test. Despite this, the system worked as expected.

On the software side, the code required only a minor update to accommodate the sensitivity of the current sensor module being used. Each module has a different sensitivity rating (mV/A), which needs to be accounted for. In this test, I used the CT433 Large Carrier variant (**Figure 7**), which has a sensitivity of 20 mV/A.

Here's the updated `readCurrent()` function:

```
float readCurrent()
{
    int16_t val_1 = ADS.readADC(0);
    // Read ADC channel 0
    float f = ADS.toVoltage(1);
    // Convert ADC reading to voltage
    float current = (val_1 * f - 1.650) / 0.020;
    // Calculate current in amps
    return current;
}
```



Where `ADS.readADC(0)` reads the raw ADC value from channel 0, `ADS.toVoltage(1)` converts the ADC reading into a voltage value based on the reference voltage and ADC resolution. `1.650` is the zero-current output voltage of the current sensor module (the sensor's output when no current flows). And `0.020` is the sensitivity of the CT433 sensor, which stands for 20 mV/A. This value is specific to the module and determines how the voltage reading translates into current.

The function calculates the current by first subtracting the zero-current voltage from the sensor's output, then dividing by the sensor's sensitivity. This simple adjustment makes the code adaptable for different sensor modules, provided their sensitivities are known. ◀

240672-01

Questions and Comments?

If you have questions about this article, feel free to email the author at saad.imtiaz@elektor.com or the Elektor editorial team at editor@elektor.com.



About the Author

Saad Imtiaz, Senior Engineer at Elektor, is a mechatronics engineer who has extensive experience in embedded systems and product development. His journey has seen him collaborate with a diverse array of companies, from innovative startups to established global enterprises, driving forward-thinking prototyping and development projects. With a rich background that includes a stint in the aviation industry and leadership of a technology startup, Saad brings a unique blend of technical expertise and entrepreneurial spirit to his role at Elektor. Here, he contributes to project development in both software and hardware.

WEB LINKS

- [1] Saad Imtiaz, "The AmpVolt Modular DC Power Meter (Part 1)," Elektor 05-06/2024: <https://elektormagazine.com/240141-01>
- [2] Pololu Current Sensor modules: www.pololu.com/category/118/current-sensors
- [3] Allegro Current Sensors: www.allegromicro.com/en/products/sense/current-sensor-ics/
- [4] CT432/CT433 TMR Current Sensor Large Carriers: www.pololu.com/category/324/ct432-ct433-tmr-current-sensor-large-carriers
- [5] ACS72981 Current Sensor Compact Carriers: www.pololu.com/category/316/acs72981-current-sensor-compact-carriers
- [6] CT432/CT433 TMR Current Sensor Compact Carriers: www.pololu.com/category/323/ct432-ct433-tmr-current-sensor-compact-carriers
- [7] Source code and PCB files: <https://github.com/ElektorLabs/AmpVolt>
- [8] Allegro's XtremeSense™ TMR technology: www.allegromicro.com/en/products/emerging-technologies/tmr

Err-electronics

Corrections, Updates, and Readers' Letters

Compiled by Jean-François Simon (Elektor)



Precision Power Supply

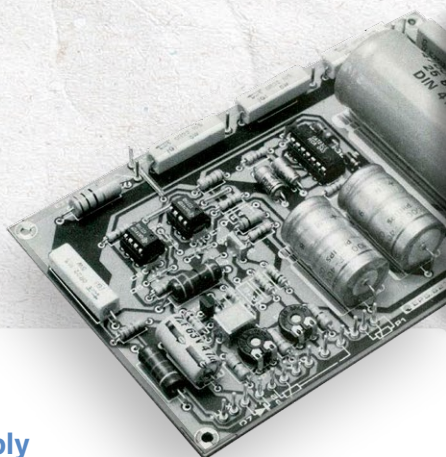
Elektor 12/1982, p. 22 (82178)

I would like to build your laboratory power supply from Elektor December 1982 with my apprentices. Is there anywhere the possibility to order the etched circuit board or to get it from elsewhere?

Holger Beck (Germany)

Thank you for your interest in this classic project. No, sorry, the PCBs are not available. If you want to have these PCBs made, there are a few options. You can redraw the PCB from scratch in your favorite PCB software. If you do, I suggest you change the footprints for the axial electrolytic capacitors and use radial ones instead, they are cheaper and easier to find these days. You could use a screenshot from the PDF article as a template, for example in Sprint Layout which has a dedicated function for that, or in KiCad using the built-in Image Converter. You'll need to count pixels between points forming a known distance (e.g., between pins 1 and 7 of the IC1) to calculate the proper scale needed when importing to KiCad. When you are done redrawing, you can export to Gerber and have the PCBs manufactured by the supplier of your choice. Good luck!

Jean-François Simon (Elektor)



KiCad 8

Elektor 11-12/2024, p. 22 (240278)

I have enthusiastically familiarized myself with KiCad. Now I am facing a problem. In order to avoid working across many files, I have created a composite project containing several circuit diagram sheets. Each circuit diagram sheet contains a separate circuit diagram corresponding to a daughterboard. All of these will be connected to a main board. However with this arrangement, I am unable to create a separate layout for each board in the PCB editor. This is also reflected in the 3D viewer. If you have a solution to the above, I would be very grateful.

Hans-Joachim Petzky (Germany)

To the best of my knowledge, it is not possible for KiCad to operate in the way that you would like. While a board may have its schematic spread over several sheets (to help with organization), it can only have a single layout. I hope this helps!

Peter Dalmaris (Author of the article)

I think it would be easier if you organize your project with subfolders for each PCB. Each folder can contain the schematic (.kicad_sch) and PCB (.kicad_pcb) files for a specific PCB. Unfortunately, this doesn't conform to your desire to minimize the number of files, sorry about that!

Jean-François Simon (Elektor)

Ideas or Feedback?
Got a bright idea or valuable feedback for Elektor? Reach out to us at editor@elektor.com. We're eager to hear from you!



Wireless Emergency Push Button

Elektor 7-8/2023, p. 20 (200578)

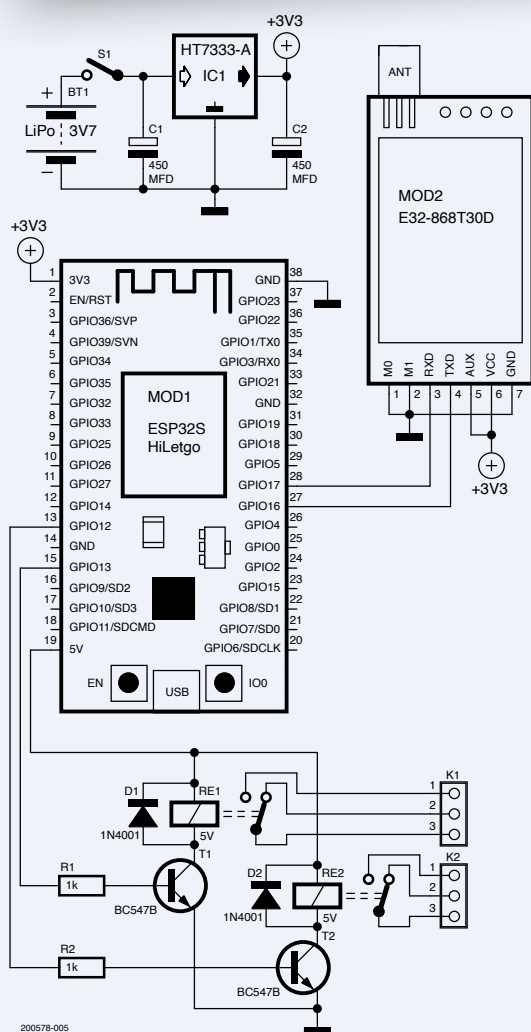
Unfortunately, the example code does not address the issue of increased security with LoRa. Quote: "Besides using interference-resistant spread-spectrum technology, they provide three parameters: channel frequency, air rates and a 4-byte ID. Communication can only take place when these three parameters are the same on both ends of the link." It is precisely these points that are missing in the article! An initialisation of the E32 module via *Serial2* should be carried out to this end. Could you clarify?

Hanspeter Schären (Switzerland)

These E32 modules are normally configured using a small, dedicated software program provided by Ebyte, the module's manufacturer. This allows you to set the baud rate, power, address, channel, etc. You will need a USB-to-serial adapter based on an FT232RL or similar circuit. Documentation for the module can be found at

<https://eltsi.ru/upload/files/E32-868T30D.pdf>. The manufacturer's download page is www.cdebyte.com/Resources-Download. After configuring the two modules with identical settings, the wireless serial link connection between the two E32 modules is automatically established. So if you take the trouble to initialize the E32 modules in advance, you won't have to do it later in the code, which is why this configuration is not done by the program available for download on the article page. Of course, it is also possible to configure the modules directly via a microcontroller's serial interface on both sides of the link. All the configuration carried out via the Ebyte software is encoded in 5 bytes, which can be sent via `Serial.print` or other means. A video under www.youtube.com/watch?v=FB-ePscCcOU clearly illustrates the procedure. The author of the video uses a Forth-based microcontroller, which is not so common, but you can of course easily adapt the procedure with Arduino or ESP32 code.

Jean-François Simon (Elektor)



Dogan Ibrahim, LTspice Essentials, Elektor, 2024

I am going through this excellent book and came across a small problem with Chapter 7: "Thyristors, Diacs and Triacs – Importing a SPICE model". I downloaded the needed files for the Diac and the Triac from ST and imported them, but when the circuit was run, an error box appeared about an errant "*" in the code. I eventually found that it was the Diac code that was causing the error. The problem was caused by a typo in the STMicro Diac spice model library `st_diacs.lib`.

Line 79 of this file is:

```
R_R1 N02098 TRG 1.462*{Tr}
```

but instead ought to be:

```
R_R1 N02098 TRG {1.462*Tr}
```

I hope this can help other readers of the book!

Adrian Hirst

Thank you very much for this very valuable feedback! Indeed, it will be helpful to others. It's a pity that ST let this error creep in their file, but it's a very good thing that you were able to spot the error and fix it!

Jean-François Simon (Elektor)



Unveiling Ethical Transparency

Insights from Ethics in Electronics's 2024 Survey

By The Elektor Content Team

A 2024 survey from Ethics in Electronics (EiE) uncovers significant transparency gaps within the electronics industry. Project leader Niek Poortman shares the key findings and discusses steps companies need to take to meet rising ESG standards.



▲ Niek Poortman (Project Leader, EiE).

As the electronics industry faces growing scrutiny over ethics and sustainability, Ethics in Electronics's (EiE) 2024 survey reveals significant gaps in transparency among electronics companies. In this interview, EiE's project leader, Niek Poortman, discusses the survey's key findings and what companies must do to meet evolving ESG standards.

Elektor: Before we dive into the details of EiE's 2024 survey, can you tell us a bit about Ethics in Electronics as an organization?

Poortman: Ethics in Electronics was founded in 1994, as part of Lenthe Foundation (Editor's note: Lenthe is the corporate foundation of Elektor), years before the electronic industry started to care about ethics and/or sustainability. Ethics in Electronics was raising awareness by triggering columns and articles in Elektor, a magazine and platform for European engineers. Nowadays Lenthe supports communication managers of middle sized companies with research, content and awards. Our ambition is to inspire and assist them in making transparent (internal and external) corporate ethical communication.

Elektor: What were the main objectives you had in mind when you created EiE's 2024 survey? What were you hoping to uncover?

Poortman: When we designed the 2024 survey for Ethics in Electronics, our primary objective was to gain a clearer understanding of how companies in the electronics industry communicate their commitment to ethics and sustainability. With the upcoming regulatory requirements around ESG reporting, particularly

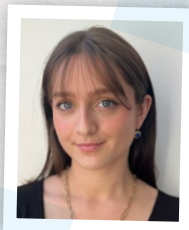
From January 2025, Morgan de Saint Jorre will join the Lenthe Foundation as the 2nd Project Leader of the EiE project.

The board thanks Niek for managing the research with the exhibitors of electronica and for his efforts to prioritize ethical corporate communication among directors and CEOs.

Morgan will begin her role at the Lenthe Foundation by mobilizing communication managers and decision-makers at M- and C-level to invest at least €4K in producing an honest, objective ethical profile to publish on their websites.

CONTACT:

Morgan de Saint Jorre, Elektor
morgan.saintjorre@elektor.com





for large enterprises with over 500 employees and, soon, for SMEs in 2025, we wanted to assess how prepared companies were for these shifts.

The goal was to uncover the extent to which these companies are transparent about key aspects, such as their ethical commitments, sustainability practices, employee relations, revenue, and whether they publish reports like annual or sustainability reports. We also aimed to see how well these companies align with emerging trends and stakeholder expectations, such as the integration of Sustainable Development Goals (SDGs).

By benchmarking 100 exhibitors at Messe München 2024, we hoped to highlight the industry's strengths and weaknesses in this area, offering companies an opportunity to identify gaps in their own communications and improve their transparency. Ultimately, our goal was to provide insights that would help companies not only meet legal obligations but also enhance their market positioning, credibility, and attractiveness to employees, clients, and stakeholders.

Elektor: How did you go about selecting the companies that participated in the 2024 survey? Was there a particular criterion or segment of the electronics industry you were focusing on?

Poortman: For the 2024 survey, we specifically targeted exhibitors from Electronica 2024 at Messe München. Our focus was on European SMEs (small and medium-sized enterprises) within the electronics sector. The companies we included were randomly selected within this criterion.

The decision to focus on SMEs in Europe was quite intentional. We wanted to assess how well mid-sized companies — often the backbone of the industry — are preparing for the upcoming regulatory changes related to ESG and sustainability reporting. While larger corporations may already have established reporting mechanisms, we were particularly interested in SMEs because they may face more significant challenges in adapting to these new requirements. By concentrating on European companies, we also acknowledged the stricter compliance landscape across the EU, which often sets the standard for global sustainability efforts.

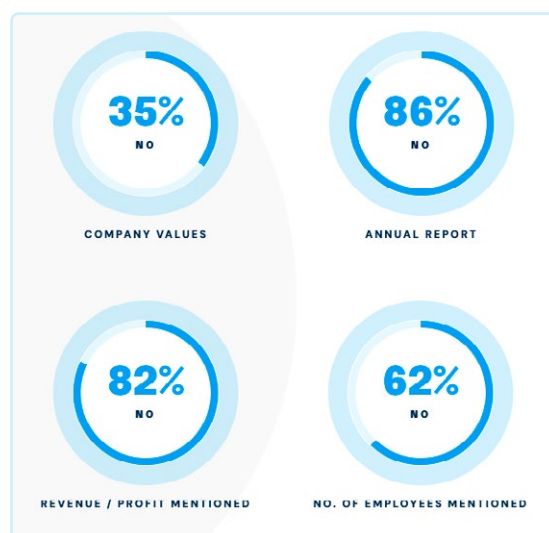
Our goal was to see how these SMEs, who play a critical role in driving innovation within the electronics industry, are positioning themselves in terms of ethical and sustainable practices and how they are communicating these efforts both publicly and within their stakeholder networks.

Elektor: Your survey revealed that only 16% of companies explicitly reference the UN's Sustainable Development Goals (SDGs) on their websites. Why do you think there is such a low alignment with these global sustainability standards?

Poortman: The low percentage of companies explicitly referencing the SDGs likely reflects a few key factors. First, while the SDGs are widely recognized as global sustainability standards, many companies — especially SMEs — may struggle with how to integrate these broader goals into their specific business models and operations. For smaller businesses, aligning with SDGs might seem like an additional layer of complexity, particularly if they lack the resources or expertise to connect these global objectives with their day-to-day activities.

Second, many companies may be engaging in sustainable practices without explicitly framing them in the context of the SDGs. They may be addressing issues like reducing carbon footprints, improving labor practices, or enhancing transparency but don't necessarily use the language of the SDGs in their communication. This could be due to a lack of awareness or simply a disconnect between their actions and how they market their sustainability efforts.

Lastly, SMEs might feel that aligning with such global standards is more relevant for larger corporations with a greater global reach. However, with the growing emphasis on transparency and compliance, especially in Europe, there's a clear opportunity for companies of all sizes to improve their communication and showcase how their efforts contribute to



◀ In a randomized survey of 100 European exhibitors, several striking findings emerged. (Source: EiE)

broader societal goals, like the SDGs. As compliance regulations tighten, we expect more businesses to recognize the importance of aligning their strategies with international standards like the SDGs.

Elektor: One of the key findings was that only 14% of companies make their annual reports publicly available. What are the potential risks for companies that are not transparent about their financial health?

Poortman: Companies that fail to make their annual reports publicly available risk losing trust with key stakeholders like investors, clients, and employees, who increasingly prioritize transparency and accountability. In a competitive market, non-transparency can damage a company's reputation and limit opportunities for growth. Additionally, with tightening ESG regulations, especially in Europe, companies that aren't proactive in sharing financial and sustainability information may face compliance challenges, making them less attractive to both partners and talent.

Elektor: You found that 62% of companies do not disclose their number of employees. Why might this be a problem? Do you think this lack of transparency negatively affects a company's perception among potential employees and other stakeholders?

Poortman: The lack of employee information can raise concerns about transparency and trust, especially for potential employees and stakeholders looking for insight into a company's workforce. For job seekers, knowing the size of a company can influence their decision to apply, as it often reflects resources, opportunities for growth, and company culture. For stakeholders, especially those focused on ESG factors,

workforce data is key to evaluating a company's social impact and employee relations. Not disclosing this information could make a company seem secretive or less accountable, potentially harming its reputation and attractiveness in a competitive market.

Elektor: You conducted a similar survey in 2022, and the 2024 results show little improvement in transparency. Why do you think electronics companies are struggling to make progress in this area, despite increasing regulatory and stakeholder pressure?

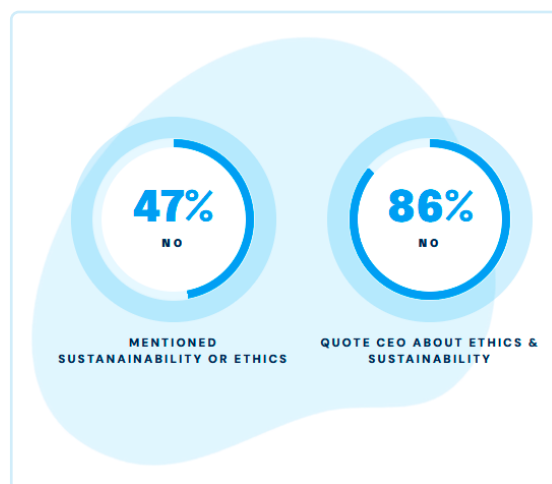
Poortman: Despite growing regulatory and stakeholder pressure, many electronics companies are likely struggling with transparency due to the complexity of aligning internal processes with new reporting standards. Implementing transparent ESG and financial reporting requires significant time, resources, and expertise, especially for SMEs, which often lack the infrastructure of larger corporations. Additionally, there may be hesitation or uncertainty about how best to present this information publicly without compromising competitive advantage. As regulatory frameworks evolve, many companies might still be in the process of adapting, which explains the slow progress despite external pressures.

Elektor: Ethical leadership endorsement was low, with only 14% of companies featuring a CEO quote on ethics and sustainability. How important do you think visible leadership support is in building stakeholder trust?

Poortman: Visible leadership support, such as a CEO endorsing ethics and sustainability, plays a crucial role in building stakeholder trust. When leaders openly champion ethical values, it signals to employees, investors, and clients that these priorities are integral to the company's mission. It fosters credibility, demonstrating a top-down commitment to sustainability that goes beyond compliance. Without this visible endorsement, stakeholders may question whether ethical initiatives are superficial or lack true backing, potentially undermining the company's reputation and its ability to engage meaningfully with audiences who prioritize ethical business practices.

Elektor: What role can the Ethics in Electronics organization play in helping electronics companies bridge the communication gap, particularly with services like the Ethical Profile?

Poortman: Ethics in Electronics plays a crucial role in helping electronics companies close the



►
Roughly 47% communicate about sustainability or ethics, while only 14% feature a CEO quote addressing these crucial topics. (Source: EiE)



communication gap on ethics and sustainability, particularly through services like the Ethical Profile. This service offers companies a structured, editorial approach to sharing their ethical commitments and sustainability efforts. With increasing regulatory demands such as ESG reporting and SDG alignment, companies often struggle to present a clear, comprehensive picture of their initiatives. The Ethical Profile not only highlights a company's actions but also ensures that these efforts are communicated effectively across key platforms — whether through the company's website, social media, corporate reports, or inclusion in the 2025 Ethical Guide. This increases visibility and credibility among stakeholders, from customers to investors, who are increasingly prioritizing ethics and sustainability in their decision-making.

Moreover, the Ethical Profile helps companies build trust by guiding them to adopt best practices in transparency and corporate responsibility. Ethics in Electronics provides insights based on industry benchmarking, helping businesses identify gaps in their communication and improve how they convey their values. By publicly showcasing their ethical practices, companies can differentiate themselves in the market, attract potential employees, and solidify their reputation as leaders in responsible innovation. This service offers not only compliance with regulations but also a competitive advantage by positioning companies as trustworthy and future-focused.

Elektor: Looking to the future, what do you think will be the biggest challenge for electronics companies in terms of ethics and sustainability communication?

Poortman: Looking to the future, the biggest challenge for electronics companies in terms of ethics and sustainability communication will likely

be maintaining transparency while keeping up with increasingly complex regulatory requirements and stakeholder expectations. As ESG reporting becomes more standardized and detailed, companies will need to find ways to align their internal processes with these frameworks, while also ensuring that their communication is clear, credible, and authentic. Striking a balance between regulatory compliance and meaningful, engaging communication that resonates with customers, investors, and employees will be key.

Additionally, as the public becomes more informed and discerning about ethical practices, companies will face the challenge of avoiding “greenwashing” — making superficial claims about sustainability without substantive backing. Electronics companies will need to provide concrete evidence of their initiatives and demonstrate measurable impacts, all while competing for attention in a market increasingly saturated with sustainability messaging. Ensuring that their communication remains genuine and data-driven, while also aligning with global sustainability goals, will be critical for building long-term trust and maintaining competitive advantage. ◀

Editor's note: Elektor and eeNews Europe — trusted media partners of Ethics in Electronics — are interested in driving ethical innovation in electronics. Ethics in Electronics was founded in 1994. Producer Lenthe Foundation started that year raising awareness with popular columns and articles in Elektor.

240631-01



Niek Poortman
PROJECT LEADER



Phylcia Akkermans
MANAGER COMMUNICATION AND SOCIALS



Johan Dijk
PUBLISHER



Harmen Heida
ART DIRECTOR



Büsra Kas
CURRENT EXECUTIVE



Prof. Stefan Heinemann
ADVISOR SCIENCE CONTENT

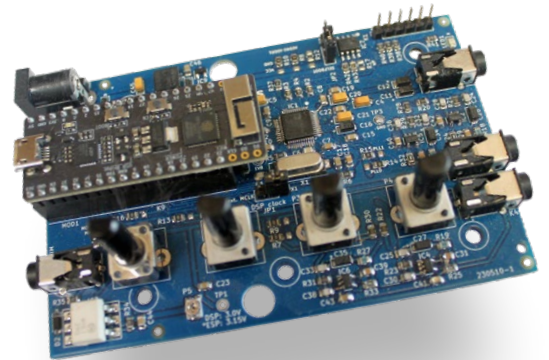
Empowering Ethical Communication in the European Electronics Industry.

◀
The Ethics in Electronics team. (Source: EiE)



Elektor Audio DSP FX Processor Board

Part 2: Creating Applications



By Clemens Valens (Elektor)

The Elektor Audio DSP FX Processor board combines a powerful ESP32 microcontroller with an ADAU1701 audio DSP. Together, they allow for high-quality audio generation and processing applications. In the first part of the project, we presented the board and its features. We also showed you how to set up a development system to create applications for the board. In this second part, we look at application development in more detail.

The Elektor Audio DSP FX Processor board is essentially an ESP32 microcontroller enhanced with high-quality audio inputs and outputs. What distinguishes this board from others is its integrated DSP, which can handle audio processing independently. This feature adds both power and flexibility to the board, making it highly versatile. In the previous article [1], we explored the board's design in depth. Now, we'll focus on the software side of the system.

For your convenience, as a refresher or a reminder, we have reproduced the Audio DSP FX Processor board's block diagram in **Figure 1**. It shows the two processors, how they are connected to each other and how the other peripherals fit in. For more details on the design of the Audio DSP FX Processor and its applications, please refer to Part 1 of this series [1].

Applications for the Audio DSP FX Processor can be created from scratch, ported from another platform or project, or by adapting one

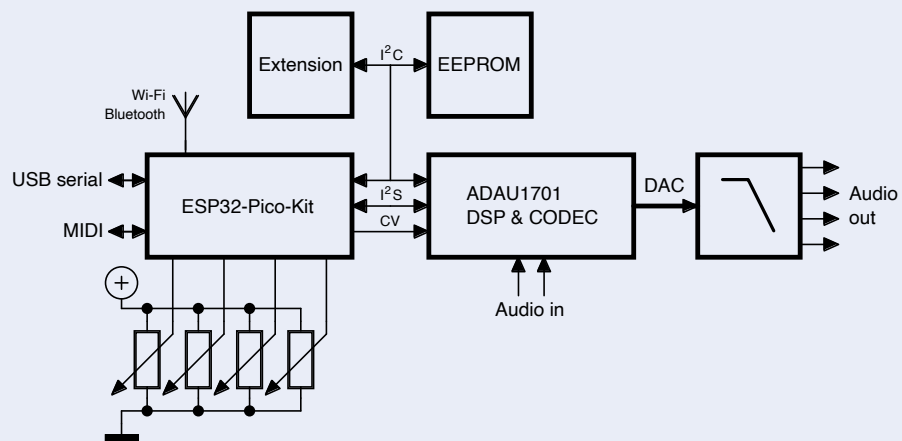


Figure 1:
The functional block
diagram of the Audio
DSP FX Processor.

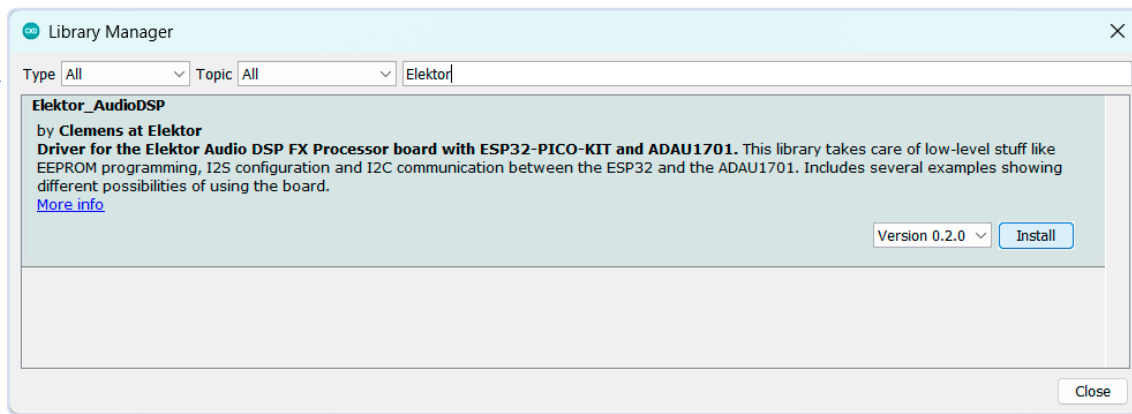


Figure 2:
The `Elektor_AudioDSP` library is available in the Library Manager of the Arduino IDE.

of the example programs. Applications consist in most cases of an ESP32 program together with an ADU1701 DSP algorithm. ESP32 programs are created in the usual way (using Arduino [2], ESP-IDF, etc.) whereas DSP programs are built in SigmaStudio 4.7, a free, visual programming environment from Analog Devices. It lets you create ADAU1701 programs by interconnecting algorithm blocks with virtual wires on a canvas. Note that there exist two versions of SigmaStudio, a new version (*SigmaStudio+*) and an old one (*SigmaStudio*). We are obliged to use the old, abandoned version (4.7) as SigmaStudio+ does not support the ADAU1701 (which is a pity).

Arduino

In order to simplify Arduino program development, we have created the `Elektor_AudioDSP` library ([3], see **Figure 2** and insert **About the ESP32 Boards Package**). This library handles most of the low-level operations of the board like EEPROM programming and updating, and routing potentiometer and MIDI data. Together with certain third-party libraries (see the examples included in the library, **Figure 3**) it gives access to controlling the DSP and even programming it directly. The library also exports some constants that are intended for simplifying porting of other I²S based sound applications (see e.g., the example `ml_synth_organ`) to the board.

An application using the `Elektor_AudioDSP` library starts by creating (instantiating) an object from the `Elektor_AudioDSP` class. In the case the ESP32 must send I²S data to the DSP, then the application can create an `Elektor_AudioDSP_I2S_Out` object instead as it provides some I²S helper functions. Refer to the file `Elektor_AudioDSP.h` for details about the available methods and properties of the object.

The object's `begin()` method allows specifying an EEPROM file for the DSP that will only be programmed when needed. Furthermore, it will configure the potentiometers, the DAC multiplexer and the MIDI port. The code snippet below shows how an `audiodsp` object from the `Elektor_AudioDSP` class is declared and intended to be used. The DSP firmware used in the snippet is part of the collection included in the library.

```
#define SAMPLE_RATE (48000)
#include "Elektor_AudioDSP.h"
Elektor_AudioDSP audiodsp = Elektor_AudioDSP();

void setup(void)
{
    audiodsp.begin(
```

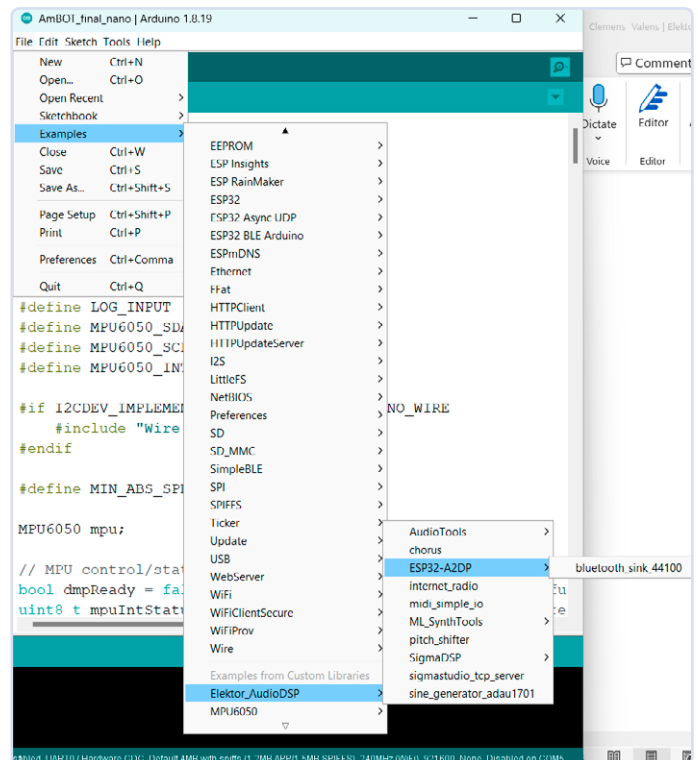


Figure 3: The `Elektor_AudioDSP` library includes a few examples to help you get started. Here is how to find them.

About the ESP32 Boards Package

To use the ESP32 module with the Arduino IDE the ESP32 Boards Package must be installed first. For details on how to do this, please refer to [2]. Note that it is highly recommended to install a version before 3.0.0 (e.g., 2.0.17) because certain drivers have been completely overhauled in version 3.0.0 (e.g., I²S, ADC, and DAC). It will take a while before other libraries using these peripherals will have integrated the modifications and again compile without errors. We have also observed severe code bloating with applications based on version 3.0.x that will no longer fit in the ESP32 module's memory. Notably, the Bluetooth examples suffer from this update.



```
adau1701_firmware_i2s_pass_through_48000,
ADAU1701_FIRMWARE_I2S_48000_SIZE);
}

void loop(void)
{
    // Read potentiometer P1 (returns a 12-bit value)
    uint16_t p1 =
        audiodsp.potentiometer[audiodsp.P1].read();
    p1 >>= 4; // Scale down
              // because DAC is only 8-bit

    // Send to DSP pin MP9,
    // but only if the value has changed.
    if (audiodsp.dac[audiodsp.MP9] != p1)
    {
        audiodsp.dac[audiodsp.MP9] = p1;
    }
    audiodsp.dac.refresh(); // Call regularly

    if (audiodsp.midi.available())
    {
        /* do something with MIDI data */
    }

    // etc.
}
```

JP1 — DSP Clock Source

When the ESP32 and the ADAU1701 do not have to exchange audio data over the I²S bus, it is simplest to make the DSP have its own clock source in the shape of crystal X1. For this, JP1 must be in position *X1* (pins 1 and 2).

When the board is used in a configuration where the DSP is an I²S slave device, the ESP32 (the I²S master) must provide an MCLK signal with a frequency exactly 256 times higher than the sample rate used in SigmaStudio. If this ratio is something else, the DSP will not output any audio. Of course, the I²S master should use the same sample rate on the I²S bus. The MCLK signal must be output on IO0 of the ESP32 and jumper JP1 must be placed in the position *ext. MCLK* (pins 2 and 3).

As the ESP32 provides the clock to the DSP, the latter will not do anything before the clock signal is present. Furthermore, the DSP may show undefined behavior when this clock is being set up or unstable. Therefore, keep the DSP in reset until the I²S bus is configured properly. You can do this by pulling port IO12 of the ESP32 low during I²S configuration and releasing it (to high) once the bus is ready. The *bluetooth_sink_44100* example shows how to do this.

JP2 — DSP Selfboot or Not?

The ADAU1701 DSP is capable of standalone operation, but it must be told to do so. This mode is called *Selfboot* and it is selected with jumper JP2 (pins 2 and 3) or R12. In Selfboot mode and with a valid clock signal, the ADAU1701 will load a program and execute it every time it is reset (at power-up, for instance). In this mode, a host processor such as the ESP32 is not required, but may be useful for controlling the ADAU1701 through its I²C port.

In Selfboot mode, the DSP expects that a program is stored in an EEPROM that it can access. In the case of the Audio DSP FX Processor, the EEPROM must be on the I²C bus on address 0x50 (in 7-bit format).

If JP2 is set to pins 1 and 2, i.e. not Selfboot, then the DSP will not try to load a program and instead wait for a host to upload something. This is again over the I²C bus and the ESP32 can take care of it. The *sigmastudio_tcp_server* example shows how this can be done.

This all would have been straightforward if the formats of the Selfboot EEPROM file and the file used by the host to program the DSP (the host-boot program) had been the same, but they aren't. Neither burning a Host-boot program into the EEPROM nor uploading a Selfboot EEPROM file in Host-boot mode will result in a running DSP.

Whether in Selfboot mode or not, a clock source is always required. In the absence of a host processor, this would be crystal X1 (JP1 on pins 1 and 2). When the host is providing a clock signal, then the DSP will not boot before this signal is present. This sounds logical but is easily forgotten. Therefore, if an application is not functioning as expected, check the DSP clock first.

SigmaStudio

Programs for the ADAU1701 DSP are made with SigmaStudio. This is a free visual programming environment in which you drop DSP algorithm blocks on a canvas and interconnect them with virtual wires to create more complex algorithms. A library of predefined algorithms is included in the tool. As said, for the Audio DSP FX Processor, we need SigmaStudio 4.7 and not SigmaStudio+ as it doesn't know the ADAU1701.

Make sure that the Audio DSP Board is configured properly for the type of algorithm you plan to create. See the inserts **JP1 — DSP Clock Source** and **JP2 — DSP Selfboot or Not?** for details. Also refer to the first part of this article series [1].

Mini Tutorial

Note that since we are not using a board that is officially supported by SigmaStudio, at some point during the creation of the schematic below you will see a message mentioning USB problems. You can safely ignore this message.

- Start SigmaStudio
- Select *File* → *New Project* and wait for the project to be created. You will see a list of elements in the toolbox on the left. Select the *ADAU1701* block, drag it to the *Hardware Configuration* window and drop it somewhere. Repeat the procedure for a *USBi* block and an *E2Prom* block.
- Link one of the blue dots of the *USBi* block to the green dot of the

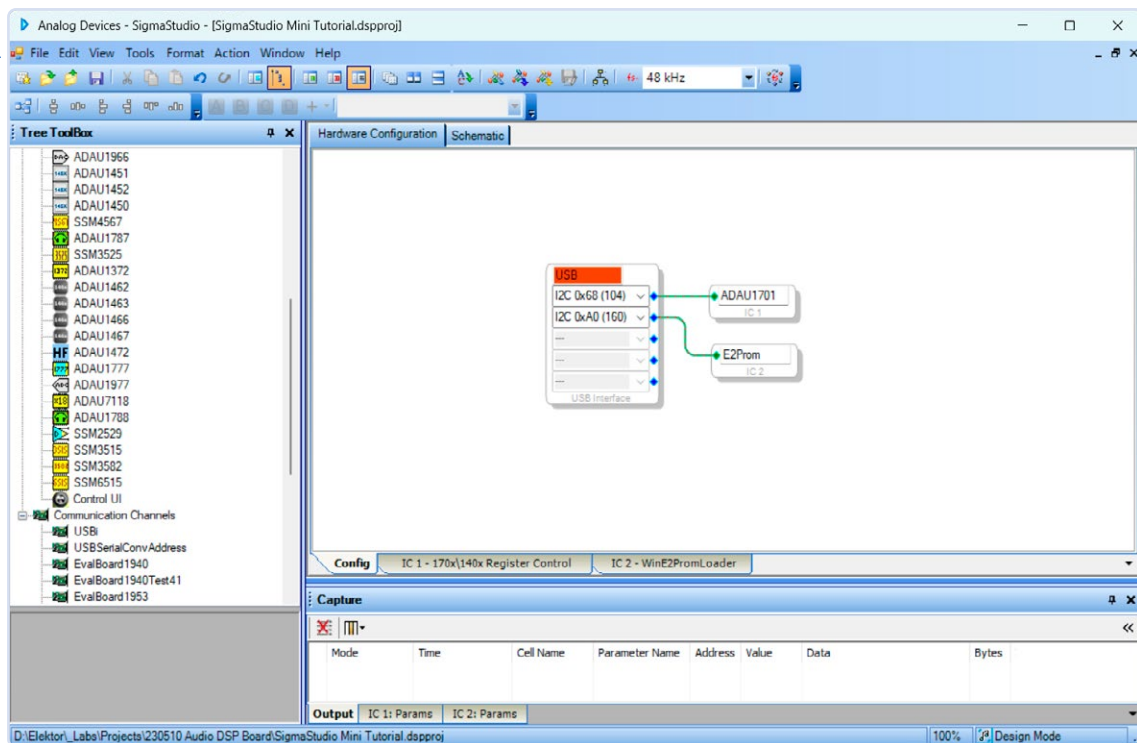


Figure 4: This is how you begin a program for the ADAU1701 with EEPROM in SigmaStudio.

ADAU1701. Link the other blue *USBi* dot to the green dot of the *E2Prom*. The result should look like **Figure 4**.

- Save the project (as *Mini Tutorial*, for instance) in a folder of the same name.
- Click on the *Schematic* tab. Notice the change in the toolbox on the left.
- From *IO* → *Input*, drag an *Input* element to the schematic and drop it.
- From *IO* → *Output*, drag an *Output* element to the schematic and drop it. Repeat this step to place a second output.
- From *IO* → *GPIO* → *Input*, drag the *Auxiliary ADC Input* element to the schematic and drop it.
- From *Volume Controls* → *Adjustable Gain* → *Ext Control* → *Click-less SW Slew*, drag the *Single slew ext vol* to the schematic and drop it.

- Right-click on the *SW vol 1* block and select *Grow Algorithm* → *1. Ext vol (SW slew)* → *1*. The block now has three inputs and two outputs.
- From *Filters* → *Second order* → *Single precision* → *2 Ch* drag the *Medium Size Eq.* to the schematic and drop it. Right-click on the *Mid EQ 1* block and select *Grow Algorithm* → *1. 2 Channel - Single Precision* → *3*. The block now has four sliders.
- Connect the blocks as shown in **Figure 5**.

Now we must configure the DSP pin MP9 (ADC0) as an auxiliary ADC input:

- Return to the *Hardware Configuration* tab and then click *IC1 -170x140x Register Control* tab at the bottom of the window.
- Select *MP9* In the *GPIO* block and change *Input GPIO Debounce*

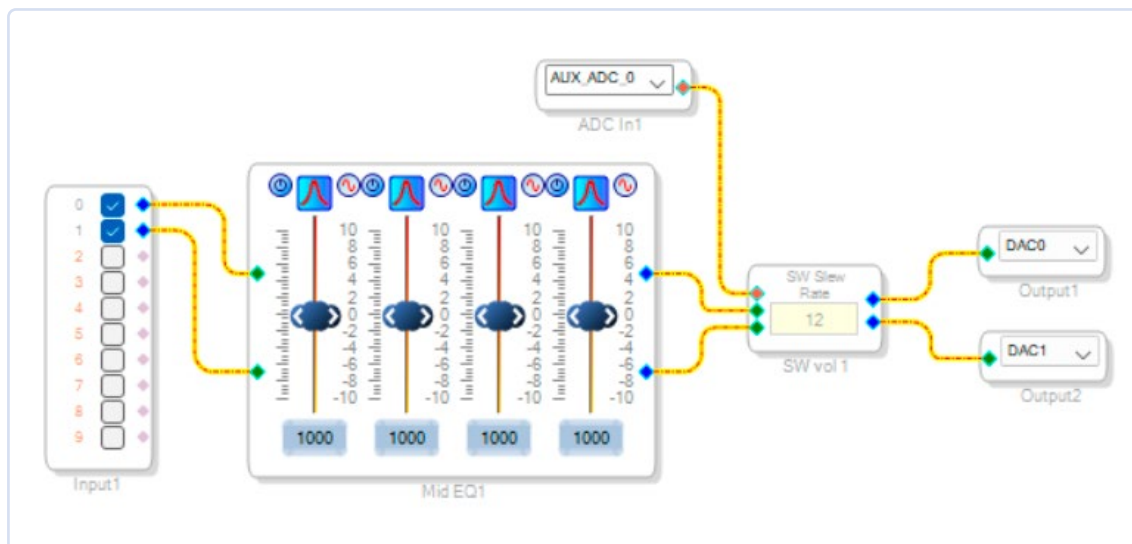


Figure 5: Programming in SigmaStudio consists of dropping blocks on a canvas and then drawing wires between them.

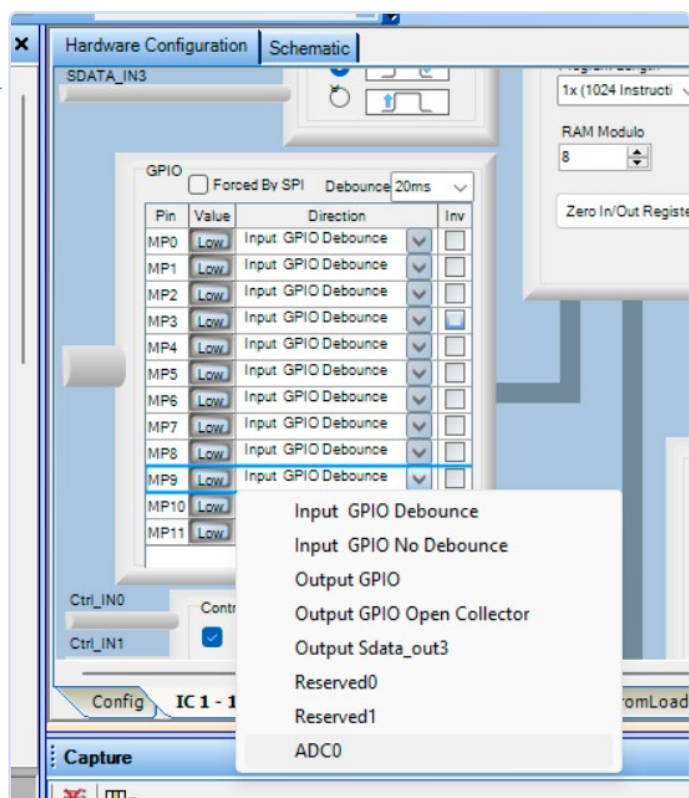


Figure 6: Configure the DSP's GPIO pin MP9 as an analog input.

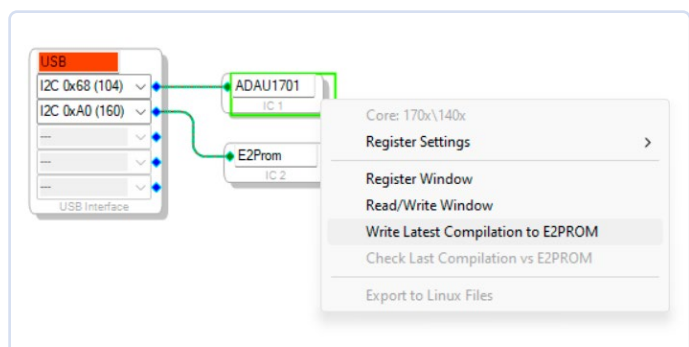


Figure 7: A right-click on the ADAU1701 block provides access to the function to create a HEX file for the EEPROM.

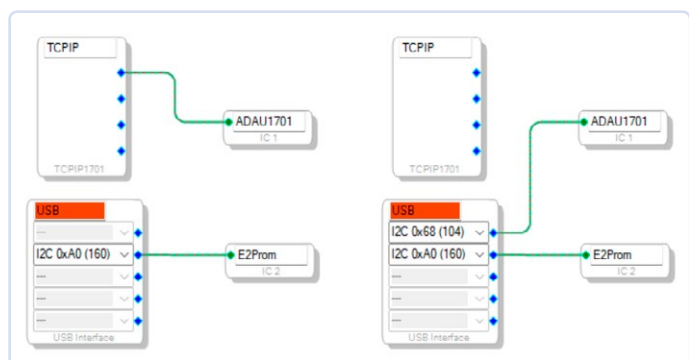


Figure 8: Use a TCPIP1701 block (left) to connect to an ADAU1701 over a (wireless) network connection. This block can coexist with a USBi block, which allows the creation of a HEX file after rewiring the Hardware Configuration (right).

to ADC0 (see **Figure 6**). Ignore any connection warnings that may pop up.

- Return to the *Schematic* and change the values of the slider frequencies in the equalizer and set the gain to your taste.
- The project is ready, save it.
- Press *F7* or select from the menu *Action* → *Link Compile Download*. Ignore any communication errors.
- Return to the *Config* tab of the *Hardware Configuration* window. Right-click on *IC1* (the ADAU170, not the EEPROM) and select *Write Latest Compilation to E2PROM* (see **Figure 7**). This will create a file *E2Prom.Hex* in the subfolder *my_project_IC2* (where *my_project* is the name of your project). Program this file into the EEPROM. How? We'll get to that below. But first, we introduce a faster method to upload HEX files to the DSP, for test and development purpose.

SigmaStudio Over Wi-Fi

A program developed in SigmaStudio must be transferred to the DSP on our board. When the program is ready, it is best exported as a HEX file. You can also add it to the E2PROM collection (*adau1701_e2prom_collection*) included in the *Elektor_AudioDSP* library. However, when the application is still under development, it has to be uploaded regularly for testing. Normally, this is done by using a development board with a special USB connection, but our board doesn't support that method. Luckily, SigmaStudio also supports uploading DSP executables over a TCP/IP connection, and this we do support. Doing this over Wi-Fi is an easy task for the ESP32 and adds over-the-air (OTA) capabilities to the system.

The *sigmastudio_tcp_server* example included in the *Elektor_AudioDSP* library implements TCP/IP communication with SigmaStudio. Upload the sketch to the ESP32 on the Audio DSP FX Processor board and open the Serial Monitor. Here you will find the IP address of the board.

In the SigmaStudio project, instead of connecting a *USBi* block to the ADAU1701 you now connect a *TCPIP1701* block (**Figure 8**). Right-click on it to open the TCP/IP configuration panel (*Show TCPIP Settings*) and enter the IP address of the Audio DSP FX Processor. Click *Open Connection*. If the Serial Monitor shows a connection message, you're good to go (**Figure 9**).

Draw your DSP algorithm and when it is ready, click the *Link Compile Download* button (or press *F7*). The program is now sent to the board where it is immediately executed. Program parameters can be adjusted in real time. Not only is this a very fast and convenient way of developing, but it also allows you to leave the board in its test environment (which doesn't have to be on your bench next to your computer).

Unfortunately, it is not possible to program the EEPROM this way. Trying to generate a HEX file for the ADAU1701 in SigmaStudio 4.7 in TCP/IP mode is broken and produces an error message. The only way to generate it is by adding a *USBi* block to the canvas, connect the ADAU1701 to it and then generate the HEX file in the usual way.

More Resources

SigmaStudio

There are quite a few projects out there that use the ADAU1701 for guitar effect pedals ("stomp boxes"), crossover filters for audio/loudspeaker systems and more. There are also (Arduino) libraries for programming and controlling the DSP. Providing an exhaustive list is, of course, undoable, but a few interesting resources are listed here. You can find more by searching, e.g. on GitHub, on keywords such as "ADAU1701" and "Sigma Studio."

Aida DSP Arduino Shield

Although the Aida DSP Arduino Shield is not perfectly compatible with the Elektor Audio DSP FX Processor board, the repository includes a good collection of SigmaStudio projects ranging from simple examples to virtual microphone preamplifiers.

https://aidadsp.github.io/aida_dsp_arduino_shield.html

SigmaDSP

Based on Aida DSP and some reverse engineering, this library focuses on controlling ADAU1701 algorithms from a microcontroller over I²C. It can be installed from the Arduino IDE's library manager and includes several examples. The documentation also features detailed instructions for converting *System files* exported from SigmaStudio to something usable in Arduino.

<https://github.com/MCUdude/SigmaDSP>

Dayton Audio

Manufacturer of high-end audio amplifiers, Dayton Audio also has a range of amplifier modules based on the ADAU1701 with Bluetooth. These modules ship with default software but are user programmable. The company has created a nice user manual for Sigma Studio and provides the SigmaStudio project plus examples. The files can be found in e.g. the download section of the KABD-4100 module.

<https://daytonaudio.com>

ESP32 & Arduino

There exist many libraries for producing and processing sound with an ESP32. Although far from being exhaustive, here are a few resources that you might find useful.

Espressif Audio Development Framework

The official audio development framework for the ESP32 family. This library focuses on audio streaming of many file formats from different sources. Supported applications are internet radio, Bluetooth streaming, VoIP, MP3, and much more.

<https://github.com/espressif/esp-adf>

Faust

Faust, short for Functional Audio Stream, is a programming language for real-time signal processing and synthesis developed by Grame, the Centre National de Creation Musicale in Villeurbanne near Lyon in France. Faust can be used on many platforms, and the ESP32 is one of them. The code and detailed documentation are on GitHub.

<https://github.com/grame-cncm/faust>

Phil Schatzmann

The GitHub space of Phil Schatzmann has several repositories that are of interest for the Audio DSP FX Processor. ESP32-A2DP is great for creating Bluetooth audio devices. The Arduino Audio Tools library features audio sources and sinks, filters, effects, decoders, and converters and much more. Some examples also require Phil's Arduino Audio Driver library. These libraries must be downloaded from GitHub, as they are not available in the Arduino IDE's Library Manager.

<https://github.com/pschatzmann>

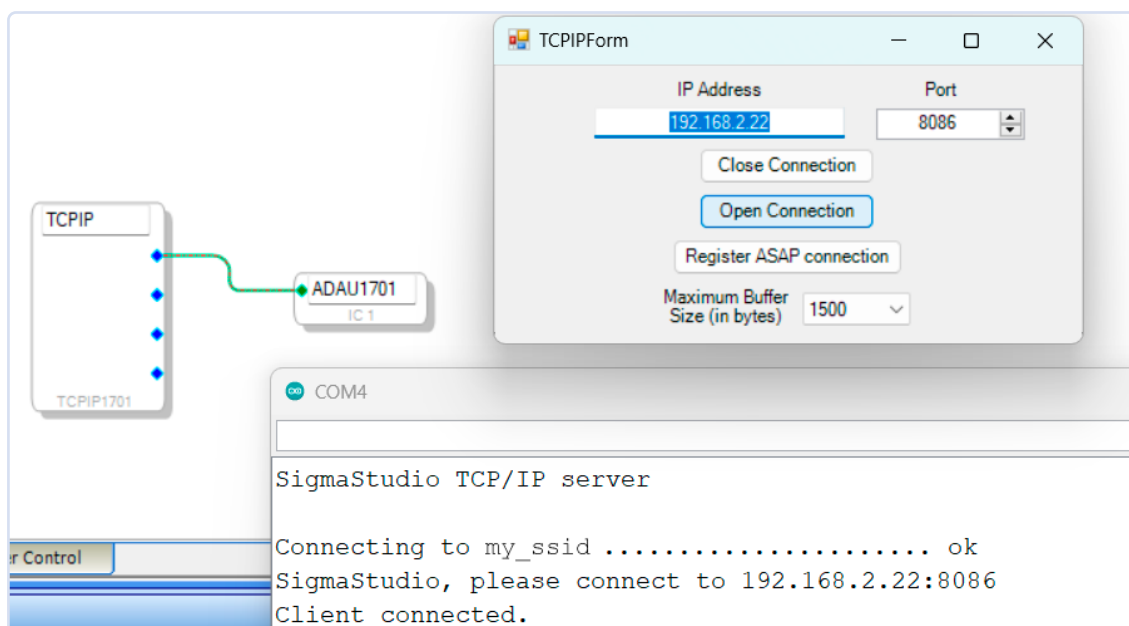


Figure 9: Use the *sigmastudio_tcp_server* example (included in the *Elektor_AudioDSP* library) to establish a wireless connection between SigmaStudio and the Audio DSP FX Processor.

The Elektor AudioDSP library includes a sketch `e2prom_writer_tcpip` that can be used to program the EEPROM over a (wireless) network. Together with a terminal program like Tera Term, capable of sending files over a network without protocol (raw mode, **Figure 10**), you can use it to upload E2Prom files directly into the EEPROM (**Figure 11**). The way it works is quite simple: you send the `.bin`-file in raw mode and then type the command `write` followed by hitting the **Enter** key to start programming (make sure *new-line* is encoded as CR+LF characters, see **Figure 12**).

This terminates the long description of the Elektor Audio DSP FX Processor board, from its design to using it. Now it is up to you to turn it into a cool application. Refer to the **More Resources** insert for inspiration. If you do, please let us know by leaving a comment at [4].

230510-B-01

Questions or Comments?

Do you have technical questions or comments about this article? Email the author at clemens.valens@elektor.com, or contact Elektor at editor@elektor.com.

About the Author

Clemens Valens started working for Elektor in 2008, and he has held various positions since. Currently, he is part of the product development team. His main interests in electronics are (digital) signal processing and its applications in music production and sound synthesis.

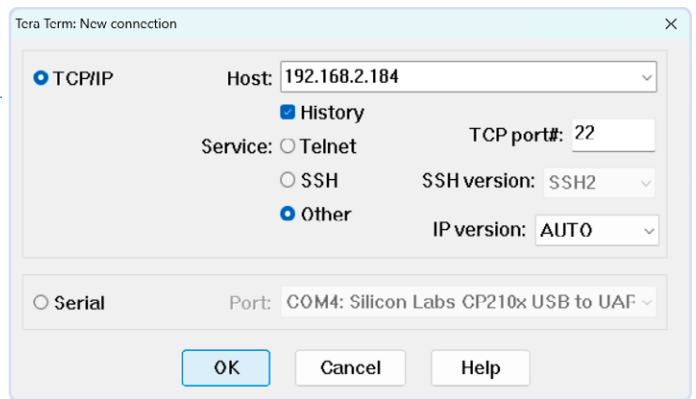


Figure 10: In Tera Term, choose the service "Other" to enable sending files over TCP/IP without using complex protocols.

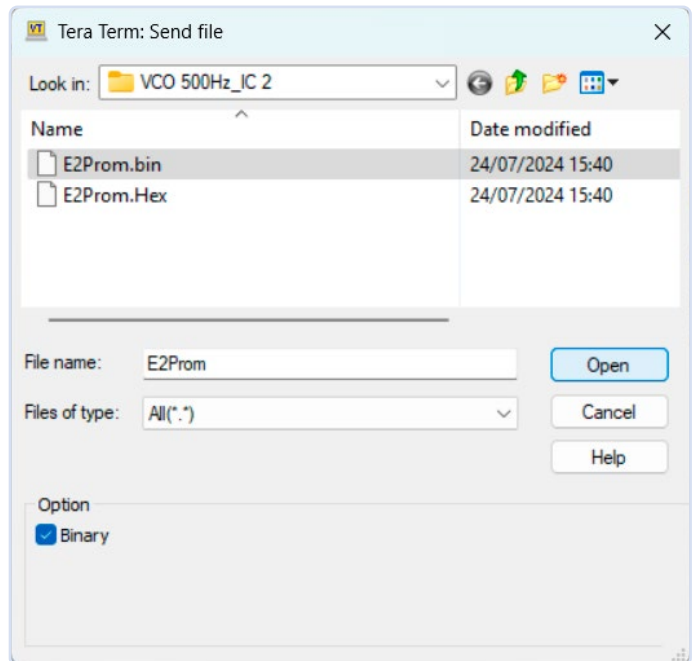


Figure 11: SigmaStudio creates the executable in two flavors: BIN and HEX. Using Tera Term's "Send File" option, transmit the binary (.bin) file, not the HEX file (.hex).

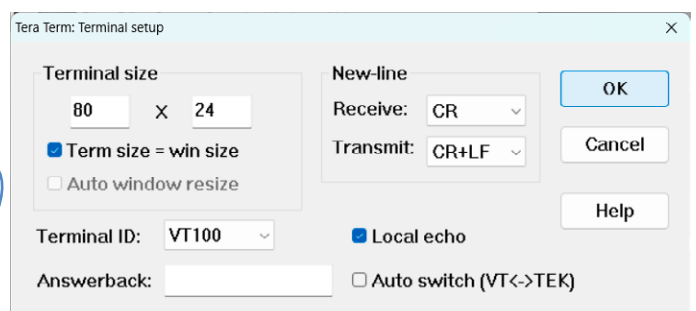


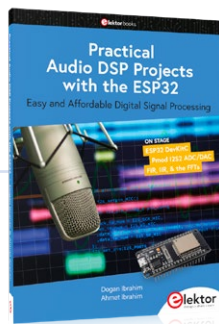
Figure 12: Terminate the remote EEPROM programming procedure by sending "write" (just type it on the keyboard) followed by pressing <Enter>. Make sure the new-line terminator is defined as CR+LF.



Related Products

> **Elektor Audio DSP FX Processor**
www.elektor.com/20895

> **Dogan and Ahmet Ibrahim, Practical Audio DSP Projects with the ESP32 (Elektor, 2023)**
www.elektor.com/20558



WEB LINKS

- [1] Clemens Valens, "Audio DSP FX Processor Board," Elektor 11-12/2024: <https://elektormagazine.com/230510-01>
- [2] ESP32 FAQ, How-to & Getting Started, elektor-labs.com: <https://elektormagazine.com/esp32-faq>
- [3] The Elektor_AudioDSP library at GitHub: https://github.com/ClemensAtElektor/Elektor_AudioDSP
- [4] The Audio DSP FX Processor on Elektor Labs: <https://elektormagazine.com/labs/audio-dsp-fx-processor>

PROTEUS DESIGN SUITE



Driving forward with Manual Routing

Push and Shove Routing
for dense layouts

Dedicated Differential
Pairs Routing mode

Length Matching and
Net Tuning Support

Visual DRC shows legal
paths for route placement

HEAVY
TRAFFIC

FASTER
ROUTING
AVAILABLE

labcenter
Electronics

www.labcenter.com

info@labcenter.com



